2006

Structural performance of approach slab and its effect on vehicle induced bridge dynamic response

Xiaomin Shi
Louisiana State University and Agricultural and Mechanical College, xshi1@lsu.edu

STRUCTURAL PERFORMANCE OF APPROACH SLAB AND ITS EFFECT ON VEHICLE INDUCED BRIDGE DYNAMIC RESPONSE

A Dissertation

Submitted to the Graduate Faculty of the
Louisiana State University and
Agricultural and Mechanical College
in partial fulfillment of the
requirements for the degree of
Doctor of Philosophy

in

The Department of Civil and Environmental Engineering

by
Xiaomin Shi
B.S., Tongji University, P.R.China, 1999
M.S., Tsinghua University, P.R.China, 2002
December, 2006

To my husband and my parents.

ACKNOWLEDGEMENTS

I would like to express my sincere appreciation to Professor Steve C.S. Cai, my advisor, who provided me the opportunity to work in the academic area of civil/structural engineering. Without his expert advice, patient guidance, timely corrections, and strong support at all levels, this dissertation would not have been accomplished. Deep thanks and special gratitude are also due to his effort on shaping my attitude to my research work.

I also want to express my sincere gratitude to my committee members: Dr. George Z. Voyiadjis, Dr. Su-Seng Pang, Dr. Ayman Okeil, and Dr. Chunyan Li for reading this dissertation and offering constructive comments.

My special thanks go to Dr. Zhongjie Zhang at Louisiana Transportation Research Center, for his generous advice in my research and help in bridge test.

Thanks are also extended to my friends and fellow graduate students: Dr. Suren Chen, Dr. Wenjie Wu, Marcio Araujo, Xianzhi Liu, Anand Chandolu, Archana Nair, Staneley Oghumu, Yin Zhang, Miao Xia, and Lu Deng for their help and company in my study.

The financial support for this research provided by Louisiana Transportation Research Center (LTRC), and the Graduate School Supplemental Fellowship offered by Louisiana State University are all fully acknowledged.

Last but not least, I am grateful to my husband and my parents for their strong support. This dissertation would not appear without their consistent encouragement, love, and patience.

TABLE OF CONTENTS

LIST OF TABLES

LIST OF FIGURES

ABSTRACT

Differential settlement often occurs between the bridge abutment and the embankment soil. It causes the approach slab to lose its contacts and supports from the soil and the slab will bend in a concave manner. Meanwhile, loads on the slab will also redistribute to the slab ends, which may result in faulting (or "bump") at the slab ends. Once a bump forms, repeating traffic vehicles can deteriorate the expansion joint in turn. In this case, the vehicle receives an initial disturbance before it reaches the bridge. This excitation introduces an extra impact load on the bridge and affects its dynamic responses. The present research targets at the structural performance of the approach slab as well as its effect on the vehicle induced bridge vibration.

Firstly, the structural performance of the approach slab is investigated. Based on a parametric study, a correlation among the slab parameters, deflections, internal moments, and the differential settlements has been established. The predicted moments make it much easier to design the approach slab considering different levels of embankment settlements. While flat approach slab may be used for some short span applications, large span length would require a very thick slab. In such case, ribbed approach slabs are proposed, providing advantages over flat slabs. Based on finite element analysis, internal forces and deformations of ribbed slabs have been predicted and their designs are conducted.

Secondly, a fully computerized vehicle-bridge coupled model has been developed to analyze the effect of approach slab deformation on bridges' dynamic response induced by moving vehicles. With this model, the dynamic performance of vehicles and bridges under different road conditions (including approach slab deformation) can be obtained for different numbers and types of vehicles, and different types of bridges. A parametric study reveals that the deformation at the approach span causes significant dynamic responses in short span bridges. AASHTO specifications may underestimate the impact factors for short bridges with uneven joints at the bridge ends.

Finally, this study investigated the possibility of using tuned mass damper (TMD) to suppress the vehicle-induced bridge vibration under the condition of uneven bridge expansion joints.

CHAPTER 1 INTRODUCTION

This dissertation consists of eight chapters based on papers that have been published, or are under review, or are to be submitted to peer-reviewed journals. It uses the technical paper format approved by the Graduate School, which is intended to facilitate and encourage technical publications. Therefore, each chapter is relatively independent. For this reason, some essential information may be repeated in some chapters for the completeness of each chapter. This introductory chapter gives a general background on the present research. More detailed information can be found in each individual chapter.

1.1 Structural Performance of Approach Slab

Bridge approaches are normally constructed with reinforced concrete slabs that connect the bridge deck with the adjacent paved roadway. Their main function is to provide a smooth transition between the bridge deck and the roadway pavement. However, complaints about the ride quality of bridge approach slabs still need to be resolved. These complaints usually involve a "bump" that motorists feel when they approach or leave bridges. Field observations indicate that either faulting near the slab and the pavement joint or a sudden change in the slope grade of the approach slab (as shown in Fig. 1-1) causes this "bump". The faulting and change of slope are partly due to the bending of the slab as the embankment settles (LQI 2002).

Concrete approach slabs can lose their contacts and supports from soil for various reasons. The major reason is the settlement of embankment soil on which the slabs are built (Fig. 1-1). When settlement occurs, the slabs will bend in a concave manner that causes a sudden change in the slope grade of the approach slab. Load and the self-weight of the slab will also be redistributed to the ends of the slab and results in vertical faulting or bump across the roadway. Eventually, the rideability of the bridge approach slabs will deteriorate.

Several comprehensive studies on the performance of approach slabs have been sponsored over the years by various state DOTs. Stewart (1985) identified the original ground subsidence and fill settlement as primary causes of approach maintenance problems. Kramer and Sajer (1991) summarized findings from various state DOTs and recommended guidelines for the use and construction of approach slabs. Mahmood (1990) indicated that the type of abutment affects the magnitude of approach settlement and thus recommended the use of various ground improvement techniques, including wick drains and surcharging, to mitigate the soil settlement. The use of lightweight fill materials was also proposed as a means of reducing the vertical loading exerted on the soil. Chini et al. (1992) summarized critical items in the design and construction of bridge approaches. Their recommendations included removal and replacement of compressible foundation soils, dynamic compaction, surcharging, use of selected borrow fill materials, and minimum compaction requirements of 95% of the Standard Proctor, along with increased construction inspections. An NCHRP synthesis report on the settlement of approach slabs (Briaud et al. 1997) recommended more stringent requirements for fill material specifications and inspection practice. The study concluded that good cooperation among geotechnical, structural, pavement, construction, and maintenance engineers reduces reported incidences of excessive approach settlement. Wahls (1990) summarized that the performance of a bridge approach is affected by the design and construction of the bridge abutment and

foundation. According to Wahls' study, causes of bridge-approach settlements are one or more of the following: time-dependent consolidation of the embankment foundation, time-dependent consolidation of approach embankment, poor compaction of abutment backfill caused by restricted access of standard compaction equipment, erosion of soil at the abutment face and poor drainage of the embankment and abutment backfill. Hence, the approach slab design and the type of abutment and foundation affect the performance of the approach slab. The differential settlement can be minimized by the sequence of construction of the embankment, approach pavement, abutment, and superstructure. The design of approach slab may minimize the effects of the embankment settlement on the performance of the bridge-approach system. Other researches have been carried out by different investigators (Stark et al. 1995; Tadros and Benak 1989; Zaman et al. 1991; Hoppe 1999; Ha et al. 2003; Seo et at. 2003).

In summary, the majority of previous research can be categorized as (1) syntheses of practice, (2) identification of the sources of differential settlement, and (3) soil improvement. Numerical studies on approach slab and embankment settlement interaction have been rare. There are no guidelines in the AASHTO code specifications regarding the structural design of approach slabs considering the differential settlement (AASHTO 2002; AASHTO 2004). The LaDOTD (2002) design manual specifies minimum reinforcement requirements without specifications on how to conduct the structural design. Therefore, there is a need to establish design alternatives with construction guidelines to mitigate this problem.

Although the bump-related problems have been commonly recognized and the causes identified, no unified engineering solutions have emerged, primarily because of the number and complexity of the factors involved. One scope of this research is to establish correlations of the approach slab's faulting and deflection with approach embankment settlement and to help design engineers develop a solution to resolve the stated problem. This feasible solution allows the approach slabs strong enough to lose a portion of their contact supports without detrimental deflection. In this solution, the flexural rigidity (EI) of the approach slabs will be enhanced by increasing the moment of inertia at the slab's cross sections, therefore, allowing some embankment settlement without a decrease in ride quality. This solution requires a thorough understanding on the interaction among bridge approach slab, bridge abutment, and underneath embankment settlement.

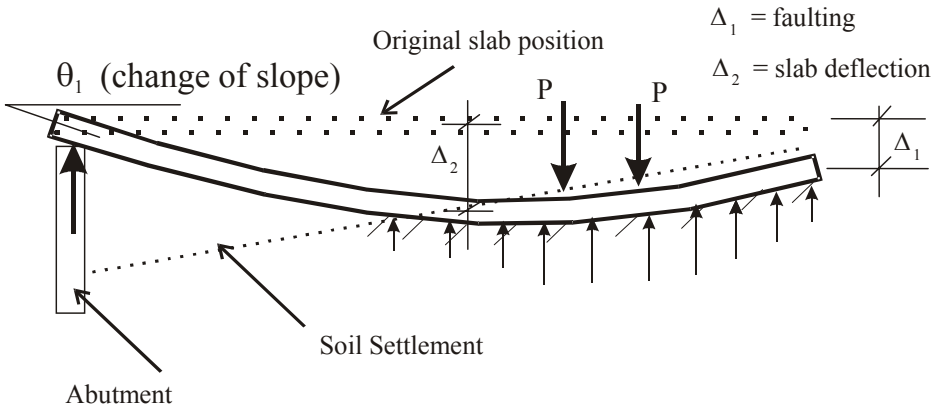

Fig. 1-1 Illustration of approach slab and its interaction with soil

1.2 Vehicle-Induced Bridge Dynamic Response

As a vehicle passes over a bridge, it acts as an oscillator as well as a time variant force on the bridge. Small irregularities of the bridge's surface might induce excitation to the vehicle, which in turn can generate dynamic loads that may be far more significant than the static loads. Vibration in bridges can amplify the propagation of existing cracks resulting in further damage to the bridge. This reduces bridge's life and renders the structure unsafe for driving. Over the years there has been interest in modeling the interaction between bridge and vehicles to predict the dynamic response of this complex system.

In early studies, it was generally accepted to model vehicles by using relatively simple-moving force (Frayba 1973; Hino et al. 1984; Lin and Trethewey 1990), moving mass (Blejwas et al. 1979), and moving single degree of freedom (SDOF) oscillator-models (Pesterev et al. 2002). A moving-force model was used when the inertia of the vehicle was small compared to that of the bridge, whereas a moving-mass model was used instead when the inertia of the vehicle could not be ignored. These two models, although, in some cases, capable of providing the designer with reasonable approximate solutions, neglect the dynamics of the moving vehicle and are not applicable to the case of uneven bridge surface, which is known to be the main cause of high-magnitude bridge vibrations. The SDOF oscillator model is free of these drawbacks. However, it fails to take into account the fact that a real vehicle moving along an uneven surface produces contact forces in a wide frequency range. With the increase in the proportion of heavy vehicles and high-speed vehicles in highway traffic, more complicated and real vehicle model, such as quarter-car model and half-car model (Todd and Kulakowski, 1991), should be adopted in the model of bridge-vehicle coupled system for more accurate results. The vehicle model used in this study is a so-called 3-D suspension model (or full truck model) that includes both primary and secondary vehicle suspension systems. It is the most realistic model because it incorporates pitching, rotating, and yawing motions of the vehicle and the variation of the axle force on the tires of each axle (Wang et al. 1991; Chatterjee et al. 1994; Liu et al 2001; Xu and Guo 2004).

In a bridge-vehicle coupled model, the interaction between the bridge and vehicle is the key part because, as the vehicle moves over the bridge, the bridge and vehicle contact point changes. Among most previous researches, the contact condition is considered through iteration, in which the displacements at the contact points are assumed first (Green and Cebon 1994; Yener and Chompooming 1994; Yang an Lin 1995); the interacting forces between the vehicle tires and bridge are then calculated by solving the equations of motion of the vehicle. These forces are in turn used in the motion equations of bridge to obtain the displacements of the contact points. In this method, the dynamic property matrices in equations of motion remain constant, and it does not consider the separation of the vehicle tire from the bridge due to large irregularities of the bridge surface. Moreover, the convergence rate of the iteration is likely to be slow especially when the bridge is subjected to a series of vehicles in motion, for the condition when there are too many contact points. The approach employed in this research to treat the interaction uses the direct integration method by updating the characteristic matrices according to the position of the contact points at each time step. The equations of motion of coupled vehicle-bridge system are solved at each time step without any iteration. The major disadvantage using this approach is that the equations of motion of the coupled system are time dependent and at each times step the equations of motion should be modified.

The present study developed a fully computerized approach to simulate the interaction of a coupled vehicle-bridge system. The road surface condition, including the approach slab deformation condition, is also taken into consideration in the analysis. The time history of dynamic response, such as displacement and acceleration, of both bridge and vehicle can be obtained. The developed program can handle more realistic models of bridges under various types of moving vehicles. It can be used to analyze not only the bridge-vehicle interaction, but also the interaction of vehicle and other infrastructures such as pavement.

1.3 Effect of Approach Slab Condition on Bridge-Vehicle Interaction

Theoretical and experimental investigations indicate that the vehicle impact to a bridge depends on many factors including: (1) the type of bridge and its natural frequencies of vibration, (2) vehicle characteristics, (3) the driving speed of the vehicle, and (4) the profiles of the approach roadway and bridge deck (Huang et al. 1992).

Among these factors, the vehicle initial condition is an important one that affects the dynamic responses of both the bridge and vehicles (Li 1996). Field observations revealed that either faulting near the slab and the pavement joint or a sudden change in the slope grade of the approach slab (as shown in Fig. 1-1) causes vehicle bumping at the joint of bridge deck and approach slab. Such bump causes the initial excitation in vehicle. Therefore, vehicle initial condition is affected not only by the road roughness of the roadway that the vehicle traveled before it enters the bridge, but also by uneven approach span conditions upon entrance to the bridge. Repeated traffic vehicles can, in turn, deteriorate the expansion joint that connects the approach slab and bridge deck. Consequently, this initial excitation of the vehicle, which is received before it reaches the bridge causes extra impact load on the bridge and affects the dynamic responses of both the bridge and the vehicle.

In previous researches, the bridge dynamic performance caused by road roughness has been excessively investigated (e.g. Green and Cebon 1994; Chompooming and Yener 1995; Kim and Nowak 1997; Wang and Liu 2000). However, these studies did not consider how the approach span condition influences the bridge-vehicle dynamic interaction, probably because most of these studies were concerned about the medium to long span bridges, upon which the effect of approach span condition may not be significant. But for short slab bridges it is worthwhile to analyze in detail the possible effect of approach span conditions on the bridge dynamic response. The present research regarding this problem is to analyze the possible effect of the approach span deformation on the dynamic behavior of short bridges caused by heavy vehicles moving across the bridge. Based on the vehicle-bridge coupled model developed in this research, the effect of approach span deformation on slab bridges and slab-on-girder bridges is investigated in details.

1.4 Suppression of Vehicle-Induced Bridge Vibration by Using Tuned Mass Damper

The importance of bridge vibrations induced by moving vehicles, which act as oscillators on a bridge as well as time variant forces, has long been recognized. This vibration can amplify the propagation of existing cracks resulting in further damage to the bridge. It has become one of the causes of reduction in long-term serviceability of the bridge, although major bridge failures are not usually caused directly by moving vehicles. It is also a critical factor to bridge's structure

fatigue and rapid deterioration (Manning 1981; Cebon, 1989; Chan and O'Connor 1989; Sammartino et al. 1999). Extensive researches (e.g., Cantieni 1984; Cheung et al. 1999; Bruni et al. 2003), including both experimental and theoretical works, have been conducted to determine the dynamic behavior of bridges under moving vehicles. The results have shown significant dynamic response exceeding expectation on certain small and medium span bridges (Huang et al. 1993; Hwang and Nowak 1991; Wang et al 1993; Li 1994; Billing 1984; O'Connor and Pritchard 1985).

One method of reducing the vibration of structures is to add an energy dissipative system to the primary structure to control the dynamic response. The tuned mass damper (TMD), which is a secondary vibration system connected to the primary structure at suitable points, is a classical device to dissipate a substantial amount of vibration energy of the main structure. A typical TMD generally consists of a mass, a spring, and a dashpot. Since Den Hartog firstly investigated the optimum values of TMD parameters using a two-degree of freedom model in 1950s, TMDs have been extensively studied and applied to suppress vibrations of buildings and bridges. They have been successfully used in some buildings and bridges for wind or seismic loads induced vibration such as Citicorp Center in New York, John Hancock tower in Boston, and the Normandy Bridge in France. Although excessive studies (e.g. Chen and Cai 2004; Chen and Kareem 2003; Jo et al. 2001) have been conducted on TMDs for wind and seismic loads induced structural vibration control, little research has been conducted on applying TMDs to control vehicle-induced bridge vibration (Li et al. 2005). Since, the vehicle-induced vibration is more critical to bridges with medium to small span lengths, it is worthwhile to investigate the possibility of applying TMDs on these bridges.

Therefore, another objective of this research is to study the possible effectiveness of TMDs for suppressing vibration of bridges under vehicle loads. In order to achieve this objective, a general formulation of the vehicle-induced bridge vibration controlled with a TMD system is developed, which takes into account the road surface conditions. Then, a comprehensive investigation is made to investigate the efficiency of the TMD for suppressing vibrations of different bridges under different traffic patterns. Such a study is helpful in evaluating the control performance before real control devices are designed in practice. These analytical results will also be useful in carrying out further studies for control strategies suppressing the vehicle-induced bridge vibration.

1.5 Organization of Dissertation

The main objective of this study is to analyze the performance of approach slab and the effect of its deformation on vehicle-induced bridge dynamic response. For this purpose, numerical modeling and field test are conducted. The following is a brief summary of the contents in each chapter.

Chapter 2 presents the strategies and results from a 3-D finite element analysis that investigates the flat approach slab performance under a given embankment settlement. It also shows how finite element procedures can help design approach slabs in this case. Parametric studies are conducted to establish the correlations of the faulting and deflection of the approach slab with approach embankment settlement and the approach slab parameters (length and

flexural rigidity). These results can be used to check the structural design of the approach slab currently used, and will eventually be used to systematically evaluate the effectiveness of approach slabs and to develop guidelines for their structural design. The established design aids will be used to predict deformation of approach slabs, such as Δ_1, Δ_2, θ_1 in Fig. 1-1.

Based on a 3-D finite element analysis, Chapter 3 analyzes systematically the structural performance of ribbed approach slabs with a span length of 60 ft as an example and to understand the interaction between ribbed approach slabs and embankment settlement. The results obtained are very useful for a proper design, which will help mitigate the slab rideability (and structural safety) problems. In this chapter, a feasible solution (ribbed approach slab) is proposed to replace the current PSAS (pile-supported approach slabs) that calls for 120 ft in length. By increasing the flexural rigidity (EI) of the approach slabs, the proposed new construction method will allow approach slabs strong enough to lose a portion of their contact supports without detrimental deflection.

To analyze the effect of approach slab deformation on vehicle-induced dynamic response of bridges, an analytical frame work of bridge-vehicle coupled system, which takes into account the road surface condition including the approach slab deformation, is developed in Chapter 4. A MATLAB program is developed to assemble the motion equations of vehicle-bridge coupled system and to solve the equations using the direct integration method. The predicted approach slab deformation obtained from Chapters 2 and 3 is used as an input to this model. The developed program can handle more realistic models of bridges under various types of moving vehicles. It can also be used to analyze not only the bridge-vehicle interaction, but also the interaction between vehicle and other infrastructures such as pavement. A case study of a pavement with an AASHTO HS20-44 truck demonstrates that the fully computerized method and the associated computer program provide an efficient and convenient tool for studying the interaction problems of infrastructures with various types of vehicles.

By using the model developed in Chapter 4, Chapter 5 investigates dynamic behavior of short slab bridges with different span lengths induced by the AASHTO HS20 truck. A parametric study is conducted to analyze the effects of different truck speeds and different road surface conditions. The approach span condition that consists of faulting at the ends and deformation along the span is considered in the analysis. While the effect of the along-span deformation on the dynamic response of bridges is trivial, the faulting condition of the approach span is found to cause significantly larger dynamic responses in short span slab bridges.

Chapter 6 analyzes the possible effect of the approach span deformation on the dynamic behavior of slab-on-girder bridges caused by heavy vehicles moving across. The bridge-vehicle coupled model is validated using experimental results obtained in static and dynamic full bridge test. Using this validated model, four multi-girder bridges with different span length are analyzed under different road surface condition. The influence of approach span conditions is investigated. The distribution of impact factors and load distribution factors in different girders are also analyzed and are compared with values specified in current AASHTO codes.

In order to study the possible usage of TMDs for suppressing vibration of bridges under vehicle loads, Chapter 7 develops a general formulation of the vehicle-induced bridge vibration

controlled with a TMD system. It takes into account the road surface conditions. Then, a comprehensive investigation is made to investigate the efficiency of the TMD for suppressing vibrations of different bridges under different vehicle load patterns. Such study is helpful in evaluating the control performance before real control devices are designed in practice. These analytical results will also be useful in carrying out further studies of control strategies in order to suppress the vehicle-induced bridge vibration.

Finally, Chapter 8 summarizes the research done in this dissertation and recommends possible future research. A discussion of a few issues raised by DOTD engineers are added in the appendix.

1.6 References

American Association of State Highway and Transportation Officials (AASHTO). (2004). *LRFD bridge design specifications*, Washington, D.C.

American Association of State Highway and Transportation Officials (AASHTO). (2002). *Standard specifications for highway bridges*, Washington, DC.

Billing, J.R. (1984). "Dynamic loading and testing of bridges in Ontario." *Canadian Journal of Civil Engineering*, Vol. 11, 833-843.

Blejwas, T. E., Feng, C. C., and Ayre, R. S. (1979). "Dynamic interaction of moving vehicles and structures." Journal of Sound and Vibration, Vol. 67, 513-521.

Briaud, J. L., James, R. W., and Hoffman, S. B. (1997). "Settlement of bridge approaches (the bump at the end of the bridge)." *NCHRP Synthesis 234*, Transportation Research Board, National Research Council, Washington, D.C.

Bruni, S., Bocciolone, M., and Beretta, S. (2003). "Simulation of bridge-heavy road vehicle interaction and assessment of structure durability." *Journal of Heavy Vehicle System*, Vol. 10, No. 1-2, 70-85.

Cantieni, R. (1984). "Dynamic load testing of highway bridges." *J. of Transportation Research Record*, Vol. 2, 141-148.

Cebon, D. (1989). "Vehicle-generated road damage: a review." *Journal of Vehicle System Dynamics*, Vol. 18, No. 1-3, 107-150.

Chan, T.H.T., and O'Connor, C. (1989). "Wheel loads form highway bridge strains: Field studies." *Journal of Structural Engineering*, ASCE, Vol. 116, No. 7, 1751-1771.

Chatterjee, P.K., Datta, T. K., and Surana, C. S. (1994). "Vibration of continuous bridges under moving vehicles." *Journal of Sound and Vibration*, 169(5), 619-632.

Chen, S. R. and Cai, C. S**.** (2004). "Coupled Vibration Control with Tuned Mass Damper for Long-Span Bridges ", *Journal of Sound and Vibration,* Elsevier, 278(1-2), 449-459.

Chen, X. Z. and Kareem, A. (2003). "Efficacy of tuned mass dampers for bridge flutter control." *Journal of Structural Engineering*, 129(10), 1290-1300

Cheung, Y.K., Au, F.T.K., Zheng, D.Y., and Cheng, Y.S. (1999). "Vibration of multi-span non-uniform bridges under moving vehicles and trains by using modified beam vibration function." *Journal of Sound and Vibration*, Vol. 228, No. 3, 611-628.

Chini, S. A., Wolde-Tinsae, A.M., & Aggour, M.S. (1992). "Drainage and backfill provisions for approaches to bridges." Ph.D. Thesis. University of Maryland, College Park, Md.

Chompooming, K. and Yener, M. (1995). "The influence of roadway surface irregularities and vehicle deceleration on bridge dynamics using the method of lines." *Journal of Sound and Vibration*, Vol. 183, 567-589.

Frayba, L. (1973). *Vibration of Solids and Structures under Moving Loads*. Groningen, Noordhoff International Publishing.

Ha, H., Seo, J.B., and Briaud, J.L. (2003). "Investigation of settlement at bridge approach slab expansion joint: Survey and site investigations." *Rep. No. 4147-1*, to the Texas Department of Transportation, published by the Texas Transportation Institute, Texas A&M Univ. System, College Station, Tex.

Hino, J., Yoshimura, T., Konishi, K., and Ananthanarayana, N. (1984). "A finite element method prediction of the vibration of a bridge subjected to a moving vehicle load." *Journal of Sound and Vibration*, Vol. 96, 45-53.

Hoppe, E. J. (1999). "Guidelines for the use, design, and construction of bridge approach slabs." *Final Rep. No. VTRC 00-R4*, Virginia Transportation Research Council, Charlottesville, Va.

Huang, D.Z., Wang, T.L., and Shahawy, M. (1992). " Impact analysis of continuous multigirder bridges due to moving vehicles." *Journal of Structural Engineering*, ASCE, Vol. 118, No. 2, 3427-3443.

Huang, D.Z., Wang, T.L., and Shahawy, M. (1993). "Impact studies of multi-girder concrete bridges," *Journal of Structural Engineering*, 119(8), 2387-2402.

Hwang, E. S. and Nowak, A. S. (1991). "Sumulation of dynamic load for bridges." *Journal of Structural Engineering*, 117(5), 1413-1434.

Jo, B. W., Tae, G. H., and Lee, D. W. (2001). "Structural vibration of tuned mass damper-installed three-span steel box bridge." *International Journal of Pressure Vessels and Piping*, 78(10), 667-675

Karoumi, R. (2000). "Modeling of cable-stayed bridges for analysis of traffic induced vibrations." *Proceedings of the International Modal Analysis Conference – IMAC,* v 1, p 842-848

Kramer, S.L., & Sajer, P. (1991). "Bridge approach slab effectiveness." Washington State Transportation Center, Seattle.

Kim, S. and Nowak, A.S. (1997). "Load distribution and impact factors for I-girder bridges." *Journal of Bridge Engineering.* 2(3), 97-104.

Louisiana Department of Transportation and Development (LaDOTD). (2002). *Bridge design metric manual*, Baton Rouge, LA.

Li, C.Y. and Fafitis, A. (1994). "Study of bridge vibration due to moving vehicles." American Society of Mechanical Engineers, Petroleum Division (Publication) PD, Vol. 64, No. 7, *Structural Dynamics and Vibrations*, 59-66.

Li, C.Y. (1996). "Bridge vibration and impact under moving vehicles." *Proceedings of the 1996 3rd Joint Conference on Engineering Systems Design and Analysis, ESDA*. Jul 1-4 1996*,* Montpellier, v 81, n 9, p 17-23.

Li, J. Z., Su, M. B., and Fan, L. C. (2005). "Vibration control of railway bridges under high-speed trains using multiple tuned mass dampers." *Journal of Bridge Engineering*, 10(3), 312-320

Lin, Y.H. and Trethewey, M.W. (1990). "Finite element analysis of elastic beams subjected to moving dynamic loads." *Journal of Sound and Vibration*, Vol. 136, 323-342.

Liu, C.H., Wang, T.L., and Huang, D.Z. (2001). "Impact study of multi-girder bridge based on correlated road roughness." *Journal of Structural Engineering and Mechanics*, Vol. 11, No. 3, 259-272.

Louisiana Quality Initiative (LQI). (2002). *Preservation of bridge approach ride ability*, Baton Rouge, LA.

Mahmood, I. U. (1990). "Evaluation of causes of bridge approach settlement and development of settlement prediction models." Ph.D. Thesis, University of Oklahoma, Norman, Okla.

Manning, D.G. (1981). Effects of traffic-induced vibrations on bridge-deck repairs. Washington, D.C. : Transportation Research Board, National Research Council.

O'Connor, C., and Pritchard, R.W. (1985). "Impact studies on small composite girder bridge." *Journal of Structural Engineering*, ASCE, Vol. 111, No. 3, 641-653.

Pesterev, A.V., Bergman, L.A., and Tan, C.A., (2002). "Pothole-induced contact forces in a simple vehicle model." *Journal of Sound and Vibration*, Vol. 256, No. 3, 565-572.

Sammartino, G., Amirouche, F., Chen, Z. L., and Wang, M. L. (1999). "Effects of heavy vehicle speeds on the structure and vibration of bridges." *American Society of Mechanical Engineers, Design Engineering Division (Publication) DE*, v 101, 139-147.

Seo, J. B., Ha, H., and Briaud, J. L. (2003). ."Investigation of settlement at bridge approach slab expansion joint: Numerical simulations and model tests," *Rep. No. 4147-2*, to the Texas Department of Transportation, published by the Texas Transportation Institute, Texas A&M Univ. System, College Station, Tex.

Stark, T. D., Olson, S. M., & Long, J. H. (1995). "Differential movement at the embankment/structure interface: Mitigation and rehabilitation." *Rep. No. IAB-H1, FY 93*, Illinois Department of Transportation, Springfield, ILL.

Stewart, C.F. (1985). "Highway structure approaches." California Department of Transportation, Sacramento, Calif.

Tadros, M. K., & Benak, J. V. (1989). "Bridge abutment and approach slab settlement (Phase1)." University of Nebraska, Lincoln, Neb.

Todd, K.B. and Kulakowski, B.T. (1991) "Simple computer models for predicting ride quality and pavement loading for heavy trucks", Transportation Research Record, n 1215, p 137-150.

Wahls, H. E. (1990) "Design and construction of bridge approaches." *Rep. No. NCHRP Synthesis 159*, Transportation Research Board, National Research Council, Washington, D.C.

Wang, T.L., Garg, V.K., and Chu, K.H. (1991). "Railway bridge/vehicle interaction studies with a new vehicle model." *Journal of Structural Engineering*, ASCE, Vol. 117, No. 7, 2099-2116.

Wang, T.L., Huang, D.Z., and Shahaway, M. (1992). "Dynamic response of multigirder bridges." *Journal of Structural Engineering*, ASCE, Vol. 118, No. 8, 2222-2238.

Wang, T.L., Huang, D.Z., and Shahawy, M. (1993), "Vibration and impact in multigirder steel bridges." *Transportation Research Record, Transportation Research Board* (TRB), National Research Council, Washington, D.C., No. 1393, Aug., 96-103.

Wang, T. L. and Liu, C.H. (2000). "Influence of Heavy Trucks on Highway Bridges," Rep. No. *FL/DOT/RMC/ 6672-379*, Florida Department of Transportation, Tallahassee, FL.

Xu, Y.L. and Guo, W.H. (2004). "Effects of bridge motion and crosswind on ride comfort of road vehicles**",** *Journal of Wind Engineering and Industrial Aerodynamics*, Vol. 92, No. 7-8, 641-662.

Yang, Y.B. and Lin B.H. (1995). "Vehicle-bridge interaction analysis by dynamic condensation method." *Journal of Structural Engineering*, Vol. 121, 1636-1643.

Yener, M. and Chompooming, K. (1994). "Numerical method of lines for analysis of vehicle-bridge dynamic interaction." *Journal of Computer and Structures*, Vol. 53, 709-726.

Zaman, M., Gopalasingam, A. and Laguros, J. G. (1991). "Consolidation settlement of bridge approach foundation", *J. of Geotech. Eng.,* 117(2) 219-239.

CHAPTER 2 EFFECT OF EMBANKMENT SETTLEMENT ON THE PERFORMANCE OF CONCRETE APPROACH SLABS*

2.1 Introduction

Bridge approaches in Louisiana are normally constructed with reinforced concrete slabs that connect the bridge deck with the adjacent paved roadway. Their function is to provide a smooth transition between the bridge deck and the roadway pavement. However, complaints about the ride quality of bridge approach slabs still need to be resolved. The complaints usually involve a "bump" that motorists feel when they approach or leave bridges. Field observations indicated that either faulting near the slab and the pavement joint or a sudden change in the slope grade of the approach slab causes this "bump." The faulting and change of slope are partly due to the bending of the slab as the embankment settles (LQI 2002).

Concrete approach slabs can lose their contacts and supports from soils due to various reasons. The major reason is the settlement of embankment soil on which the slabs are built. When settlement occurs, the slabs will bend in a concave manner that causes a sudden change in the slope grade of the approach slab. Load and the self-weight of the slab will also redistribute to the ends of the slab, resulting in vertical faulting or a bump across the roadway. Eventually, the rideability of the bridge approach slabs will deteriorate. Although the bump-related problems have been commonly recognized and the causes identified, no unified engineering solutions have emerged, primarily because of the number and complexity of the factors involved. Very seldom can the embankment settlement at bridge approaches be traced to a single cause. Typically, the embankment settlement reflects an accumulated effect of many factors such as subsoil conditions, materials, construction techniques, drainage provisions, and quality control methods during construction.

Several comprehensive studies on the performance of approach slabs have been sponsored over the years by various state DOTs. Stewart (1985) identified the original ground subsidence and fill settlement as primary causes of approach maintenance problems. Kramer and Sajer (1991) summarized findings from various state DOTs and recommended guidelines for the use and construction of approach slabs. Mahmood (1990) indicated that the type of abutment affects the magnitude of approach settlement and thus recommended the use of various ground improvement techniques, including wick drains and surcharging, to mitigate the soil settlement. The use of lightweight fill materials was also proposed as a means of reducing the vertical loading exerted on the soil. Chini et al. (1992) summarized critical items in the design and construction of bridge approaches. Their recommendations included removal and replacement of compressible foundation soils, dynamic compaction, surcharging, use of selected borrow fill materials, and minimum compaction requirements of 95% of the Standard Proctor, along with increased construction inspections. An NCHRP synthesis report on the settlement of approach slabs (Briaud et al. 1997) recommended more stringent requirements for fill material specifications and inspection practice. The study concluded that good cooperation among geotechnical, structural, pavement, construction, and maintenance engineers reduces reported incidences of excessive approach settlement. Other researches were also carried out by different

* Reprinted by permission of "Journal of Bridge Engineering"

investigators (Stark et al. 1995; Tadros and Benak 1989; Wahls 1990; Zaman et al. 1991; Hoppe 1999; Ha et al. 2003; Seo et at. 2003).

The majority of the previous researches can be categorized as (1) syntheses of practice, (2) identification of the sources of differential settlements, and (3) soil improvement. Numerical studies on approach slab and embankment settlement interaction have been rare. There are no guidelines in the AASHTO code specifications (AASHTO 1998, AASHTO 2002) regarding the structural design of approach slabs considering the effects of embankment settlements. Similarly, the Louisiana Department of Transportation and Development (LaDOTD) design manual (LaDOTD 2002) specifies minimum reinforcement requirements but provide no specifications for the structural design of the approach slabs.

2.2 Objective and Research Approach

LaDOTD has launched a major effort under the Louisiana Quality Initiative (LQI) program to solve the "bump" problems. This program involves structural, geotechnical, pavement construction, maintenance, and quality control engineers as well as university researchers, aiming to improve ride quality by changing the design of approach slabs where a differential settlement is expected. The objective is to find a feasible solution that allows the approach slabs to be strong enough to lose a portion of their contact supports without detrimental deflection. This solution requires a thorough understanding of the interaction between the bridge approach slab and the embankment settlement underneath.

One extreme case assumes that the slab fully contacts the embankment soil and that the slab's performance is the same as that of the concrete floors on the ground. This assumption is not realistic in many cases due to the embankment settlement discussed above, and it may result in an unconservative design. In the other extreme case, an approach slab can be designed as a simple beam spanning the bridge end and the pavement end, assuming no soil supports the beam between the two ends. This assumption, while conservative, will definitely result in an uneconomical design. In the majority of these cases, the slab is both partially separating from and partially contacting the soil. The spring supports provided to the concrete slab by the embankment soil will reduce the internal force in the slab. The extent of this support and reduction depends on the slab and soil interaction for a given embankment settlement.

This chapter presents the strategies and results from a 3-D finite element analysis that investigated the approach slab performance under a given embankment settlement. These results were used to check the structural design of the approach slab currently used by LaDOTD, and will eventually be used to systematically evaluate the effectiveness of approach slabs and to develop guidelines for their structural design. This information will also help determine when settlement controls are necessary for an economical approach slab design.

Length of a typical approach slab used in Louisiana (Fig. 1-1) is 6000 mm (20 ft.) or 12,000 mm (40 ft.) depending on whether it is a cut or filled embankment (LaDOTD 2002). Since the left end of the slab sits on the pile-supported abutment while the right end is on embankment soil, a differential movement occurs between the two ends of the slab, resulting in a gap between the slab and the embankment soil. The amplitude and distribution of soil

settlements can be very complicated and will be determined in another ongoing research project supported by the LaDOTD LQI program. Therefore, in the present finite element analysis, the embankment settlement was given and a linear settlement was assumed, as shown in Fig. 1-1. When the self-weight of the slab and live loads were applied, the slab deformed and interacted with the soil, resulting in partial contact of the slab with the soil, as seen in Fig. 1-1. The present research will provide essential information needed for the structural design of the approach slab considering embankment settlements.

2.3 Finite Element Modeling

Louisiana is currently using approach slabs with a length of either 6,096 mm (20 ft) or 12,195 mm (40 ft) depending on whether it is a cut or filled embankment (LaDOTD 2002). For the demonstration purposes of analysis, an approach slab with 12,195mm (40 ft.) in span length, 305 mm (12 in.) in thickness and the other dimensions shown in Fig. 2-1 was chosen with a 1,220mm (4 ft.) sleeper slab. A 3D finite element model was established, as shown in Fig. 2-3, where eight-node hexahedron elements (ANSYS© Solid 45) were used to form the finite element mesh. In addition to the dead load of the slab, two AASHTO (2002) HS20 truck loads were applied on the slab. The two HS20 truck loads were moved along the slab length to produce the worst loading scenario for the slab deflection and internal bending moments, the same way as in the bridge live load analysis. These predicted internal moments will provide information for the structural evaluation and design of the approach slabs by selecting appropriate slab reinforcement, section dimensions and length. The current LaDOTD Bridge Design Manual (LaDOTD 2002) does not require structural calculation in the approach slab design, and standard reinforcement is specified in the standard drawings, as shown in Fig. 2-2. Perhaps a simple yet reliable calculation method is not available for the routine design of approach slabs.

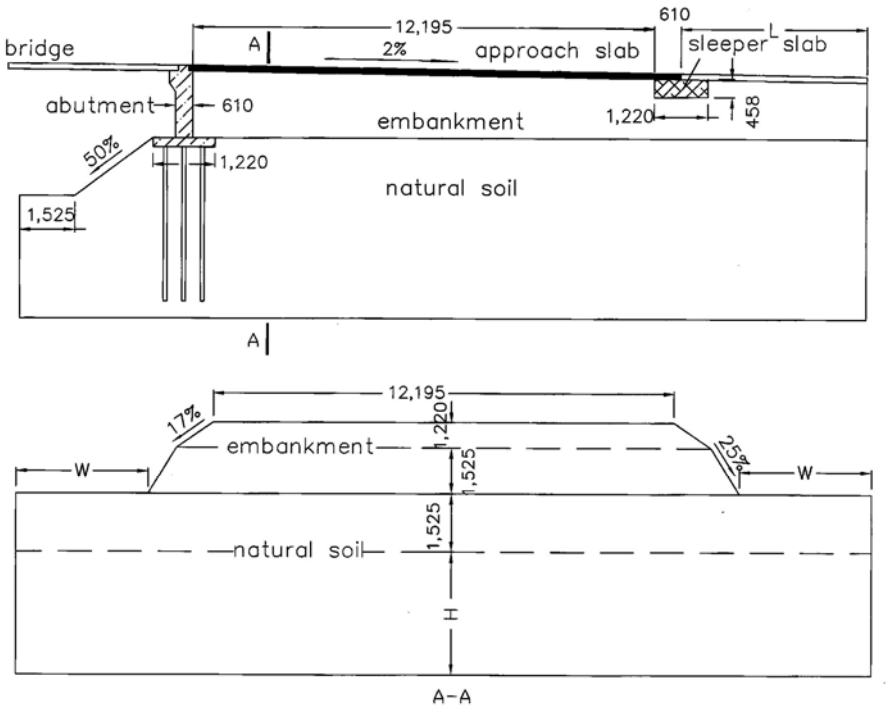

Fig. 2-1 Sketch of bridge abutment (unit: mm)

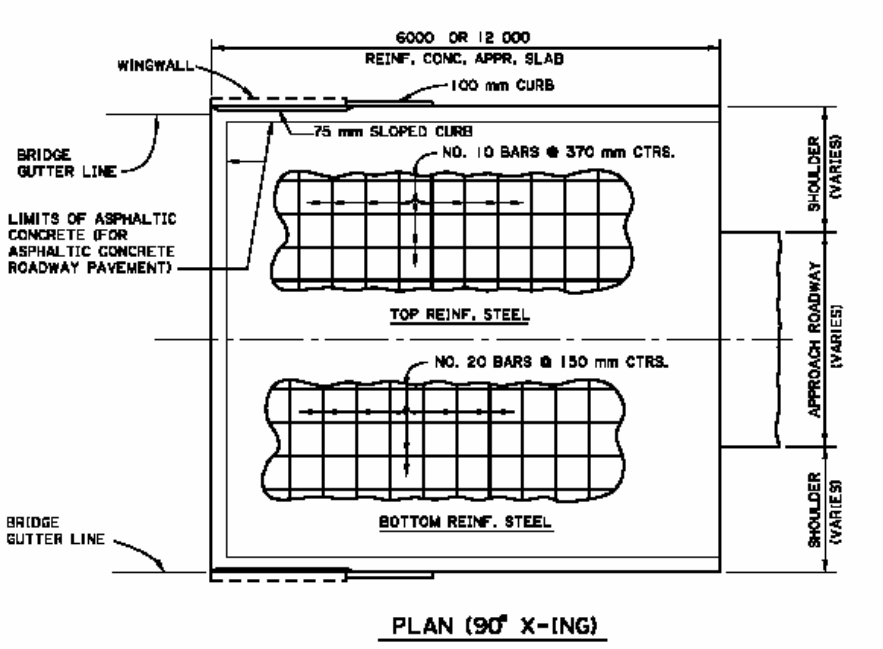

Fig. 2-2 Standard approach slab used in Louisiana

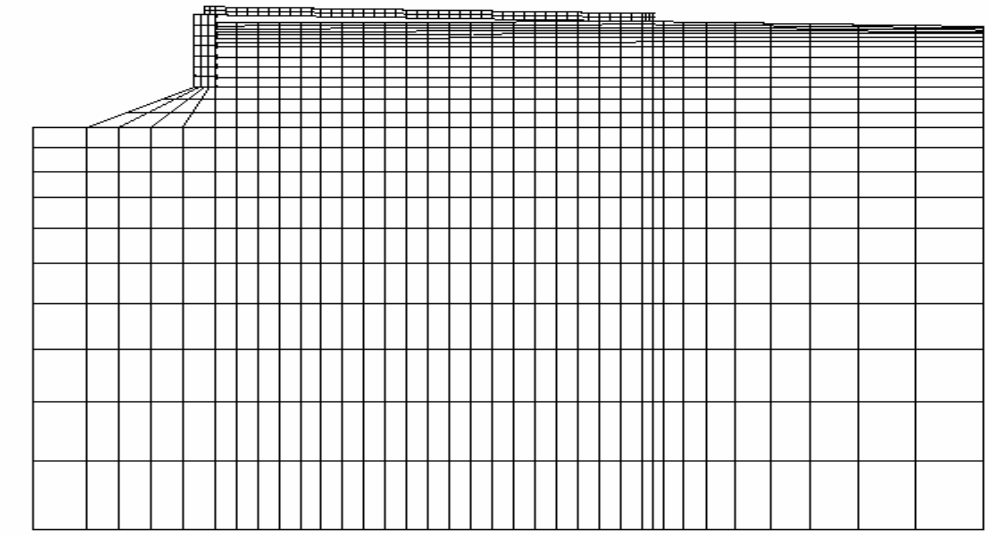

Fig. 2-3 Typical finite element mesh with 8 node cubic element

The soil profile under the approach slab consisted of compacted embankment and silty clay subgrade soil. A contact and target pair surface element available in the ANSYS© element library was used to simulate the interaction between the soil and the slab. This surface element is compressive only and can thus model the contacting and separating process between the slab and soil. When the soil is in tension, the slab and soil separate automatically. The Drucker-Prager model was used to define the yield criteria for both embankment soil and subgrade soil in the following form:

$$f(I_1, J_2) = \sqrt{J_2} - \alpha I_1 - \kappa = 0 \quad (2\text{-}1)$$

where α and κ are material constants which are related to the constants *c* and φ, the cohesion coefficient and internal friction angle, respectively, and can be determined from test results. Table 2-1 lists the material parameters used in the finite element analysis of the present study.

Table 2-1 Material parameters

	Elastic modulus E MPa (psi)	Poisson ratio μ	Cohesion c kPa (psi)	Friction angle φ(°)	Density γ kg/m³(pcf)
Embankment Soil	260 (37700)	0.3	80 (11.6)	30	2000 (127.4)
Natural Soil	30 (4360)	0.3	50 (7.25)	30	1500 (95.6)

2.4 Determination of Boundary Conditions

The soil underneath the approach span is theoretically semi-infinite. Sensitivity analysis was conducted to determine how far the boundaries, laterally, vertically, and longitudinally, should be included in the finite element model. Three parameters, W, L, and H shown in Fig. 2-1 were investigated in the sensitivity study as follows:
(1) W was varied from 1524, 3049, 4573, 6098, 7622, 9146, 13720 mm (5, 10, 15, 20, 25, 30, to 45 ft.) for the fixed L = 9146 mm (30 ft.) and H = 9146 mm (30 ft.);
(2) L was varied from, 3049, 6098, 9146, 12195, 15244, 36585 mm (10, 20, 30, 40, 50, to 120 ft.) for the fixed H = 9146 mm (30 ft.) and W = 7622 mm (25 ft.);
(3) H was varied from 1524, 3049, 6098, 9146, 10671, 12195, 15244, 18293, 30488, 60976 mm (5, 10, 20, 30, 35, 40, 50, 60, 100, to 200 ft.) for the fixed W = 7622 mm (25 ft.) and L = 9146 mm (30 ft.).

For each case, two truck loads (HS 20) on two lanes and the slab's self-weight were applied to the approach slab. In this sensitivity study, a 610 mm (2 ft.) differential settlement between the abutment and the approach slab was used to model the extreme case in which there are essentially no soil supports between the two ends.

The deflection of the approach slab and the vertical stress in the embankment soil under the sleeper slab for the three conditions are shown in Figs. 2-4 and 2-5. As shown in these figures, it is clear that *W* has insignificant effects on the results. When *L* is larger than 12,195 mm (40 ft.), it insignificantly affects the results of both the deflection and the soil stress. When *H* is larger than 15,244 mm (50 ft.), its effect on deflection reduces, but still makes some impact on the soil stress. From the above sensitivity analysis and considering the computational efficiency, the boundary conditions for the slab-soil interaction analysis were determined as: *W* = 4,573 mm (15 ft.); *L* = 12,195 mm (40 ft.); and *H* = 15,244 mm (50 ft.). It is noted that based on the Saint-Venant Principle, different settlement scenarios should not significantly affect this sensitivity study. Therefore, these boundary dimensions along with the slab and embankment dimensions are used in the analyses hereafter unless otherwise specified.

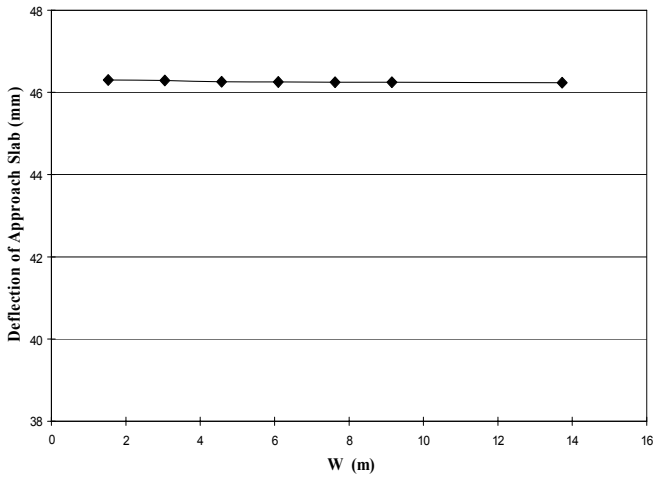

(a) Deflection versus W

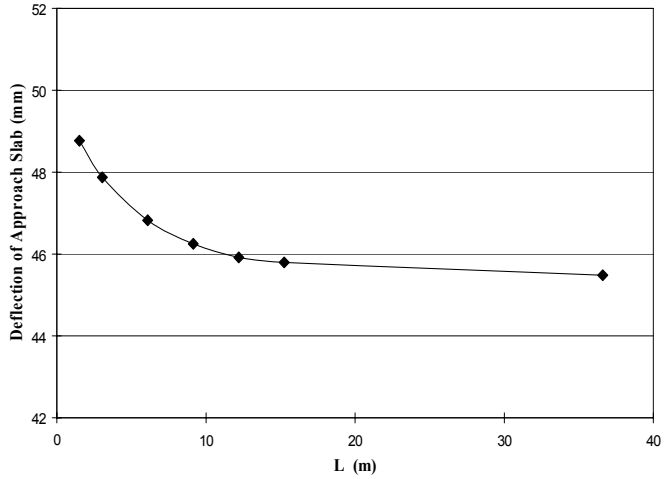

(b) Deflection versus L

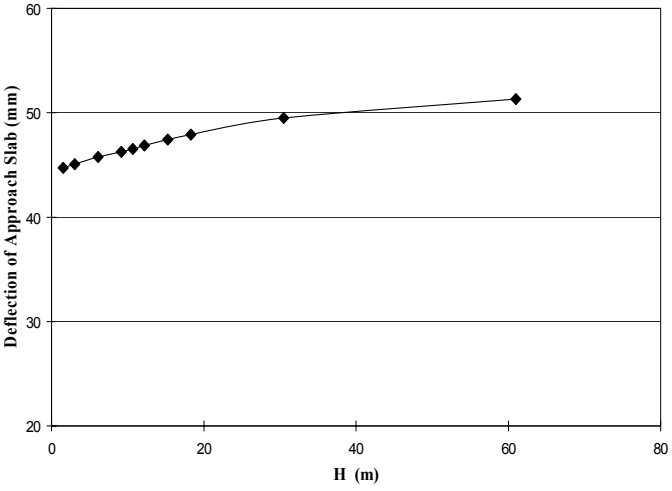

(c) Deflection versus H

Fig. 2-4 Effects of parameters on deflection of approach slab

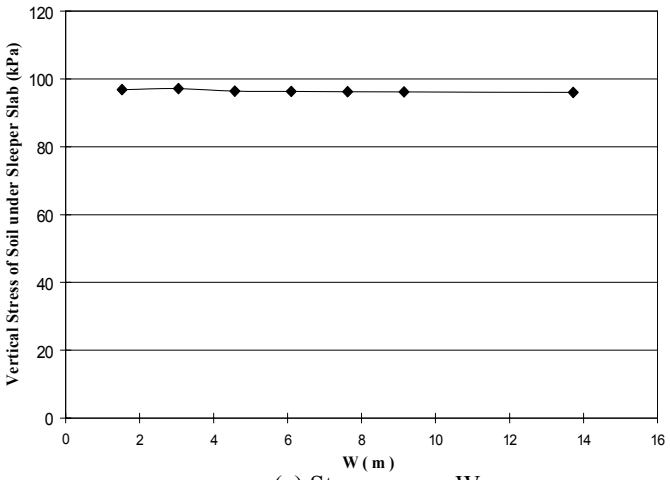

(a) Stress versus W

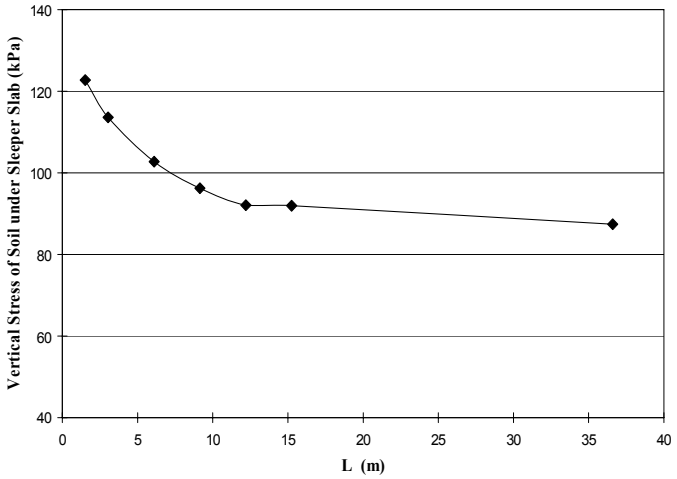

(b) Stress versus L

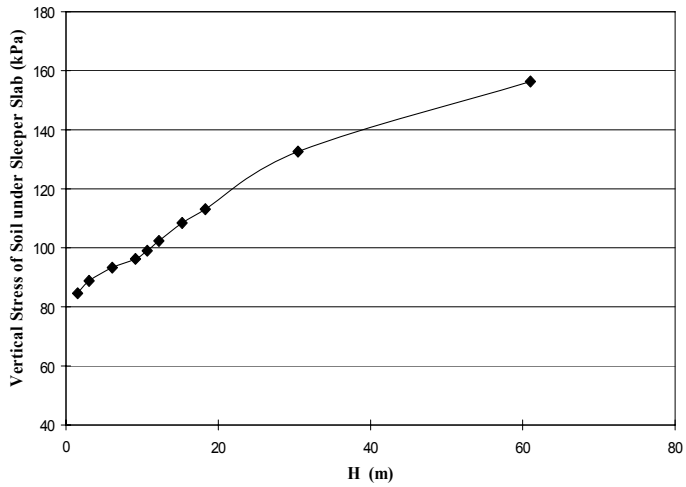

(c) Stress versus H

Fig. 2-5 Effects of parameters on vertical stress of soil

2.5 Effects of Embankment Settlements on Slab Performance

With the dimensions (i.e., boundaries) of the finite element model determined above, a parametric study was conducted to examine the mechanism of interaction between the embankment soils and the approach slab under different embankment settlements. The maximum deflections and internal moments of the approach slab under different settlements were obtained by moving the truck loads along the slab. In the finite element analysis for a given embankment settlement, the dead load (*DL*) was applied first; then the dead load and live loads (*DL+LL*) were applied together. The live load effects (*LL*) were then calculated from the total load effect minus the dead load effect, i.e., *(DL+LL)–DL*. This procedure was necessary since the loading sequence affects the contacting and separating process between the slab and the soil. Therefore, the live load could not be applied independently without including the dead load for a proper solution.

As shown in Figs. 2-6 and 2-7, the magnitude of the slab maximum deflections and internal moments increases with the increase of embankment settlements. When the differential settlement increases from 152 mm (6.0 inches) to a larger value, there is almost no change in the deflection and internal moment of the approach slab. This is because the settlement no longer affects the slab performance since the approach slab loses almost all contact with the soil and then performs as a simple beam. With L/800 as the live load deflection control that is typically used in bridge engineering, the allowable live load deflection will be 12,195 mm/800 = 15 mm (0.6 in.), which corresponds to an allowable embankment settlement of about 127 mm (5 in.) as shown in Fig. 2-6.

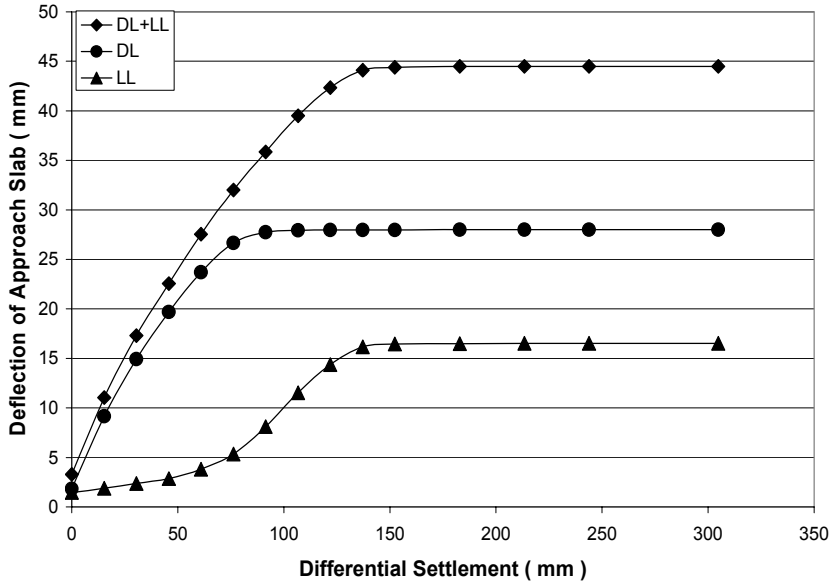

Fig. 2-6 Deflection of approach slab versus settlement
(slab length = 12,195 mm and thickness = 305 mm)

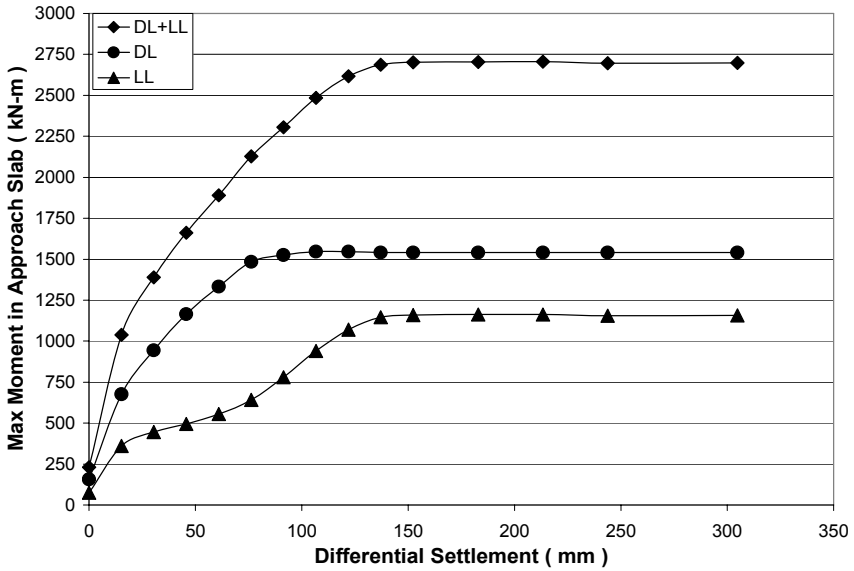

Fig. 2-7 Internal moment of approach slab versus settlement
(slab length = 12,195 mm and thickness = 305 mm)

Similarly, as shown in Fig. 2-8, the maximum vertical stress of the embankment soil under the sleeper slab continued to increase with the increase of the differential settlement. Since the slab lost more support from the soil as the settlement increased, a larger portion of the slab self-weight and truck loads was distributed to the sleeper slab and then to the soil under the sleeper slab. In comparison with the slab deflection and internal moments (Figs. 2-6 and 2-7), the stress in the soil kept increasing with a reduced rate even when the settlement exceeded 152 mm (6.0 in.). Even after the complete loss of contact between the slab and the soil, the increase in settlement changed the geometry of the soil around the sleeper slab so that the stress in the soil underneath the sleeper slab was slightly affected. A typical vertical stress distribution along the span in the soil under the approach slab and under the sleeper slab is shown in Fig. 2-9.

As discussed earlier, the differential settlement between the two ends of the approach slab formed a gap between the approach slab and the embankment. Due to the action of the truck loads and slab self-weight, the approach slab deformed downward and was supported by the embankment at the contacting points. Fig. 2-10 shows the assumed settlement lines of the embankment and the predicted deflection shape of the slab under different differential settlements. The figure clearly exhibits the contact area between the slab and the embankment near the sleeper slab and the gap near the abutment. As the settlement increased, the gap became deeper and longer, and the contact area decreased. If the settlement is large enough, the slab and embankment will have no contact, and the slab will lose the support from the embankment, except near the sleeper slab. Thus, the deflection and internal moment of the approach slab will not change with the increase of the embankment settlement as indicated in Figs. 2-6 to 2-7.

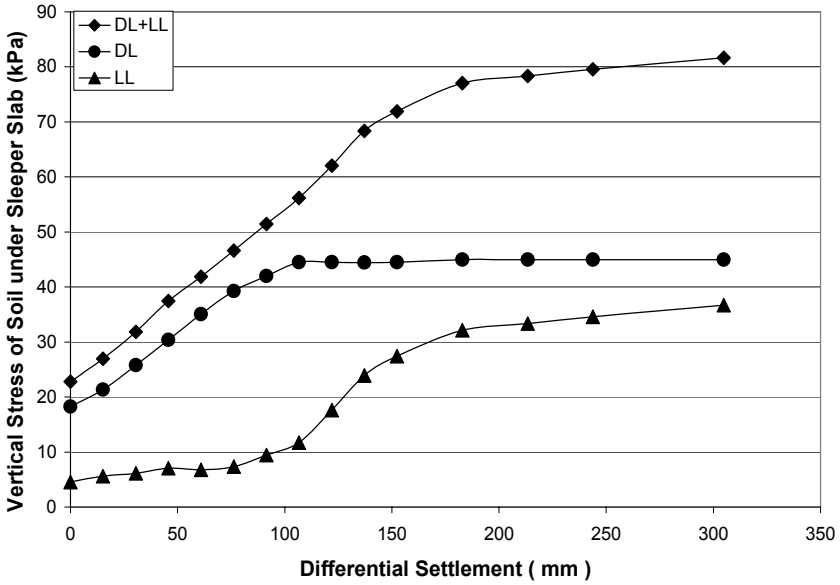

Fig. 2-8 Vertical stress of soil under sleeper slab versus settlement
(slab length = 12,195 mm and thickness = 305 mm)

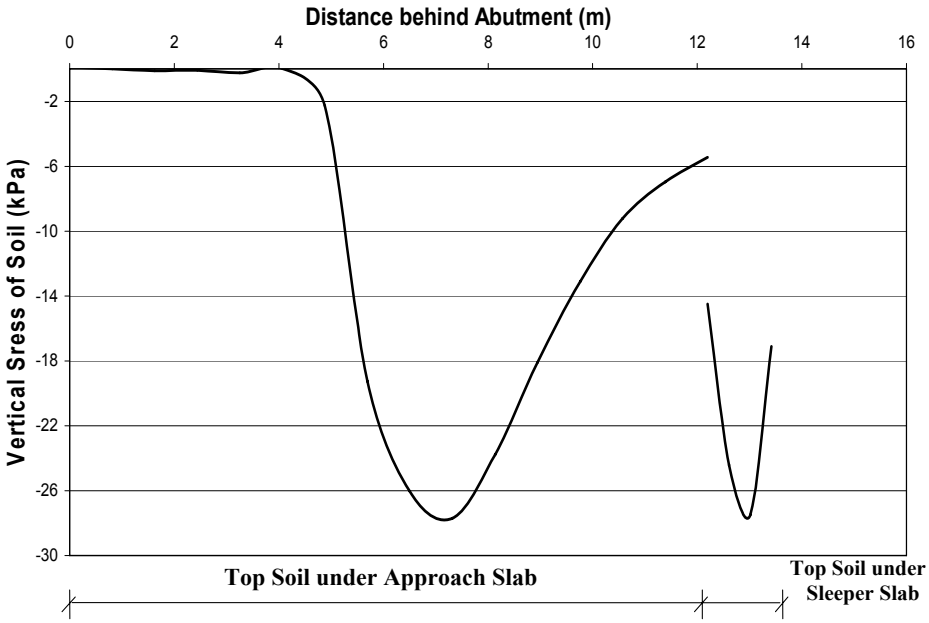

Fig. 2-9 Stress distribution in soil near interface
(slab length = 12,195 mm, thickness = 305 mm, settlement = 15 mm)

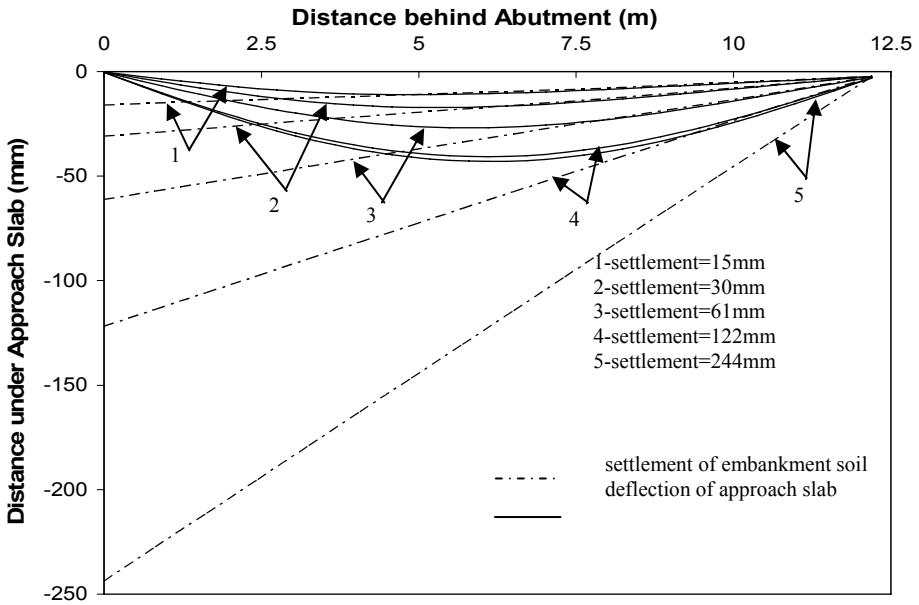

Fig. 2-10 Interface between approach slab and embankment soil
(slab length = 12,195 mm and thickness = 305 mm)

2.6 Effects of Embankment Settlements on Slab Design

Since the increase of the embankment settlement results in the separation of the slab from the soil and subsequent increase of the internal moment in the approach slab, the slab must be designed to provide enough strength for an expected embankment settlement. To this end, the results from the finite element analysis were used to evaluate the structural design of the approach slabs that are used by the LaDOTD. Currently, the LaDOTD standard drawing (LaDOTD 2002) calls for #20 @ 150 mm (#6@6") for the bottom reinforcement of the approach slab.

When the approach slab is subjected to bending, the stresses that are induced by the concentrated loads are not uniformly distributed over the whole width of the slab. If the width of the slab is large, only part of the slab is effective in resisting a given bending load. The non-uniform distribution of the stresses in the slab means that a simple beam theory cannot be applied for the slab analysis without some modifications. Therefore it is convenient, for design purposes, to consider a width for the slab (an effective width), which, if uniformly stressed, would represent the same amount of flexural resistance as the real slab. The effective width in slabs may be affected by the following parameters: (1) position of load, (2) ratio of the span length of the slab to its width, and (3) type of loading.

For the simply supported slab, the case of the two trucks applied at the mid-span was chosen as the basic loading type and a uniformly distributed dead load was considered. By moving the trucks along the transverse direction of the slab, the critical scenario was observed when the trucks move to one side of the slab. The effective width w_e is defined as:

$$w_e = \frac{\int_0^w \sigma_y dx}{\sigma_{y\max}} \tag{2-2}$$

where σ_y = bending stress in section, σ_{ymax} = maximum bending stress in section; and w = width of the slab.

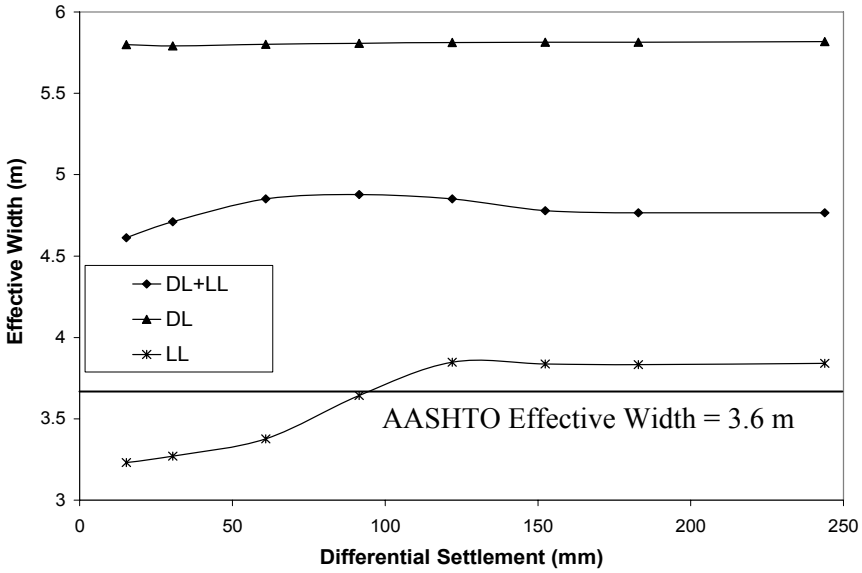

Fig. 2-11 Effective width of slab versus differential settlement
(slab length = 12,195 mm and thickness = 305 mm)

For an approach slab with the span length of 12,195 mm (40 ft.), width of 12,195 mm (40 ft.), and thickness of 305 mm (12 in.), the effective width, w_e, for the truck loads on the side of the slab were calculated by varying the differential settlement from 15 mm (0.6 in.) to 183 mm (7.2 in.). The effective width corresponding to one truck load is plotted in Fig. 2-11. As expected, the dead load is much more uniformly distributed across the bridge width and thus the effective width is larger than that of the live load. The effective width per truck was also determined to be 3,600 mm (11.8 ft.) per AASHTO code (1998), which is within the range of the prediction. Therefore, when no more accurate information is available, the effective width specified in the AASHTO specifications can be used. As shown in Fig. 2-11, when the differential settlement is small, then the predicted effective width for live loads is smaller than that specified in the codes, implying that using the code effective width is not conservative for design. However, small settlement is not the critical condition. For larger settlement (about 76 mm or 3 in. in this case), the code effective width is more conservative

Checking the strength of the approach slab was conducted according to the AASHTO Standard Specifications (AASHTO 2002), namely, with load factors of 1.3 for dead load, 2.17 for live load, and 1.3 for impact factor, and with an equivalent slab width of 3,600 mm. The results of the reinforcement design considering the effects of different differential settlements are shown in Table 2-2

Table 2-2 Design of approach slab

Settlement mm (in.)	M kN-m (ft.-kips) DL	LL	1.3DL +2.17(LL+IM)	ρ	ρ_{max}	A_s mm^2/mm ($in.^2/ft.$)	Reinforcement[2]
0 (0)	270.9 (195.8)	37.5 (27.1)	458.0 (331.0)	0.0050	0.0214	1.27 (0.60)	#16@150mm (#5@6.0")
15 (0.6)	423.7 (306.2)	180.6 (130.5)	1060.4 (766.3)	0.0125	0.0214	3.18 (1.50)	#19@90mm (#6@3.5")
30 (1.2)	466.3 (337.0)	222.7 (160.9)	1234.5 (892.1)	0.0149	0.0214	3.77 (1.78)	#22@100mm (#7@4.0")
46 (1.8)	498.2 (360.0)	244.9 (177.0)	1346.2 (972.8)	0.0165	0.0214	4.19 (1.98)	#25@110mm (#8@4.5")
61 (2.4)	510.1 (368.6)	277.6 (200.6)	1446.1 (1045.0)	0.0180	0.0214	4.57 (2.16)	#29@140mm (#9@5.5")
76 (3.0)	526.1 (380.2)	321.0 (232.0)	1589.7 (1148.8)	0.0202	0.0214	5.14 (2.43)	#32@150mm (#10@6.0")
91 (3.6)	526.1 (380.2)	389.3 (281.3)	1782.0 (1287.8)	0.0235	0.0214	NA[1]	NA
106.7 (4.2)	531.4 (384.0)	469.7 (339.4)	2015.8 (1456.7)	0.0280	0.0214	NA	NA
122 (4.8)	531.4 (384.0)	535.4 (386.9)	2201.1 (1590.6)	0.0321	0.0214	NA	NA
137 (5.4)	530.0 (383.0)	572.2 (413.5)	2303.2 (1664.4)	0.0347	0.0214	NA	NA
152 (6.0)	530.0 (383.0)	579.4 (418.7)	2323.5 (1679.1)	0.0353	0.0214	NA	NA
183 (7.2)	530.0 (383.0)	581.1 (419.9)	2328.2 (1682.5)	0.0354	0.0214	NA	NA
213 (8.4)	530.0 (383.0)	581.2 (420.0)	2328.5 (1682.7)	0.0354	0.0214	NA	NA
244 (9.6)	526.1 (380.2)	580.5 (419.5)	2321.3 (1677.5)	0.0352	0.0214	NA	NA
305 (12.0)	526.1 (380.2)	582.6 (421.0)	2327.5 (1682.0)	0.0354	0.0214	NA	NA

Note: (1) The required reinforcement ratio ρ exceeds the allowed maximum reinforcement of flexure, i.e., $\rho > \rho_{max} = 0.75\rho_b$, meaning that section dimension needs to be increased.
(2) Some rebar size listed in the table may not be practical for a slab with a thickness of 12 inches.

It is interesting to observe in Table 2-2 that when the settlement is zero, the required reinforcement at the bottom of slab is 1.27 mm^2/mm (0.6 $in.^2/ft.$) and it increases to 3.175 mm^2/mm (1.5 $in.^2/ft.$) when the settlement increases to 15 mm (0.6 in.). This indicates that the current design (LaDOTD 2002, Fig. 2-2), 1.86 mm^2/mm (0.88 $in.^2/ft.$), is good only for the case of zero settlement and is not adequate for a settlement larger than 15 mm (0.6 in.). When the embankment settlement increases, more reinforcement is required. When the settlement exceeds 76 mm (3.0 in.), then the required reinforcement ratio, ρ, will exceed the allowed maximum

reinforcement ratio, ρ_{max}, namely 75% of the balanced reinforcement ratio (AASHTO 2002). In this case, either the slab thickness should be increased or the soil should be improved to control the settlement within the allowable limit.

2.7 Development of Design Aids

A parametric study was conducted by changing the slab thickness and length to establish the relationship between the slab responses, parameters, and the corresponding differential settlements, which can be used in routine design. The slab parameters, length (L) and thickness (h), were investigated in the parametric study for the following cases: (1) h was varied from 305, 457, to 610 mm (1, 1.5, to 2 ft.) for the fixed L = 12,195 mm (40 ft.); and (2) h was varied from 457, 686, to 915 mm (1.5, 2.25, to 3 ft.) for the fixed L = 18,288 mm (60 ft.).

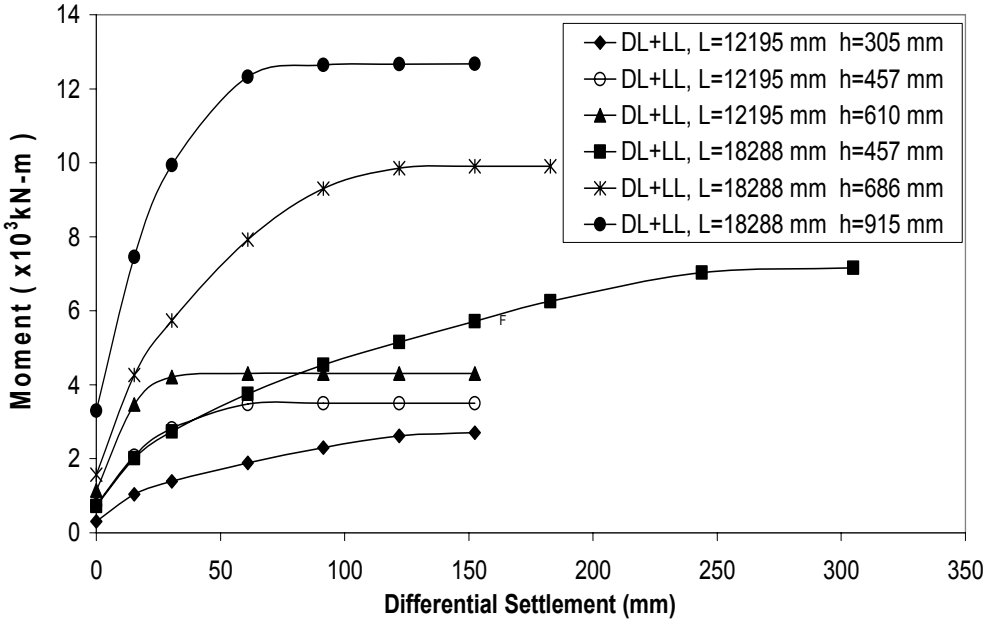

Fig. 2-12 Internal moment of approach slab versus differential settlement

As shown in Figs. 2-12 to 2-14, with the increase of embankment settlement, the magnitude of the maximum internal moments, deflections, and rotation angles in the slab increases to some constant values. For example, with L = 12,195 mm (40 ft.) and h = 305 mm (12 in.), when the settlement is increased from 152 mm (6.0 in.) to larger values, there is almost no change in the internal moment, deflection, and rotation angle since the approach slab has become a simply-supported beam. For the same differential settlement, with the increase of approach slab thickness (h), the deflection in the slab decreases. Smaller deflections of the approach slab reduce the contact area between the slab and embankment soil. As a result, the value of the differential settlement beyond which the settlement ceases to affect the slab behavior decreases.

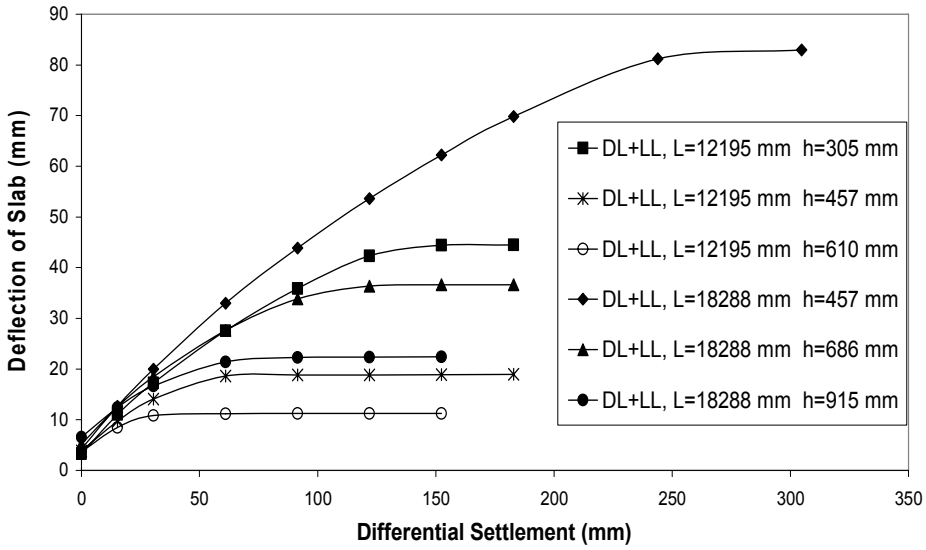

Fig. 2-13 Deflection of slab versus differential settlement

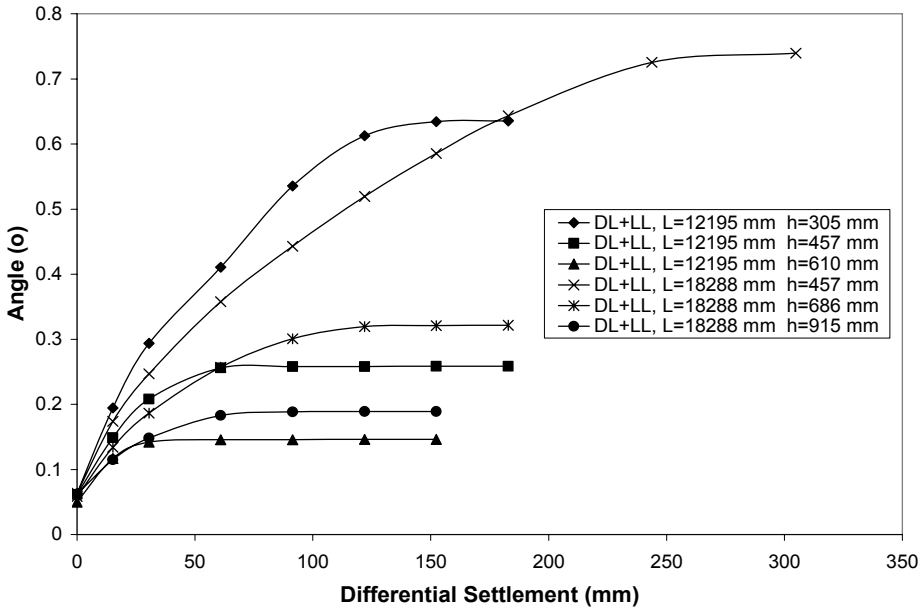

Fig. 2-14 Rotation angle of slab versus differential settlement

By analyzing the results from the finite element analysis, this study established a correlation among the slab parameters, deflection and angle of the slab, internal moment of the slab, and the differential settlement. The results were then normalized with respect to the traditional simply-supported (pin and roller supports) beams, i.e., without considering the contact between the slab and the soil, and without considering the settlement of the end supports. Engineers can conveniently obtain the slab response, such as deflections and moments, by multiplying the slab response of the simply-supported beam with a computed coefficient. These coefficients are developed next.

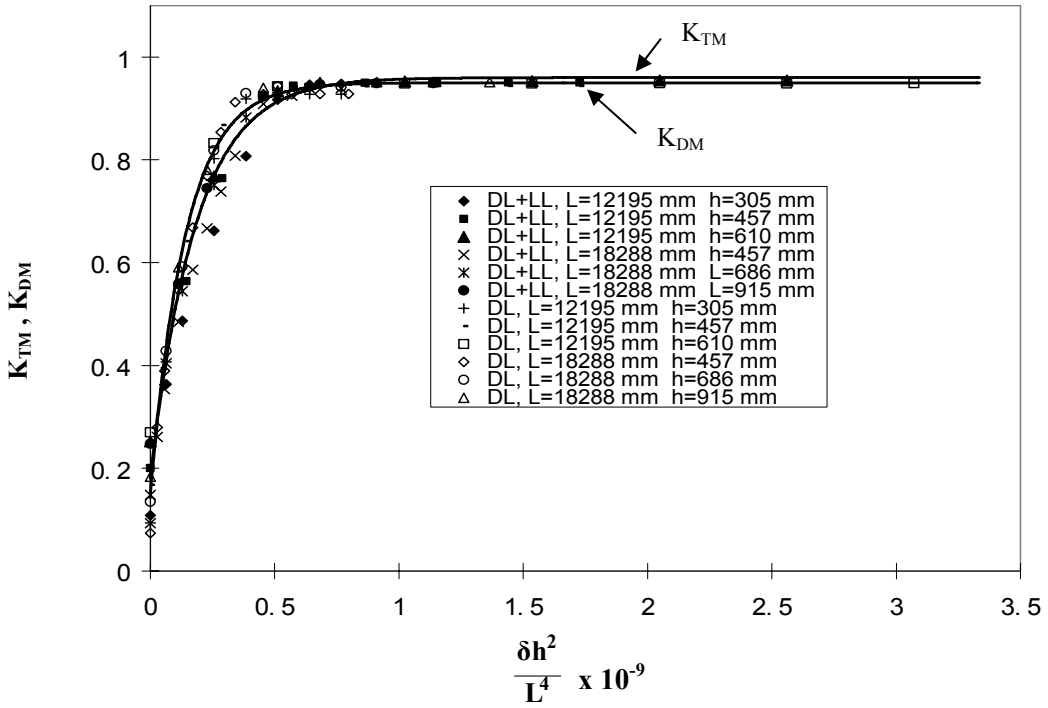

Fig. 2-15 K_{TM} and K_{DM} curve

The predicted maximum internal moments in approach slabs due to total load (dead load plus live load without considering dynamic impact effect) and dead load only were normalized and represented in Fig. 2-15. They can be expressed by an exponential function with a regression analysis as follows:

$$M_T = \left(0.955 - 0.78 \ \ e^{-5.49\times10^9 (\frac{\delta h^2}{L^4})} \right) M_{T0} = K_{TM} M_{T0} \tag{2-3}$$

$$M_D = \left(0.95 - 0.8 \ \ e^{-7.02\times10^9 (\frac{\delta h^2}{L^4})} \right) M_{D0} = K_{DM} M_{D0} \tag{2-4}$$

where M_T = maximum moment of approach slab due to total load; M_D = maximum moment of approach slab due to dead load; δ = differential settlement (mm); h = thickness of approach slab (mm); L = length of approach slab (mm); K_{DM} and K_{TM} are moment coefficients that are self-evidenced in the equations; M_{T0} = maximum moment of simply supported beam due to total load; and M_{D0} = maximum moment of simply supported beam due to dead load.

The maximum internal moment in approach slab due to live load is then calculated as:

$$M_L = K_{TM} M_{T0} - K_{DM} M_{D0} \tag{2-5}$$

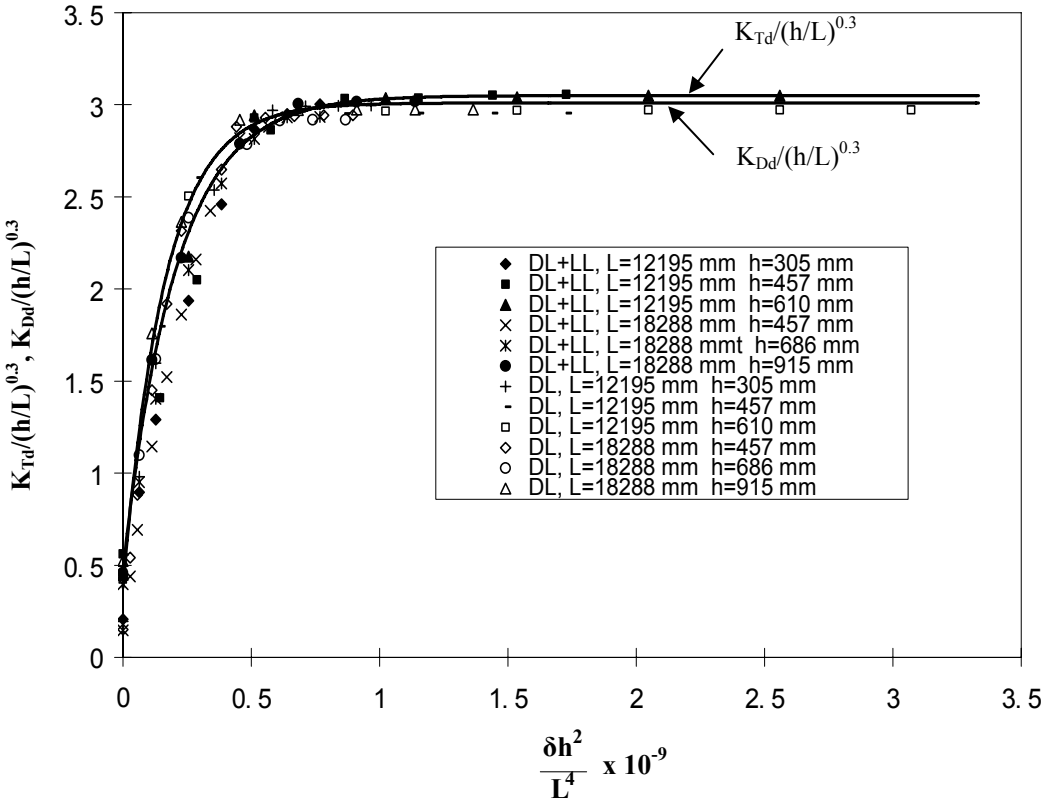

Fig. 2-16 K_{Td} and K_{Dd} curve

Similarly, the maximum deflections (Δ_2 in Fig. 1-1, including both slab deflection and load-induced support deformation) in the approach slab due to the total load and dead load only are represented by the curves shown in Fig. 2-16 and can be expressed by the an exponential function as:

$$d_T = \left((3.05 - 2.58 \quad e^{-4.88\times10^9 (\frac{\delta h^2}{L^4})}) \times (\frac{h}{L})^{0.3} \right) d_{T0} = K_{Td} d_{T0} \tag{2-6}$$

$$d_D = \left((3.01 - 2.63 \quad e^{-6.10\times10^9 (\frac{\delta h^2}{L^4})}) \times (\frac{h}{L})^{0.3} \right) d_{D0} = K_{Dd} d_{D0} \tag{2-7}$$

where d_T = maximum deflection of approach slab due to total load; d_D = maximum deflection of approach slab due to dead load; K_{Dd} and K_{Td} are deflection coefficients that are self-evidenced in the equations; d_{T0} = maximum deflection of simply supported beam due to total load; and d_{D0} = maximum deflection of simply supported beam due to dead load.

The maximum deflection in approach slab due to live load is then calculated as:

$$d_L = K_{Td} d_{T0} - K_{Dd} d_{L0} \tag{2-8}$$

Finally, the end rotation angle also shown in Fig. 1-1 is represented in Fig. 2-17 and the formulas are obtained as

$$\theta_T = (1.86 - 1.44e^{-5.9\times10^9(\frac{\delta h^2}{L^4})}) \bullet (\frac{h}{L})^{0.2} \bullet \theta_{T0} = K_{T\theta}\theta_{T0} \quad (2-9)$$

$$\theta_D = (1.84 - 1.45e^{-7.32\times10^9(\frac{\delta h^2}{L^4})}) \bullet (\frac{h}{L})^{0.2} \bullet \theta_{D0} = K_{D\theta}\theta_{D0} \quad (2\text{-}10)$$

where θ_T = maximum rotation of approach slab due to total load; θ_D = maximum rotation of approach slab due to dead load; $K_{D\theta}$ and $K_{T\theta}$ are moment coefficients that are self-evidenced in the equations; θ_{T0} = angle of simple beam due to total load; and θ_{D0} = angle of simple beam due to dead load.

The maximum rotation angle in the approach slab due to live load is then calculated as:

$$\theta_L = K_{T\theta}\theta_{T0} - K_{D\theta}\theta_{D0} \quad (2\text{-}11)$$

These developed formulas provide information (deflection, rotation, and internal force) for the structural evaluation and design of approach slabs without conducting complicated finite element analysis. For example, the predicted internal moments can be used to design the slab reinforcement for a given settlement. Engineers can also control the excessive settlement by either improving embankment fills or foundations, or by selecting a stiffer approach slab based on the predicted deformation.

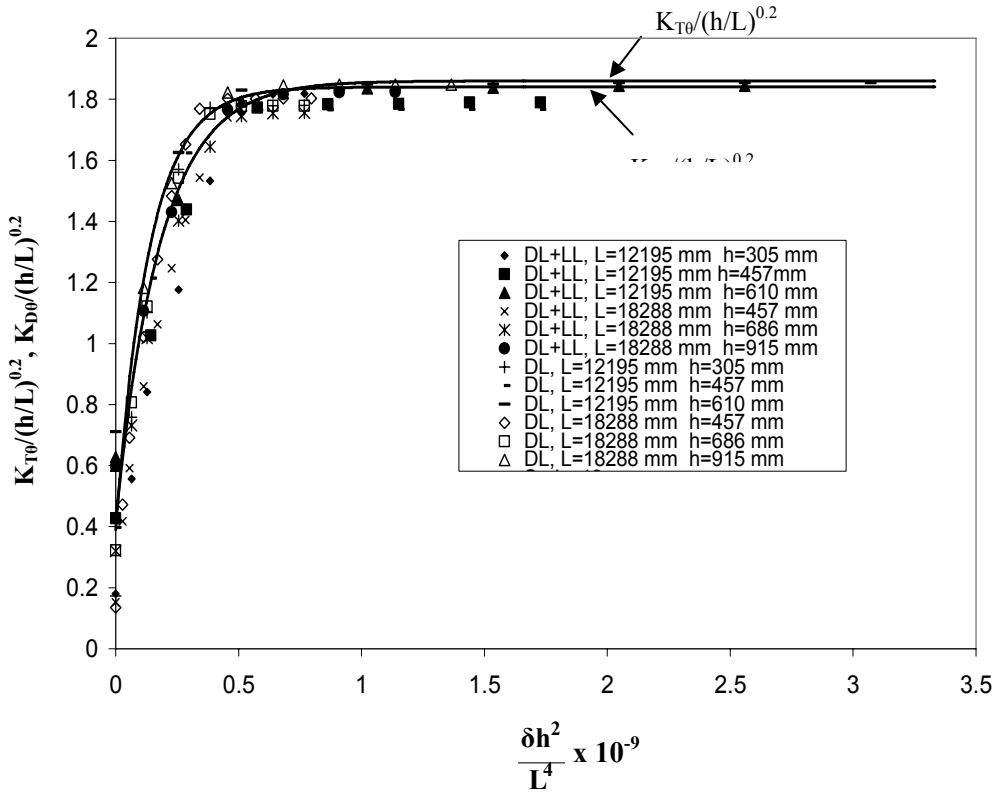

Fig. 2-17 $K_{T\theta}$ and $K_{D\theta}$ curve

2.8 Summary and Conclusions

An appropriate approach slab design directly affects the safety and economy of the transportation infrastructure. A rational design is necessary not only for the serviceability requirement of the transition approach slab, but also for the life-expectancy of the whole highway system including bridges and pavements. While the "bump" problem has existed for years, the design of the approach slab is still more an art than a science. Engineering calculations of the approach slab are typically not conducted or the approach slab is simply designed as a simply-supported beam since the information about the interaction of the approach slab and the embankment settlement is unknown for a routine office design. There are no AASHTO guidelines for designing approach slabs with embankment settlements.

The present study investigated the effect of embankment settlement on the structural performance of the approach slab. Deflections and internal moments of the slab and stresses of the embankment soil were predicted with finite element modeling; they increased with the increase of the embankment settlement. For the particular example used in the present study, when the settlement increased to 152 mm (6.0 in.), the approach slab became a simply-supported beam. Predicted results indicated that LaDOTD's current slab design is good for cases without embankment settlement, but the ultimate strength is not adequate if settlement greater than 15 mm is considered, implying that either more reinforcement, thicker slab section, and/or settlement control are needed to satisfy the AASHTO structural design requirement. Similar issues may exist in other states and modifications of concrete slab design may be warranted.

This research shows how finite element procedures can help design approach slabs for a given embankment settlement. Parametric studies were then conducted to develop a simpler design procedure so that engineers do not need to use complicated finite element analysis in a routine design. Instead, the developed coefficients can be multiplied with the simple beam response to consider the interaction of the embankment soil and slab under a given embankment settlement. The more rational design considering a given settlement will eventually lead to a more reliable practice in using approach slabs. LaDOTD has initiated a large effort under the Louisiana Quality Initiative program to resolve the "bump" problems related to approach spans, and this study is one of the components necessary to eventually resolve this issue.

2.9 References

American Association of State Highway and Transportation Officials (AASHTO). (1998). *LRFD bridge design specifications*, Washington, D.C.

American Association of State Highway and Transportation Officials (AASHTO). (2002). *Standard specifications for highway bridges*, Washington, DC.

Briaud, J. L., James, R. W., and Hoffman, S. B. (1997). "Settlement of bridge approaches (the bump at the end of the bridge)." *NCHRP Synthesis 234*, Transportation Research Board, National Research Council, Washington, D.C.

Chini, S. A., Wolde-Tinsae, A.M., & Aggour, M.S. (1992). "Drainage and backfill provisions for approaches to bridges." University of Maryland, College Park, Md.

Ha, H., Seo, J.B., and Briaud, J.L. (2003). "Investigation of settlement at bridge approach slab expansion joint: Survey and site investigations." *Rep. No. 4147-1*, to the Texas Department of Transportation, published by the Texas Transportation Institute, Texas A&M Univ. System, College Station, Tex.

Hoppe, E. J. (1999) "Guidelines for the use, design, and construction of bridge approach slabs." *Final Rep. No. VTRC 00-R4*, Virginia Transportation Research Council, Charlottesville, Va.

Kramer, S.L., & Sajer, P. (1991). "Bridge approach slab effectiveness." Washington State Transportation Center, Seattle.

Louisiana Department of Transportation and Development (LaDOTD). (2002). *Bridge design metric manual*, Baton Rouge, LA.

Louisiana Quality Initiative (LQI). (2002). *Preservation of bridge approach ride ability*, Baton Rouge, LA.

Mahmood, I. U. (1990). "Evaluation of causes of bridge approach settlement and development of settlement prediction models." Ph.D. Thesis, University of Oklahoma, Norman, Okla.

Seo, J. B., Ha, H., and Briaud, J. L. (2003). ."Investigation of settlement at bridge approach slab expansion joint: Numerical simulations and model tests," *Rep. No. 4147-2*, to the Texas Department of Transportation, published by the Texas Transportation Institute, Texas A&M Univ. System, College Station, Tex.

Stark, T. D., Olson, S. M., & Long, J. H. (1995). "Differential movement at the embankment/structure interface: Mitigation and rehabilitation." *Rep. No. IAB-H1, FY 93*, Illinois Department of Transportation, Springfield, ILL.

Stewart, C.F. (1985). "Highway structure approaches." California Department of Transportation, Sacramento, Calif.

Tadros, M. K., & Benak, J. V. (1989). "Bridge abutment and approach slab settlement (Phase1)." University of Nebraska, Lincoln, Neb.

Wahls, H. E. (1990) "Design and construction of bridge approaches." *Rep. No. NCHRP Synthesis 159*, Transportation Research Board, National Research Council, Washington, D.C.

Zaman, M., Gopalasingam, A. and Laguros, J. G. (1991). "Consolidation settlement of bridge approach foundation", *J. of Geotech. Eng.,* 117(2) 219-239.

CHAPTER 3 PERFORMANCE OF RIBBED CONCRETE APPROACH SLAB BASED ON ITS INTERACTION WITH EMBANKMENT*

3.1 Introduction

Bridge approaches in Louisiana are usually constructed with reinforced concrete slabs that connect the deep founded bridge end with the shallow founded adjacent roadway as shown in Fig. 1-1. Their functions are to bridge the differential settlement and provide a smooth transition between the bridge and roadway pavement. However, complaints about the ride quality of bridge approach slabs still arise and need to be resolved. The complaints are usually described as a "bump" that motorists feel when they approach or leave bridges. Field observations indicate that either faulting or a sudden change in slope grades of approach slabs causes this "bump". These faulting and change of slope are partly due to the bending of the slab as the embankment settles. Similar problems have been reported nationwide and currently cost millions of dollars for maintenance (estimated as 100 million per year) with 6.3 million dollars annually for Texas alone (Ha et al. 2003).

Several studies of the performance of approach slabs have been sponsored over the years by various state DOTs. The majority of the previous researches can be categorized as (1) syntheses of practice (Wahls 1990, Kramer and Sajer, 1991, Chini et al. 1992, Briaud et al., 1997, Hoppe 1999); (2) identification of the sources of differential settlement (Stewart 1985, Tadros 1989 et al.); and (3) soil improvement (Mahmood 1990). Although the bump-related problems have been commonly recognized and the causes are identified, no unified engineering solutions have emerged, primarily because of the number and complexity of the factors involved. There are no guidelines in the AASHTO code specifications (AASHTO 2002, AASHTO 1998) regarding the structural design of approach slabs considering the effects of embankment settlements.

Louisiana Department of Transportation and Development (LA DOTD) has launched a major effort to alleviate this problem by changing the design of approach slabs where differential settlement is expected (LQI 2002). Currently, 6.10 m (20 ft) or 12.19 m (40 ft) long approach slabs, directly sitting on embankment soil (called soil-supported approach slab, or SSAS, hereafter), are used for slab spans and girder bridges except weak soil areas. However, concrete approach slabs can lose their contacts from soil due to the embankment settlement. Finite element analysis conducted by Cai et al. (2004) considering the differential settlement has shown that the current reinforcement requirement of the SSAS is not adequate and design methodology considering the differential settlement has been developed.

For approach embankments sitting directly on weak foundation soils, 36.58 m (120 ft) long pile-supported approach slabs (called piled-approach approach slab, or PSAS, hereafter) are often used in Louisiana, hopefully to achieve a reasonable transition as shown in Fig. 3-1. However, this approach sometimes works, but at other times it does not work with broken slabs since it is not possible to accurately predict pile settlement. Currently, no simple and reliable design procedure for PSAS is available and such details as specified reinforcement requirement are to be in accordance with the guidelines (LA DOTD 2002).

---

* Reprinted by permission of "Journal of the Transportation Research Board"

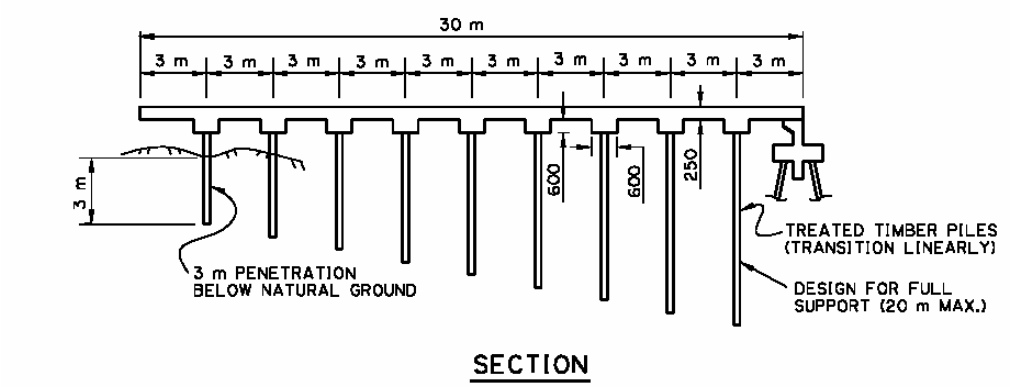

Fig. 3-1 Typical pile-supported approach slab in Louisiana

The motivation of the present study is to find a feasible solution to replace the current PSAS that calls for 36.58 m (120 ft) in length. The drawback of the PSAS is the cost and the unpredictable performance, evidenced by the observed inconsistent performance in field. The proposed new construction method will allow approach slabs strong enough to lose a portion of their contact supports without detrimental deflection, perhaps by increasing the flexural rigidity (EI) of the approach slabs. Previous studies indicated that SSAS may be used for some short span applications. Large span length would require a very thick slab. In such a case, ribbed approach slabs (similar to slab-on-beam bridge decks) are more economical and are thus proposed in the present study, providing advantages over both the SSAS and PSAS for some span ranges.

This chapter presents strategies and results from a 3-D finite element analysis. The objective is to analyze systematically the structural performance of ribbed approach slab with span length of 18.29 m (60 ft) as example and to understand the interaction of ribbed approach slab and embankment settlement. In this study, 3 different beam spacings were considered. The results obtained are very useful for a proper design which will help mitigate the slab ride ability (and structural safety) problems.

3.2 Description of Finite Element Model

Two extreme cases are currently used in practical design of approach slabs. In the first case, the slab is assumed in full contact with the soil and without considering differential settlement. This assumption may result in un-conservative design. In the other extreme case, an approach slab is designed as a simple beam, assuming a complete separation between the slab and the embankment except for the two bridge ends. This assumption, while conservative, will definitely result in uneconomical design. In many real cases, the slab is in partial separation and partial contact with the soil along the span length. The spring supports provided from the embankment soil to the concrete slab will reduce the internal force of the slab. The extent of this support depends on the slab and soil interaction for a given embankment settlement.

The present finite element analysis simulates the interaction of the approach slab and the embankment soil by assuming a linear settlement of embankment shown in Fig. 1-1. While some

real cases may be different, this assumption is justified since the embankment height varied roughly in a linear manner along the pavement. The actual embankment settlement will be determined on a case-by-case basis in another ongoing research project supported by the LaDOTD LQI program which is assumed as a known parameter in the present finite element analysis. Since the left end of the slab sits on the relatively stiffer abutment while the right end on the relatively weaker soil or sleeper slab, the linear movement results in a linear gap between the slab and the embankment soil. When the self-weight of the slab and live loads are applied, the slab deforms and interacts with the soil, which results in partial contact of the slab with the soil as illustrated in the figure. The present research will provide essential information needed for structural design of the ribbed approach slab considering embankment settlement.

For demonstration purposes, a ribbed approach slab with 18.29 m in span length and beam spacing of 4.88 m (3 beams) is used and the other dimensions are shown in Fig. 3-2 with a 1.22 m sleeper slab. For modeling convenience, the beams are modeled as rectangular section with the equivalent section properties of ASSHTO Type II beam. A 3-D finite element model was established using eight-node hexahedron elements (ANSYS© Solid 45) in meshing. In addition to the dead load of the slab, the AASHTO truck loads were applied on the slab. The two HS20 truck loads were moved along the slab length to produce the worst loading scenario for the slab deflection and internal bending moments.

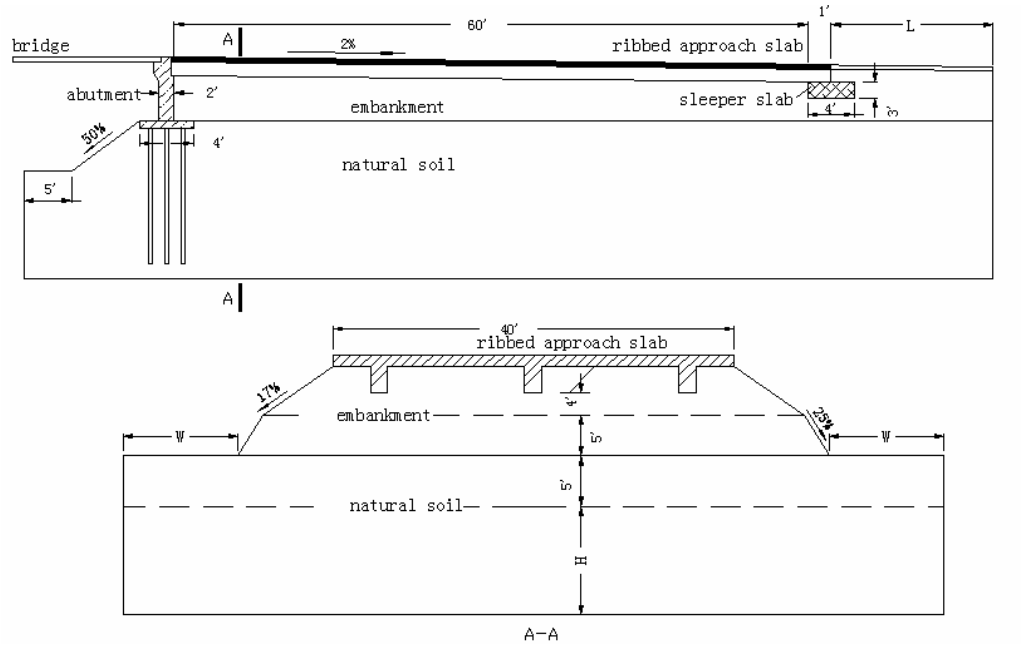

Fig. 3-2 Sketch of bridge abutment

The soil profile under the approach slab consists of compacted embankment and silty clay subgrade soil which is typical for Louisiana. A contact and target pair surface element available in ANSYS© element library was used to simulate the interaction between the soil and the slab. This surface element is in compression only and can thus model the contacting and separating process between the slab and soil. When the soil is in tension, the slab and soil will separate automatically. The Drucker-Prager model is used to define the yield criteria for both embankment soil and subgrade soil. The material parameters used in the finite element analysis

of the present study are Elastic modulus 260 and 30 MPa, Poisson ratio 0.3 and 0.3, Cohesion coefficient 80 and 50 KPa, friction angle 30 and 30 degrees, and gravity density 20 and 15 KN/m^3, for embankment soil and subgrade natural soil, respectively. The concrete weight is considered to be 2404 Kg/m^3. Investigations for wider range of material properties are in the progress in order to develop general design guidelines for the approach slab design.

The soil underneath the approach span is theoretically semi-infinite. Sensitivity analysis was conducted in order to locate the appropriate location of the boundaries, laterally, vertically, and longitudinally, for the finite element model. Three parameters, W, L, and H shown in Fig. 3-2, were investigated in the sensitivity study and determined to be: W = 4.57 m; L = 12.19 m; H = 15.24 m for the analyses of different settlements described below.

3.3 Predicted Results

In this study, 2, 3, and 4 beam alternatives for a given approach slab width of 12.19 m were studied, which corresponds to beam spacings of 9.75, 4.88 and 3.66 m, respectively. By moving the truck loads along the slab, maximum deflections, internal moments and reaction forces of the ribbed approach slab at the sleeper slab end under different settlements were obtained. In order to simulate the interaction of the approach slab and the embankment soil, for a given embankment settlement, the dead load (DL) was applied first; then the dead load and live loads (DL+LL) were applied together. The live load effects (LL) were then calculated with (DL+LL) – DL. This procedure is necessary since the loads affect the contacting and separating process between the slab and soil. The live load cannot be applied without the dead load for a correct/proper solution due to the nonlinear effect of the interaction.

Figs 3-2 to 3-4 show the increase of magnitude of the beam's maximum deflections and internal moment of interior beam with the increase of embankment differential settlement. If the differential settlement is increased to larger than 76 mm (3 in), there is almost no change in the deflection and internal moment of the approach slab, which indicates that the settlement no longer affects the performance of the slab since the approach slab almost completely loses its contact with the soil except at the end near the sleeper slab, thus becoming a simply-supported beam.

Similarly, as shown in Fig. 3-5, the total reaction force of beams at the sleeper slab end keeps increasing with the increase of the differential settlement. Since the slab loses more support from soil as the settlement increases, a larger portion of the slab self-weight and truck loads are passed to the sleeper slab instead of directly to the soil under the ribbed slab, and consequently to the soil under the sleeper slab. In comparison with the slab deflection and internal force (Figs. 3-3 and 3-4), the reaction force keeps increasing but with a reduced rate even after the settlement exceeds 76 mm. This is because even after the complete loss of contact between the ribbed slab and soil, the increase in settlement will change the geometry of the soil around the sleeper slab so that the interaction of the ribbed slab, sleeper slab and embankment soil will be slightly affected.

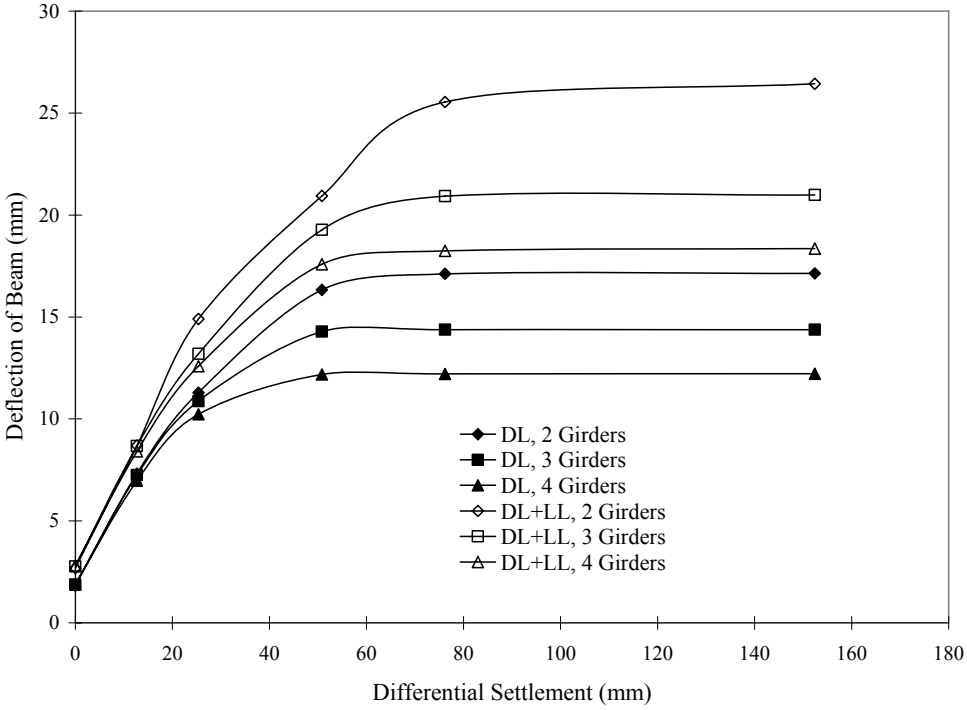

Fig. 3-3 Deflection of beam versus differential settlement

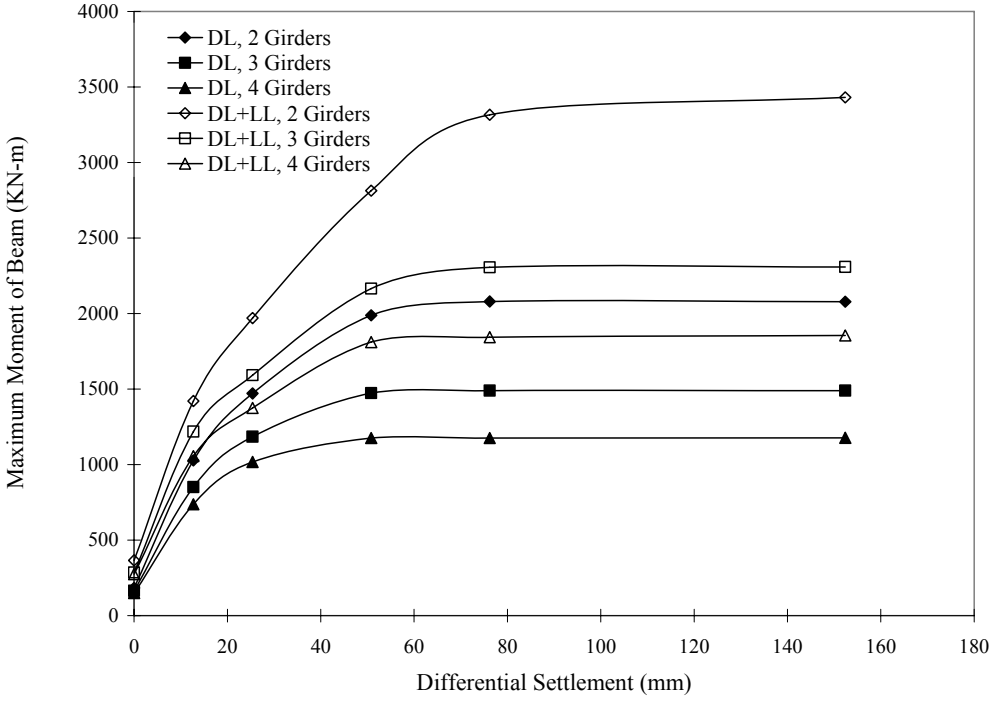

Fig. 3-4 Maximum moment of interior beam versus differential settlement

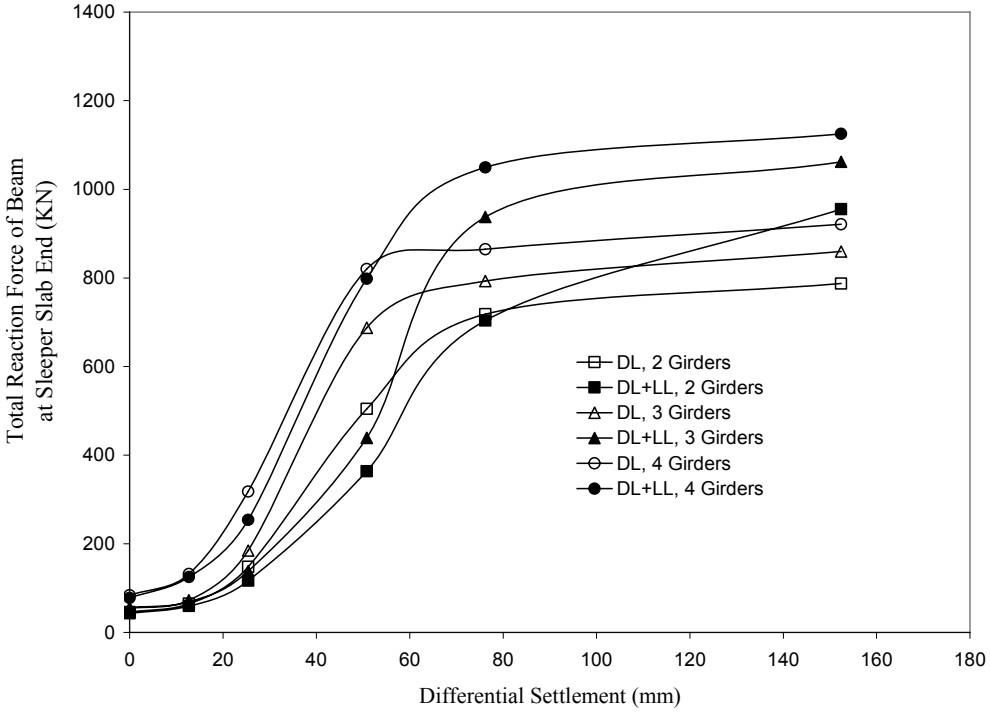

Fig. 3-5 Total reaction force of beams at sleeper slab end versus differential settlement

Tables 3-1 to 3-4 show that the mid-span deflection and internal moment of beams with smaller beam spacing are smaller than those of beams with larger spacing, which means using smaller beam spacing can control the mid span deflection and therefore control the change of the slope angle (θ_1 in Fig 1-1). However, Tables 3-2 to 3-4 and Fig. 3-5 also show that for a given settlement, with the decrease of beam spacing, the total reaction force (corresponding to maximum internal moment) of beams at the sleeper slab end increases, which means more percentage of the forces is transferred to the sleeper slab. Correspondingly, as shown in Table 3-1, the smaller the beam spacing, the more deflection of beam at the sleeper slab end (Δ_1 in Fig. 1-1). This is because the higher stiffness of the beam with smaller spacing makes the beam lose more portion of contact support with the soil and therefore transfers more load to its sleeper slab end for the same embankment settlement. Therefore, it should be noted that a more rigid approach slab will decrease the change of slope angle (θ_1 in Fig 1-1) and mid-span deflection(Δ_2 in Fig. 1-1), but may also increase the reaction force beneath the contact area (sleeper slab), thereby may increase the faulting deflection (Δ_1 in Fig. 1-1). In such cases, a spread footing may be necessary to distribute this force.

Simultaneously, Tables 3-2 to 3-4 show that in some cases when settlement is small the reaction force of the beam at the sleeper slab end due to self-weight of the ribbed slab is surprisingly larger than the reaction force due to the self-weight and truck load together. Since the beam has more deflection due to total load than due to self-weight, when settlement is small, beams subjected to the total load have more contact support from soil than those subjected to self-weight only, thus may have smaller reaction forces. The interaction of the ribbed slab and the soil is affected by the magnitude of the external load as well as the embankment settlement and the stiffness of the structure.

Table 3-1 Deflection of beam

Differential Settlement (mm)	Beam Spaced at 32 ft				Beam Spaced at 16 ft				Beam Spaced at 12 ft			
	DL		DL+LL		DL		DL+LL		DL		DL+LL	
	Total Deflection (mm)		Total Deflection (mm)		Total Deflection (mm)		Total Deflection (mm)		Total Deflection (mm)		Total Deflection (mm)	
	at Mid-span	at End of Sleeper Slab	at Mid-span	at End of Sleeper Slab	At Mid-span	at End of Sleeper Slab	at Mid-span	at End of Sleeper Slab	at Mid-span	at End of Sleeper Slab	at Mid-span	at End of Sleeper Slab
0	1.83	2.13	2.67	2.39	1.88	2.24	2.77	2.51	1.88	2.29	2.82	2.59
13	7.32	2.44	8.71	2.57	7.24	2.49	8.69	2.77	6.96	2.57	8.41	2.84
25	11.30	2.51	14.91	2.74	10.87	2.72	13.18	3.00	10.24	2.82	12.57	3.10
51	16.33	2.87	20.93	3.07	14.27	3.12	19.28	3.45	12.19	3.12	17.58	3.58
76	17.12	3.00	25.53	3.48	14.38	3.18	20.93	3.73	12.22	3.15	18.24	3.73
152	17.15	3.02	26.44	3.68	14.38	3.20	20.98	3.81	12.22	3.20	18.36	3.78

Table 3-2 Internal force of beam spaced at 9.75 m (32 ft)

Differential Settlement (mm)	Moment (KN-m)		Reaction Force at Sleeper Slab End (KN)			
	DL	DL+LL	Beam 1		Beam 2	
			DL	DL+LL	DL	DL+LL
0	184.2	366.4	22.2	20.5	23.6	22.7
13	1027.8	1421.5	32.9	26.3	32.0	33.4
25	1471.5	1969.5	73.4	46.7	74.7	70.3
51	1988.5	2813.7	251.4	141.0	253.2	222.9
76	2079.7	3316.8	359.1	334.6	359.1	369.3
152	2078.8	3431.5	393.8	530.8	394.2	424.5

3.4 Effect of Embankment Settlement on Beam Design

Since the ribbed approach slab has partial contact support from the embankment soil for a given embankment settlement, it is necessary to design the slab in order to provide enough strength for the given predicted settlement. When the ribbed approach slab is subjected to bending, the stresses that are induced by the concentrated loads are not uniformly distributed over the whole width of the slab. If the spacing of the beams is large, only part of the slab is effective in resisting a given bending load. It is traditional, for design purposes, to consider a portion of the slab (an effective width) as the top flange of the beam. Therefore, to conduct structural design, the effective width of the approach slab is important and needed in design. However, such information is not available in the design codes for a partially contact ribbed slab system.

For the simply supported ribbed slab, the case of the two trucks applied at the mid-span was chosen as the basic loading type and a uniformly distributed dead load was considered. By moving the trucks along the transverse direction of the slab, the critical scenario was observed for exterior and interior beams. The effective width, w_e, is defined as:

$$w_e = \frac{\int_0^w \sigma_y dx}{\sigma_{y\max}} \qquad (3\text{-}1)$$

where σ_y is the bending stress in the section, σ_{ymax} is the maximum bending stress in the section; and w is the spacing of the beams.

Table 3-3 Internal force of beam spaced at 4.88 m (16 ft)

Differential Settlement (mm)	Exterior Beam								Interior Beam							
	Moment (KN-m)		Reaction Force at Sleeper Slab End (KN)						Moment (KN-m)		Reaction Force at Sleeper Slab End (KN)					
			Beam 1		Beam 2		Beam 3				Beam 1		Beam 2		Beam 3	
	DL	DL+LL	DL	DL+LL	DL	DL+LL	DL	DL+LL	DL	DL+LL	DL	DL+LL	DL	DL+LL	DL	DL+LL
0	126.0	232.7	15.1	14.7	22.7	24.5	16.5	16.9	164.8	286.8	15.1	14.7	22.7	25.4	16.5	15.6
13	732.6	1114.9	22.2	16.9	29.4	28.5	21.4	21.8	851.5	1218.2	22.2	20.9	29.4	26.3	21.4	21.8
25	1035.0	1478.2	62.3	29.8	59.6	45.4	63.2	62.3	1185.5	1592.6	62.3	46.3	59.6	36.9	63.2	54.7
51	1308.0	2041.0	228.2	116.6	229.6	171.3	229.6	226.9	1473.3	2164.6	228.2	173.1	229.6	132.1	229.6	133.9
76	1313.5	2093.6	259.8	326.6	272.3	311.0	260.7	272.3	1489.4	2305.7	259.8	313.7	272.3	323.9	260.7	299.4
152	1313.0	2102.8	279.9	401.3	299.9	355.5	279.9	296.3	1490.6	2308.4	279.9	351.9	299.9	380.0	279.9	330.1

Table 3-4 Internal force of beam spaced at 3.66 m (12 ft)

Differential Settlement (mm)	Exterior Beam										Interior Beam									
	Moment (KN-m)		Reaction Force at Sleeper Slab End (KN)								Moment (KN-m)		Reaction Force at Sleeper Slab End (KN)							
			Beam 1		Beam 2		Beam 3		Beam 4				Beam 1		Beam 2		Beam 3		Beam 4	
	DL	DL+ LL	DL	DL+ LL	DL	DL+ LL	DL	DL+ LL	DL	DL+ LL	DL	DL+ LL	DL	DL+ LL	DL	DL+ LL	DL	DL+ LL	DL	DL+ LL
0	108.9	203.4	21.8	23.6	20.5	21.4	20.5	22.2	21.4	22.7	149.9	275.3	21.8	18.7	20.5	17.8	20.5	18.7	21.4	22.2
13	610.7	902.6	37.8	32.5	28.9	24.9	28.5	29.8	36.9	37.4	736.9	1056.0	37.8	32.5	28.9	24.9	28.5	29.8	36.9	37.4
25	855.2	1196.4	92.1	58.7	66.3	41.8	66.7	59.6	92.5	90.3	1017.5	1374.8	92.1	63.2	66.3	40.5	66.7	56.5	92.5	89.0
51	995.5	1649.6	208.2	192.2	203.3	176.2	202.0	211.3	206.9	214.0	1176.3	1811.8	208.2	202.0	203.3	170.8	202.0	207.8	206.9	218.0
76	996.2	1707.8	214.9	308.8	218.5	267.8	218.5	249.6	213.6	219.8	1176.8	1843.6	214.9	299.0	218.5	270.1	218.5	254.9	213.6	225.6
152	996.5	1712.4	222.9	326.6	238.0	295.0	238.5	272.3	221.6	229.6	1177.0	1855.0	222.9	315.4	238.0	297.7	238.5	277.6	221.6	234.9

For a ribbed approach slab with a span length of 18.28 m, width of 12.19 and beam spacing of 9.75, 4.88 and 3.66 m, the effective width, w_e, for exterior beam and interior beam respectively was calculated by varying the differential settlement from 0 to 152 mm, and was plotted in Figs. 3-6 to 3-8. To avoid stress concentration caused by point load that represents truck wheel load, the effective width obtained is the average effective width within 0.61 m range of the point load along the longitudinal direction. As expected, the dead load is much more uniformly distributed across the bridge width and thus the effective width is larger than that of the live load. The effective width for exterior and interior beam was also determined per AASHTO code (1998) respectively and shown in Figs 3-6 to 3-8. It is noted that these AASHTO calculations are based on a simply supported beams (partial contact case is not available) that correspond to the case with a very large differential settlement of embankment.

As shown in Figs. 3-6 and 3-7, for beams spaced at 9.75 and 4.88 m, when the differential settlement is small, the predicted effective width for live loads is smaller than that specified in the codes, implying that using the code effective width is slightly not conservative for design of partial contact slab. This is because the partial contact of the beam and soil decreases the effective span length of the beam. However, small settlement is not the critical condition. For larger settlement, the code effective width is more conservative. For beams spaced at 3.66 m, as shown in Fig. 3-8, the predicted effective width is smaller than the code effective width for both the exterior beams and the interior beams, namely 2.44 and 3.66 m respectively. In the code specifications (AASHTO 2002), the effective width is controlled by the span length, the slab thickness, and the beam spacing. In the case of 3.66 m beam spacing, the slab effective width, controlled by the beam spacing, is the same as the beam spacing. This means that in this case, the whole slab width is effective, which equivalently assumes that the stress distribution in the slab is perfectly uniform. Since the predicted slab effective width from the finite element analysis is obtained by using Eq. (3-1) and the stress distribution cannot be perfectly uniform, the predicted values must be smaller than those of the code specifications in this small beam spacing case.

After the maximum internal moments of the exterior beam and interior beam and the effective width were obtained respectively, checking the strength of the beam of the ribbed slab was conducted according to the AASHTO Standard Specifications (AASHTO 2002), namely, with load factors of 1.3 for dead load, and 2.17 for live load. Since the beam used in finite element analysis has the same section properties as AASHTO Type II section, the latter is used in strength checking. For the extreme case when the ribbed slab loses contact with the soil, regular reinforced concrete beam cannot provide the required stiffness, and therefore prestressed concrete beams are used here. The results of the prestressed reinforcement design considering the effects of different differential settlements are shown in Table 3-5.

It is obvious in Table 3-5 that when the embankment settlement increases, more prestressing strands are required. For the ribbed slab with a beam spacing of 9.75 m, when the settlement exceeds 76 m, the required prestressing strands will exceed the allowed maximum value (i.e., we cannot reasonably design the section). In this case, either the beam spacing should be reduced or the soil should be improved to control the settlement within the allowable limit. Table 3-5 also indicates that ribbed slabs with beam spaced at 4.88 and 3.66 m can provide enough strength in the case of a given settlement that exceeds 76 mm.

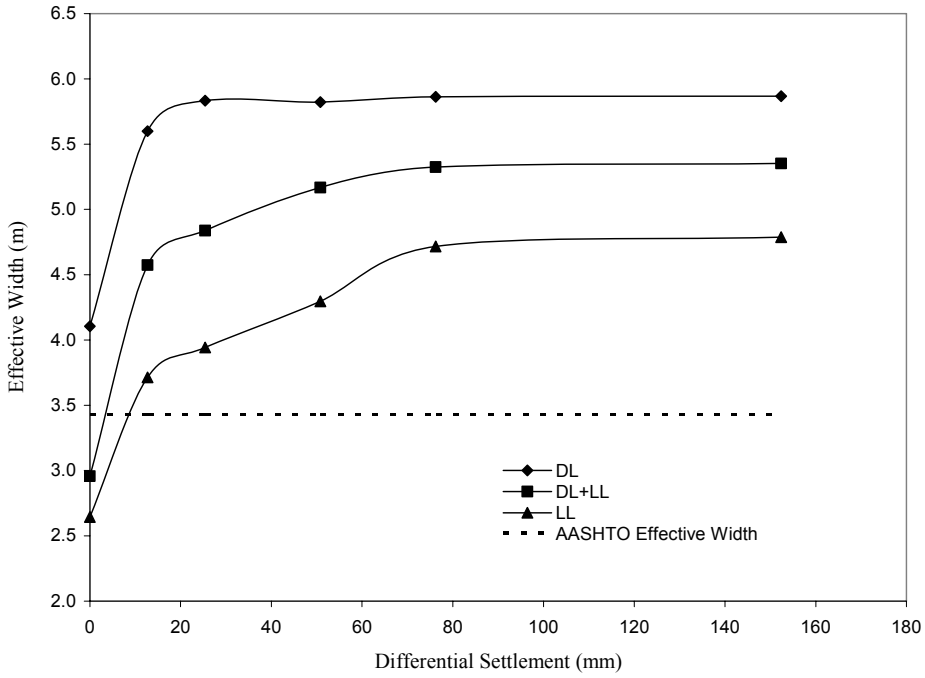

Fig. 3-6 Effective width of beam spaced at 32 ft

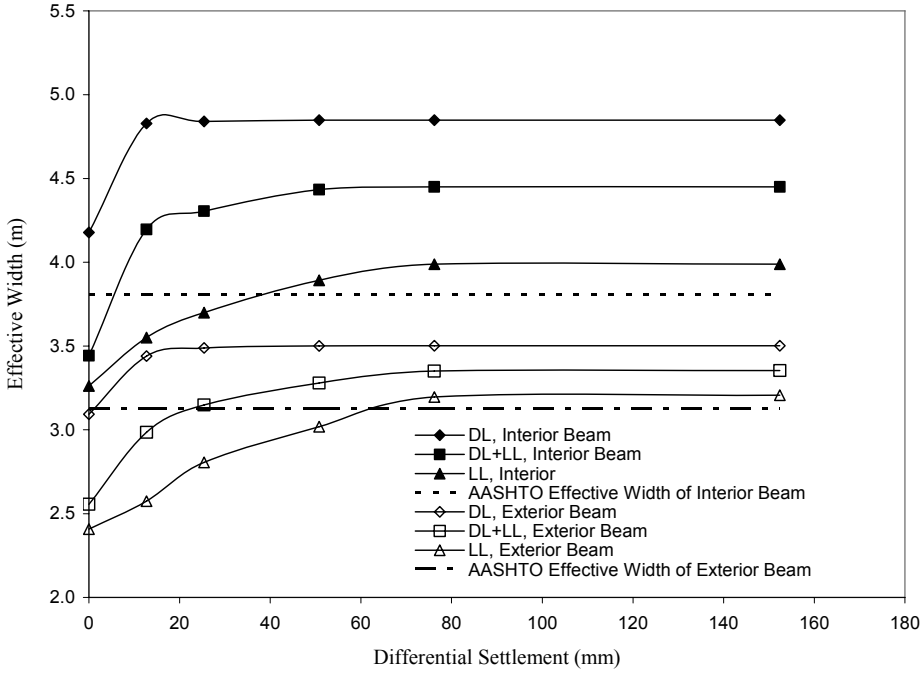

Fig. 3-7 Effective width of beam spaced at 16 ft

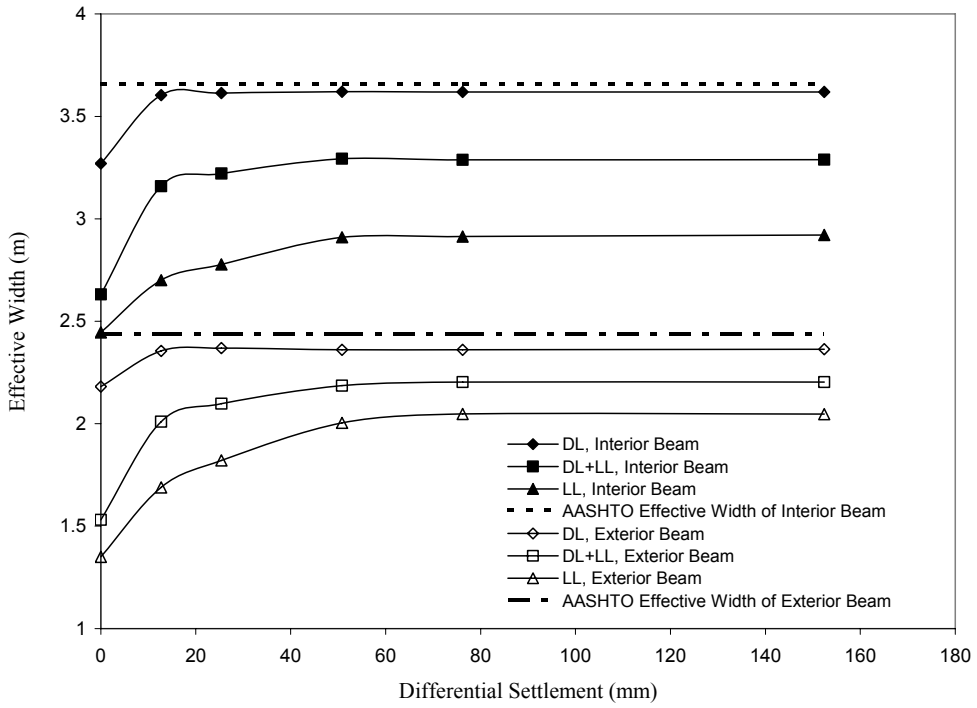

Fig. 3-8 Effective width of beam spaced at 12 ft

3.5 Conclusions

An appropriate approach slab design directly affects the safety and economy of the transportation infrastructure. A rational design is not only necessary for serviceability requirement of the transition approach, but also for the life-expectation of the whole highway system including bridges and pavements. While the "bump" problem has existed for years, the design of approach slab is still more an art than a science. Engineering calculations of approach slabs are typically either underdesigned or overdesigned since the information between the interaction of the approach slab and the embankment settlement is unknown for a routine office design. There are no AASHTO guidelines for designing the approach slabs considering embankment settlements.

The present study recommended and analyzed a stiffer approach slab, namely a ribbed slab that can reduce the slab thickness compared with the flat approach slabs. It investigated the effect of the embankment settlement on the structural performance of the ribbed approach slab. Deflections and internal moments of the beam, and reaction forces of the beam at the sleeper slab end were predicted; they increase with the increase of the embankment settlement. Since the beams with different spacings were also investigated, with the given settlement and deflection limit, proper beam spacing can be determined. Preliminary results indicated that the beam spaced at 9.76 m is good for cases with an embankment settlement less than 76 mm. The strength of beam with spacing of 4.88 and 3.66 m is adequate when the settlement is larger.

This research shows how the finite element procedure can be used to help design ribbed approach slabs for a given differential settlement. This performance based design (for a given

settlement) will eventually lead to a more reliable practice in using approach slabs. The LA DOTD has initiated a large effort under the Louisiana Quality Initiative program to resolve the "bump" problems related to the approach spans. The information from the present study, along with other information, such as time-dependent embankment settlement, comfort criteria of bump from other related studies, will help decide when settlement controls are necessary and how to choose an appropriate configuration in order to have an economical design for the approach slabs.

3.6 References

AASHTO (2002). "Standard specifications for highway bridges." American Association of State Highway and Transportation Officials, Washington, D.C.

AASHTO (1998). *LRFD Bridge Design Specifications.* American Association of State Highway and Transportation Officials, Washington, DC.

Briaud, J. L., James, R. W., and Hoffman, S. B. (1997). "Settlement of Bridge Approaches (the Bump at the End of the Bridge)." NCHRP Synthesis 234, Transportation Research Board, National Research Council, Washington, D.C.

Cai, C. S., Shi, X. M., Voyiadjis, G. Z. and Zhang, Z. J. (2005) "Structural Performance of Bridge Approach Slab under Given Embankment Settlement." Journal of Bridge Engineering, ASCE, 10(4), 482-489.

Chini, S.A., Wolde-Tinsae, A.M., & Aggour, M.S. (1992). "Drainage and Backfill Provisions for Approaches to Bridges." University of Maryland, College Park.

Hoppe, E. J. (1999) "Guidelines for the use, design, and construction of bridge approach slabs", Virginia Transportation Research Council, final report VTRC 00-R4.

Kramer, S.L., & Sajer, P. (1991). "Bridge Approach Slab Effectiveness." Washington State Transportation Center, Seattle.

LaDOTD (2002) "Bridge Design Metric Manual." Louisiana Department of Transportation and Development, Baton Rouge, LA.

LQI (2002). Louisiana Quality Initiative: Preservation of Bridge Approach Ride Ability. Louisiana Department of transportation and Development, Baton Rouge, LA.

Mahmood, I. U. (1990). "Evaluation of Causes of Bridge Approach Settlement and Development of Settlement Prediction Models." Ph.D. Thesis, University of Oklahoma, Norman.

Ha, H., Seo, J. B., Briaud, J.L. (2003) "Investigation of Settlement at Bridge Approach Slab Expansion Joint: Survey and Site investigations", Report No. 4147-1 to the Texas Department of Transportation, published by the Texas Transportation Institute, Texas A&M University System.

Stewart, C.F. (1985). “Highway Structure Approaches.” California Department of Transportation, Sacramento.

Tadros, M.K., & Benak, J.V. (1989). “Bridge Abutment and Approach Slab Settlement (Phase1).” University of Nebraska, Lincoln.

Wahls, H. E. (1990) “Design and Construction of Bridge Approaches”, NCHRP Synthesis 159, Transportation Research Board, National Research Council, Washington, D.C.

Zaman, M., Gopalasingam, A. and Laguros, J. G. (1991). “Consolidation settlement of bridge approach foundation”, J. of Geotechnical Engineering, 117(2) 219-239.

CHAPTER 4 VEHICLE AND BRIDGE COUPLED MODEL

4.1 Introduction

Vibration that occurs in bridges can amplify the propagation of existing cracks resulting in further damage to the bridge, which reduces their life and render the structure unsafe for driving. Prediction of the dynamic responses of bridges resulting from moving vehicles is of significance because a moving vehicle may produce a larger response on the structure than a static vehicle does. Over the years there has been interest in modeling the interaction between bridge and vehicle to predict the dynamic response of this system.

The dynamic interaction between vehicle and bridge has been studied by many researchers since the middle of 19th century. Due to the limitation of computational capacity in early stage, only simplified vehicle-bridge models could be considered. For example, a moving load excluding the effect of inertia force was used to model a moving vehicle, and later a moving-mass model was used to consider the inertia force (Blejwas et al. 1979; Frayba 1973; Hino et al. 1984; Lin and Trethewey 1990). These two models, although capable, in many cases, of providing the designer with reasonable approximate solutions, neglect the dynamics of the moving vehicle. They are not applicable to the case of uneven bridge surface, which is known to be the main cause of high-magnitude bridge vibration. Nowadays, the vehicle load, the vehicle speed, and the traffic volume have increased considerably, and the configurations of vehicles have also changed dramatically. More sophisticated and rational models and computerized approaches are thus needed (Todd and Kulakowski, 1991, Gillespie and Karamihas 2000).

In bridge-vehicle coupled model, the interaction between bridge and vehicle is the key part because, as the vehicle moves over the bridge, the bridge and vehicle contact point changes. Among most previous researches, the contact condition is considered through iteration, in which the displacements at the contact points are assumed first (Green and Cebon 1994); the interacting forces between the vehicle tires and bridge are then calculated by solving the equations of motion of vehicles. These forces are in turn used in motion equations of the bridge to obtain the displacements of the contact points. In this method, the dynamic property matrices in equations of motion remain constant, and the convergence rate of the iteration is likely to be slow, especially when the bridge is subjected to a series of vehicles in motion and thus have many contact points. Moreover, it cannot model the separation of the vehicle tire from the bridge due to large irregularities of the bridge surface.

The present study developed a fully computerized approach to simulate the interaction of the coupled vehicle-bridge system. The vehicle model used in this study is a so-called 3-D suspension model (or full truck model) that includes both primary and secondary vehicle suspension systems. This is a more realistic model because it incorporates pitching, rotating, and yawing motions of the vehicle and also the variation of the axle force on the tires of each axle (Chatterjee et al. 1994, Xu and Guo 2004). The proposed approach uses the direct integration method to treat the interaction by updating the characteristic matrices according to the position of contact points at each time step. Therefore, the equations of motion are time dependent and they should be modified, updated, and solved by the Rounge-Kutta method (Bathe and Wilson 1976) at each time step. The road surface roughness is also taken into consideration in the analysis. It also considers the separation of the vehicle tire from the bridge due to large irregularities of the

road surface. Based on this methodology, a MATLAB program was developed to assemble and to solve the motion of equations using the method described previously. The developed program can be used to analyze not only the bridge-vehicle interaction, but also the interaction between vehicle and other infrastructures such as pavement. A case study of a real pavement with an AASHTO HS20-44 truck demonstrates that this fully computerized method provide an efficient and convenient tool for studying the interaction problems of infrastructures with moving vehicles.

4.2 Methodology

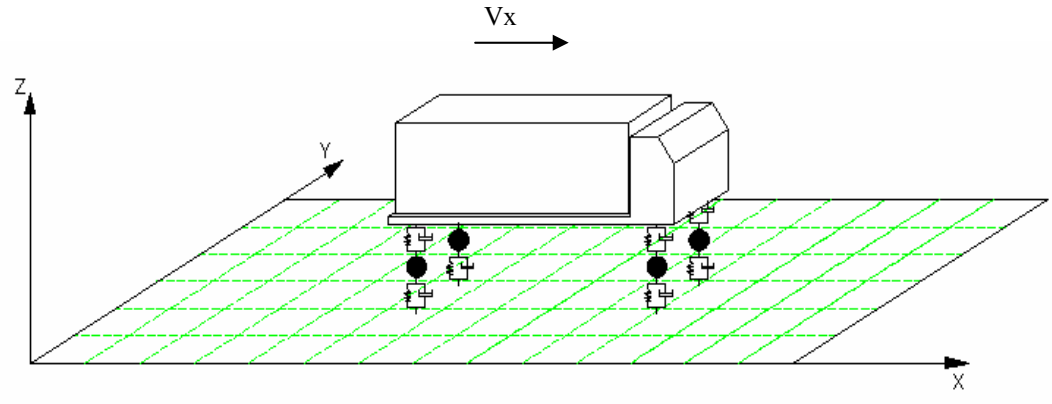

Fig. 4-1 Sketch of moving vehicle on bridge

In the present study, the vehicle-bridge coupled problem is firstly characterized by two sets of differential equations of motion, one for the bridge and the other for the vehicle. Then the two systems are coupled through the contact condition.

The vehicle is modeled as a combination of several rigid bodies connected by a series of springs and damping devices (Fig. 4-1). Vehicle bodies are represented by rigid bodies. The tires and suspension systems are idealized as linear elastic spring elements and dashpots. The contact between the bridge deck and the moving tire is assumed to be a point contact. The model can be used to simulate vehicles on highway roads or bridges with axle number varying from two to five. For demonstration purposes, a 5-axle articulated truck is shown in Fig. 4-2. The equation of motion for the vehicle is given by the following matrix form:

$$[M_v]\{\ddot{d}_v\} + [C_v]\{\dot{d}_v\} + [K_v]\{d_v\} = \{F_v{}^G\} + \{F_c\} \tag{4-1}$$

where $[M_v]$, $[C_v]$, and $[K_v]$ are mass matrix, damping matrix, and stiffness matrix, respectively; $\{F_v{}^G\}$ is the self-weight of vehicle; $\{F_c\}$ is the vector of wheel-road contact forces acting on the vehicle.

A three-dimensional dynamic model of the bridge can be obtained through finite element method using convenient elements. This allows the motion of the structure to be described by the system of equations:

$$[M_b]\{\ddot{d}_b\} + [C_b]\{\dot{d}_b\} + [K_b]\{d_b\} = \{F_b\} \tag{4-2}$$

where $\{F_b\}$ is the equivalent nodal force of wheel-bridge contact forces on bridge.

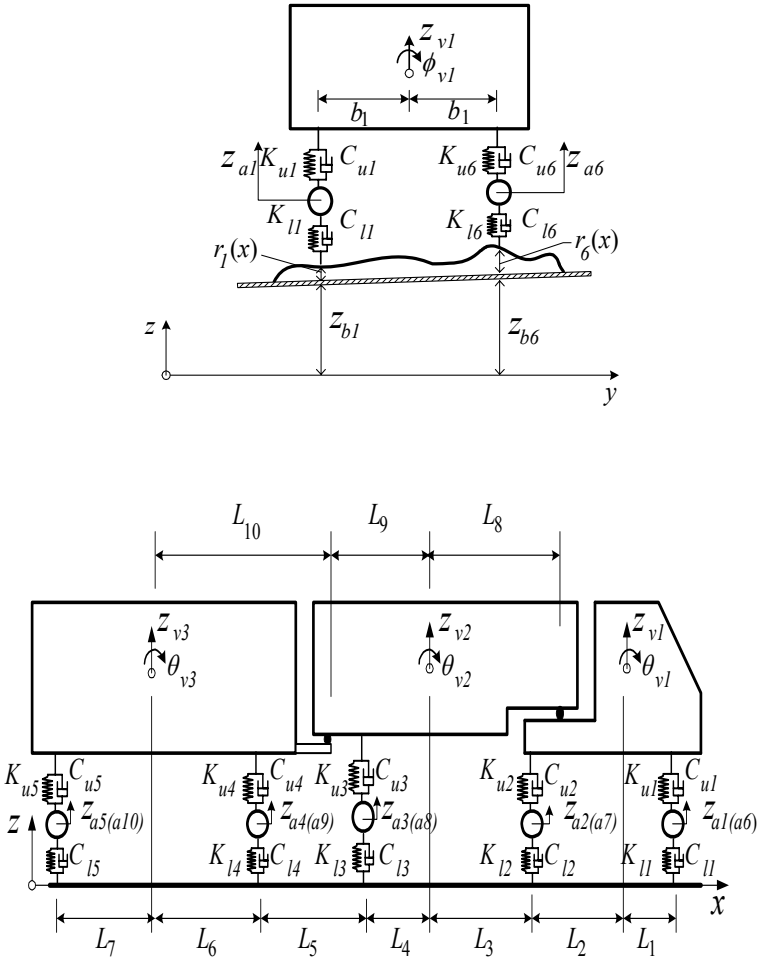

Fig. 4-2 Vehicle model

These two systems of motion equations for the vehicle and bridge are coupled through the contact condition, i.e., the interaction forces $\{F_b\}$ and $\{F_c\}$, which are action and reaction forces existing at the contact points of the two systems. To simulate bridge-vehicle interaction, Equation (4-1) is used for each vehicle; and Equation (4-2) for bridge in conjunction with:

(i) a relation among vehicle axle suspension displacement Z_a in vertical direction, displacement of bridge at wheel-road contact points Z_b, deformation of lower springs of vehicle Δ_L, and road surface profile $r(x)$ (as shown in Fig. 4-3):

$$\Delta_L = Z_a - Z_b - r(x) \tag{4-3}$$

$$\dot{\Delta}_L = \dot{Z}_a - \dot{Z}_b - \dot{r}(x) \tag{4-4}$$

in which $\dot{r}(x) = \frac{dr(x)}{dx}\frac{dx}{dt} = \frac{dr(x)}{dx}V(t)$, and *V(t)* is the vehicle velocity;

(ii) an expression for the bridge-vehicle contact forces as a function of deformation of vehicle lower spring:

$$\{F_b\} = -\{F_c\} = [K_L]\{\Delta_L\} + [C_L]\left\{\dot{\Delta}_L\right\} \tag{4-5}$$

where $[K_L]$ and $[C_L]$ are coefficients of vehicle lower spring and damper.

The mass matrices, damping matrices, and stiffness matrices of these two sets of systems and the coupled mass, damping, and stiffness matrices and the contact force vectors in Equations (4-1) through (4-5) will be automatically assembled using the fully computerized approach in the developed program. It will be explained in details in the following sections.

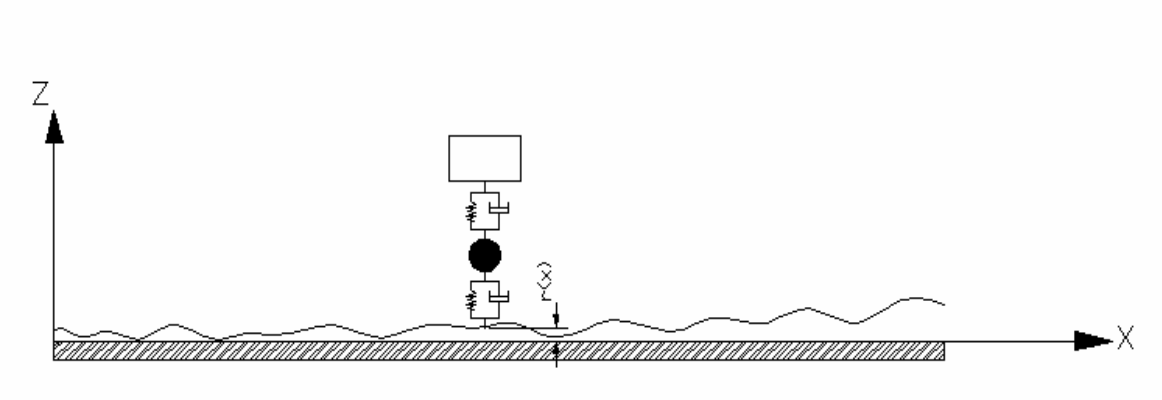

Fig. 4-3 Vehicle and bridge contact condition

4.2.1 Modeling of Vehicle

There are varieties of vehicle types in reality, including the tractor-trailers having different axle spacings. In the present study, the vehicle is modeled as a combination of several rigid bodies connected by a series of axle mass blocks, springs, dashpots, and pivots. For demonstration purpose, a five-axle vehicle model is shown in Fig.4-2. The vehicle bodies are represented by rigid bodies, and the centroid of each rigid body is treated as a node. The mass of axle set including suspensions and tires is lumped as idealized mass blocks on each side of the vehicle, and the center of mass block is also abstracted as a node. The suspension and tire systems are idealized as linear elastic spring elements and dashpots connecting one rigid body with one mass block (upper spring and dashpots in Fig. 4-2) or one mass block with one contact point (lower spring and dashpots in Fig. 4-2). The pivots may be used to connect the trailer to the tractor, for which the constraint equations will be developed accordingly. The coordinate system for the vehicle is as shown in Fig. 4-2. The X, Y, and Z axis are set in the longitudinal, lateral, and vertical directions of the bridge, respectively, following the right-hand rule.

To develop the three-dimensional model of a vehicle, the stiffness matrix, mass matrix, damping matrix, and force vector in Equation (4-1) should be first defined. The 5-axle

tractor-trailer shown in Fig. 4-2 is taken as an example vehicle in this section to demonstrate how the vehicle model is developed. The vehicle model consists of 3 rigid bodies: one for the tractor, two for two trailers, and 10 mass blocks for five axle sets (Fig. 4-2). On each side of an axle, the suspension system is represented by a vertical unit and a transverse unit, which connects the rigid body and the axle. The vertical unit comprises one spring (with stiffness of $K_{Uz}^{\ i}$, where U denotes the devices in upper position and i denotes the i^{th} axle) and one dashpot (with damping coefficient $C_{Uz}^{\ i}$) in Z direction. Similarly, the transverse unit contains one spring with stiffness of $K_{Uy}^{\ i}$ and one dashpot with damping coefficient of $C_{Uy}^{\ i}$ in Y direction. Two similar units (lower springs and dashpots), connecting the axle and the bridge deck, are also used to simulate the dynamic characteristics of the tire.

In general, there are six degrees of freedom at each node, representing the vehicle body in Fig. 4-2: three translational degrees and three rotational degrees. The corresponding displacements and rotations are assumed to remain small throughout the analysis so that the cosine of the rotation angles may be taken as unity and the sine of the angles may be taken equal to angles themselves. For the nodes of mass block denoting the axle suspensions and tires, only three translation degrees are considered because the dimension of suspensions and tires, compared to the volume of vehicle body, is relatively small and ignorable.

If only the lateral and vertical vibration of the vehicle are considered, the vehicle rigid body has only five degrees of freedom, and the mass block has only two degrees of freedom. The displacement of mass block at j^{th} axle are represented by: lateral displacement $Y_{val}^{\ j}$ and $Y_{var}^{\ j}$, and vertical displacement $Z_{val}^{\ j}$ and $Z_{var}^{\ j}$, where the subscription "*va*" denotes the vehicle axle and the subscriptions "*l*" and "*r*" denote the left and right side of the vehicle, respectively. The displacements of the i^{th} rigid body of the vehicle are expressed as: lateral displacement $Y_{vr}^{\ i}$, vertical displacement $Z_{vr}^{\ i}$, rolling displacement about the longitudinal axis $\Phi_{vr}^{\ i}$, pitching displacement about the lateral axis $\theta_{vr}^{\ i}$, and yawing displacement about the vertical axis $\varphi_{vr}^{\ i}$, in which the subscript "*vr*" represents the vehicle rigid body. In addition, four constraint equations as follows should be considered because there are two pivots connecting the three rigid bodies.

$$\begin{cases} Z_{vr}^{\ 1} + \theta_{vr}^{\ 1} L_8 = Z_{vr}^{\ 2} - \theta_{vr}^{\ 2} L_9 \\ Z_{vr}^{\ 2} + \theta_{vr}^{\ 2} L_{10} = Z_{vr}^{\ 3} - \theta_{vr}^{\ 3} L_{11} \\ Y_{vr}^{\ 1} - \varphi_{vr}^{\ 1} L_8 = Y_{vr}^{\ 2} + \varphi_{vr}^{\ 2} L_9 \\ Y_{vr}^{\ 2} - \varphi_{vr}^{\ 2} L_{10} = Y_{vr}^{\ 3} + \varphi_{vr}^{\ 3} L_{11} \end{cases} \tag{4-6}$$

Therefore, the total degrees of freedom of the entire vehicle are not 35 but only 31. The displacement vector of the five-axle vehicle, i.e. the *{dv}* defined in Equation (4-1), can be written as

$$\begin{aligned} \{d_v\} = \{ & Y_{val}^{\ 1}\ Z_{val}^{\ 1}\ Y_{\mathrm{var}}^{\ 1}\ Z_{\mathrm{var}}^{\ 1}\ Y_{val}^{\ 2}\ Z_{val}^{\ 2}\ Y_{\mathrm{var}}^{\ 2}\ Z_{\mathrm{var}}^{\ 2}\ Y_{val}^{\ 3}\ Z_{val}^{\ 3}\ Y_{\mathrm{var}}^{\ 3}\ Z_{\mathrm{var}}^{\ 3}\ Y_{val}^{\ 4}\ Z_{val}^{\ 4}\ Y_{\mathrm{var}}^{\ 4}\ Z_{\mathrm{var}}^{\ 4} \\ & Y_{val}^{\ 5}\ Z_{val}^{\ 5}\ Y_{\mathrm{var}}^{\ 5}\ Z_{\mathrm{var}}^{\ 5}\ Y_{vr}^{\ 1}\ Z_{vr}^{\ 1}\ \phi_{vr}^{\ 1}\ Y_{vr}^{\ 2}\ Z_{vr}^{\ 2}\ \phi_{vr}^{\ 2}\ Y_{vr}^{\ 3}\ Z_{vr}^{\ 3}\ \phi_{vr}^{\ 3}\ \theta_{vr}^{\ 1}\ \varphi_{vr}^{\ 1}\ \}^T \end{aligned} \tag{4-7}$$

Based on the given geometric condition in Fig. 4-2, the deformation of each upper spring is as follows.

$$
\begin{cases}
\Delta_{U\_Zl}{}^{1} = Z_{vr}{}^{1} - L_1\theta_{vr}{}^{1} + b\phi_{vr}{}^{1} - Z_{val}{}^{1} \\
\Delta_{U\_Zr}{}^{1} = Z_{vr}{}^{1} - L_1\theta_{vr}{}^{1} - b\phi_{vr}{}^{1} - Z_{\mathrm{var}}{}^{1} \\
\Delta_{U\_Yl}{}^{1} = Y_{val}{}^{1} - (Y_{vr}{}^{1} + L_1\varphi_{vr}{}^{1}) \\
\Delta_{U\_Yr}{}^{1} = Y_{\mathrm{var}}{}^{1} - (Y_{vr}{}^{1} + L_1\varphi_{vr}{}^{1}) \\
\\
\Delta_{U\_Zl}{}^{2} = Z_{vr}{}^{1} + L_2\theta_{vr}{}^{1} + b\phi_{vr}{}^{1} - Z_{val}{}^{2} \\
\Delta_{U\_Zr}{}^{2} = Z_{vr}{}^{1} + L_1\theta_{vr}{}^{1} - b\phi_{vr}{}^{1} - Z_{\mathrm{var}}{}^{2} \\
\Delta_{U\_Yl}{}^{2} = Y_{val}{}^{2} - (Y_{vr}{}^{1} - L_2\varphi_{vr}{}^{1}) \\
\Delta_{U\_Yr}{}^{2} = Y_{\mathrm{var}}{}^{2} - (Y_{vr}{}^{1} - L_2\varphi_{vr}{}^{1}) \\
\\
\Delta_{U\_Zl}{}^{3} = Z_{vr}{}^{2} + L_4\theta_{vr}{}^{2} + b\phi_{vr}{}^{2} - Z_{val}{}^{3} \\
\Delta_{U\_Zr}{}^{3} = Z_{vr}{}^{2} + L_4\theta_{vr}{}^{1} - b\phi_{vr}{}^{2} - Z_{\mathrm{var}}{}^{3} \\
\Delta_{U\_Yl}{}^{3} = y_{val}{}^{3} - (y_{vr}{}^{2} - L_4\varphi_{vr}{}^{2}) \\
\Delta_{U\_Yr}{}^{3} = y_{\mathrm{var}}{}^{3} - (y_{vr}{}^{2} - L_4\varphi_{vr}{}^{2}) \\
\\
\Delta_{U\_Zl}{}^{4} = Z_{vr}{}^{3} - L_6\theta_{vr}{}^{3} + b\phi_{vr}{}^{3} - Z_{val}{}^{4} \\
\Delta_{U\_Zr}{}^{4} = Z_{vr}{}^{3} - L_6\theta_{vr}{}^{3} - b\phi_{vr}{}^{3} - Z_{\mathrm{var}}{}^{4} \\
\Delta_{U\_Yl}{}^{4} = Y_{val}{}^{4} - (Y_{vr}{}^{3} + L_6\varphi_{vr}{}^{3}) \\
\Delta_{U\_Yr}{}^{4} = Y_{\mathrm{var}}{}^{4} - (Y_{vr}{}^{3} + L_6\varphi_{vr}{}^{3}) \\
\\
\Delta_{U\_Zl}{}^{5} = Z_{vr}{}^{3} + L_7\theta_{vr}{}^{3} + b\phi_{vr}{}^{3} - Z_{val}{}^{5} \\
\Delta_{U\_Zr}{}^{5} = Z_{vr}{}^{3} + L_7\theta_{vr}{}^{3} - b\phi_{vr}{}^{3} - Z_{\mathrm{var}}{}^{5} \\
\Delta_{U\_Yl}{}^{5} = Y_{val}{}^{5} - (Y_{vr}{}^{3} - L_7\varphi_{vr}{}^{3}) \\
\Delta_{U\_Yr}{}^{5} = Y_{\mathrm{var}}{}^{5} - (Y_{vr}{}^{3} - L_7\varphi_{vr}{}^{3})
\end{cases}
\tag{4-8}
$$

Substitute the constraint conditions in Equation (4-6) into the above equations of spring deformation, the relation of spring deformation and vehicle displacement is as follows:

$$
\begin{cases}
\Delta_{U\_Zl}{}^{1} = -Z_{val}{}^{1} + Z_{vr}{}^{1} + b\phi - L_1\theta_{vr}{}^{1}{}_{vr}{}^{1} \\
\Delta_{U\_Zr}{}^{1} = -Z_{\mathrm{var}}{}^{1} + Z_{vr}{}^{1} - b\phi_{vr}{}^{1} - L_1\theta_{vr}{}^{1} \\
\Delta_{U\_Yl}{}^{1} = Y_{val}{}^{1} - (Y_{vr}{}^{1} + L_1\varphi_{vr}{}^{1}) \\
\Delta_{U\_Yr}{}^{1} = Y_{\mathrm{var}}{}^{1} - (Y_{vr}{}^{1} + L_1\varphi_{vr}{}^{1}) \\
\Delta_{U\_Zl}{}^{2} = -Z_{val}{}^{2} + Z_{vr}{}^{1} + b\phi_{vr}{}^{1} + L_2\theta_{vr}{}^{1} \\
\Delta_{U\_Zr}{}^{2} = -Z_{\mathrm{var}}{}^{2} + Z_{vr}{}^{1} - b\phi_{vr}{}^{1} + L_1\theta_{vr}{}^{1} \\
\Delta_{U\_Yl}{}^{2} = Y_{val}{}^{2} - Y_{vr}{}^{1} + L_2\varphi_{vr}{}^{1} \\
\Delta_{U\_Yr}{}^{2} = Y_{\mathrm{var}}{}^{2} - Y_{vr}{}^{1} + L_2\varphi_{vr}{}^{1} \\
\Delta_{U\_Zl}{}^{3} = -Z_{val}{}^{3} - \dfrac{L_4}{L_9}Z_{vr}{}^{1} + \dfrac{L_4+L_9}{L_9}Z_{vr}{}^{2} + b\phi_{vr}{}^{2} - \dfrac{L_4L_8}{L_9}\theta_{vr}{}^{1} \\
\Delta_{U\_Zr}{}^{3} = -Z_{\mathrm{var}}{}^{3} - \dfrac{L_4}{L_9}Z_{vr}{}^{1} + \dfrac{L_4+L_9}{L_9}Z_{vr}{}^{2} - b\phi_{vr}{}^{2} - \dfrac{L_4L_8}{L_9}\theta_{vr}{}^{1} \\
\Delta_{U\_Yl}{}^{3} = Y_{val}{}^{3} + \dfrac{L_4}{L_9}Y_{vr}{}^{1} - \dfrac{L_4+L_9}{L_9}Y_{vr}{}^{2} - \dfrac{L_4L_8}{L_9}\varphi_{vr}{}^{1} \\
\Delta_{U\_Yr}{}^{3} = Y_{\mathrm{var}}{}^{3} + \dfrac{L_4}{L_9}Y_{vr}{}^{1} - \dfrac{L_4+L_9}{L_9}Y_{vr}{}^{2} - \dfrac{L_4L_8}{L_9}\varphi_{vr}{}^{1} \\
\Delta_{U\_Zl}{}^{4} = -Z_{val}{}^{4} - \dfrac{L_6L_{10}}{L_9L_{11}}Z_{vr}{}^{1} + \dfrac{L_6(L_9+L_{10})}{L_9L_{11}}Z_{vr}{}^{2} + \dfrac{L_{11}-L_6}{L_{11}}Z_{vr}{}^{3} + b\phi_{vr}{}^{3} - \dfrac{L_6L_8L_{10}}{L_9L_{11}}\theta_{vr}{}^{1} \\
\Delta_{U\_Zr}{}^{4} = -Z_{\mathrm{var}}{}^{4} - \dfrac{L_6L_{10}}{L_9L_{11}}Z_{vr}{}^{1} + \dfrac{L_6(L_9+L_{10})}{L_9L_{11}}Z_{vr}{}^{2} + \dfrac{L_{11}-L_6}{L_{11}}Z_{vr}{}^{3} - b\phi_{vr}{}^{3} - \dfrac{L_6L_8L_{10}}{L_9L_{11}}\theta_{vr}{}^{1} \\
\Delta_{U\_Yl}{}^{4} = Y_{val}{}^{4} + \dfrac{L_6L_{10}}{L_9L_{11}}Y_{vr}{}^{1} - \dfrac{L_6(L_9+L_{10})}{L_9L_{11}}Y_{vr}{}^{2} - \dfrac{L_{11}-L_6}{L_{11}}Y_{vr}{}^{3} - \dfrac{L_6L_8L_{10}}{L_9L_{11}}\varphi_{vr}{}^{1} \\
\Delta_{U\_Yr}{}^{4} = Y_{\mathrm{var}}{}^{4} + \dfrac{L_6L_{10}}{L_9L_{11}}Y_{vr}{}^{1} - \dfrac{L_6(L_9+L_{10})}{L_9L_{11}}Y_{vr}{}^{2} - \dfrac{L_{11}-L_6}{L_{11}}Y_{vr}{}^{3} - \dfrac{L_6L_8L_{10}}{L_9L_{11}}\varphi_{vr}{}^{1} \\
\Delta_{U\_Zl}{}^{5} = -Z_{val}{}^{5} + \dfrac{L_7L_{10}}{L_9L_{11}}Z_{vr}{}^{1} - \dfrac{L_7(L_9+L_{10})}{L_9L_{11}}Z_{vr}{}^{2} + \dfrac{L_{11}+L_7}{L_{11}}Z_{vr}{}^{3} + b\phi_{vr}{}^{3} + \dfrac{L_7L_8L_{10}}{L_9L_{11}}\theta_{vr}{}^{1} \\
\Delta_{U\_Zr}{}^{5} = -Z_{\mathrm{var}}{}^{5} + \dfrac{L_7L_{10}}{L_9L_{11}}Z_{vr}{}^{1} - \dfrac{L_7(L_9+L_{10})}{L_9L_{11}}Z_{vr}{}^{2} + \dfrac{L_{11}+L_7}{L_{11}}Z_{vr}{}^{3} - b\phi_{vr}{}^{3} + \dfrac{L_7L_8L_{10}}{L_9L_{11}}\theta_{vr}{}^{1} \\
\Delta_{U\_Yl}{}^{5} = Y_{val}{}^{5} - \dfrac{L_7L_{10}}{L_9L_{11}}Y_{vr}{}^{1} + \dfrac{L_7(L_9+L_{10})}{L_9L_{11}}Y_{vr}{}^{2} - \dfrac{L_{11}-L_7}{L_{11}}Y_{vr}{}^{3} + \dfrac{L_7L_8L_{10}}{L_9L_{11}}\varphi_{vr}{}^{1} \\
\Delta_{U\_Yr}{}^{5} = Y_{\mathrm{var}}{}^{5} - \dfrac{L_7L_{10}}{L_9L_{11}}Y_{vr}{}^{1} + \dfrac{L_7(L_9+L_{10})}{L_9L_{11}}Y_{vr}{}^{2} - \dfrac{L_{11}-L_7}{L_{11}}Y_{vr}{}^{3} + \dfrac{L_7L_8L_{10}}{L_9L_{11}}\varphi_{vr}{}^{1}
\end{cases}
\tag{4-9}
$$

The above equations can be represented by the following matrix format:

$$\{\Delta_{upper}\} = \{\Delta_{U\_Yl}^{1}\ \Delta_{U\_Yr}^{1}\ \Delta_{U\_Zl}^{1}\ \Delta_{U\_Zr}^{1}\ \Delta_{U\_Yl}^{2}\ \Delta_{U\_Yr}^{2}\ \Delta_{U\_Zl}^{2}\ \Delta_{U\_Zr}^{2}\ \Delta_{U\_Yl}^{3}\ \Delta_{U\_Yr}^{3}\ \Delta_{U\_Zl}^{3}\ \Delta_{U\_Zr}^{3}\ \Delta_{U\_Yl}^{4}\ \Delta_{U\_Yr}^{4}\ \Delta_{U\_Zl}^{4}\ \Delta_{U\_Zr}^{4}\ \Delta_{U\_Yl}^{5}\ \Delta_{U\_Yr}^{5}\ \Delta_{U\_Zl}^{5}\ \Delta_{U\_Zr}^{5}\}^{T} = [N_v]\{d_v\} \quad (4\text{-}10)$$

where $[N_v]$ is the matrix obtained from Equation (4-9), expressing the relation between the vehicle displacement at each degree of freedom and the deformation of the each springs.

The motion equations of vehicle are generally obtained by using either the principle of virtual work or D'alembert's principle or the Hamilton's principle. In this study, the virtual work principle is used to derive Equation (4-1). The virtual work is given by

$$\{\delta W_{VI}\} = \{\delta d_v\}^T [M_v]\{\ddot{d}_v\} \quad (4\text{-}11)$$

$$\{\delta W_{VD\_upper}\} = \{\delta\Delta_{upper}\}^T [C_{upper\_dashpot}]\left\{\dot{\Delta}_{upper}\right\} = \{\delta d_v\}^T [N_v]^T [C_{upper\_dashpot}][N_v]\left\{\dot{d}_v\right\} = \{\delta d_v\}^T [C_{v\_upper}]\left\{\dot{d}_v\right\} \quad (4\text{-}12)$$

$$\{\delta W_{VE\_upper}\} = \{\delta\Delta_{upper}\}^T [K_{upper\_spring}]\{\Delta_{upper}\} = \{\delta d_v\}^T [N_v]^T [K_{upper\_spring}][N_v]\{d_v\} = \{\delta d_v\}^T [K_{v\_upper}]\{d_v\} \quad (4\text{-}13)$$

where $\{\delta W_{VI}\}$, $\{\delta W_{VI}\}$, and $\{\delta W_{VI}\}$ are virtual work done by inertial forces, damping forces of upper dashpots, and spring forces of upper springs, respectively; $[M_v]$ is the matrix of vehicle mass and the mass moment of inertia computed from the weight distribution and dimension of the vehicle at each node; $[C_{upper\_dashpot}]$ and $[C_{v\_upper}]$ are damping matrices corresponding to upper dashpot deformation and vehicle displacement at each degree of freedom, respectively. Similarly, $[K_{upper\text{-}spring}]$ and $[K_{v\_upper}]$ are stiffness matrices. The virtual work done by the contact force between the vehicle and the bridge, the elastic and damping force of vehicle lower springs and dashpots in Equation (4-5), is discussed in the following sections.

4.2.2 Modeling of Bridge

The bridge can be modeled by using different types of elements such as beam element, plate element, and solid element, depending on the bridge type. The mass matrix and stiffness matrix can be obtained by the conventional finite element method. To simplify the modeling procedure in bridge-vehicle coupled system, the bridge mode superposition technique is used. The bridge mode shape $\{\Phi_i\}$ and the corresponding natural circular frequencies ω_i are firstly obtained from bridge modal analysis by using conventional finite element software such as ANSYS. The bridge dynamic response $\{d_b\}$ can be expressed as:

$$\{d_b\} = [\{\Phi_1\}\ \ \{\Phi_2\}\ldots\{\Phi_n\}]\{\xi_1\ \ \xi_2\cdots\xi_n\}^T = [\Phi_b]\{\xi_b\} \quad (4\text{-}14)$$

where n is the total number of modes for the bridge under consideration; $\{\Phi_i\}$ and ξ_i are the i^{th} mode shape and its generalized coordinates. Each mode shape is normalized such that $\{\Phi_i\}^T[M_b]\{\Phi_i\}=1$ and $\{\Phi_i\}^T[K_b]\{\Phi_i\}=\omega_i^2$. The damping matrix $[C_b]$ is assumed to be $2\omega_i\eta_i[M_b]$,

where ω_i denotes the natural circular frequency of the bridge and η_i is the percentage of the critical damping for the bridge's i^{th} mode. Equation (4-2) can be rewritten as:

$$[I]\left\{\ddot{\xi}_b\right\}+[2\omega_i\eta_i I]\left\{\dot{\xi}_b\right\}+\left[\omega_i{}^2 I\right]\{\xi_b\}=[\Phi_b]\left\{F_b{}^N\right\} \tag{4-15}$$

The mode superposition approach makes it possible to separate the bridge modal analysis from vehicle-bridge coupled model. Consequently, the coupled vehicle-bridge system vectors contain the modal components of the bridge rather than its physical components, and the physical components of the vehicles. The degrees of freedom, the number of equations in Eq. (4-2), and the complexity of the whole procedure are greatly reduced.

In terms of finite element method, the interaction force between vehicle tire and bridge deck may not apply at element node as the vehicle passes over the bridge. Therefore, the interaction force, i.e. $\{F_b\}$ in equation (4-2), needs to be transformed to equivalent nodal force ($\{F_b{}^N\}$) in the analysis. A bridge deck of solid elements shown in Fig.4-4 is taken as an example in order to demonstrate how the contact force is transformed to the equivalent nodal force.

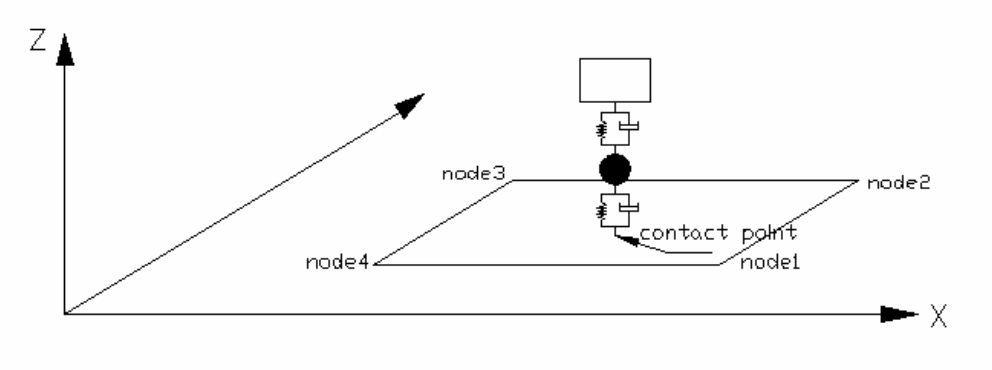

Fig. 4-4 Interaction at a contact point

According to the virtual work principle, the works done by equivalent nodal force and actual force should be equal:

$$\{d_{b\_nodal}\}^T\left\{F_b{}^N\right\}=\{d_{b\_contact}\}^T\{F_b\}=([N_b]\{d_{b\_nodal}\})^T\{F_b\}=\{d_{b\_nodal}\}^T([N_b]^T\{F_b\}) \tag{4-16}$$

$$\left\{F_b{}^N\right\}=[N_b]^T\{F_b\} \tag{4-17}$$

where $\{d_{b\_nodal}\}$ is the bridge deck nodal displacement, $\{d_{b\_contact}\}$ is the displacement of bridge-vehicle contact points, and $[N_b]$ is the shape function of the bridge deck element.

4.2.3 Road Surface Condition

The road surface profile is an important factor that affects the dynamic responses of both the bridge and vehicles. Road surface profile is simulated in space domain and acts as an input to the bridge-vehicle model. To take into account the effect of approach slab deformation on the interaction of bridge and vehicle, the road profile needs to contain this deformation as well as the road roughness of the whole roadway (including bridge deck and approach slab), because the latter cannot represent the local unevenness of the expansion joints and slope change at the slab end due to large deformation of the approach slab.

The road surface roughness can be described as a realization of a random process that can be described by its power spectral density (PSD) (Dodds and Robson 1973). A concise spectral model is used in this study as:

$$\varphi(n) = \varphi(n_0)(\frac{n}{n_0})^{-2} \qquad (n_1 < n < n_2) \tag{4-18}$$

where φ(n) is the PSD function (m^3/cycle/m) for the road surface elevation; n is the spatial frequency (cycle/m); n_0 is the discontinuity frequency of 1/2π (cycle/m); and $\varphi(n_0)$ is the roughness coefficient (m^3/cycle) whose value is chosen depending on the road condition; n_1 and n_2 are lower and upper cut-off frequencies. In this study, classification of road roughness based on the International Organization for Standardization (ISO 1995) is used. The ISO has proposed road roughness classification (Classes A (very good) to H (very poor)) according to different values of $\varphi(n_0)$.

The road surface roughness is assumed to be a zero-mean stationary Gaussian random process. It can be generated through an inverse Fourier transformation as:

$$r(X) = \sum_{k=1}^{N} \sqrt{2\varphi(n_k)\Delta n}\cos(2\pi n_k X + \theta_k) \tag{4-19}$$

where θ_k is the random phase angle uniformly distributed from 0 to 2π.

4.2.4 Assembling of Bridge-Vehicle Motion Equation

Since the interaction force is on the bridge deck, the equivalent nodal force only applies to the nodes on the deck. For the solid element shown in Fig. 4-4, the degree of freedom of each node is $\{x, y, z\}^T$. For the contact point *i*, the equations of compatible displacement (Equations (4-3) and (4-4)) are rewritten in matrix form as follows:

$$\begin{Bmatrix} \Delta_{L\_Y} \\ \Delta_{L\_Z} \end{Bmatrix}^i = \begin{Bmatrix} Y_{va} \\ Z_{va} \end{Bmatrix}^i - \left(\begin{Bmatrix} Y_{b\_contact} \\ Z_{b\_contact} \end{Bmatrix}^i + \begin{Bmatrix} 0 \\ r(X) \end{Bmatrix}^i \right) \tag{4-20}$$

$$\begin{Bmatrix} \dot{\Delta}_{L\_Y} \\ \dot{\Delta}_{L\_Z} \end{Bmatrix}^i = \begin{Bmatrix} \dot{Y}_{va} \\ \dot{Z}_{va} \end{Bmatrix}^i - \left(\begin{Bmatrix} \dot{Y}_{b\_contact} \\ \dot{Z}_{b\_contact} \end{Bmatrix}^i + \begin{Bmatrix} 0 \\ \dot{r}(X) \end{Bmatrix}^i \right) = \begin{Bmatrix} \dot{Y}_{va} \\ \dot{Z}_{va} \end{Bmatrix}^i - \left(\begin{Bmatrix} \dot{Y}_{b\_contact} \\ \dot{Z}_{b\_contact} \end{Bmatrix}^i + \begin{Bmatrix} 0 \\ \frac{dr(X)}{dX}\frac{dX}{dt} \end{Bmatrix}^i \right) \tag{4-21}$$

In bridge model, the contact point is not necessarily at the node. To get the local displacement of contact point the shape function of bridge deck element is used:

$$\begin{Bmatrix} Y_{b\_contact} \\ Z_{b\_contact} \end{Bmatrix}^i = [N_b]^i \{d_{b\_nodal}\}^i \tag{4-22}$$

where $\{d_{b\_nodal}\}$ is the nodal displacement of element for each contact point. Then the contact force at contact position *i* is:

$$\{F_{contact}\}^i = \begin{bmatrix} K_{LY}{}^i & \\ & K_{LZ}{}^i \end{bmatrix} \begin{Bmatrix} \Delta_{L\_Y}{}^i \\ \Delta_{L\_Z}{}^i \end{Bmatrix} + \begin{bmatrix} C_{LY}{}^i & \\ & C_{LZ}{}^i \end{bmatrix} \begin{Bmatrix} \dot{\Delta}_{L\_Y}{}^i \\ \dot{\Delta}_{L\_Z}{}^i \end{Bmatrix}$$
$$= \begin{bmatrix} K_{LY}{}^i & \\ & K_{LZ}{}^i \end{bmatrix} \left(\begin{Bmatrix} Y_{va}{}^i \\ Z_{va}{}^i \end{Bmatrix} - [N_b{}^i] \{d_{b\_nodal}{}^i\} - \begin{Bmatrix} 0 \\ r(X)^i \end{Bmatrix} \right) \quad (4\text{-}23)$$
$$+ \begin{bmatrix} C_{LY}{}^i & \\ & C_{LZ}{}^i \end{bmatrix} \left(\begin{Bmatrix} \dot{Y}_{va}{}^i \\ \dot{Z}_{va}{}^i \end{Bmatrix} - \frac{d[N_b{}^i]}{dX}\frac{dX}{dt}\{d_{b\_nodal}{}^i\} - [N_b{}^i]\{\dot{d}_{b\_nodal}{}^i\} - \begin{Bmatrix} 0 \\ \frac{dr(X)^i}{dX}\frac{dX}{dt} \end{Bmatrix} \right)$$

Contact force of contact position *i* on vehicle: $\{F_{contact}\}_v{}^i = -\{F_{contact}\}^i$. For a vehicle with n contact points, the total contact forces in the direction of vehicle d.o.f. are:

$$\{F_{contact}\}_v = \sum_{i=1}^{n} \begin{bmatrix} K_{LY}{}^i & \\ & K_{LZ}{}^i \end{bmatrix} \left(-\begin{Bmatrix} Y_{va}{}^i \\ Z_{va}{}^i \end{Bmatrix} + [N_b{}^i]\{d_{b\_nodal}{}^i\} + \begin{Bmatrix} 0 \\ r(X)^i \end{Bmatrix} \right)$$
$$- \sum_{i=1}^{n} \begin{bmatrix} C_{LY}{}^i & \\ & C_{LZ}{}^i \end{bmatrix} \left(\begin{Bmatrix} \dot{Y}_{va}{}^i \\ \dot{Z}_{va}{}^i \end{Bmatrix} - \frac{d[N_b{}^i]}{dX}\frac{dX}{dt}\{d_{b\_nodal}{}^i\} - [N_b{}^i]\{\dot{d}_{b\_nodal}{}^i\} - \begin{Bmatrix} 0 \\ \frac{dr(X)^i}{dX}\frac{dX}{dt} \end{Bmatrix} \right) \quad (4\text{-}24)$$
$$= -[K_{v\_lower}]\{d_v\} + [K_{v\_b}]\{d_b\} + \{F_{ev\_r}\}_v - [C_{v\_lower}]\{\dot{d}_v\} + [K_{cv\_vb}]\{d_b\} + [C_{v\_b}]\{\dot{d}_b\} + \{F_{cv\_r}\}_v$$

During the deduction of the above equation, the local bridge nodal displacement has been transformed into global bridge nodal displacement by tracing the element where each contact point locates in the whole bridge model. Since the vehicle is moving on the bridge, the contact position changes with time, so $[N_b{}^i]$, $\{d_{b\_nodal}{}^i\}$, $r(X)$ are time dependent. Consequently, $[K_{v\_b}]$, $\{F_{ev\_r}\}_v$, $[K_{cv\_vb}]$, $[C_{v\_b}]$ and $\{F_{cv\_r}\}_v$ are all time dependent terms.

Contact force of contact position *i* on bridge: $\{F_{contact}\}_b{}^i = \{F_{contact}\}^i$. The contact force is not necessarily acting on element nodes in bridge FE model. Therefore the force needs to be transformed into equivalent nodal force by using the shape function:

$$\{F_b{}^N\}^i = [N_b{}^i]^T \{F_{contact}\}_b{}^i = [N_b{}^i]^T \{F_{contact}\}^i \quad (4\text{-}25)$$

For a vehicle with *n* contact points, the total contact forces on the bridge are:

$$\{F_b{}^N\} = \sum_{i=1}^{n} [N_b{}^i]^T \begin{bmatrix} K_{LY}{}^i & \\ & K_{LZ}{}^i \end{bmatrix} \left(\begin{Bmatrix} Y_{va}{}^i \\ Z_{va}{}^i \end{Bmatrix} - [N_b{}^i]\{d_{b\_nodal}{}^i\} - \begin{Bmatrix} 0 \\ r(X)^i \end{Bmatrix} \right)$$
$$+ \sum_{i=1}^{n} [N_b{}^i]^T \begin{bmatrix} C_{LY}{}^i & \\ & C_{LZ}{}^i \end{bmatrix} \left(\begin{Bmatrix} \dot{Y}_{va}{}^i \\ \dot{Z}_{va}{}^i \end{Bmatrix} - \frac{d[N_b{}^i]}{dX}\frac{dX}{dt}\{d_{b\_nodal}{}^i\} - [N_b{}^i]\{\dot{d}_{b\_nodal}{}^i\} - \begin{Bmatrix} 0 \\ \frac{dr(X)^i}{dX}\frac{dX}{dt} \end{Bmatrix} \right) \quad (4\text{-}26)$$
$$= [K_{b\_v}]\{d_v\} - [K_{ev\_bb}]\{d_b\} - \{F_{ev\_r}\}_b + [C_{b\_v}]\{\dot{d}_v\} - [K_{cv\_bb}]\{d_b\} - [C_{cv\_bb}]\{\dot{d}_b\} - \{F_{cv\_r}\}_b$$

where $[N_b{}^i]$, $\{d_{b\_local}{}^i\}$, $r(X)$ are time dependent, similar to Eq. (4-24). And $[K_{b\_v}]$, $[K_{ev\_bb}]$, $\{F_{ev\_r}\}_b$, $[C_{b\_v}]$, $[K_{ev\_bb}]$, $[C_{cv\_bb}]$ and $\{F_{cv\_r}\}_b$ are all time dependent terms as well. For the case of multiple vehicles on a bridge, the total contact forces on the bridge can be accumulated by the above equation for all vehicles.

By substituting contact forces into Eqs. (4-1) and (4-2), the equations of motion become:

$$\begin{aligned}[M_v]\{\ddot{d}_v\}+[C_{v\_upper}]\{\dot{d}_v\}+[K_{v\_upper}]\{d_v\}&=-\{F^G\}_v+\{F_{contact}\}_v\\ &=-\{F^G\}_v-[K_{v\_lower}]\{d_v\}+[K_{v\_b}]\{d_b\}+\{F_{ev\_r}\}_v-[C_{v\_lower}]\{\dot{d}_v\}+[K_{cv\_vb}]\{d_b\}+[C_{v\_b}]\{\dot{d}_b\}+\{F_{cv\_r}\}_v\end{aligned} \tag{4-27}$$

$$\begin{aligned}[M_b]\{\ddot{d}_b\}+[C_b]\{\dot{d}_b\}+[K_b]\{d_b\}&=\{F_b^N\}\\ &=[K_{b\_v}]\{d_v\}-[K_{ev\_bb}]\{d_b\}-\{F_{ev\_r}\}_b+[C_{b\_v}]\{\dot{d}_v\}-[K_{cv\_bb}]\{d_b\}-[C_{cv\_bb}]\{\dot{d}_b\}-\{F_{cv\_r}\}_b\end{aligned} \tag{4-28}$$

These two equations can be combined as follows.

$$\begin{bmatrix}M_b & \\ & M_v\end{bmatrix}\begin{Bmatrix}\ddot{d}_b\\ \ddot{d}_v\end{Bmatrix}+\begin{bmatrix}C_b+C_{bb} & C_{bv}\\ C_{vb} & C_v\end{bmatrix}\begin{Bmatrix}\dot{d}_b\\ \dot{d}_v\end{Bmatrix}+\begin{bmatrix}K_b+K_{bb} & K_{bv}\\ K_{vb} & K_v\end{bmatrix}\begin{Bmatrix}d_b\\ d_v\end{Bmatrix}=\begin{Bmatrix}F_b^r\\ F_v^r+F_v^G\end{Bmatrix} \tag{4-29}$$

In comparison with equations (4-1) and (4-2), there are additional terms C_{bb}, C_{bv}, C_{vb}, K_{bb}, K_{bv}, K_{vb}, F_{br} and F_v^r in equation (4-29), which are due to expansion of the contact force. When the vehicle is moving across the bridge, the bridge-vehicle contact points change with the vehicle position. Then the road roughness r(x) at the contact point changes as well. Consequently, the contact force between the bridge and vehicle changes, indicating that the additional terms in equation (4-29) are time dependent terms and will change as the vehicle moves across the bridge.

The mode superposition makes it possible to separate the bridge modal analysis from vehicle-bridge coupled model. Equation (4-29) follows:

$$\begin{aligned}&\begin{bmatrix}I & \\ & M_v\end{bmatrix}\begin{Bmatrix}\ddot{\xi}_b\\ \ddot{d}_v\end{Bmatrix}+\begin{bmatrix}2\omega_i\eta_i I+\Phi_b{}^T C_{bb}\Phi_b & \Phi_b{}^T C_{bv}\\ C_{vb}\Phi_b & C_v\end{bmatrix}\begin{Bmatrix}\dot{\xi}_b\\ \dot{d}_v\end{Bmatrix}\\ &\quad+\begin{bmatrix}\omega_i{}^2 I+\Phi_b{}^T K_{bb}\Phi_b & \Phi_b{}^T K_{bv}\\ K_{vb}\Phi_b & K_v\end{bmatrix}\begin{Bmatrix}\xi_b\\ d_v\end{Bmatrix}=\begin{Bmatrix}\Phi_b{}^T F_b^r\\ F_v^r+F_v^G\end{Bmatrix}\end{aligned} \tag{4-30}$$

The coupled vehicle-bridge system vectors contain the modal components of the bridge and the physical components of the vehicles. Consequently, the number of equations in equation (4-29) and the complexity of the whole procedure are greatly reduced.

Equation (4-30) is solved by the Rounge-Kutta method in time domain. At each time step, the contact force at each contact point is calculated by Eq. (4-5). If this force is in tension, which means the corresponding vehicle tire leaves the riding surface, then the force at this contact point is set to zero and the corresponding time dependent terms in Eq. (4-30) are also modified. In this model, the vehicle can jump or leave the riding surface, i.e., the vehicle tires are not necessary to remain in contact with the bridge deck at all time.

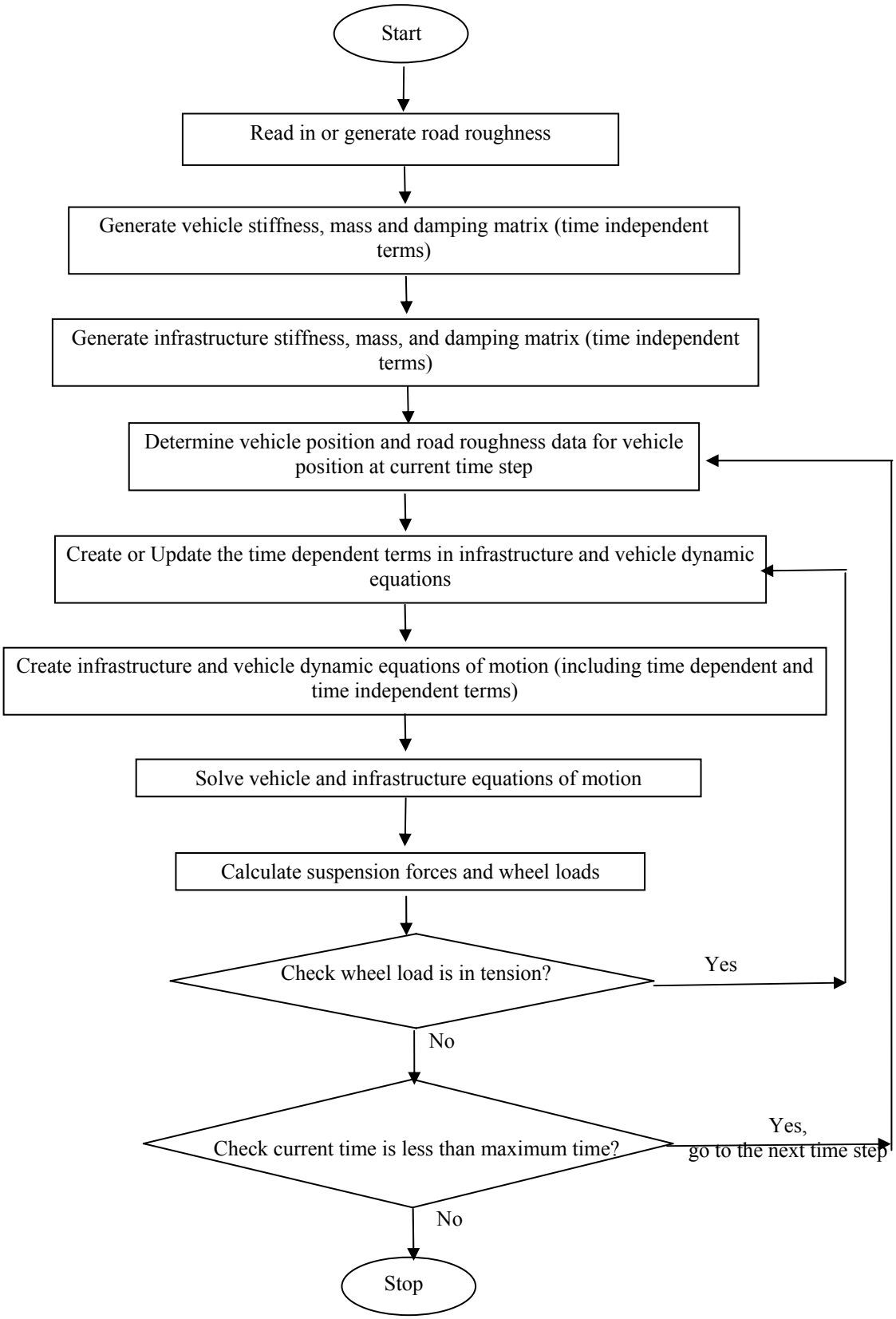

Fig. 4-5 Flowchart of the program

Based on the above methodology, a MATLAB program was developed to assemble the motion equations of vehicle-bridge coupled system and to solve the equations using the direct integration method. The flowchart of this program is shown in Fig. 4-5. The developed program can handle more realistic models of bridges under various types of moving vehicles. The solution to this system contains the interaction force and dynamic response of both bridge and vehicle, such as the displacement and acceleration at each time step. The application of this model to analyze the bridge dynamic response will be conducted in Chapters 5 and 6. Meanwhile, this model can also be used to analyze the interaction of vehicle with other infrastructures such as pavement. In the following sections of this chapter, a numerical example regarding the interaction of a real pavement with an AASHTO HS20-44 truck is demonstrated.

4.3 Numerical Example

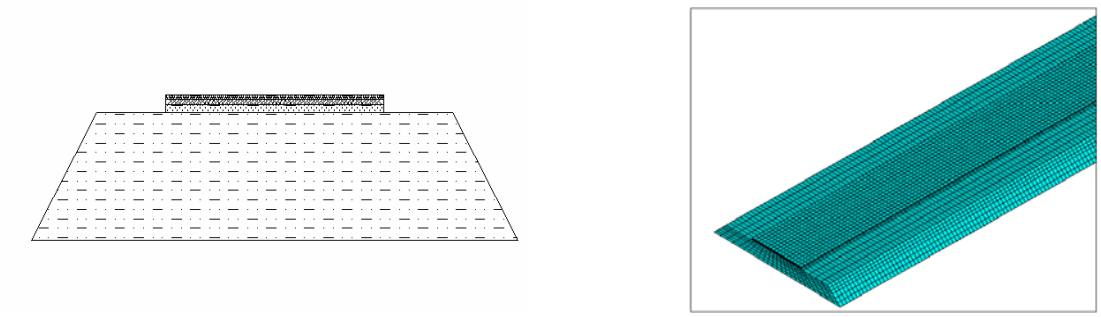

Fig. 4-6 Pavement model

A 3-axle truck (AASHTO HS20-44) passing through a pavement with different velocities is analyzed. The pavement, 280.42 m (920 ft) long, 12.19 m (40 ft) wide and 3.66 m (12 ft) thick, is assumed at rest before the vehicle enters the pavement. The finite element model of pavement is shown in Fig. 4-6 and the model parameters are listed in Table 4-1.

Table 4-1 Parameters of pavement model

	Material	Thickness (m)	Modulus E (MPa)	Poisson's Ratio γ
Layer1	RAP	0.09	221	0.35
Layer2	crushed stone base	0.10	259	0.35
Layer3	cement stabilized soil	0.15	490	0.35
Layer4	subgrade soil	3.30	38	0.45

The geometry, mass distribution, damping and stiffness of the tires and suspension systems of the HS20-44 truck (AASHTO bridge design truck) are shown in Fig. 4-7 and Table 4-2 (Wang and Liu 2000). The static wheel loads for the first, second and third axle of this truck are 4 kips, 16 kips and 16 kips, which make the total weight of the truck 72 kips. Modal frequencies of the vehicle are calculated as 1.52, 2.14, 2.69, 5.94, 7.74, 7.82, 8.92, 13.87, 13.99, 14.63 and 17.95 Hz.

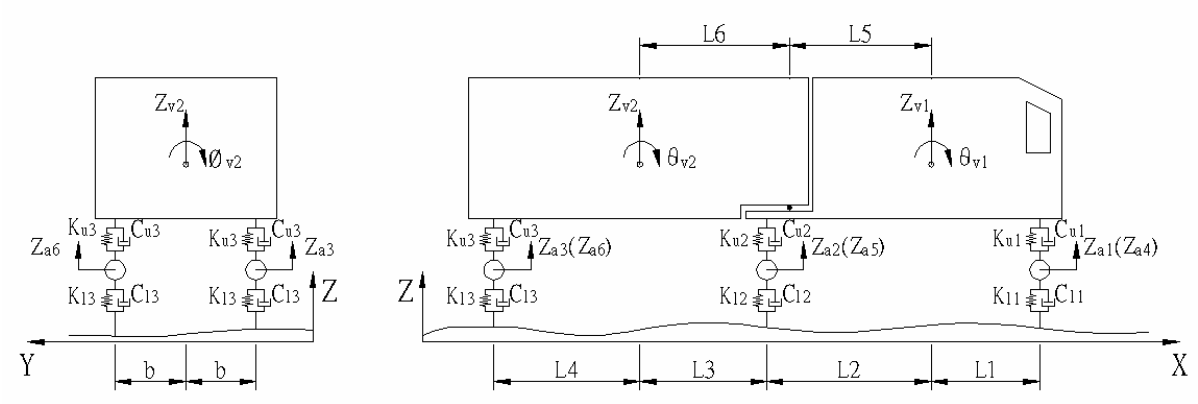

Fig. 4-7 Vehicle model

Table 4-2 Major parameters of vehicle (HS20)

Mass of truck body 1	2612 (kg)
Pitching moment of inertia of truck body1	2022 (kg.m^2)
Rolling moment of inertia of tuck body 1	8544 (kg.m$^{2)}$
Mass of truck body 2	26113 (kg)
Pitching moment of inertia of truck body 2	33153 (kg.m^2)
Rolling moment of inertia of tuck body 2	181216 (kg.m^2)
Mass of the first axle suspension	490 (kg)
Upper spring stiffness of the first axle	242604 (N/m)
Upper damper coefficient of the first axle	2190 (N.s/m)
Lower spring stiffness of the first axle	875082 (N/m)
Lower damper coefficient of the first axle	2000 (N.s/m)
Mass of the second axle suspension	808 (kg)
Upper spring stiffness of the second axle	1903172 (N/m)
Upper damper coefficient of the second axle	7882 (N.s/m)
Lower spring stiffness of the second axle	3503307 (N/m)
Lower damper coefficient of the second axle	2000 (N.s/m)
Mass of the third axle suspension	653 (kg)
Upper spring stiffness of the third axle	1969034 (N/m)
Upper damper coefficient of the third axle	7182 (N.s/m)
Lower spring stiffness of the third axle	3507429 (N/m)
Lower damper coefficient of the third axle	2000 (N.s/m)
L1	1.698 (m)
L2	2.569 (m)
L3	1.984 (m)
L4	2.283 (m)
L5	2.215 (m)
L6	2.338 (m)
B	1.1 (m)

4.3.1 Impact Factor and Dynamic Load Coefficient

The impact factor (*IM*) is defined as:

$$IM(\%) = (\frac{F_d}{F_s} - 1) \times 100\% \tag{4-31}$$

in which F_d and F_s are the maximum dynamic load and static load of the vehicle on pavement, respectively.

The dynamic tire forces are characterized by a Dynamic Load Coefficient (*DLC*) defined as the ratio of standard deviation over mean tire force:

$$DLC = \frac{1}{\bar{F}} \sqrt{\frac{\sum_{i=1}^{N} (F_i - \bar{F})}{N-1}} \times 100\% \tag{4-32}$$

where F_i is the tier force at the i^{th} time step, $\bar{F}$ is the mean tire force, and N is the total time step.

The *IM* and *DLC* are two important variables of pavement dynamic loads. The *IM* indicates the magnitude of the dynamic tire force; and the DLC represents the variation of the dynamic loads.

4.3.2 Effect of Road Roughness

In order to analyze the effect of road roughness on pavement dynamic loading, four road conditions have been considered as inputs to the pavement-vehicle coupled model respectively: (1) very good; (2) good; (3) average; and (4) poor road surface conditions. According to ISO, n1 and n2 in Eq. (4-18) are proposed to be 0.01 (cycle/m) and 2.0 (cycle/m), respectively, for pavement. The speed of the HS20-44 truck is assumed to be 20m/s (44.7mph) in the simulation unless otherwise specified.

The dynamic wheel loads (for the second axle) under four different road conditions are shown in space domain (which corresponds to time domain) in Fig. 4-8. Since the first axle tire force is much less than the other two, wheel loads of the second and third axles are concerned. The figure shows that the pavement road condition has greatly affected the dynamic load, and the magnitude of tire force increases as the road condition deteriorates.

Table 4-3 listed the IM and DLC of the three different axle tire forces under different road conditions. The IM and DLC of the 2nd axial tire forces are as high as 71.7% and 22.25%, respectively, when the road condition is poor for the specific case of HS20-44 truck with a velocity of 20m/s.

The road surface condition is divided into different levels with different road surface roughness coefficient, φ(n0), in Eq. (4-18). According to ISO, the pavement surface condition decreases by one level when the φ(n0) value increases to four times of its initial value. The results given in Table 4-3 show that the decline of pavement surface condition by one level

results in about two times increase in IM and DLC of the tire force on such a pavement. The relation between DLC and road surface condition level, obtained in this study, agrees with the conclusion of Sun and Deng (1998).

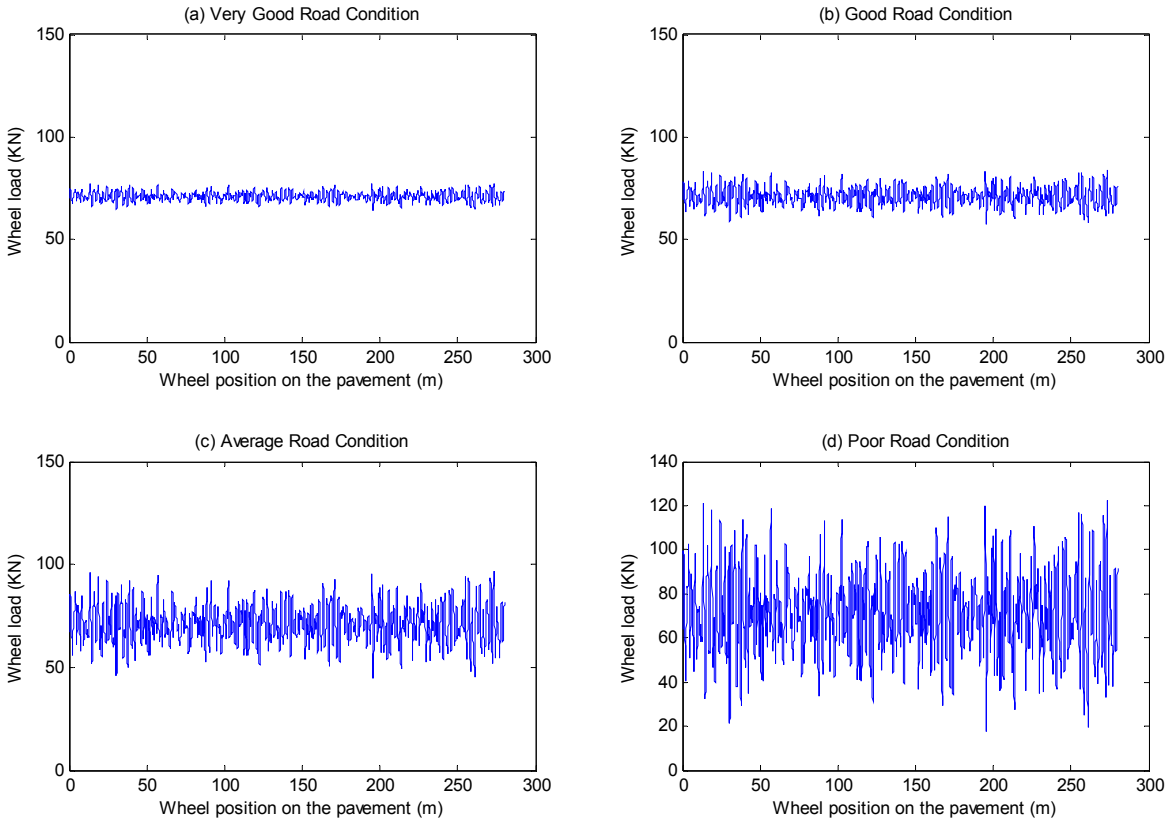

Fig. 4-8 Dynamic tire force in space domain (corresponding to time domain)

Table 4-3 Impact factor and dynamic load coefficient under different road surface condition

Road Condition	Impact Factor (*IM*)			Dynamic Load Coefficient(*DLC*)		
	1st axle	2nd axle	3rd axle	1st axle	2nd axle	3rd axle
Very good	0.128	0.087	0.081	0.0307	0.0278	0.0235
Good	0.259	0.177	0.162	0.0613	0.0557	0.0469
Average	0.520	0.357	0.325	0.1226	0.1113	0.0938
Poor	1.044	0.717	0.651	0.2451	0.2225	0.1875

In order to obtain statistical results for IM, more samples of road roughness profiles have been generated. IM is obtained by taking the mean value of the predicted impact factors from these random road surface profiles. More runs of different pavement confirmed this result, which indicated in addition to DLC, the peak value of the pavement dynamic force also increases by two times as road surface condition decreases by one level.

4.3.3 Effect of Vehicle Damping

The vehicle damping is studied assuming average road surface condition and a truck speed of 20 m/s. Denote the vehicle damping coefficient in Table 4-2 as C, the dynamic tire loads for four different damping coefficients, 0.5C, C, 2C and 3C have been analyzed.

The influence of vehicle damping coefficient on IM and DLC are shown in Fig. 4-9. As the damping coefficient increases, the IM and DLC decrease. When the damping coefficient increases from 0.5C to 2C, the IM of the second axle decreases from 48.7% to 35.7%, while the DLC declines from 15.64% to 11.13%.

However, when the damping coefficient is beyond some value, the *IM* and *DLC* decrease in a very slow rate and become constants. For the HS20-44 truck, when the damping coefficient reaches 2*C*, there are almost no changes in the values of *IM* and *DLC*. Further study of vehicle acceleration shows that after the damping reaches a certain value, it affects the rideability more than the pavement dynamic load. For this reason, the vehicle damping coefficient of 2*C* is used in the rest parts of this paper, which can exclude vehicle damping as a variable.

4.3.4 Effect of Vehicle Rigidity

The effect of vehicle rigidity was also analyzed for the average road condition and truck speed of 20m/s. With the vehicle spring rigidity listed in Table 4-2 as *K*, the dynamic tire loads have been analyzed for four different stiffness conditions: 0.5*K*, *K*, 2*K* and 3*K*.

Fig. 4-10 shows the results of *IM* and *DLC* for these four conditions. The vehicle rigidity affects pavement dynamic loads. As the vehicle stiffness increases, the IM increases. As the vehicle rigidity increases from 0.5K to 2K, the *IM* for the second axle increases from 31.4% to 73.0%, and the *DLC* increases from 8.83% to 24.24%.

4.3.5 Effect of Vehicle Weight

Vehicle weight is another important factor that influences the magnitude of pavement dynamic loads. In order to analyze its effect on *IM* and *DLC* of dynamic loads, four vehicle weight conditions of 0.5*M*, *M*, 1.5*M* and 2*M* have been studied, where *M* is to designate the vehicle weight shown in Table 4-2.

Fig. 4-11 gives the variation of *IM* and *DLC* with different vehicle weight. The results were obtained based on the 20 m/s vehicle speed and average road surface condition. Lighter vehicles cause larger *IM* and *DLC*. For example, the *IM* decreases form 63.4% to 39.4%, and *DLC* from 20.07% to 10.91%, when the weight of the vehicle increases from 0.5*M* to 2*M*.

However, if the vehicle weight keeps increasing to some large value, it will no longer affect the *IM* and *DLC*. Moreover, heavier vehicle will increase the absolute magnitude of dynamic loads, which is the direct cause of pavement damage.

4.3.6 Effect of Vehicle Speed

The vehicle speeds of 10, 20, 30 and 40 m/s were considered to analyze the influence of vehicle speed on pavement dynamic loads for an average road surface condition.

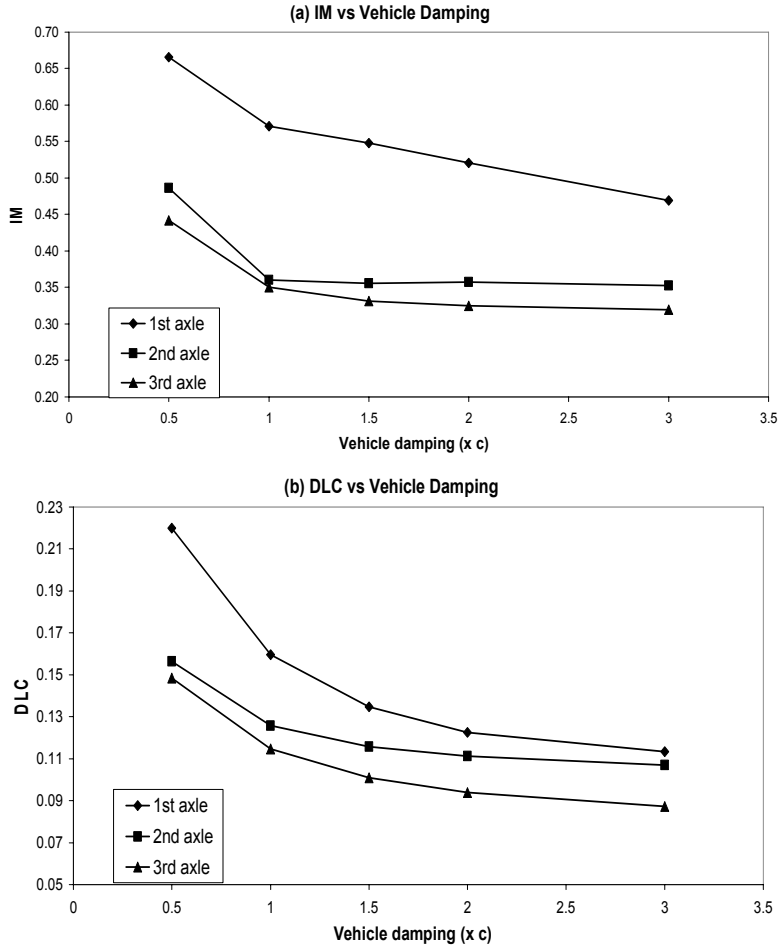

Fig. 4-9 Effect of vehicle damping

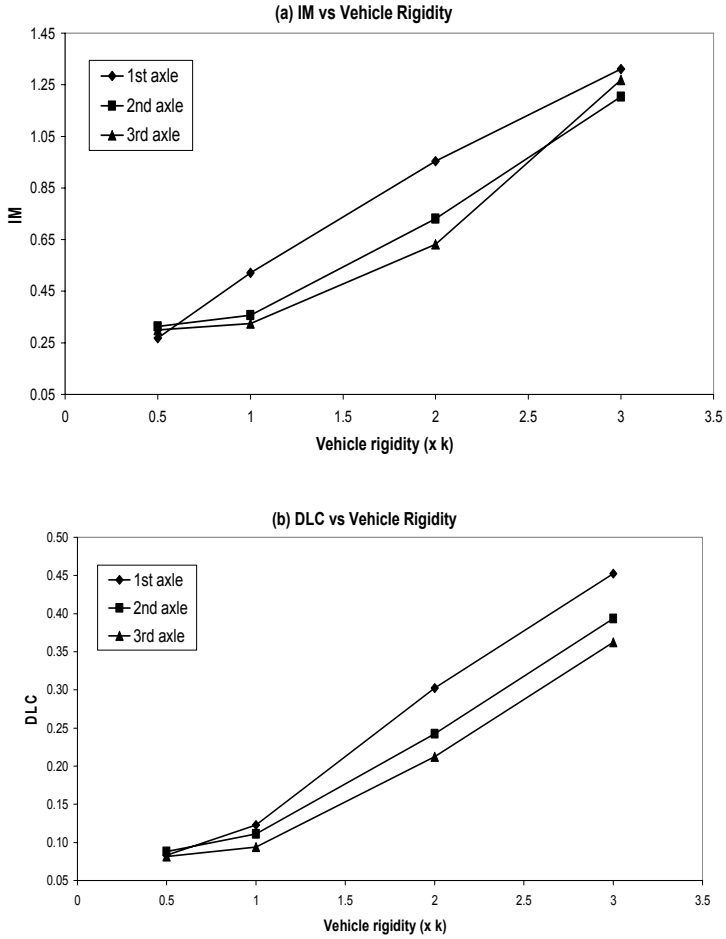

Fig. 4-10 Effect of vehicle rigidity

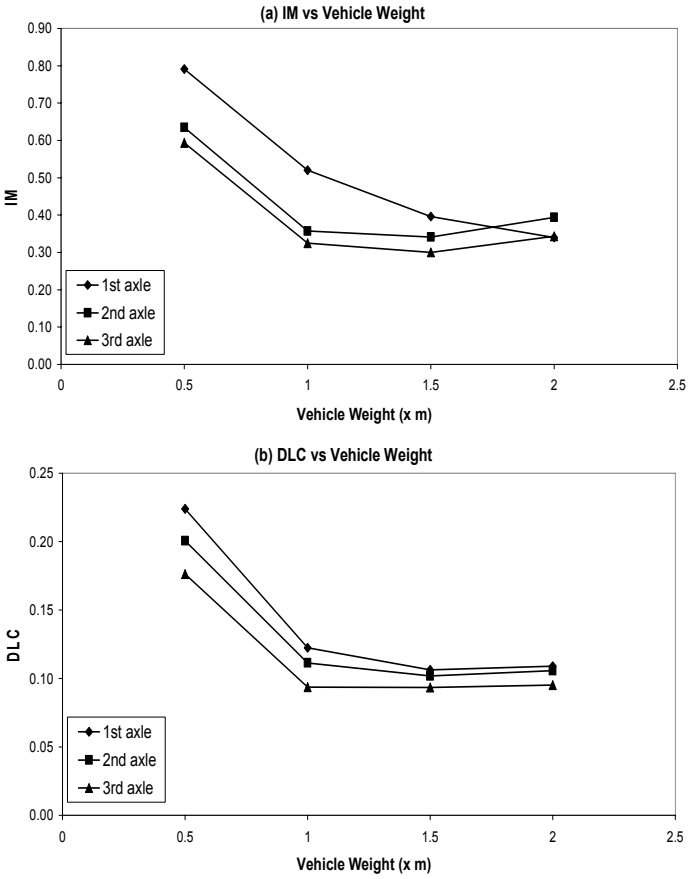

Fig. 4-11 Effect of vehicle weight

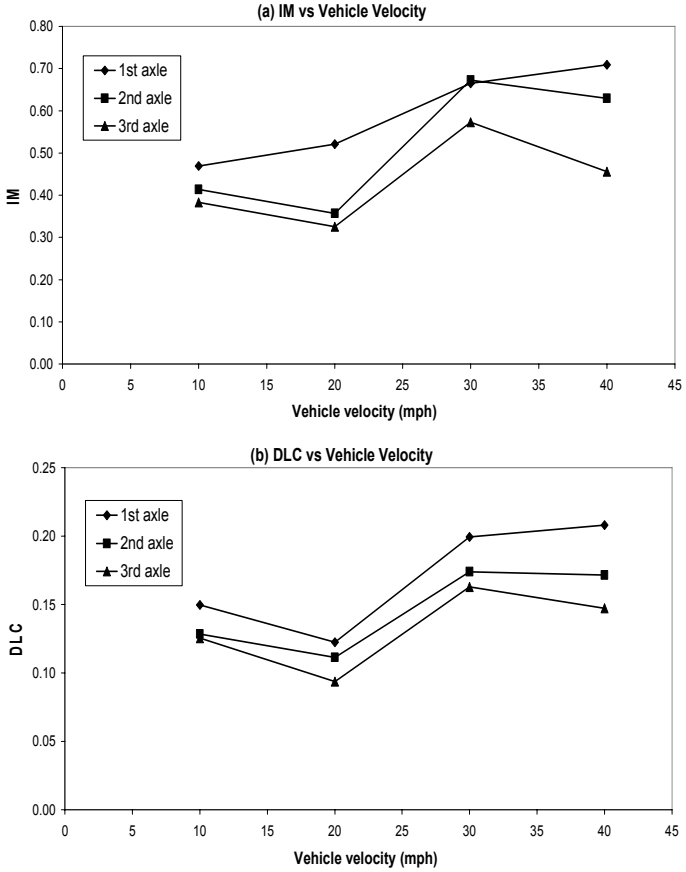

Fig. 4-12 Effect of vehicle speed

Fig. 4-12 shows the variation of *IM* and *DLC* with vehicle speeds. They do not necessarily increase as the vehicle speed increases. When the vehicle speed increases from 10 m/s to 20 m/s, and then to 30 m/s, the *IM* of the second axle declines from 41.4% to 35.7%, and then increase to 67.2%, while the DLC changes from 12.85% to 11.13%, and then to 17.41%. This phenomenon is complicated because the vehicle speed affects the product of vehicle speed and cut-off values of the roughness spatial frequency, which will be further explained in the frequency domain later.

As far as the vehicle parameters of HS20-44 truck are concerned, the pavement dynamic loads can be 63% (IM) higher than its static load under the conditions of average road roughness and a vehicle speed of 89.4 mph (40 m/s). The dynamic load coefficient falls into a range of 3%-30%, if the road surface is no worse than the average level condition and vehicle speed is within 40 m/s.

4.3.7 Results in Frequency Domain

To study the frequency distribution of the pavement dynamic loads (one of the important characteristics of the load for pavement damage analysis), the results obtained in the time domain have been transformed into the frequency domain and the spectral density amplitudes are shown in Figs. 4-13 to 4-15.

It can be seen in Fig. 4-13 that as the vehicle rigidity increases, the peak frequencies (the frequencies corresponding to peak values) shift to the right side of the frequency axle. Actually, the increase of rigidity results in the increase of vehicle modal frequencies. Similarly, when the vehicle weight increases, the vehicle frequencies decrease and the peak frequencies in Fig. 4-14 shift to the left side of the frequency axle. This means that the dominant frequency of the dynamic loads is affected when the vehicle frequency changes.

It is found in Figs. 4-13 and 4-14 that the peak frequencies for dynamic loads of the first axle are close to the third and sixth vehicle modal frequencies, and that the peak frequencies for the second and third axles are close to the second and seventh vehicle modal frequencies. Take the dynamic wheel load of the second axle for instance, when the vehicle rigidity are 0.5K, K, 2K and 3K, the vehicle's second modal frequencies are 1.51, 2.14, 3.02 and 3.71 Hz, respectively, and the seventh modal frequencies are 6.31, 8.90, 12.61 and 15.45 Hz, respectively. Peaks corresponding to these frequencies are shown in Fig. 9 (a-2), (b-2), (c-2), and (d-2). These results indicate that the main frequency of pavement dynamic loads is mostly dominated by the vehicle resonance frequency.

Moreover, among the peak frequencies, which are close to the vehicle frequencies, the main peak frequency is not corresponding to the same vehicle mode when the vehicle frequencies change. As shown in Fig. 4-13 (a-2) and (d-2), the two peaks switch order. It indicates that vehicle frequency is not the only factor that affects the dominant frequency of pavement dynamic loads.

The spectral analysis (Fig. 4-15) shows that the variation of vehicle speeds results in changes in the main frequency and frequency bandwidth of the pavement dynamic loads. With a low vehicle speed, the dynamic load concentrated in a low frequency zone less than 5 Hz and the

frequency bandwidth is narrow. At a high speed, the main frequency of dynamic loads does not shift, but more peaks appear, which means higher vehicle speed results in wider frequency band. Actually, it is the higher vehicle speed that causes the larger product of vehicle speed and the cut-off spatial frequency of pavement road roughness, vn_1 and vn_2. Consequently, the vehicle's higher frequency modes are excited, which contributes to the dynamic loads with higher frequency.

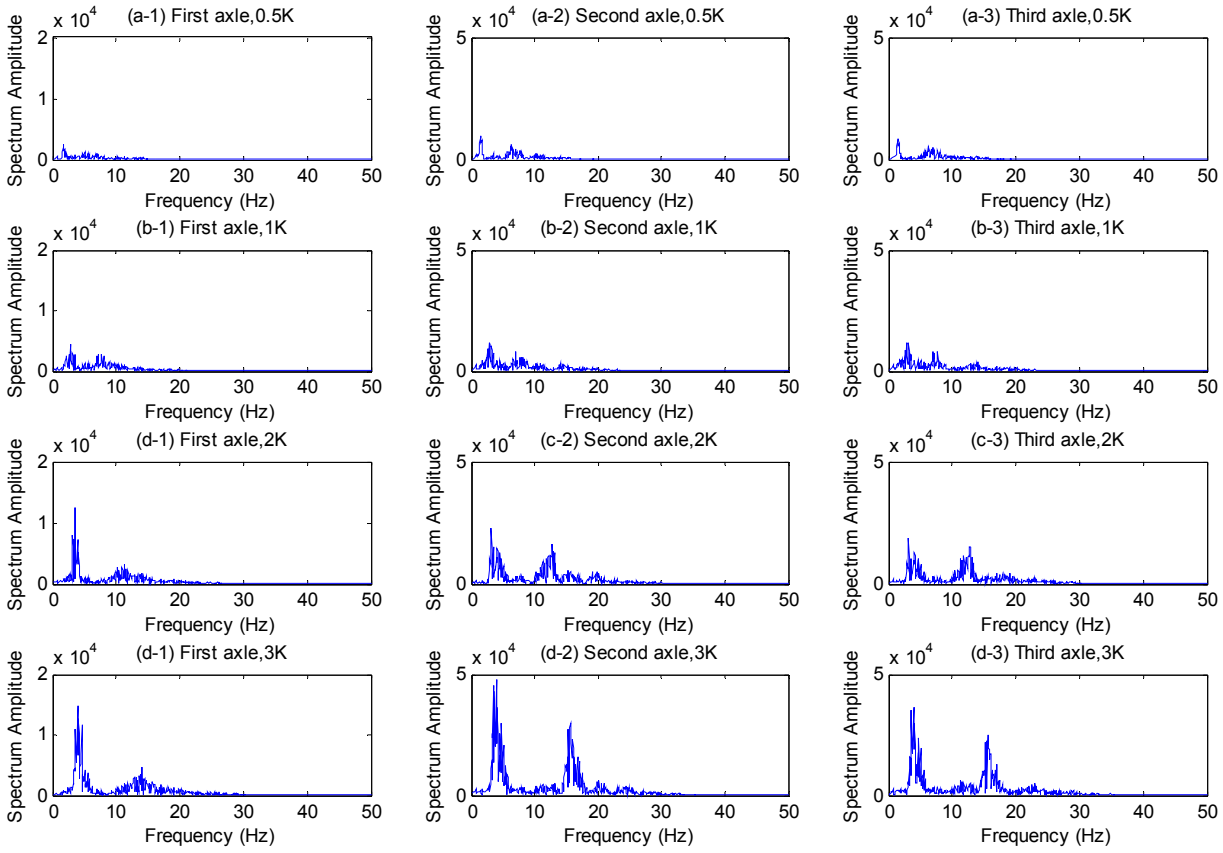

Fig. 4-13 Effect of vehicle rigidity in frequency domain

The dynamic load frequencies are dominated by vehicle frequencies. However, which vehicle frequency will be excited and which frequency will determine the main dynamic load frequency is affected by the product of the vehicle velocity and the cut-off values of road roughness spatial frequency. The frequencies of commercial trucks (used in U.S.) range from 1 to 25 Hz (Gillespie et al., 2000). Therefore the main frequencies (corresponding to peaks) of dynamic loads will distribute within this bandwidth. The upper limit of the dynamic load frequency range (frequency bandwidth) is determined by the value of the vehicle frequency and the product of the vehicle speed and the upper cut-off value of the road surface spatial frequency.

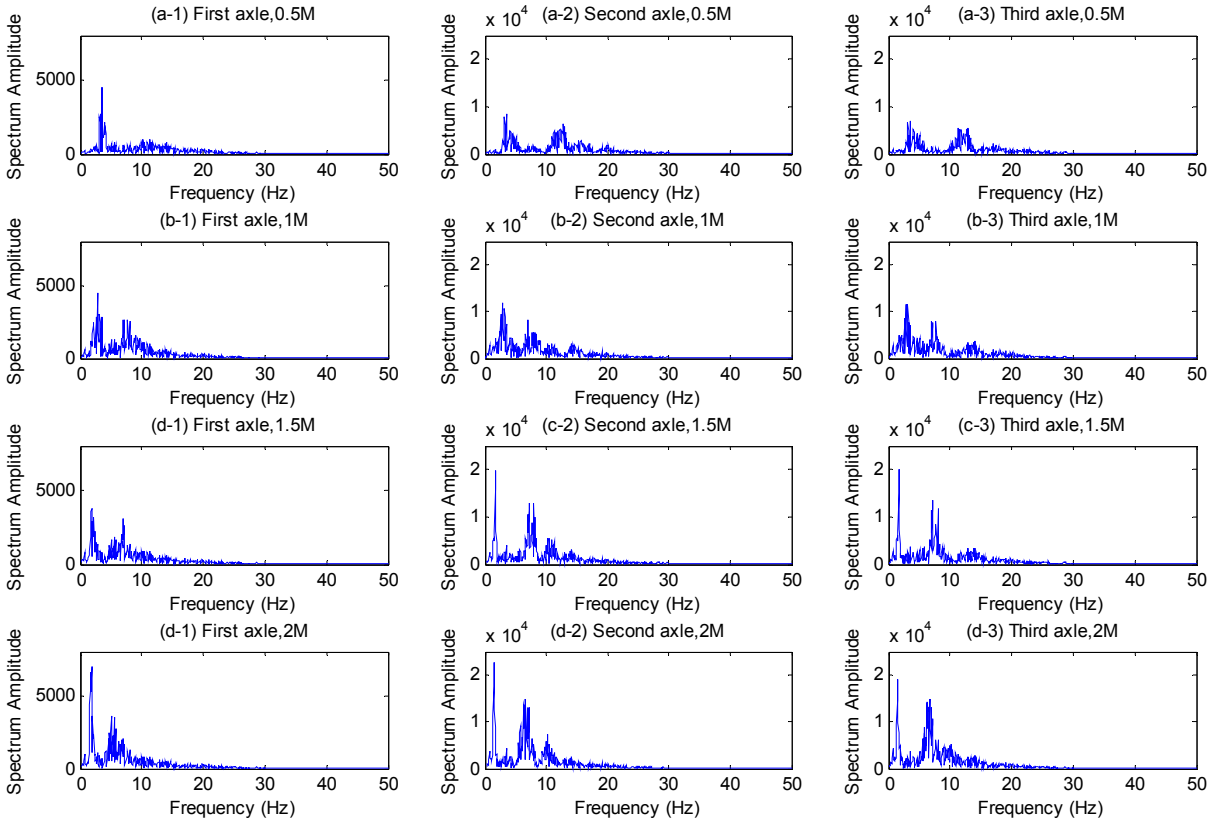

Fig. 4-14 Effect of vehicle weight in frequency domain

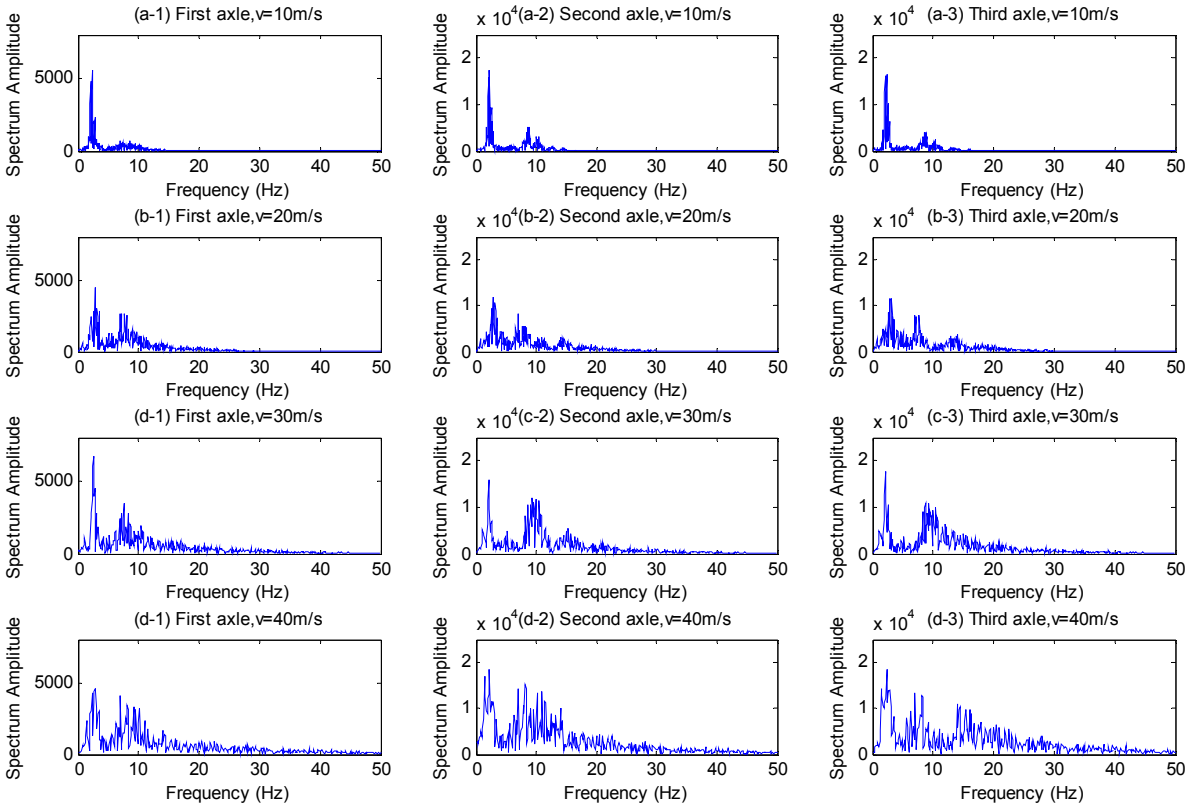

Fig. 4-15 Effect of vehicle speed in frequency domain

4.4 Conclusions

In this study, a fully computerized approach to simulate the interaction of coupled vehicle-bridge system is developed. By calculating the interaction force at each time step, it also considers the separation of the vehicle tire from the riding surface. The time history of dynamic response, such as displacement and acceleration, of both bridge and vehicle can be obtained. The developed program can handle more realistic models of bridges under various types of moving vehicles. It can be used to analyze not only the bridge-vehicle interaction, but also the interaction of vehicle and other infrastructures such as pavement.

Based on this model, the pavement dynamic loads caused by the AASHTO HS20-44 truck is obtained by solving the pavement-vehicle coupled equations in the time domain. With the help of this method, effects of road surface conditions and vehicle parameters on pavement dynamic loads are analyzed. The impact factor (*IM*), dynamic load coefficient (*DLC*), and frequency distribution of pavement loads are concerned. The developed methodology can be used to further study the vehicle-induced pavement response and the information will be useful in analyzing pavement damage.

It is found that, given the vehicle parameters and constant speed, *IM* and *DLC* of dynamic loads are proportional to road surface condition level, i.e., $\varphi(n_0)$ in Eq. (4-18). The *IM* and *DLC*

increase by about two times when the pavement surface condition declines by one level. Increase in vehicle damping coefficient will reduce the *IM* and *DLC* of wheel loads. But the effect of increasing the damping coefficient is very slight after the damping reaches some value. For the HS20-44 truck, after the damping coefficient reaches 2*C, IM* and *DLC* remains the same. Increase in vehicle rigidity will result in larger *IM* and *DLC*. Heavier vehicle causes less *IM* and *DLC*. If the vehicle weight keeps increasing after the weight reaches some value, it will no longer affect the *IM* and *DLC*, but the absolute magnitude of dynamic load will increase. The vehicle speed affects the *IM* and *DLC*. A higher speed does not necessarily increase the *IM* and *DLC*. The vehicle speed affects the time frequency of road roughness by changing the product of the vehicle speed and the cut-off values of the roughness spatial frequency.

The main frequency of the dynamic load is dominated by the vehicle modal frequency and is affected by the vehicle speed. Since trucks used in U.S. have modal frequencies in the 1-25 Hz range, the main frequencies (corresponding to peaks) of dynamic pavement loads may distribute within this range. The upper limit of frequency of dynamic loads is determined not only by the value of vehicle frequency but also the product of the vehicle speed and the upper cut-off value of the road surface spatial frequency.

For the HS20-44 truck, the impact factor can be as high as 63% for average road roughness and a vehicle speed of 89.4 mph (40 m/s). The dynamic load coefficient falls into the range of 3-30%, if the road surface is no worse than the average level condition and vehicle speed is within 40 m/s.

4.5 References

Bathe, K.J. and Wilson, E.L. (1976). *Numerical Methods in Finite Element Analysis*. Englewood Cliffs, N.J.: Prentice-Hall.

Blejwas, T. E., Feng, C. C., and Ayre, R. S. (1979). "Dynamic interaction of moving vehicles and structures." Journal of Sound and Vibration, Vol. 67, 513-521.

Chatterjee, P.K., Datta, T. K., and Surana, C. S. (1994). "Vibration of continuous bridges under moving vehicles." *Journal of Sound and Vibration*, 169(5), 619-632.

Dodds, C.J., and Robson, J.D. (1973) "The description of road surface roughness," Journal of Sound and Vibration, Vol. 31, No. 2, 175-183.

Frayba, L. (1973). *Vibration of Solids and Structures under Moving Loads*. Groningen, Noordhoff International Publishing.

Gillespie, T.D. and Karamihas, S.M. (2000) "Simplified models for truck dynamic response to road inputs", Heavy Vehicle Systems, v 7, n 2-3, 2000, p 231-247.

Green, M.F. and Cebon, D. (1994). "Dynamic response of highway bridges to heavy vehicle loads: theory and experimental validation." Journal of Sound and Vibration, Vol. 170, No. 1, 51-78.

Hardy, M.S.A. and Cebon, D. (1994) "Importance of speed and frequency in flexible pavement response," Journal of Engineering Mechanics, v. 120, n 3, p 463-482.

Hino, J., Yoshimura, T., Konishi, K., and Ananthanarayana, N. (1984). "Afinite element method prediction of the vibration of a bridge subjected to a moving vehicle load." *Journal of Sound and Vibration*, Vol. 96, 45-53.

ISO 8068: 1995 (E), "Mechanical Vibration –Road Surface Profiles-Reporting of Measured Data," 1995.

Lin, Y.H. and Trethewey, M.W. (1990). "Finite element analysis of elastic beams subjected to moving dynamic loads." *Journal of Sound and Vibration*, Vol. 136, 323-342.

Markow, M.J., Hedrick, J.K., and Brademeyer, B.D. (1988) "Analyzing the interactions between dynamic vehicle loads and highway pavements," Transportation Research Record, n 1196, p 161-169.

Sun, L. and Deng, X.J.(1998) "Prediding vertical dynamic loads caused by vehicle-pavement interaction", Journal of Transportation Engineering, v. 124, n 5, p 470-478.

Todd, K.B. and Kulakowski, B.T. (1991) "Simple computer models for predicting ride quality and pavement loading for heavy trucks", Transportation Research Record, n 1215, p 137-150.

Xu, Y.L. and Guo, W.H. (2004). "Effects of bridge motion and crosswind on ride comfort of road vehicles**",** *Journal of Wind Engineering and Industrial Aerodynamics*, Vol. 92, No. 7-8, 641-662.

Zafir, Z., Siddharthan, R, and Sebaaly, P.E., (1994) "Dynamic pavement strain histories from moving traffic load", Journal of Transportation Engineering, v 120, n 5, Sept-Oct, p 821-842.

CHAPTER 5 VEHICLE INDUCED DYNAMIC BEHAVIOR OF SHORT SPAN SLAB BRIDGES CONSIDERING EFFECT OF APPROACH SPAN CONDITION

5.1 Introduction

Prediction of the dynamic responses of bridges resulting from moving vehicles is of significance in bridge design because a moving vehicle may produce a larger response on the structure than a static vehicle does. The bridge dynamic response is caused by vehicles acting as oscillators, as well as time variant forces, on the bridge. Theoretical and experimental investigations indicate that the vehicle impact to a bridge depends on many factors including: (1) the type of bridge and its natural frequencies of vibration, (2) vehicle characteristics, (3) the driving speed of the vehicle, and (4) the profiles of the approach roadway and bridge deck (Huang et al. 1993). Among the factors influencing the bridge-vehicle interaction, the vehicle initial condition is an important factor that affects the dynamic responses of both bridges and vehicles (Li 1996). A vehicle's initial condition before entering a bridge is caused not only by the roughness of the roadway that the vehicle has traveled before it enters the bridge, but also by the uneven approach span conditions upon entrance to the bridge. An uneven approach span condition is caused by the differential settlement between the embankment soil and the abutments, and/or bridge approach span deformation. However, the effect of bridge approach span condition on bridge dynamic performance has seldom been analyzed.

Bridge approach spans are normally constructed as slabs laid on the embankment soil to connect the bridge deck with the adjacent paved roadway. Their function is to provide a smooth transition between the bridge deck and the roadway pavement. However, soil embankment settlement causes the approach slabs of bridges to lose their contacts and supports from the soil. When this occurs, the slab will bend and deform in a concave manner (Cai et al. 2005). Meanwhile, loads on the slab will also redistribute to its ends, which may result in faulting across the roadway at the ends of the approach slab ($\Delta 1$ and $\Delta 3$ in Fig. 5-1). On the other hand, the expansion joint that connects the approach slab and bridge deck will form a faulting between the bridge deck and approach span ($\Delta 1$ in Fig. 5-1) due to the poor maintenance.

Field observations as shown in Fig. 5-2 indicate that the faulting between the bridge deck and approach slab can be as large as 0.038 m (1.5 inches) (White et al. 2005). This unevenness triggers vehicle bumping at the joint; consequently, the vehicle receives an initial disturbance before reaching the bridge. This initial excitation of the vehicle causes an extra impact load on the bridge and has an effect on the dynamic responses of both the bridge and the vehicle. Traditionally a 0.3 impact factor has been used in AASHTO Standard code (AASHTO 2002) for many years. Recently, the significant effect of the uneven joints (bumps) on vehicle induced impact loads has been recognized in the AASHTO LRFD code (AASHTO 2004) that specifies an impact factor of 0.75 for joint design.

The bump-related problems have been commonly recognized, and the causes have been identified. However, previous studies took little account of how the approach span condition influences the bridge-vehicle dynamic interaction, probably because most of these studies were concerned about the medium to long span bridges, upon which the effect of the approach span condition may not be significant. But for short slab bridges it is worthwhile to analyze in detail the possible effect of approach span conditions on the bridge dynamic response.

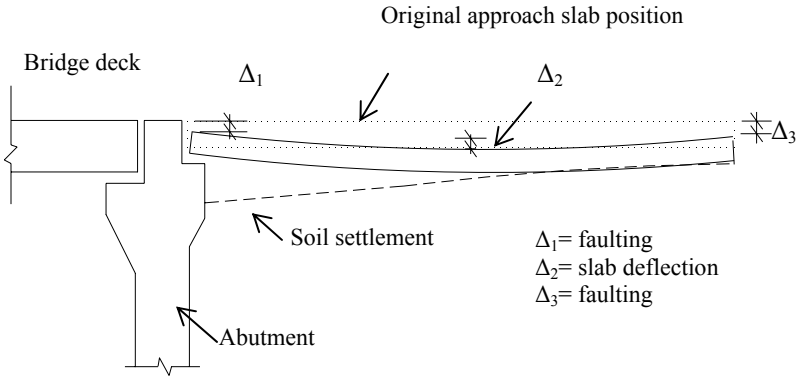

Fig. 5-1 Illustration of approach span deformation

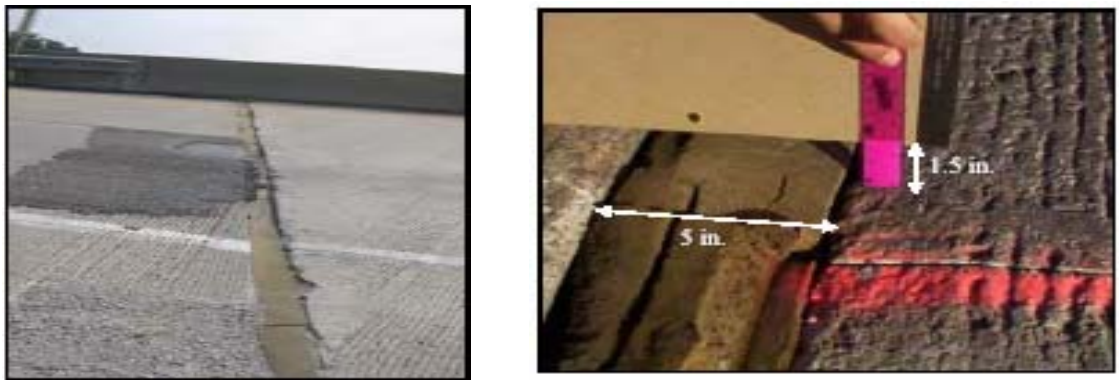

Fig. 5-2 Uneven joint of approach slab an bridge deck (White et al. 2005)

In this chapter a fully computerized vehicle-bridge coupled model has been developed. Using this model, the present study investigates the dynamic behavior of slab bridges with different span lengths under conditions of various vehicle speeds and different road surface conditions. Furthermore, the approach span condition is taken into account in this model, and its effect on bridge dynamic response has been analyzed.

5.2 Vehicle-Bridge Dynamic System

5.2.1 Vehicle-Bridge Coupled Model

In the present study the vehicle is considered as an oscillator moving on the bridge. The tires and suspension systems are ideally modeled as linear elastic spring elements and dashpots. This model can be used to simulate vehicles on highway roads or bridges with axle numbers varying from two to five. For demonstration purposes a 3-axle articulated truck consisting of up

to 11 independent degrees of freedom is shown in Fig. 5-3. The equation of motion for the vehicle is derived based on the following matrix form:

$$[M_v]\{\ddot{d}_v\} + [C_v]\{\dot{d}_v\} + [K_v]\{d_v\} = \{F_v^G\} + \{F_c\} \tag{5-1}$$

where the vehicle mass matrix $[M_v]$, damping matrix $[C_v]$, and stiffness matrix $[K_v]$ are obtained by considering the equilibrium of the forces and the moments of the system; $\{d_v\}$ is the vehicle displacement vector; $\{F_v^G\}$is the self-weight of the vehicle; and $\{F_c\}$is the vector of wheel-road contact forces acting on the vehicle. The contact between the bridge and the moving vehicle is assumed to be a point contact.

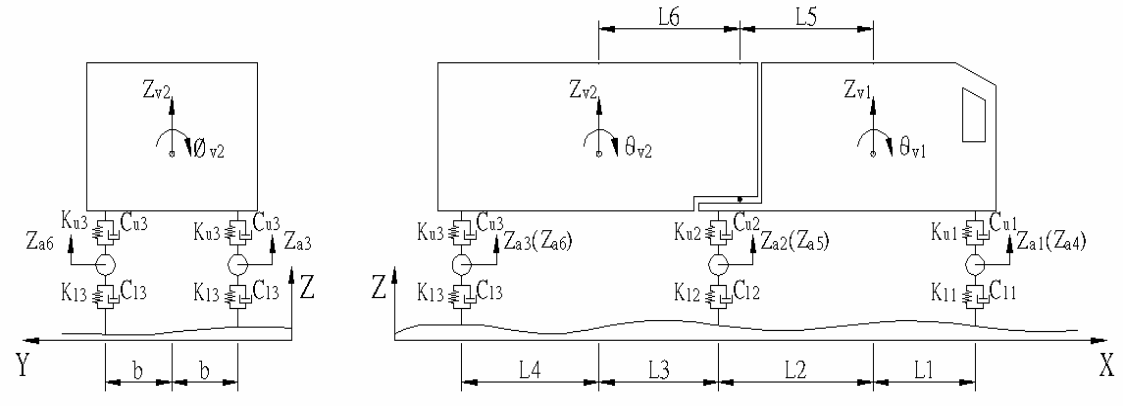

Fig. 5-3 Vehicle model

A dynamic model of the bridge can be obtained through finite element modeling. This allows the motion of the structure to be described by the following equations with similar definitions to Eq. (5-1), namely, by changing the subscript v to b for bridge as:

$$[M_b]\{\ddot{d}_b\} + [C_b]\{\dot{d}_b\} + [K_b]\{d_b\} = \{F_b\} \tag{5-2}$$

where $\{F_b\}$is the wheel-bridge contact force on the bridge.

The equations of motion for the vehicle and bridge are coupled through the interaction forces, i.e. $\{F_b\}$ and $\{F_c\}$. $\{F_b\}$ and $\{F_c\}$are action and reaction forces existing at the contact point of the two systems.

5.2.2 Interaction of Vehicle and Bridge

To simulate the bridge-vehicle interaction, Eq. (5-1) is used for each vehicle and Eq. (5-2) is used for the bridge in conjunction with:

i) a relation among the displacement of vehicle axle suspension Z_a, the displacement of bridge at the wheel-road contact point Z_b, the deformation of lower springs of vehicle Δ_l, and the road surface profile $r(x)$ (as shown in Fig. 5-3):

$$Z_a = Z_b + r(x) + \Delta_l \tag{5-3}$$

$$\dot{Z}_a = \dot{Z}_b + \dot{r}(x) + \dot{\Delta}_l \tag{5-4}$$

in which $\dot{r}(x) = \frac{dr(x)}{dx}\frac{dx}{dt} = \frac{dr(x)}{dx}V(t)$ and *V(t)* is the vehicle velocity;

ii) an expression for the bridge-vehicle contact forces as a function of the deformation of the vehicle's lower spring:

$$\{F_b\} = -\{F_c\} = [K_l]\{\Delta_l\} + [C_l]\left\{\dot{\Delta}_l\right\} \tag{5-5}$$

where K_l and C_l are coefficients of vehicle's lower spring and damper, respectively. By substituting Eqs. (5-3) and (5-4) into Eq. (5-5), the contact force between the bridge and vehicle can be expressed as

$$\{F_b\} = -\{F_c\} = [K_l](Z_a - Z_b - r(x)) + [C_l](\dot{Z}_a - \dot{Z}_b - \dot{r}(x)) \tag{5-6}$$

The positive F_b indicates the contact force between the vehicle and bridge is in tension and the vehicle tire is separating from the bridge. Under this condition, the contact force should be set equal to zero. From Eq. (5-6) it is apparent that the interaction force depends on the motion of both the bridge and the vehicle and that the vehicle displacement is related to bridge displacement, road surface profile, and the position of the vehicle. Substituting Eq. (5-6) into Eqs. (5-1) and (5-2), the final equations of motion for the coupled system are written as:

$$\begin{bmatrix} M_b & \\ & M_v \end{bmatrix}\begin{Bmatrix} \ddot{d}_b \\ \ddot{d}_v \end{Bmatrix} + \begin{bmatrix} C_b + C_{bb} & C_{bv} \\ C_{vb} & C_v \end{bmatrix}\begin{Bmatrix} \dot{d}_b \\ \dot{d}_v \end{Bmatrix} + \begin{bmatrix} K_b + K_{bb} & K_{bv} \\ K_{vb} & K_v \end{bmatrix}\begin{Bmatrix} d_b \\ d_v \end{Bmatrix} = \begin{Bmatrix} F_b^{\,r} \\ F_v^{\,r} + F_v^{\,G} \end{Bmatrix} \tag{5-7}$$

In comparison with Eqs. (5-1) and (5-2), there are additional terms C_{bb}, C_{bv}, C_{vb}, K_{bb}, K_{bv}, K_{vb}, $F_b^{\,r}$, and $F_v^{\,r}$ in Eq. (5-7), which are the interaction terms and are due to the expansion of the contact force vectors. When the vehicle moves across the bridge, the bridge-vehicle contact points change with the vehicle position. Thus, the road roughness *r(x)* at the contact point no longer remains the same. Consequently, the contact force between the bridge and vehicle changes, indicating that the interaction terms in Eq. (5-7) are time-dependent and will change as the vehicle moves across the bridge.

To simplify the modeling procedure, the bridge mode superposition technique is used based on the obtained bridge mode shape $\{\Phi_i\}$ and the corresponding natural circular frequencies ω_i. The bridge dynamic response $\{d_b\}$ can be expressed as:

$$\{d_b\} = [\{\Phi_1\} \quad \{\Phi_2\} \ldots \{\Phi_n\}]\{\xi_1 \quad \xi_2 \cdots \xi_n\}^T = [\Phi_b]\{\xi_b\} \tag{5-8}$$

where n is the total number of modes considered for the bridge, and $\{\Phi_i\}$ and ξ_i are the i^{th} mode shape and its generalized coordinates, respectively. If each mode shape is normalized to the mass matrix, i.e. $\{\Phi_i\}^T[M_b]\{\Phi_i\}=1$ and $\{\Phi_i\}^T[K_b]\{\Phi_i\}=\omega_i^2$, and if the damping matrix $[C_b]$ is assumed to be $2\omega_i\eta_i[M_b]$, where ω_i is the natural circular frequency of the bridge and η_i denotes the percentage of the critical damping for the i^{th} mode of the bridge, then Eq. (5-7) can be rewritten as:

$$\begin{bmatrix} I & \\ & M_v \end{bmatrix}\begin{Bmatrix} \ddot{\xi}_b \\ \ddot{d}_v \end{Bmatrix}+\begin{bmatrix} 2\omega_i\eta_i I+\Phi_b{}^T C_{bb}\Phi_b & \Phi_b{}^T C_{bv} \\ C_{vb}\Phi_b & C_v \end{bmatrix}\begin{Bmatrix} \dot{\xi}_b \\ \dot{d}_v \end{Bmatrix} + \begin{bmatrix} \omega_i{}^2 I+\Phi_b{}^T K_{bb}\Phi_b & \Phi_b{}^T K_{bv} \\ K_{vb}\Phi_b & K_v \end{bmatrix}\begin{Bmatrix} \xi_b \\ d_v \end{Bmatrix}=\begin{Bmatrix} \Phi_b{}^T F_b{}^r \\ F_v{}^r+F_v{}^G \end{Bmatrix} \tag{5-9}$$

The mode superposition makes it possible to separate the bridge modal analysis from the vehicle-bridge coupled model. In consequence, the number of equations in Eq. (5-9) and the complexity of the entire procedure are greatly reduced.

Based on the methodology described above, a computer program has been developed to model the vehicle-bridge coupled system. The motion equations of the vehicle-bridge coupled system are assembled automatically and solved in time history using the Runge-Kutta method. The time dependent terms in Eqs. (5-7) and (5-9) are calculated precisely by determination of the vehicle position on the bridge and are updated at each time step, which makes it possible to reduce the computational effort for iterations. By determining the contact force at each time step and setting the force to be zero, once the contact force between the vehicle and bridge is found to be tensile, this model is able to consider the separation of the vehicle tires from the bridge. The developed program can handle more realistic models of bridges and various types of moving vehicles, such as when vehicles pass over a bump where separation of tires from road surface is possible.

5.2.3 Road Surface Condition

The road surface profile *r(x)* in Eqs. (5-3) to (5-6) is used as the input in the bridge-vehicle coupled model. The road surface condition considered in this study includes an artificial pseudo-random surface profile (road roughness) and approach span condition (see Fig. 5-1). Road surface roughness is normally considered as a random process with a Gaussian (normal) probability distribution (ISO 8068, 1995). A concise spectral model is used as:

$$\varphi(n)=\varphi(n_0)\left(\frac{n}{n_0}\right)^{-2} \tag{5-10}$$

where $\varphi(n)$ is the power spectral density (PSD) function (m^3/cycle/m) for the road surface elevation; n is the spatial frequency (cycle/m); n_0 is the discontinuity frequency of $1/(2\pi)$(cycle/m); and $\varphi(n_0)$ is the roughness coefficient (m^3/cycle) whose value is chosen depending on road condition. Roughness can be simulated in the space domain by applying the inverse discrete Fourier transform, as described by Wang and Huang (1992). A pseudo-random road surface profile of a roadway and bridge deck can be obtained by using this method.

However, according to ISO (ISO 8606, 1995) and Cebon (1999), occasional large local irregularities, such as potholes and faultings (bumps), should be isolated and treated separately from such pseudo-random road surface profiles. This is because the pseudo-random roughness only represents a gradual change in road surface condition, while the slope change in approach slab due to approach span deformation and the faulting at expansion joints are much more abrupt. Thus, the approach span condition (Fig. 5-1) considered in this study cannot be represented by a

Gaussian random process and needs to be treated separately. Therefore, the road surface condition is twofold: firstly, the roughness of the bridge deck and roadway, and secondly, the approach span condition, which includes the approach span deflection and the faulting at the ends of the approach slab, namely, the road surface condition r(x) is the superimposition of the approach slab deformation upon the natural road roughness of the whole roadway (including bridge deck and approach slab).

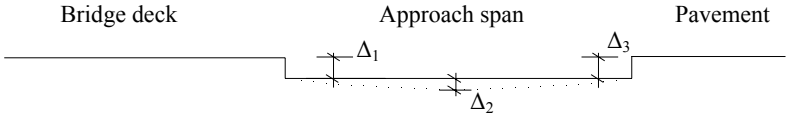

Fig. 5-4 Model of approach span deformation

As shown in Fig. 5-4, the faulting between approach slab and bridge deck can be modeled by a step up, while the faulting between pavement and approach slab by a step down (Green et al. 1997). To reduce the number of parameters in the analysis, the faulting values are assumed the same at both ends of the approach slab (Δ_1 and Δ_3). The approach slab deflection (Δ_2) and slope change in the approach slab, shown in Figs. 5-1 and 5-4, were obtained from the static analysis of approach spans (Cai et al. 2005).

5.3 Prototype of Analytical Bridge and Vehicle

To study the general dynamic behavior of short span bridges, four typical simply supported concrete slab bridges designed in accordance with AASHTO standard specifications (AASHTO 2002) are analyzed. The span lengths are 6 m, 8 m, 10 m, and 12 m, which is the normal range of span lengths for slab bridges. These bridges are of rectangular sections and are designed for a HS20-44 loading. Fig. 5-5 shows the first four vibration mode shapes of the bridge with a span length of 8 m where modes 1 and 4 correspond to bending modes, while modes 2 and 3 correspond to torsional modes. Vibration modes of other bridges are similar. Twenty modes of each bridge are taken into account in the analysis of dynamic response after a sensitivity study. The primary data of the bridges and the first ten modes of each bridge are listed in Table 5-1. The damping ratio is assumed to be 0.02.

The AASHTO HS20-44 truck is used in the numerical analysis and its sketch is shown in Fig. 5-3. The geometry, mass distribution, damping, and stiffness of the tires and suspension systems of this truck are listed in Table 5-2 (Wang and Liu 2000). The static wheel loads for the first, second, and third axle are 17.8 KN (4 kips), 71.2 KN (16 kips), and 71.2 KN (16 kips), respectively, which make the total weight of this truck 320 KN (72 kips). Modal frequencies of the vehicle are calculated as 1.52, 2.14, 2.69, 5.94, 7.74, 7.82, 8.92, 13.87, 13.99, 14.63, and 17.95 Hz.

Table 5-1 Modal frequencies (Hz) of slab bridges

First 10 modes of the slab bridge with span length of 6m and thickness of 0.30m	12.92, 15.37, 23.04, 36.06, 51.75, 54.18, 55.05, 62.57, 76.38, 80.28
First 10 modes of the slab bridge with span length of 8m and thickness of 0.40m	9.64, 12.71, 22.26, 38.57, 39.09, 41.80, 52.46, 64.01, 70.02, 85.92
First 10 modes of the slab bridge with span length of 10m and thickness of 0.50m	7.68, 11.27, 22.61, 30.72, 34.69, 43.29, 47.42, 68.34, 68.51, 72.16
First 10 modes of the slab bridge with span length of 12m and thickness of 0.60m	6.38, 10.39, 23.52, 25.52, 30.17, 44.78, 48.07, 56.72, 61.30, 66.58

Table 5-2 Major parameters of vehicle (HS20)

Mass of truck body 1	2612 (kg)
Pitching moment of inertia of truck body1	2022 ($kg.m^2$)
Rolling moment of inertia of tuck body 1	8544 ($kg.m^{2)}$
Mass of truck body 2	26113 (kg)
Pitching moment of inertia of truck body2	33153 ($kg.m^2$)
Rolling moment of inertia of tuck body 2	181216 ($kg.m^2$)
Mass of the first axle suspension	490 (kg)
Upper spring stiffness of the first axle	242604 (N/m)
Upper damper coefficient of the first axle	2190 (N.s/m)
Lower spring stiffness of the first axle	875082 (N/m)
Lower damper coefficient of the first axle	2000 (N.s/m)
Mass of the second axle suspension	808 (kg)
Upper spring stiffness of the second axle	1903172 (N/m)
Upper damper coefficient of the second axle	7882 (N.s/m)
Lower spring stiffness of the second axle	3503307 (N/m)
Lower damper coefficient of the second axle	2000 (N.s/m)
Mass of the third axle suspension	653 (kg)
Upper spring stiffness of the third axle	1969034 (N/m)
Upper damper coefficient of the third axle	7182 (N.s/m)
Lower spring stiffness of the third axle	3507429 (N/m)
Lower damper coefficient of the third axle	2000 (N.s/m)
L1	1.698 (m)
L2	2.569 (m)
L3	1.984 (m)
L4	2.283 (m)
L5	2.215 (m)
L6	2.338 (m)
B	1.1 (m)

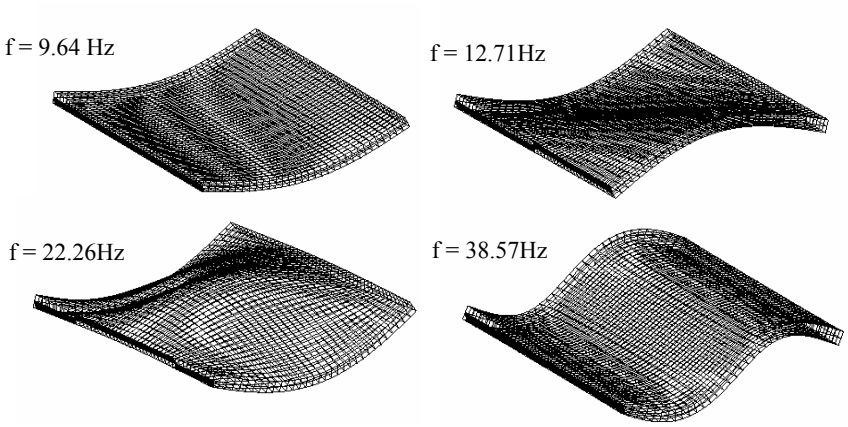

Fig. 5-5 First four modes of the 8 m slab bridge

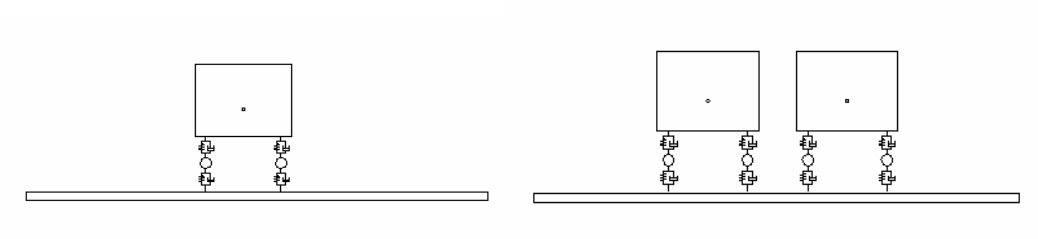

(a) **(b)**

Fig. 5-6 Vehicle position

Vehicles on the bridge may have different distribution patterns and may be located in different lanes randomly. The common practice is to use only one vehicle or a series of identical vehicles in one line (Guo and Xu 2001). Since the slab bridge considered in the present study has a very short span length, only one vehicle can be placed in each lane on the bridge at any given moment. For slab bridges with two lanes, both cases of one lane truck (Fig. 5-6(a)) and two lane trucks driving side by side (Fig. 5-6(b)) are considered, except as stated otherwise.

A 6 m long approach slab connecting the pavement and bridge deck is considered. As discussed earlier, the deformation from static analysis of the approach slab is used as an input to modify the road surface profile. The faulting between the bridge deck and approach slab and the faulting at the approach slab and pavement joint, ranging from 0.005 m to 0.038 m, have been used.

5.4 Dynamic Response of Slab Bridges

Short slab bridges have received less attention than medium length slab-on-girder bridges in terms of bridge dynamics. It will be seen that shorter bridges are actually more sensitive to uneven joint induced disturbances than longer span bridges. In the following parametric (sensitivity) study, only one truck passing over the bridge (Fig. 5-6(a)) is considered.

5.4.1 Effect of Vehicle Speed

The dynamic behavior of bridges depends on many factors, including the speed of the vehicle. While the effects of vehicle speeds on bridge vibrations have been studied by many researchers, this section focuses on the effect of vehicle speed on slab bridge dynamic response and attempt to explain and predict the observed critical speed conditions. The influence of vehicle speed, ranging from 5 m/s to 70 m/s with an interval of 5 m/s, on bridge response is studied. Although a driving speed of more than 40 m/s is beyond the legal maximum, it provides information on dynamic effects at higher speeds and helps observe the trends. To exclude the influence of other factors, a smooth road surface condition is assumed, which means the bridge deck and the pavement that the vehicle has traveled before it enters the bridge are perfectly smooth. The properties and fundamental frequencies of these bridges are given in Table 5-1.

Fig. 5-7 shows the time history of the vertical dynamic displacement at the mid-span of the 8 m long bridge. For a given time, the vehicle with different speeds is located at different places on the bridge. To compare the bridge dynamic response for different vehicle speeds at the same vehicle position, the distance between the vehicle's first axle and bridge entrance, instead of the time, is used as the x axis, with the entrance to the bridge defined as zero. It can be found that the bridge response differs under different vehicle speeds. The amplitude of dynamic displacement increases with the increase in the vehicle speed v if v is less than 20 m/s (Fig. 5-7 (a) and (b)); it decreases when v increases to 25 m/s (Fig. 5-7 (b)); and then increases again when v is not larger than 40 m/s (Fig. 5-7 (b) and (c)). After that, it decreases with the truck speed between 40 m/s and 60m/s. This phenomenon reveals that a higher vehicle speed does not necessarily increase the bridge dynamic response, and the influence of vehicle speed on the bridge response may occur in some particular pattern.

The spectral density amplitude, shown in Fig. 5-8, is obtained from spectral analysis of the time history of the 8 m bridge's mid-span dynamic displacement under different driving speeds. It is found that the bridge dynamic displacement is dominated by the first mode of the bridge, which corresponds to the first symmetric bending mode. Again, results in frequency domain show that the dynamic response reaches the maximum value when the driving speed approaches 40m/s.

Observations of the numerical results indicate that there is at least one critical speed for the HS20 truck passing through this 8 m bridge. It can be explained by the following equation:

$$\frac{v}{L_v} n = f \quad (n = 1,2,3\cdots) \tag{5-11}$$

where v = vehicle velocity; L_v= vehicle axle load spacing; and f = fundamental frequency of the bridge under vehicle loads. Eq. (5-11) was originally used to explain the train resonant speed for railway bridges (Li and Su 1999). Theoretical and numerical studies on railway bridges have shown that when n times the frequency component due to a series of moving loads is equal to the natural frequency of a bridge, the resonant effect will occur.

As mentioned previously, the numerical results (Figs. 5-7 and 5-8) show that the bridge has the maximum dynamic response when the truck speed is around 40 m/s, which is close to the critical speed 41.1 m/s obtained from Eq. (5-11) using a bridge fundamental frequency of 9.64

Hz and a HS20 truck load axle spacing of 4.26 m. This consistency between them is probably due to the short span length of the bridge. Although the number of axle loads of the truck is much less than that of a train, the multi-axle truck loads can still be considered as repeated loads on short bridges, because the bridge span of 8 m is short compared to the 4.26 m spacing of the HS20 truck axle loads.

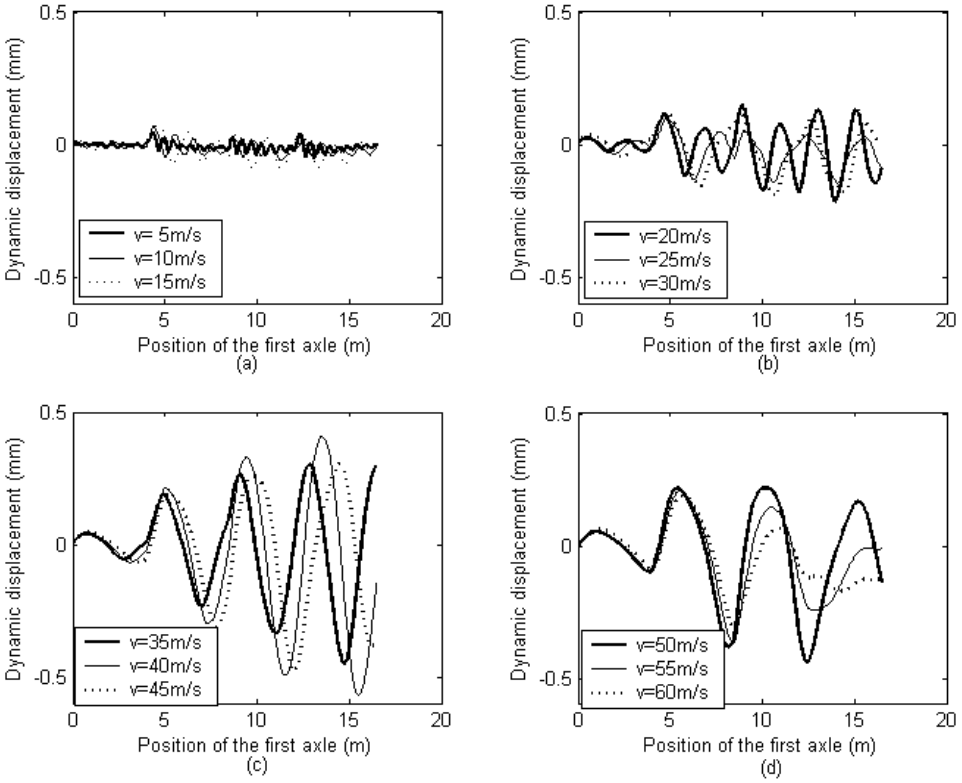

Fig. 5-7 Vertical displacement of the bridge with span length of 8m

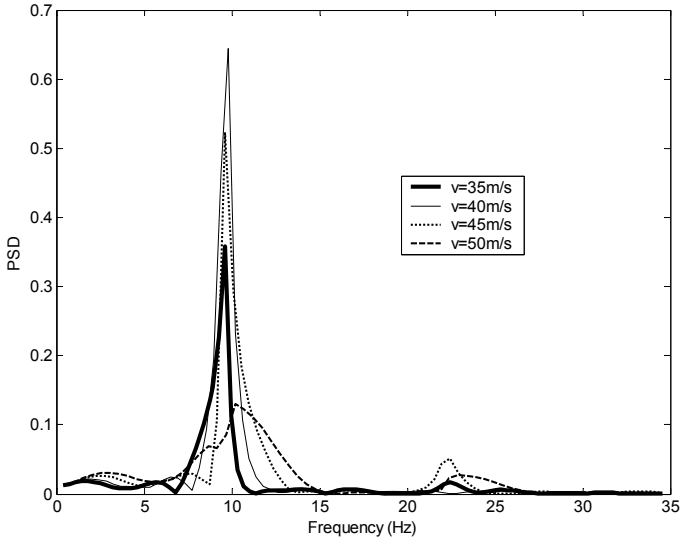

Fig. 5-8 Dynamic response of 8 m bridge in frequency domain

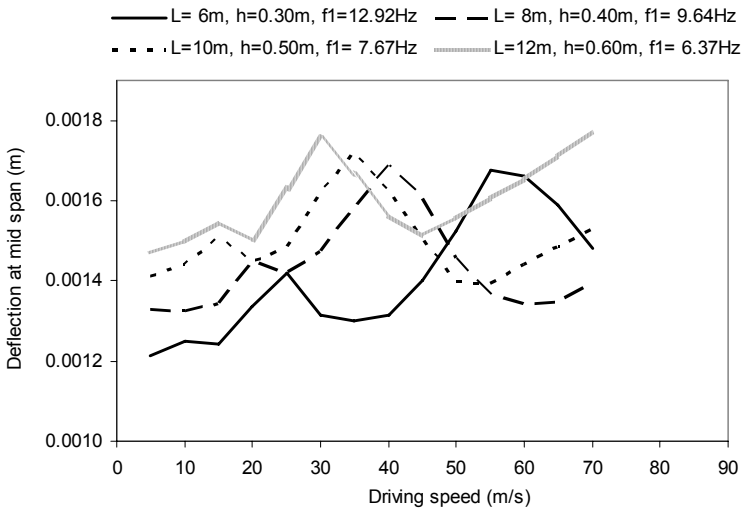

(a)

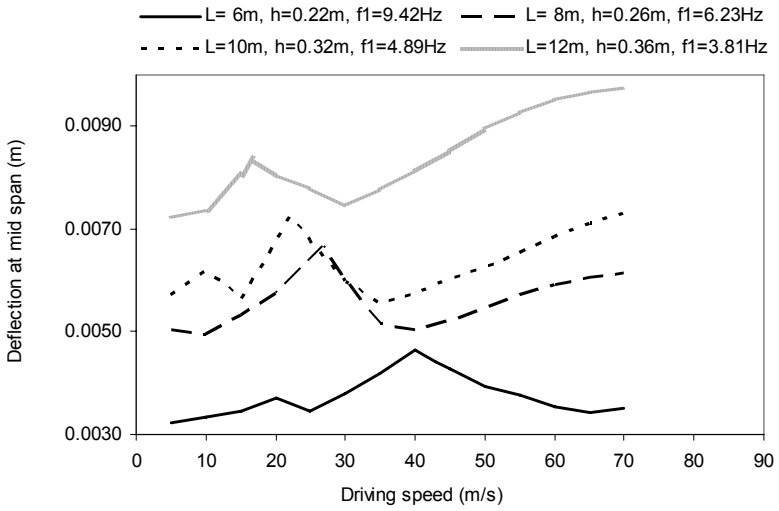

(b)

Fig. 5-9 Effect of truck speed

The deflection-speed relation curves at the mid-span are shown in Fig. 5-9 (a) for all four bridges. Moreover, the relation of truck speed and the bridge dynamic response of all four bridges are also analyzed with smaller slab thickness (Fig. 5-9(b)). Although these more flexible bridges are not designed according to AASHTO codes, the relation of truck speed and the bridge dynamic response shown in Fig 9(b) also confirmed the existence of a critical speed for more flexible slab bridges.

Fig. 5-9(a) indicates that within a possible vehicle speed range, the short bridge has a critical speed for the HS20 truck to excite the bridge's resonant response. For example, when the

truck speed is around 35 m/s, the dynamic displacement of the 10 m bridge (with slab thickness of 0.50 m) approaches the maximum value. The critical speeds calculated by Eq. (5-11) for the bridges mentioned in Fig. 5-9 are listed in Table 5-3. Compared with Table 5-3, the results shown in Fig. 5-9 have numerically proven that Eq. (5-11) is also applicable for short bridges under truck load. When the truck has multi-axle loads, the axle load can be considered as a repeating load on bridges, especially when the span length of the bridge is short compared to the axle load spacing of the truck. Consequently, it can be concluded that there exist critical speeds that excite resonant vibrations for short bridges when multi-axle trucks pass over them.

Table 5-3 Critical speed

Critical speed (m/s)	Bridges shown in Fig. 5- 9(a)				Bridges shown in Fig. 5-9 (b)			
	L=6m h=0.30m	L=8m H=0.40m	L=10m h=0.50m	L=12m h=0.60m	L=6m h=0.22m	L=8m h=0.26m	L=10m h=0.32m	L=12m h=0.36m
by using Eq. (5-11)	55.1	41.1	32.7	27.2	40.1	26.6	20.8	16.2
from numerical results	55	40	35	30	40	25	20	15

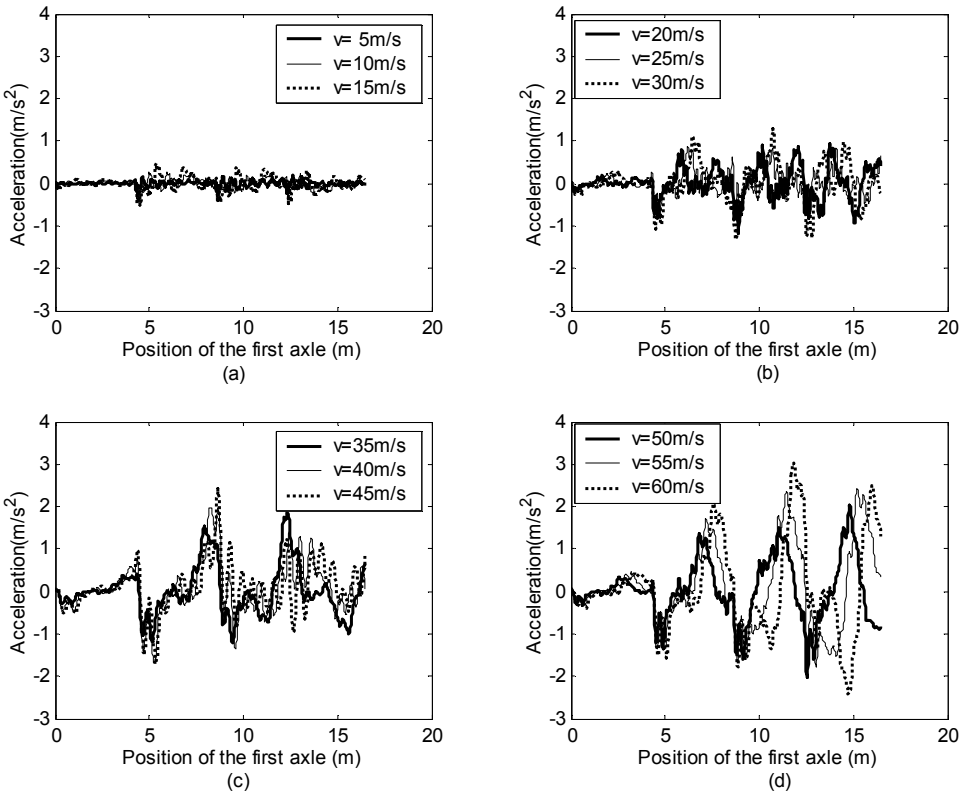

Fig. 5-10 Acceleration response of the bridge with span length of 8 m in time history

Fig. 5-10 shows the mid-span vertical acceleration of the 8 m bridge in time history. The critical speed for bridge dynamic displacement does not necessarily cause the maximum acceleration response in the bridge. According to Fig. 5-10, it is clear that the truck speed does increase the bridge acceleration response, although it does not necessarily increase the displacement response monotonically. The analyses of the vertical acceleration of the other three bridges listed in Table 5-1 also reveal the same trend. It can be explained by the fact that in bridge dynamic displacement response, the higher modes also have a contribution, but not a dominant one (Fig. 5-8). As the vehicle speed increases, the frequency component $\frac{v}{L_v}$ due to moving loads increases. The higher frequency truck loads will excite higher modes of the bridge, and although the contribution of higher modes increases (Fig. 5-7), the first bending mode is still dominant in the displacement response that is expressed as $\{d(t)\} = \sum_{i=1}^{N} \zeta_i \sin[(2\pi f_i)t + \theta_i]\{\phi_i\}$ ($\{\phi_i\}$ = the modal shape i, ζ_i = the participation factor of modal shape i, f_i = the frequency of modal shape i, and θ_i = the initial phase of modal shape i). However, the increase in contribution of higher modes will increase the acceleration response because the acceleration, $\{\frac{\partial^2 d(t)}{\partial t^2}\} = -\sum_{i=1}^{N} \zeta_i (2\pi f_i)^2 \sin[(2\pi f_i)t + \theta_i]\{\phi_i\}$, is not only affected by the mode participation factor ζ_i, but also by the frequency of each mode f_i^2. Therefore, although the higher mode is not the dominant mode in the displacement response, it may be more dominant in the acceleration response due to the higher frequency of these modes. As a result, the acceleration increases monolithically with the increase in the vehicle driving speed.

5.4.2 Effect of Approach Span Condition

To investigate the pure effect of the approach span condition and to exclude the effect of other factors such as road roughness, the surface of pavement, approach slab, and bridge deck are assumed to be perfectly smooth without any depressions, i.e., considering only the approach slab deflection and the faulting at the approach slab ends. In order to investigate the effect of approach slab deflection, bridge dynamic responses under the faulting condition and under the combination of both conditions of faulting and approach slab deflection are compared. Fig. 5-11 shows the comparison of the dynamic displacement of the 8 m bridge under these two conditions. An approach slab with a length of 6 m was used. The extreme case of a large embankment soil settlement is assumed, which causes the approach slab to lose support from the soil. The deflection of the approach slab is obtained by using the method described by Cai et al. (2005). Meanwhile, a step value of 0.005 m is used to model a small faulting condition. It is observed from Fig. 5-11 that the effect of the approach span deflection is very small compared with the faulting conditions at the approach slab ends, even though the faulting is relatively small. This may be explained by the fact that the deflection of the approach slab is more gradual compared to the faulting at the approach slab ends (Fig. 5-1). Therefore, in the following analyses the approach slab deflection is excluded, and only the faulting at the expansion joints are considered.

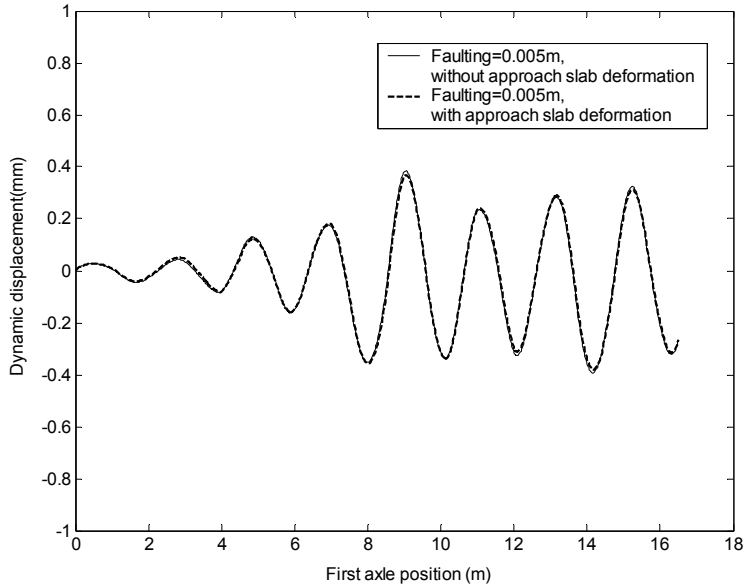

Fig. 5-11 Vertical displacement of the bridge with span length of 8 m (under conditions with/without approach slab deflection)

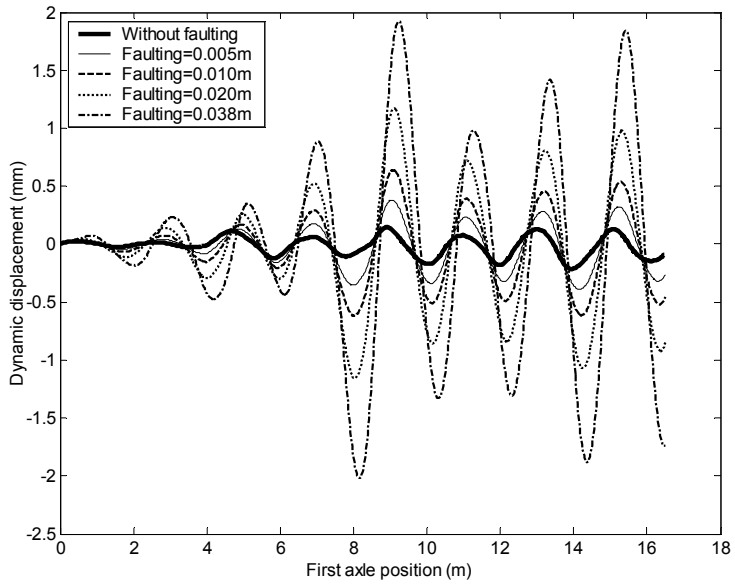

Fig. 5-12 Vertical displacement of the 8m bridge in time history (under different approach span conditions)

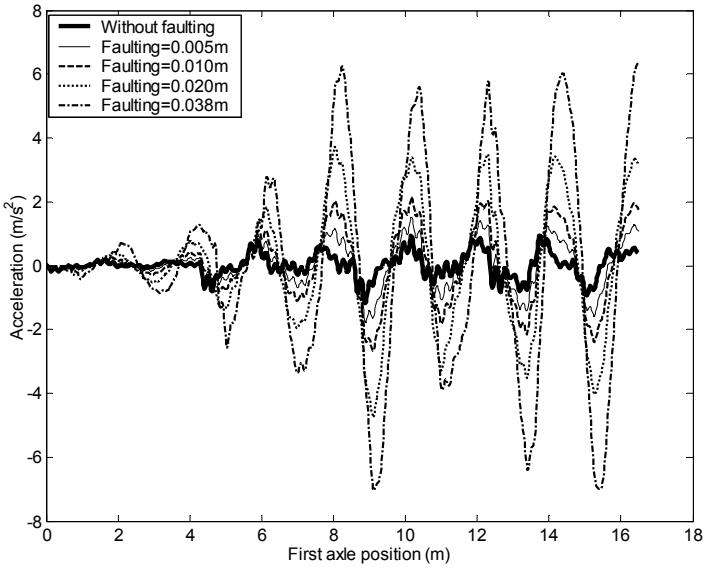

Fig. 5-13 Vertical acceleration of the 8m bridge in time history
(under different approach span deformation condition)

Five faulting conditions: Δ_1=0, 0.005, 0.01, 0.02, and 0.038 m were considered. Figs. 5-12 and 5-13 show the time history of the 8 m bridge displacement response and acceleration response under different faulting conditions, respectively. The HS20 truck speed is 20 m/s. It can be found that the bridge dynamic response undergoes a significant increase as the faulting increases. In the extreme case, the dynamic mid-span displacement of the bridge under a large faulting (Δ_1=0.038 m) condition can be as much as several times of that under the smooth road condition. Such an increase in bridge response is due to the larger dynamic load caused by the initial vehicle disturbance experienced when the vehicle passes over the uneven joints before it enters the bridge.

Fig. 5-14 shows the effects of different faulting conditions on all four bridges with a vehicle speed of 20m/s. The amplification factor plotted in the figure is the ratio of the maximum dynamic displacement to the static displacement of bridges at the mid-span. It is clear that the same faulting condition has a much larger influence on shorter bridges than it does on longer bridges. For example, for the faulting of 0.02 m, the amplification factors for bridges with span lengths of 6 m, 8 m, 10 m, and 12 m are 1.92, 1.76, 1.48, and 1.42, respectively.

Fig. 5-15 shows the dynamic tire load (contact force in Eqs. (5-5) and (5-6)) of the third axle of the truck after it passed over the faulting of 0.02 m at the bridge entrance where the bump causes a large tire force (sharp peak in the figure). Due to the damping system of the truck, the tire load dissipates very quickly after the truck received the bump from the step up. Thus, the dynamic tire load applied on a shorter bridge is larger than on a longer bridge under the same faulting condition. For longer span bridges, after the truck received the bump disturbance at the bridge end, it has more time for the vehicle to dissipate the initial disturbance and to become stable before it comes to the mid-span of the bridge. Thus, the same faulting value causes less of a dynamic response to a longer bridge than to a shorter bridge.

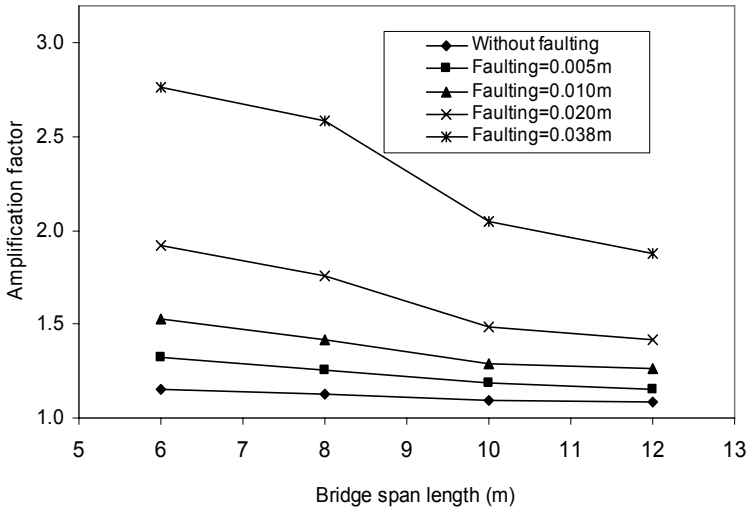

Fig. 5-14 Amplification factor caused by bump disturbed truck versus bridge span length

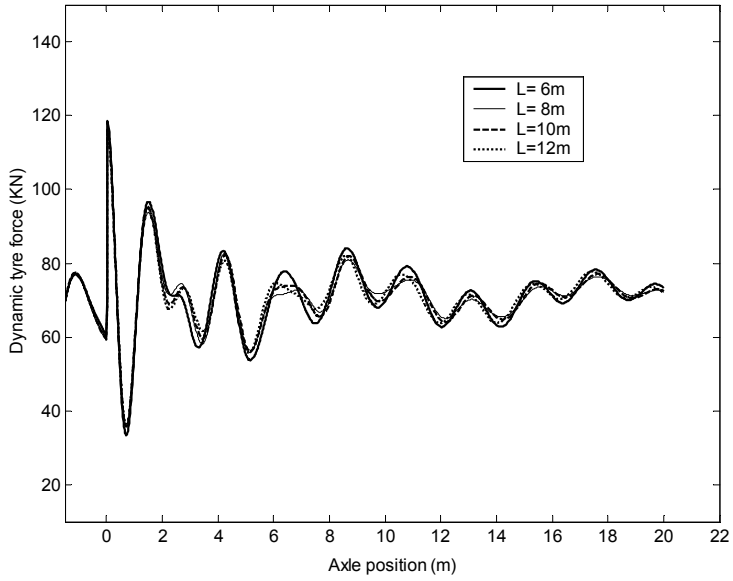

Fig. 5-15 Dynamic tire force of the third axle (faulting = 0.02 m)

5.4.3 Effect of Bridge Deck Surface Condition

The bridge deck surface condition is an important factor affecting the vehicle-bridge interaction and were more intensively studied. In this study four bridge surface conditions are used, which are classified as very good, good, average, and poor roads. According to ISO specifications, the values of 5×10^{-6}, 20×10^{-6}, 80×10^{-6}, and 256×10^{-6} for different road conditions were used as the roughness coefficient, $\varphi(n_0)$, in Eq. (5-10).

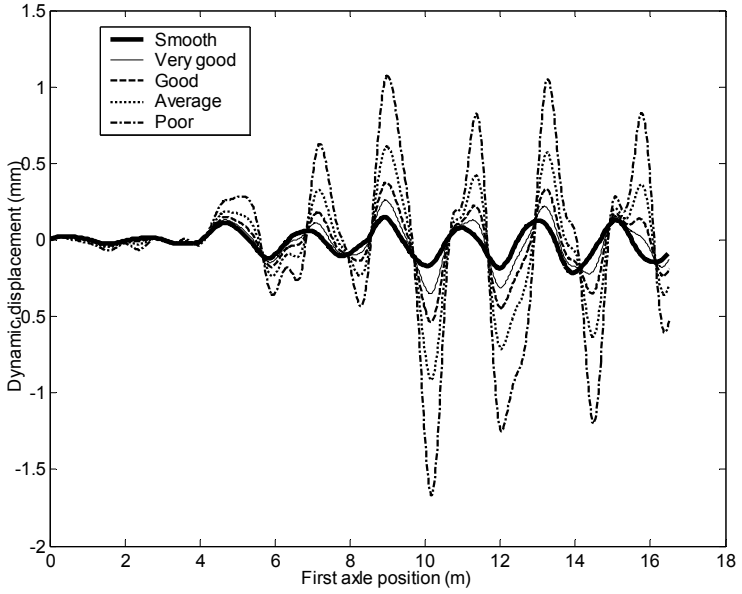

Fig. 5-16 Vertical displacement of the 8m bridge in time history (under different bridge deck surface condition)

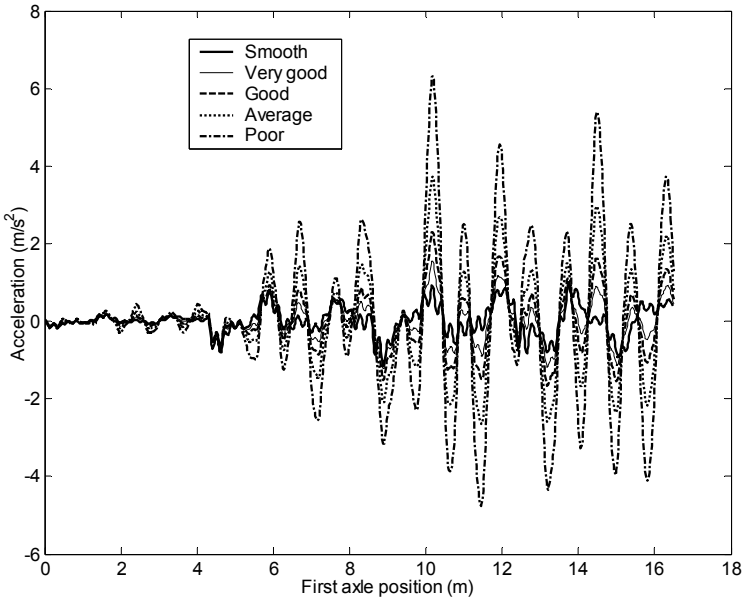

Fig. 5-17 Vertical acceleration of the 8m bridge in time history (under different bridge deck surface condition)

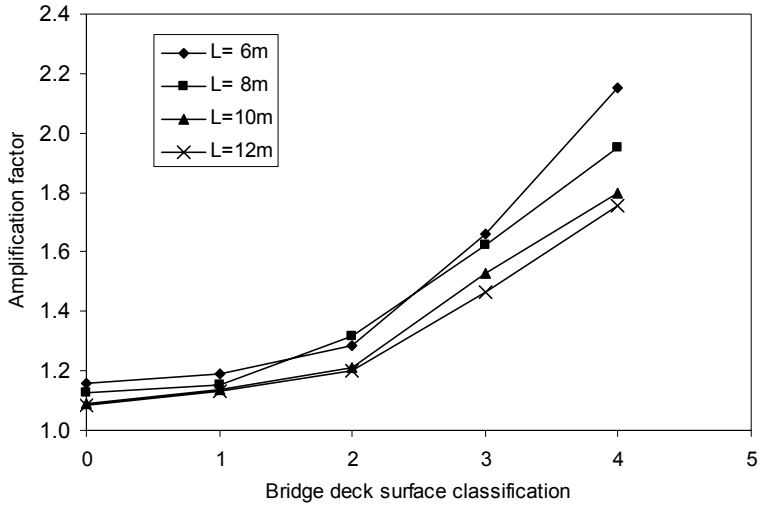

Fig. 5-18 Amplification factor versus road surface profile

Figs. 5-16 and 5-17 show the time series response of the 8 m bridge with different road roughness but without considering any approach span deformation. The displacement amplification factors of different bridges under different road roughness are also shown in Fig. 5-18. In this figure the values of 0, 1, 2, 3, and 4 at the x axis denotes the road surface classifications of perfectly smooth, very good, good, average, and poor, respectively. Figs. 5-16 to 5-18 illustrate that road surface roughness significantly influences the dynamic behavior of bridges. With increasing road roughness, the dynamic response of bridges increases considerably.

5.5 Effect of Approach Span Condition on Impact Factors of Slab Bridges

The previous discussion was meant to investigate the effect of each individual factor on the dynamic behavior of slab bridges. It has been shown that the effect of approach span condition, especially the faulting on the dynamic response of short bridges, is significant. In this section the influence of the approach span condition on the impact factor used in the bridge design is of concern.

Due to the difficulty and complexity in predicting an accurate bridge dynamic response for design, most design codes simply amplify the static response with an impact factor (IM) that is commonly defined as

$$IM(\%) = (\frac{R_d}{R_s} - 1) \times 100\% \tag{5-12}$$

in which R_d and R_s are the maximum dynamic and static responses of the bridge, respectively.

To analyze the effect of approach span condition on impact factors, four road conditions are considered as inputs to the bridge-vehicle coupled model, respectively: (i) smooth road surface without considering any surface roughness or approach span deformation; (ii) smooth road surface as in (i) plus uneven joints (faulting); (iii) rough road surface with a condition of good for the pavement, approach slab, and bridge deck, i.e. considering the road surface

roughness only, but the unevenness at the approach slab ends are not included; and (iv) rough road surface as in (iii) plus uneven joints. Meanwhile, four different joint conditions of the approach span (Δ_1=0.005 m, Δ_1=0.01m, Δ_1=0.02 m, and Δ_1=0.038 m) and two trucks passing over the bridge side by side (Fig. 5-6(b)) are considered in the analysis. For the last two conditions, the initial conditions are obtained by allowing the trucks to travel an arbitrary distance of 100 m before they enter the bridge approach slab, i.e., a 100 m lead distance is given to obtain stable initial conditions before the vehicles move onto the approach span, then continue moving until they left the end of the bridge.

Fig. 5-19 shows the results of an 8 m bridge dynamic response for displacement under the four different road surface conditions. The faulting value in these figures is 0.01 m. It is apparent that this bridge presents a much larger maximum response under conditions (ii) and (iv) than under conditions (i) and (iii), respectively, which shows that the effect of the faulting condition on bridge dynamic response is significant. Moreover, the bridge dynamic response under condition (ii) is larger than under condition (iii), indicating that the faulting of approach slab is more critical than the rough road surface condition to short bridges' dynamic response.

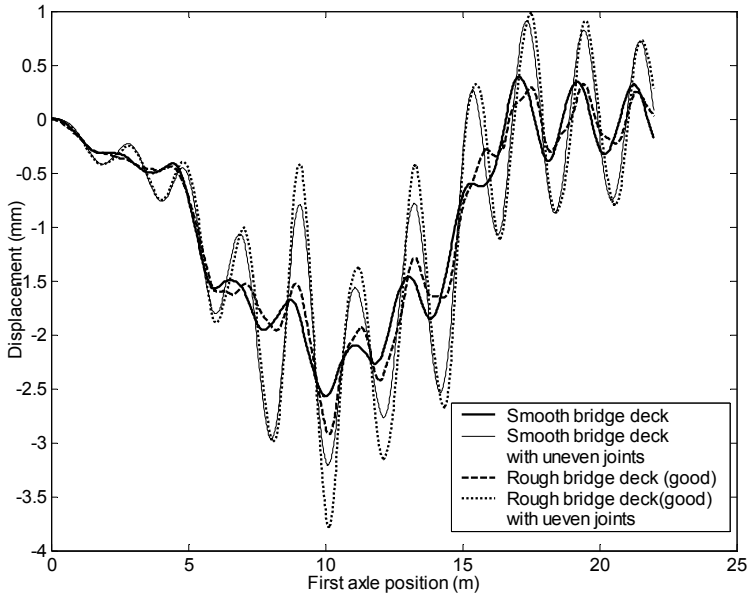

Fig. 5-19 Mid-span displacement of the 8m bridge under different conditions

Based on the four road surface conditions and a vehicle speed of 20 m/s, impact factors of moment IM(M) and mid-span displacement IM(d) for all four bridges (in Table 5-1) are listed in Table 5-4. Table 5-4 indicates that when assuming the road surface is perfectly smooth, the impact factors of moment and displacement are tremendously increased due to the uneven joints at the approach slab end (compare (i) and (ii)). When the road roughness is classified as in good condition, the impact factors are increased following the same trends (compare (iii) and (iv)).

A comparison of impact factors under conditions (ii) and (iii) in Table 5-4 confirms that the effect of faulting conditions on bridge impact factors is predominant in the road surface profile, especially when the faulting value is large. For the short bridge with a span length of 6 m, the

impact factor caused by a faulting value of 0.005 m is larger than that caused by road roughness with "good" condition. For bridges with span lengths of 8 m, 10 m, and 12 m, a faulting value of 0.01 m caused larger impact factors than road roughness. As mentioned before, this phenomenon can be explained with the fact that faulting (bump) is a more abrupt depression compared to the regular road roughness. The disturbance received by the vehicle from such abrupt depressions will not be dissipated in the short time period when the vehicle passes over the bridge. As a result, the severe vehicle vibration increases the impact factor of short bridges.

The impact factor in AASHTO (2002) specifications is presented as

$$IM = \frac{15.24}{L + 38.1} \tag{5-13}$$

where *IM* is no larger than 0.3 and L is the loaded bridge span length in meters. According to Eq. (5-13) and AASHTO specifications, the impact factor for bridges with a span length less than 12.7 m is 30%.

Table 5-4 Impact factors of short span bridges

Road surface condition		6m bridge		8m bridge		10m bridge		12m bridge	
		IM (d)	IM (M)	IM (d)	IM (M)	IM (d)	IM (M)	IM (d)	IM (M)
(i)		0.14	0.14	0.11	0.12	0.07	0.06	0.07	0.05
(ii)	Δ_1=0.038m	1.62	1.44	1.35	1.33	0.87	0.84	0.68	0.65
	Δ_1=0.020m	0.86	0.79	0.67	0.65	0.41	0.40	0.32	0.32
	Δ_1=0.010m	0.48	0.47	0.38	0.35	0.24	0.26	0.20	0.17
	Δ_1=0.005m	0.30	0.30	0.23	0.22	0.12	0.14	0.09	0.07
(iii)		0.24	0.20	0.25	0.23	0.17	0.13	0.18	0.16
(iv)	Δ_1=0.038m	1.80	1.67	1.44	1.45	0.99	0.91	0.79	0.74
	Δ_1=0.020m	1.08	0.94	0.89	0.81	0.51	0.47	0.45	0.40
	Δ_1=0.010m	0.70	0.62	0.63	0.55	0.32	0.30	0.24	0.21
	Δ_1=0.005m	0.52	0.44	0.43	0.37	0.20	0.16	0.16	0.17

In Table 5-4 it is clear that when the faulting is larger than 0.02 m, the impact factors of all bridges exceed the impact factor specified in the AASHTO code; when the faulting is 0.01 m, the impact factors of the 6 m and 8 m bridges were underestimated by Eq. (5-13). Under the good road surface condition, the impact factors of bridges with span lengths of 6 m, 8 m, and 10 m in most cases are larger than what the AASHTO code specifies, namely 30%. However, for the bridge of 12 m, most of the impact factors are lower than those values specified by the AASHTO code, except those caused by faultings of 0.038 m and 0.02 m. For all four bridges with good road surface without faulting at the bridge ends, the impact factors are smaller than those computed by the AASHTO specifications.

Similarly compared with the impact factor values specified by the AASHTO LRFD code (AASHTO 2004), i.e. 33% for bridge main components, the computed impact factors for conditions (i) and (iii) are less than those from the code specifications. However, when the expansion joints are not even, the impact factors may be higher than the values specified by AASHTO codes.

5.6 Conclusions

The dynamic responses of slab bridges under HS20 trucks are obtained by using the bridge-vehicle coupled model to simulate the interaction between the two systems in the time domain. The dynamic behavior of four short slab bridges with span lengths of 6 m, 8 m, 10 m, and 12 m has been analyzed.

The vehicle speed does affect the dynamic performance of short slab bridges. A higher vehicle speed causes a larger bridge vertical acceleration; however, the higher vehicle speed does not necessarily increase the bridge dynamic displacement response. The axle load of multi-axle trucks can be considered as a repeating load on short bridges. A vehicle speed induced resonant vibration that is usually observed in train bridges has also been predicted for short bridges.

Initial conditions of vehicles entering bridges excited by a large deformation of approach span have a significant influence on bridge dynamic response. The local unevenness of expansion joints at the approach slab ends tremendously increases the dynamic response of short slab bridges. Moreover, the bridge dynamic response under the condition of a large approach span deformation, especially the faulting, is much higher than that under the rough road surface classified in "good" condition. The same faulting value has a much larger influence on short bridges than it does on longer bridges. Longer span bridges have more time for the initial disturbance to be dissipated and for the vehicle to become stable before it comes to the critical mid-span of the bridge.

Providing that short bridges have a good road surface condition and smooth joints (small faulting) at the bridge ends, the impact factors are generally smaller than those computed by the AASHTO specifications (both standard and LRFD codes). However, AASHTO specifications may underestimate the impact factors for short bridges with uneven joints at the bridge ends. This situation should be emphasized in practice, especially in rating existing short span bridges.

5.7 References

American Association of State Highway and Transportation Officials (AASHTO). (2004). *LRFD bridge design specifications,* Washington, DC.

American Association of State Highway and Transportation Officials (AASHTO). (2002). *Standard specifications for highway bridges,* Washington, DC.

Cai, C. S., Shi, X. M., Voyiadjis, G. Z. and Zhang, Z. J. (2005). "Structural performance of bridge approach slab under given embankment settlement." *Journal of Bridge Engineering,* 10(4), 482-489.

Cebon, D. (1999). *Handbook of vehicle-road interaction*, 2nd Ed., Swets & Zeitlinger B.V., Lisse, the Netherlands.

Green, M. F., Cebon, D. and Cole, D. J. (1997). "Effects of heavy vehicle suspension design on the dynamics of highway bridges." *Journal of Structural Engineering*, 121(2), 272-282.

Guo, W. H., Xu, Y. L. (2001). "Fully computerized approach to study cable-stayed bridge-vehicle interaction," *Journal of Sound and Vibration*, 248(4), 745-761

International Organization for Standardization (ISO). (1995). "Mechanical vibration –Road surface profiles-Reporting of measured data." *ISO 8068: 1995 (E),* ISO, Geneva.

Huang, D.Z., Wang, T.L., and Shahaway, M. (1993). "Impact studies of multi-girder concrete bridges," *Journal of Structural Engineering*, 119(8), 2387-2402.

Li, C.Y. (1996). "Bridge vibration and impact under moving vehicles." *Proceedings of the 1996 3rd Joint Conference on Engineering Systems Design and Analysis, ESDA.* Jul 1-4 1996*,* Montpellier, v 81, n 9, p 17-23.

Li, J. Z. and Su, M. B. (1999). "The resonant vibration for a simply supported girder bridge under high speed trains." Journal of Sound and Vibration, 224(5), 897-915.

White, D., Sritharan, S., Suleiman,M., Mekkawy, M., and Chetlur, S. (2005). "Identification of the best practices for design, construction, and repair of bridge approaches." Rep. No. *CTRE Project 02-118*, Iowa Department of Transportation, Ames, IA.

Wang, T. L. and Liu, C.H. (2000). "Influence of Heavy Trucks on Highway Bridges," Rep. No. *FL/DOT/RMC/ 6672-379*, Florida Department of Transportation, Tallahassee, FL.

Wang, T. L. and Huang, D. Z. (1992). "Computer modeling analysis in bridge evaluation." Rep. No. *FL/DOT/RMC/0542-3394*, Florida Department of Transportation, Tallahassee, FL.

CHAPTER 6 INFLUENCE OF APPROACH SPAN CONDITION ON VEHICLE-INDUCED DYNAMIC RESPONSE IN SLAB-ON-GIRDER BRIDGES

6.1 Introduction

Vehicle-induced dynamic response in bridges is one of the primary problems concerning bridge engineers. Moving vehicles, acting as oscillators on a bridge as well as time variant forces, usually produce larger responses in the bridge than static vehicles. They have become one of the causes of deterioration and reduction in long-term serviceability of the bridge, although major bridge failures are not usually caused by moving vehicles. The effect of moving vehicles on the dynamic response of bridges is of primary importance in the design of these structures.

As playing an important role in highway transportation systems, slab-on-girder bridges raised great interest in studying bridge-vehicle interactions. Extensive researches (e.g., Green and Cebon 1994; Kim and Nowak 1997; Wang and Liu 2000), including both experimental and theoretical works, have been conducted to determine the dynamic behavior for this type of bridges. Previous investigations indicated that factors that are important in bridge dynamic performance induced by moving vehicles are the dynamic characteristics of the bridge and the vehicle, and the road surface condition of the approach roadway and bridge deck (Huang et al. 1993). Among these factors, the vehicle initial condition is an important one that affects the dynamic responses of both the bridge and vehicles (Li 1996). The vehicle initial condition is caused not only by the roughness of the roadway that the vehicle traveled on before it enters the bridge, but also by uneven approach span conditions upon entrance to the bridge. The uneven approach conditions are usually caused by the differential settlement of embankment soil and abutments and/or bridge approach deformation.

A bridge approach slab is usually constructed to connect the bridge deck with the roadway. It is intended to provide a smooth transition between the bridge deck and the roadway pavement. However, differential settlement often occurs between the bridge abutment and the embankment soil either because the soil underlying the approach slab consolidates or because the embankment soil materials are compressible and the bridge is relatively rigid. When the soil settlement occurs, the approach slab of bridges loses its contacts and supports from the soil, and the slab will bend and deform in a concave manner (Cai et al. 2005). Meanwhile, loads on the slab will also redistribute to the ends of the slab, which may result in faulting (or bump) across the roadway at the ends of the approach slab (Δ_3 in Fig. 6-1). On the other hand, the expansion joint that connects the approach slab and bridge deck will form a faulting (Δ_1 in Fig. 6-1) due to the differential settlement of the abutments and/or poor maintenance. When a "bump" forms at the bridge end, repeating traffic vehicles can deteriorate the expansion joint in turn. Thus, a rough transition region has developed with time in some bridge approaches. Consequently, the vehicle receives an initial disturbance before it reaches the bridge. This initial excitation of the vehicle causes an extra impact load on the bridge and affects the dynamic responses of both the bridge and the vehicle.

The development and cause of bump-related problems have been commonly recognized and identified; however according to current literature review (Bruni et al. 2003; Chatterjee et al. 1994; Green et al. 1997; Hwang and Nowak 1991; Wang and Huang 1994; Sammartino et al.

1999), the effect of bridge approach span conditions on the bridge dynamic performance has seldom been studied.

The objective of this study is to analyze the possible effect of the approach span deformation on the dynamic behavior of slab-on-girder bridges caused by heavy vehicles moving across the bridge. In order to achieve this objective, a bridge-vehicle coupled model, which takes into account the road roughness and approach span conditions, is first developed. Then, the model is adjusted by using experimental results obtained in a full bridge test. Using this validated model, the dynamic behavior of slab-on-girder bridges with different span lengths induced by the AASHTO HS20 truck is investigated. A parametric study is conducted to investigate the influence of approach span conditions on bridge dynamic response. The distribution of impact factors and load distribution factors is also analyzed and compared with values specified in current AASHTO codes.

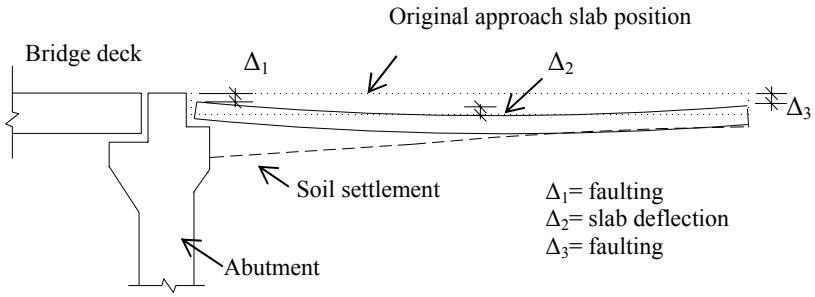

Fig. 6-1 Illustration of approach span deformation

6.2 Bridge-Vehicle Coupled System

The present study has developed a fully computerized program to simulate the interaction of any types of coupled vehicle-bridge systems, with consideration of road roughness and approach span deformations.

6.2.1 Bridge-Vehicle Numerical Model

A heavy vehicle is idealized as a combination of a number of rigid bodies connected by a series of springs and dampers while the bridge is modeled using the conventional finite element method. For demonstration purposes, a 3-axle articulated truck consisting of up to 11 independent degrees of freedoms is shown in Fig. 6-2. The equations of motion for the vehicle and bridge are derived based on the following matrix form:

$$[M_v]\{\ddot{d}_v\} + [C_v]\{\dot{d}_v\} + [K_v]\{d_v\} = \{F_v^{\,G}\} + \{F_c\} \tag{6-1}$$

$$[M_b]\{\ddot{d}_b\} + [C_b]\{\dot{d}_b\} + [K_b]\{d_b\} = \{F_b\} \tag{6-2}$$

where the vehicle mass matrix $[M_v]$, damping matrix $[C_v]$, and stiffness matrix $[K_v]$ are obtained by considering the equilibrium of the forces and moments of the vehicle system; $\{d_v\}$ is the displacement vector of vehicle; $\{F_v^G\}$ is the self-weight of the vehicle; $\{F_c\}$ is the vector of wheel-bridge contact forces acting on the vehicle; and $\{F_b\}$ is the wheel-bridge contact forces on the bridge. The contact between the bridge and the moving vehicle is assumed to be a point contact. The other variables of the bridge are similarly defined by changing the subscript v for the vehicle to b for the bridge.

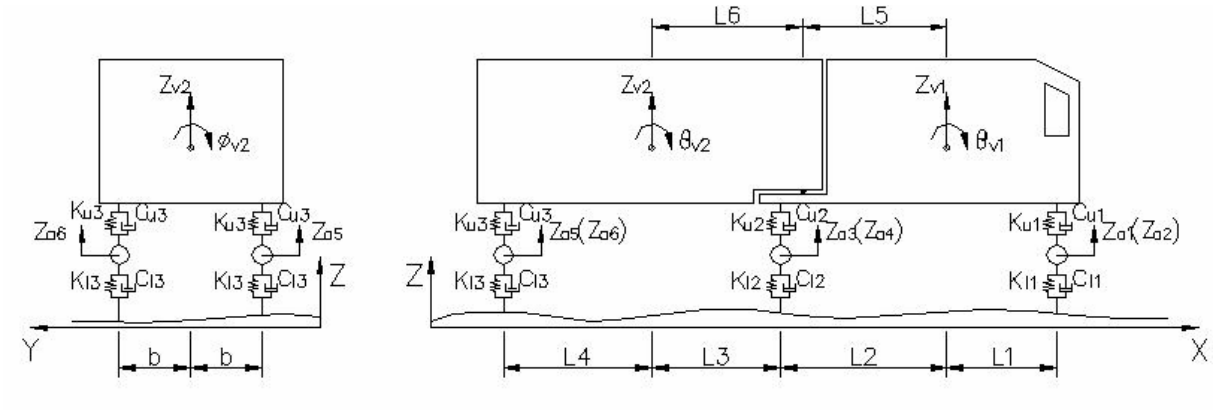

Fig. 6-2 Vehicle model

The equations of motion for the vehicle and bridge are coupled through the interaction forces, i.e. $\{F_b\}$ and $\{F_c\}$. $\{F_b\}$ and $\{F_c\}$ are action and reaction forces existing at the contact points of the two systems and are expressed as a function of the deformation of the vehicle's lower springs $\{\Delta_l\}$:

$$\{F_b\} = -\{F_c\} = [K_l]\{\Delta_l\} + [C_l]\{\dot{\Delta}_l\} \tag{6-3}$$

where $[K_l]$ and $[C_l]$ are the coefficients of the vehicle's lower springs and dampers, respectively. The relation among the vehicle axle suspension displacement Z_a, displacement of bridge at the wheel-bridge contact point Z_b, deformation of the lower springs of vehicle Δ_l, and road surface profile $r(x)$, should satisfy the compatible displacement condition and can be expressed as:

$$Z_a = Z_b + r(x) + \Delta_l, \quad \dot{Z}_a = \dot{Z}_b + \dot{r}(x) + \dot{\Delta}_l \tag{6-4}$$

in which $\dot{r}(x) = \frac{dr(x)}{dx}\frac{dx}{dt} = \frac{dr(x)}{dx}V(t)$ and $V(t)$ is the vehicle velocity. By substituting Eq. (6-4) into Eq. (6-3), the contact force vector between the bridge and the vehicle can be rewritten as

$$\{F_b\} = -\{F_c\} = [K_l](Z_a - Z_b - r(x)) + [C_l](\dot{Z}_a - \dot{Z}_b - \dot{r}(x)) \tag{6-5}$$

By substituting Eq. (6-5) into Eqs. (6-1) and (6-2), the final equations of motion for the coupled system are:

$$\begin{bmatrix} M_b & \\ & M_v \end{bmatrix}\begin{Bmatrix} \ddot{d}_b \\ \ddot{d}_v \end{Bmatrix} + \begin{bmatrix} C_b + C_{bb} & C_{bv} \\ C_{vb} & C_v \end{bmatrix}\begin{Bmatrix} \dot{d}_b \\ \dot{d}_v \end{Bmatrix} + \begin{bmatrix} K_b + K_{bb} & K_{bv} \\ K_{vb} & K_v \end{bmatrix}\begin{Bmatrix} d_b \\ d_v \end{Bmatrix} = \begin{Bmatrix} F_b^r \\ F_v^r + F_v^G \end{Bmatrix} \tag{6-6}$$

Compared with Eqs. (6-1) and (6-2), there are additional terms C_{bb}, C_{bv}, C_{vb}, K_{bb}, K_{bv}, K_{vb}, F_b^r, and F_v^r in Eq. (6-6), which are due to the expansion of the contact force vector. When the vehicle is moving across the bridge, the bridge-vehicle contact points change. Then, the road roughness r(x) at the contact points no longer remains the same. Consequently, the contact forces between the bridge and vehicle change, indicating that the additional terms in Eq. (6-6) are time-dependent terms and will change as the vehicle moves across the bridge. By solving this equation, the displacement of the vehicle and bridge can be obtained in the time history. From Eq. (6-5), the interacting forces between the vehicle and bridge can also be obtained.

To simplify the modeling procedure, the bridge mode superposition technique is used based on the obtained bridge mode shapes and the corresponding natural circular frequencies. The mode superposition makes it possible to separate the bridge modal analysis from the vehicle-bridge coupled model. Consequently, the number of equations in Eq. (6-6) and the complexity of the entire procedure are greatly reduced.

A computer program is developed based on the above methodology. The mass matrix, stiffness matrix, and damping matrix of vehicle and bridge are automatically assembled using the fully computerized approach. The equations of motion are solved in time domain by using the Runge-Kutta method. The time dependent terms in Eq. (6-6) are calculated precisely by determining the vehicle position on the bridge and are updated at each time step, which makes it possible to reduce the computation effort for iterations. By determining the contact forces at each time step and setting the force equal to zero once the tension between vehicle and bridge is found, this model is able to consider the separation of vehicle from bridge. The developed program can handle more realistic models of bridges under various types of moving vehicles.

6.2.2 Road Surface Condition Including Approach Span Condition

The road surface condition can be obtained either by measuring the road profile in field or from numerical modeling. For measured *r(x)*, the total information of the roadway, bridge deck, and the expansion joint are included, while an artificial road surface is usually considered as a random process with a Gaussian (normal) probability distribution (ISO 8068, 1995) and expressed by a PSD function as:

$$\varphi(n) = \varphi(n_0)\left(\frac{n}{n_0}\right)^{-2} \tag{6-7}$$

where $\varphi(n)$ is the PSD function (m^3/cycle) for the road surface roughness; n is the spatial frequency (cycle/m); n_0 is the discontinuity frequency of $1/(2\pi)$ (cycle/m); and $\varphi(n_0)$ is the roughness coefficient (m^3/cycle) whose value is chosen depending on the road condition. Roughness can be simulated in the space domain by applying the inverse discrete Fourier transform as described by Wang and Huang (1992). However, according to ISO (ISO8606 1995) and Cebon (1999), occasional large local irregularities, like potholes and faultings, should be isolated and treated separately from such pseudo-random road roughness.

Field observations indicated that the faulting between bridge deck and approach slab can be as much as 0.038 m (1.5 inches, Fig. 6-3) (White et al. 2005). The large faulting at the expansion joints is much more abrupt than the pseudo-random roughness that only represents a gradual

change in road surface condition. In addition, the large approach span deformation (Fig. 6-1) considered in this study cannot be represented by a Gaussian random process and needs to be treated separately. Therefore, the artificial road surface condition considered in this study is twofold: firstly, the roughness of the bridge deck and roadway, and secondly, the approach span conditions including the approach span deflection and the faulting at the ends of the approach slab. As a result, the road surface condition r(x) is the superimposition of the approach slab deformation upon the natural roughness of the whole roadway.

As shown in Fig. 6-4, the faulting between the approach slab and the bridge deck can be modeled by a step up while the faulting between the pavement and the approach slab by a step down (Green et al. 1997). The faulting values at the both ends of the approach slab are assumed the same. The approach slab deformation, the deflection (Δ_2) and the slope change of the approach slab, shown in Figs. 6-1 and 6-4 are obtained from the static analysis (Cai et al. 2005).

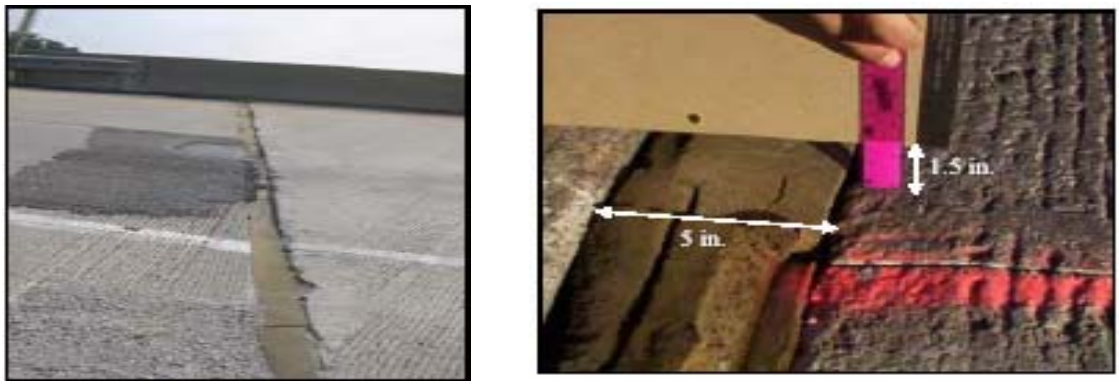

Fig. 6-3 Uneven joint of approach slab and bridge deck (White et al. 2005)

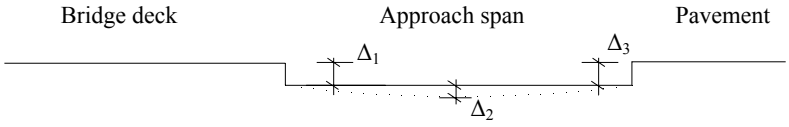

Fig. 6-4 Model of approach span deformation

6.3 Experimental Validation of Numerical Model

The field test in this study aims to validate the developed methodology. The validation consists of two main steps: the first step was the measurement of the bridge static response, which is used to adjust the bridge finite element model for predicting the dynamic response of the bridge; the second step consists of single vehicle tests in which the vehicle was passing over the bridge in different traffic lanes and the bridge dynamic responses were measured and compared with the predicted dynamic responses to validate the bridge-vehicle coupled model.

6.3.1 Brief Description of Bridge and Instrumentation Plan

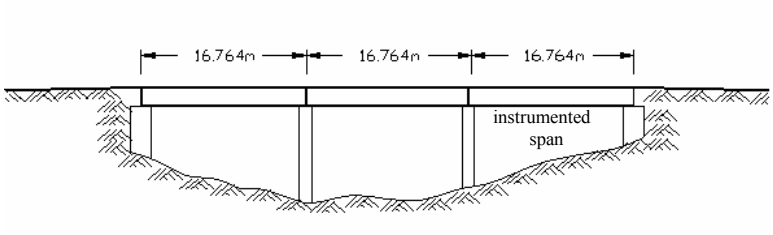

Fig. 6-5 Description of the test bridge

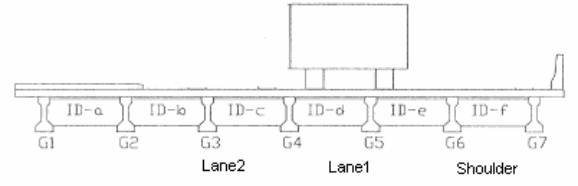

(a) Load case 1

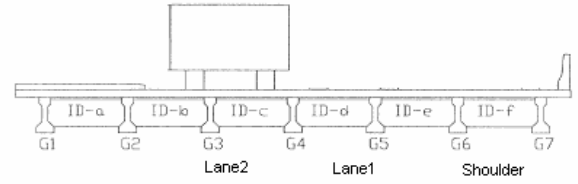

(b) Load case 2

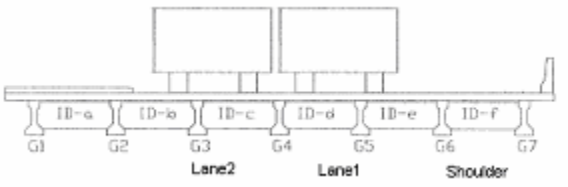

(c) Load case 3

Fig. 6-6 Cross section and the truck position in different load cases

The test bridge is located over Cypress Bayou in District 61, on LA 408 East. The location of this bridge and its easy accessibility were some of the factors which were considered. The total ADT for the structure is 11,473 according to its last bridge inspection data recorded on March 11th, 2002. This bridge structure is representative of the large majority of prestressed concrete slab-on-girder highway bridges.

There are three straight simple spans, each measuring 16.76 m (55 ft) in length with zero skew angle (Fig. 6-5). Its cross section has seven AASHTO Type II prestressed concrete girders spaced 2.13m (7 ft) from center to center (Fig. 6-6). All girders are anchored to the supports at both ends with anchor bolts on both sides of them. Each span has one intermediate diaphragm (ID) located at the mid-span; this ID is not connected to the deck.

The third span of the bridge was instrumented. The acquisition of data was concentrated on the girders. Strain gauges, accelerometers, and cable extension transducers were placed one foot away from the mid-span on all seven girders to avoid stress concentration due to the closeness to the diaphragm. Strains, accelerations, and deflections were continuously acquired in all loading paths.

The truck used in the test is a dumping truck with a single front axle and a two-axle group for the rear. The static wheel loads for the first, second, and third axle of this truck are 40.0 KN (9 kips), 47.8 KN (10.75kips), and 47.8 KN (10.75 kips), which makes the total weight of the truck as 271.2 KN (61 kips). The truck configuration is shown in Fig. 6-7.

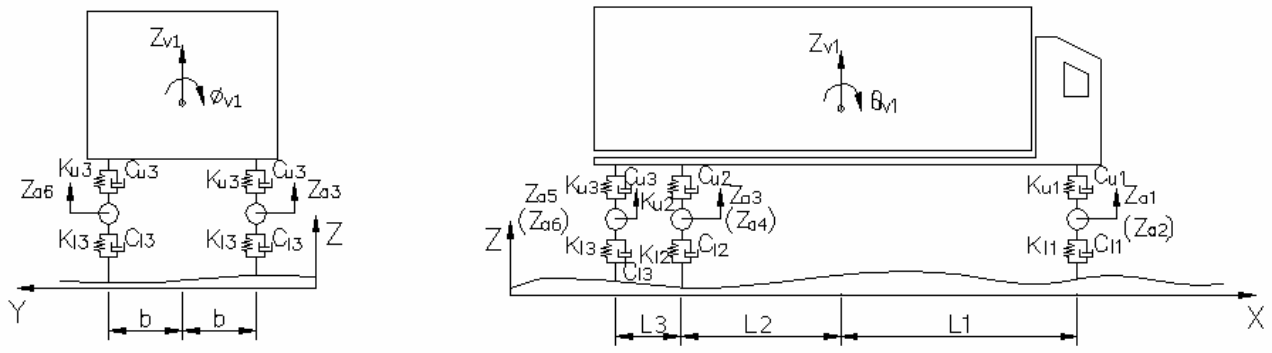

Fig. 6-7 Test truck

6.3.2 Results of Static Tests

In the static test, the bridge responses have been obtained by performing quasi-static tests, moving the truck at a crawling speed (less than 5 mph). All three load cases shown in Fig. 6-6 were conducted. The experimental and numerical results of static tests were compared in terms of vertical displacements. Fig. 6-8 shows the numerical and experimental values of the maximum vertical displacement for all seven girders. This comparison indicates the difference of the numerical model in relation to the real structure. For instance, in load case 3, the measured maximum deflection at mid-span (G4) is 3.40 mm, while the calculated value is 3.75 mm (+10.3%). Furthermore, the difference in the deflection distribution among girders is quite obvious. These differences seem to be related to the material properties of concrete used in the numerical model and to the connection between the diaphragm and girders.

The concrete elastic modulus in the numerical model was chosen as the secant value at the age of 28 days using $E_0 = w_c^{1.5}(0.043)\sqrt{f_c'}$ (w_c and f_c' are the density and strength of the concrete, respectively), i.e. E_0=24,730 MPa (3,586,616 psi) for f_c' = 24.1 Mpa (3,500 psi) concrete used for slab and diaphragm and E_0= 32,380 Mpa (4,695,982 psi) for f_c' = 41.4 Mpa (6,000 psi) concrete used for the prestressed girders. In fact, the concrete modulus in the field is higher than E_0 due to two reasons (Calcada et al. 2005): (1) the aging of concrete will usually increase the modulus and (2) use of secant modulus is not as appropriate as tangent modulus in simulation of the bridge structural behavior. Calcada et al. (2005) indicates that the elastic modulus for concrete increases by a value of about 30% compared to the initial modulus (E_0).

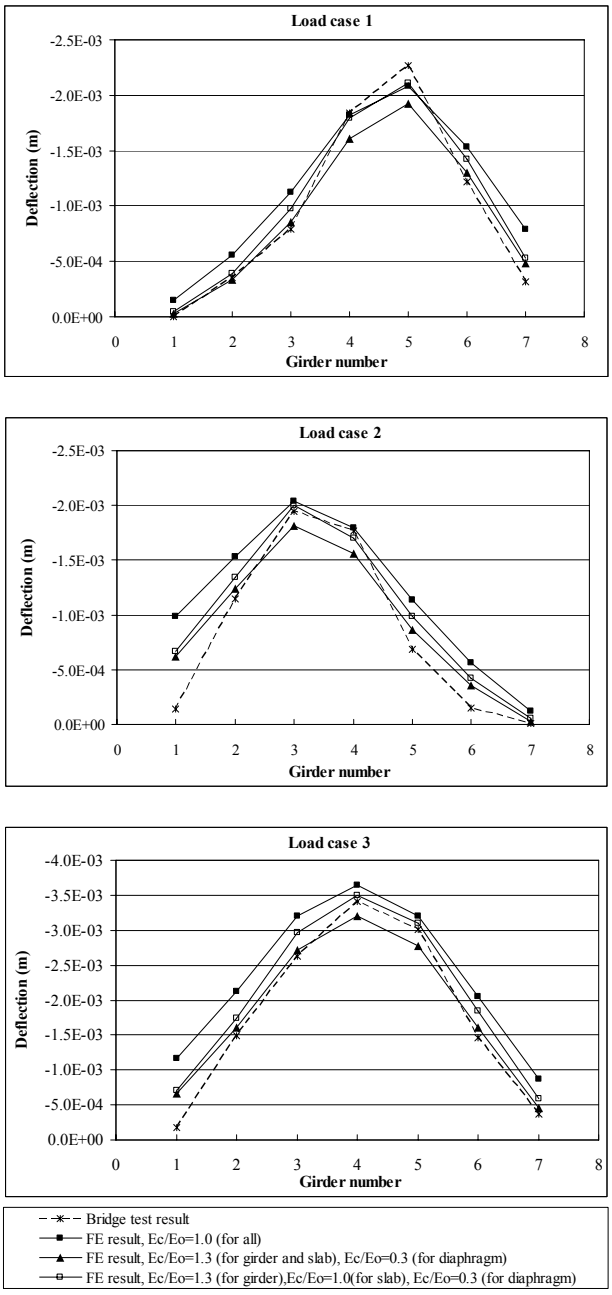

Fig. 6-8 Comparison of experimental and numerical results (static deflection)

On the other hand, the connection between the diaphragm and the girders are not as rigid as modeled in the numerical model. Field observations indicate that there are cracks in the diaphragm at the connection of the diaphragm and girders. This phenomenon is caused by the fact that the weak connection between the girder and the diaphragm causes the diaphragm to crack when the bridge is subjected to heavy load. The actual stiffness of intermediate diaphragms of field bridges is about 30% of their rigid section stiffness (Kostem et al. 1977, Cai and Shahawy 2004). Therefore, the modulus of the diaphragm needs to be reduced and the bridge model needs to be adjusted.

Fig. 6-8 also displays results from the following two adjusted bridge models: (1) the elastic modulus for girders and slab is increased by 30% and the modulus for diaphragm was reduced to 30% and (2) the same change as made in (1) except that the modulus of slab keeps its original value. The argument of (2) is that the slab deterioration such as cracks may trade off the stiffness contribution of the increased modulus. Fig. 6-8 clearly shows that the latter adjusted model reduces the difference between the maximum experimental and numerical deflection, and it has close deflection distribution among girders to the experimental results. Therefore, the latter adjusted model is adopted in the later analysis.

6.3.3 Results of Dynamic Tests

The dynamic test aims to acquire the dynamic response of the bridge under the moving truck. In addition, the bump-caused dynamic problem at the bridge end, induced by the faulting between the approach slab and the bridge deck, was also considered. A piece of wood board with a thickness of 0.038 m (1.5 in.) was placed at the end of the second span to simulate the faulting condition (Fig. 6-9).

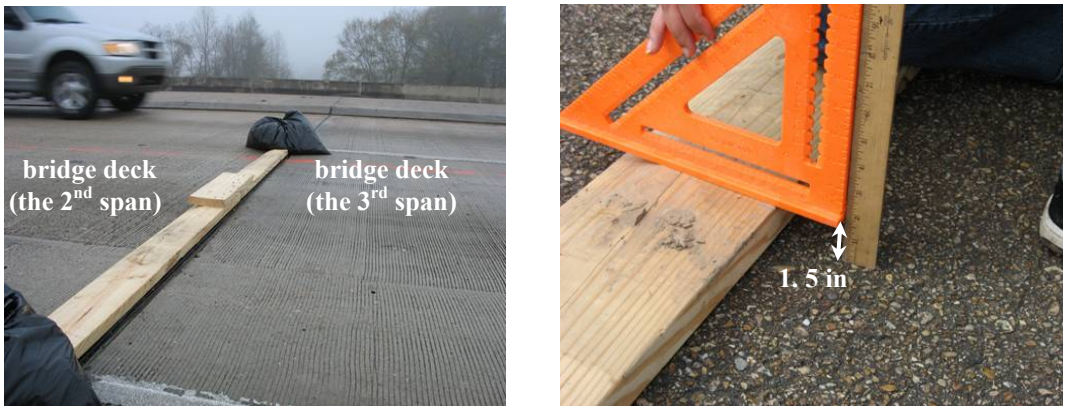

Fig. 6-9 Wood board used to simulate the faulting height of 1.5 in.

The irregularities of pavement and bridge deck are measured by a laser profiler, which obtains the longitudinal road surface profile along each wheel track. For instance, Fig. 6-10 shows the road surface profile (with/without the wood board) of the right wheel in lane 1, which has a total acquisition length of 170 m with a sample interval of 0.076 m.

Two sets of tests were conducted: the truck passed over the bridge through lane 1 (Fig. 6-6 (a)) and lane 2 (Fig. 6-6 (b)), respectively. The truck speed is 17.78 m/s (40 mph). The bridge dynamic responses at each girder's mid-span, including the strain, deflection, and acceleration, for each passage of the test vehicle were recorded in time history. The prediction of dynamic response of bridge is obtained through the developed methodology, which takes into account both the faulting condition and the irregularities of pavement and bridge deck shown in Fig. 6-10 (b). The experimental results of the dynamic tests were used to verify the predicted dynamic responses.

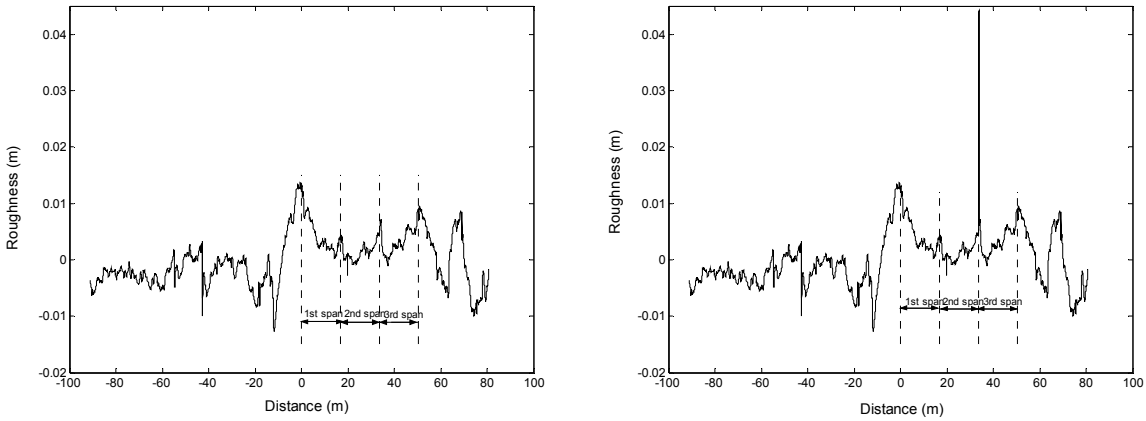

(a) roughness of lane 1 (b) roughness of lane 1 with the wood board

Fig. 6-10 Road surface profile for lane 1

Fig. 6-11 presents the time history of the experimental and numerical result of deflection in the maximum-load-taking girder for two load cases. To display the position of the vehicle on the bridge, the distance between the vehicle's first axle and the bridge entrance, instead of the time, is used as the x axis, with the entrance to the bridge is defined as zero (or origin). This comparison shows that the main pattern of the calculated deflection is satisfactory. In addition, Fig. 6-12 displays the comparison between the experimental and numerical results of accelerations. The same type of comparison is shown in Fig. 6-13 for the dynamic effect on experimental strain and numerical deflection in terms of amplification factor, which is the ratio of dynamic response to its static value. From these figures, it can be concluded that the agreement between the measurement and the prediction is generally good. The developed methodology can be used to predict the bridge dynamic response under moving vehicles.

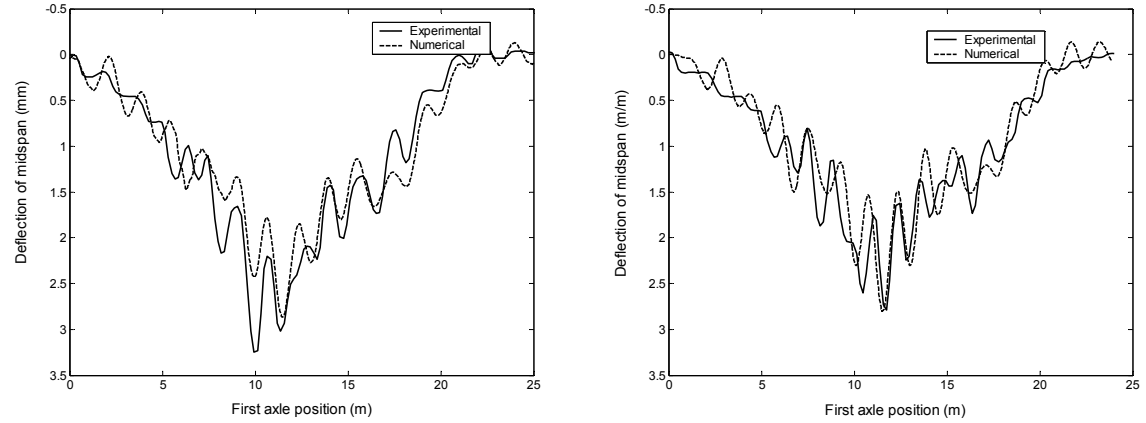

(a) results of G5 (load case 1) (b) results of G3 (load case 2)

Fig. 6-11 Comparison of experimental and numerical results (dynamic deflection)

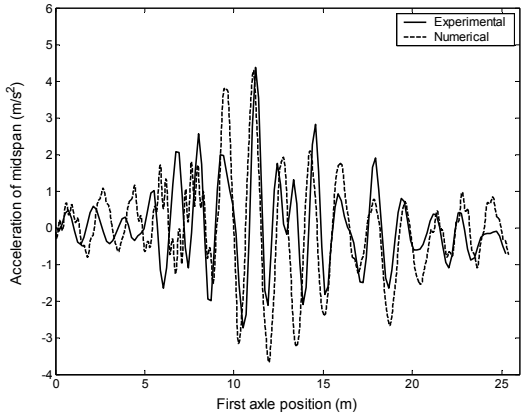

(a) results of G5 (load case 1)

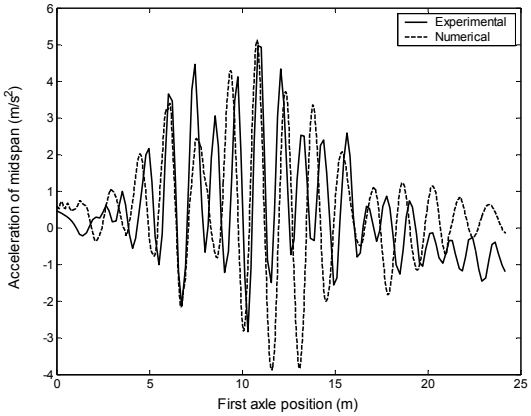

(b) results of G3 (load case 2)

Fig. 6-12 Comparison of experimental and numerical results (acceleration)

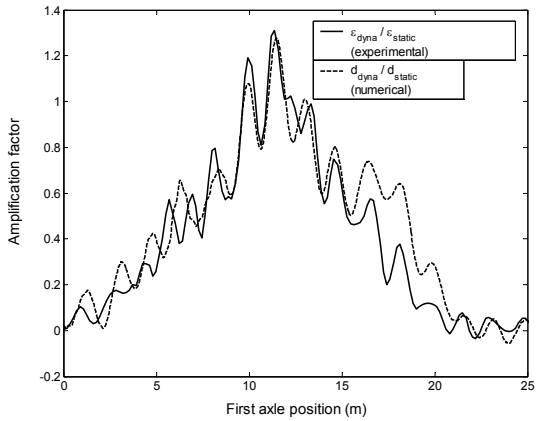

(a) Results of G5 (load case 1)

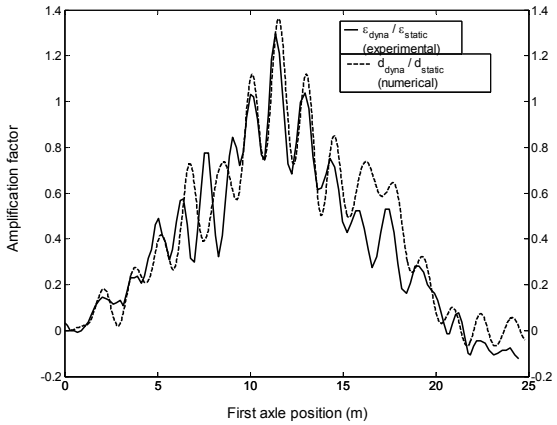

(b) Results of G3 (load case 2)

Fig. 6-13 Comparison of experimental and numerical results (amplification factors of strain and deflection)

6.4 Parametric Study on Effect of Approach Span Condition

Four typical slab-on-girder bridges, with span lengths of 16.76 m (55 ft), 24.38 m (80 ft), 30.48 m (100 ft), and 39.62 m (130 ft), were analyzed. These bridges are of Type II, Type III, Type IV and Type VI prestressed girders, respectively, which are designed for HS20-44 loading in accordance with AASHTO standard specifications (AASHTO 2002). All four bridges consist of seven girders with girder spacing of 2.13 m (7 ft) that are simply supported. The bridges have a roadway width of 14.32 m (47 ft) and a bridge deck thickness of 0.20 m (8 in). Besides end diaphragms, the seven girders are connected by intermediate diaphragms. One intermediate diaphragm is used at the mid-span of bridges with a span length less than 24.38 m, while two diaphragms are at the span third points for spans in excess of 30.48 m (100 ft). The typical cross sections of these four bridges are similar as that shown in Fig. 6-6.

Fig. 6-14 shows the first four vibration mode shapes of the bridge with a span length of 30.48 m. Vibration modes of the other bridges have nearly the same shape. The first four modes of each bridge are listed in Table 6-1. Twenty modes of each bridge were taken in the dynamic analysis. The damping characteristics of bridges were assumed as viscous damping, and the damping ratio is assumed to be 0.02.

An AASHTO HS20-44 truck shown in Fig. 6-2 is used in the numerical analysis. This vehicle was chosen mainly based on the fact that it is a major vehicle used in designing bridges according to AASHTO codes. The geometry, mass distribution, damping, and stiffness of the tires and suspension systems of this truck are shown in Table 6-2 (Wang and Liu 2000). The static wheel loads for the first, second, and third axle are 17.8 KN (4 kips), 71.2 KN (16 kips), and 71.2 KN (16 kips), which makes the total weight of the truck as 320 KN (72 kips). Modal frequencies of the vehicle are calculated as 1.52, 2.14, 2.69, 5.94, 7.74, 7.82, 8.92, 13.87, 13.99, 14.63, and 17.95 Hz. The vehicle modes can be divided into two categories: the first four modes correspond to vehicle body motion (such as bounce, pitch, or rotation of the vehicle rigid body); the other modes involve motions of the wheels (wheel hop).

Table 6-1 Modal frequencies of girder-on-slab bridges

Mode shape description	Span length			
	16.76 (m)	24.38 (m)	30.48 (m)	39.62 (m)
First bending mode (Hz)	7.56	4.45	3.44	2.64
Second bending mode (Hz)	24.47	15.98	12.54	9.69
First torsional mode (Hz)	9.34	5.77	4.50	3.50
Second torsional mode (Hz)	11.86	8.68	8.52	9.08

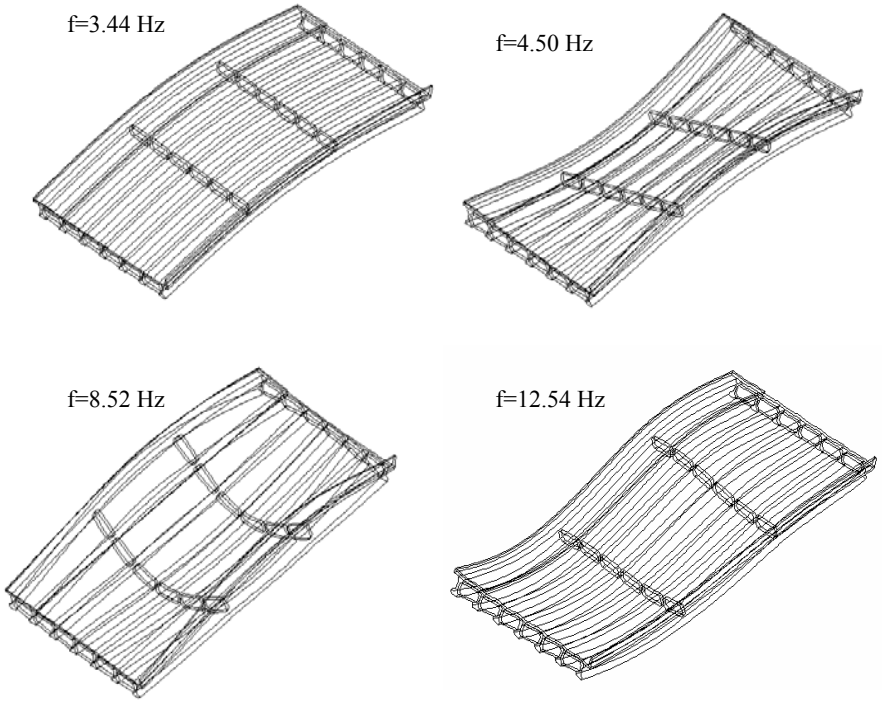

Fig. 6-14 Mode shape of bridge (30.48 m)

To study the effect of the approach span deformation on slab-on-girder bridges, a 12 m long approach slab was considered. Compared with the faulting at the expansion joint (Δ_1, Fig. 6-4), the effect of the approach span deflection (Δ_2, Fig. 6-4) is very small, even though the faulting is relatively small (Shi and Cai, 2006); thus, only the faulting condition at the slab ends is considered here, which varies from 0.005 m, 0.01 m, 0.02 m, to 0.038 m. Since this study focuses on the effect of the faulting, variations of other factors such as vehicle driving speed and bridge deck roughness are not considered. Therefore, the vehicle speed used in the following part of this chapter is 20 m/s and bridge deck roughness is in good condition. All three load cases shown in Fig. 6-6 are considered. Since the bridges considered in the present study have relatively short span lengths, only one vehicle is considered in each lane at any given moment, which agrees with the live load specifications of AASHTO codes.

6.5 Results and Discussion

6.5.1 Bridge Dynamic Response under Different Conditions

With the aim of comparing the effect of approach span faulting condition with the effect of bridge deck roughness, four road conditions are considered for all four bridges, respectively: (i) smooth road surface, which means that the surface of the pavement, approach slab, and bridge deck are assumed perfectly smooth without any depressions; (ii) smooth road surface as in (i) plus faulting at the approach slab ends; (iii) road roughness classified as good, i.e. considering the road surface only without considering the faulting; and (iv) considering the road roughness (good) plus faulting at the approach slab ends. For the last two conditions, before the vehicle enters the bridge approach slab, its initial conditions are obtained by allowing it to travel a distance of 100 m, i.e., a 100 m lead distance is given to obtain stable initial conditions before the vehicle moves on to the approach span. It continues moving until the entire vehicle has left the end of the bridge. The same class of road surface, i.e. good, is assumed for the pavement, approach slab, and bridge deck.

Fig. 6-15 shows the time history of a typical bridge (16.76 m) response in terms of an interior girder's (G4) deflection at the mid-span for load case 3. In this case, the faulting value is 0.02 m. The results indicate that the maximum bridge responses under conditions (ii) and (iv) are larger than under conditions (i) and (iii), respectively, which shows the effect of the faulting condition on bridge dynamic response is significant. Moreover, the bridge dynamic response under condition (ii) is larger than under condition (iii), indicating that the faulting at approach slab ends is more critical than the rough road surface condition to short bridges' dynamic response. Consequently, only road surface condition (ii) is considered in the following part of this section to analyze the effect of different faulting conditions and to exclude other factors.

In order to investigate the effect of the different faulting conditions, the time history of mid-span deflection of all four bridges under different faultings is presented in Fig. 6-16. It is clear in the figure that for all four bridges, higher faulting values cause larger bridge dynamic response. Concerning the results obtained in the spectral domain for all four bridges (Fig. 6-17), the major contribution to the dynamic response arises from the participation of the first four natural modes. With the increase of the faulting value, the contribution of higher modes increases.

Table 6-2 Major parameters of vehicle (HS20)

Mass of truck body 1	2612 (kg)
Pitching moment of inertia of truck body1	2022 (kg.m^2)
Rolling moment of inertia of tuck body 1	8544 (kg.m$^{2)}$
Mass of truck body 2	26113 (kg)
Pitching moment of inertia of truck body2	33153 (kg.m^2)
Rolling moment of inertia of tuck body 2	181216 (kg.m^2)
Mass of the first axle suspension	490 (kg)
Upper spring stiffness of the first axle	242604 (N/m)
Upper damper coefficient of the first axle	2190 (N.s/m)
Lower spring stiffness of the first axle	875082 (N/m)
Lower damper coefficient of the first axle	2000 (N.s/m)
Mass of the second axle suspension	808 (kg)
Upper spring stiffness of the second axle	1903172 (N/m)
Upper damper coefficient of the second axle	7882 (N.s/m)
Lower spring stiffness of the second axle	3503307 (N/m)
Lower damper coefficient of the second axle	2000 (N.s/m)
Mass of the third axle suspension	653 (kg)
Upper spring stiffness of the third axle	1969034 (N/m)
Upper damper coefficient of the third axle	7182 (N.s/m)
Lower spring stiffness of the third axle	3507429 (N/m)
Lower damper coefficient of the third axle	2000 (N.s/m)
L1	1.698 (m)
L2	2.569 (m)
L3	1.984 (m)
L4	2.283 (m)
L5	2.215 (m)
L6	2.338 (m)
B	1.1 (m)

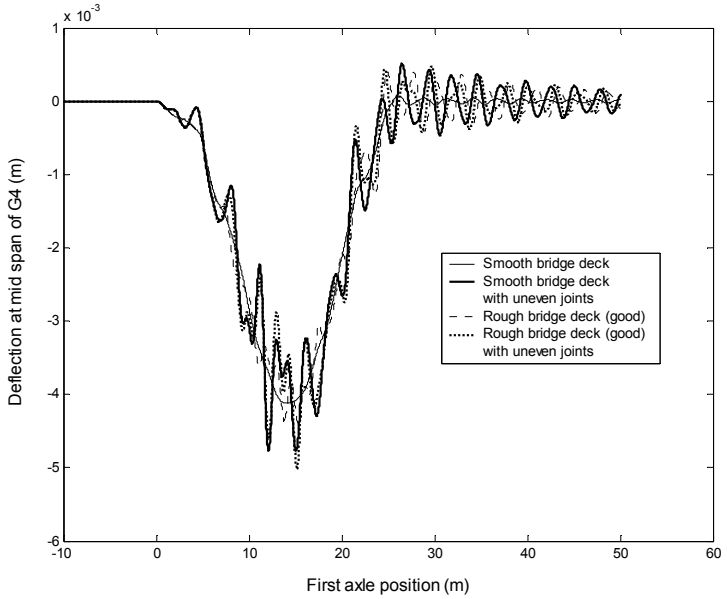

Fig. 6-15 Dynamic deflection of the bridge under four different road surface conditions (L=16.76 m)

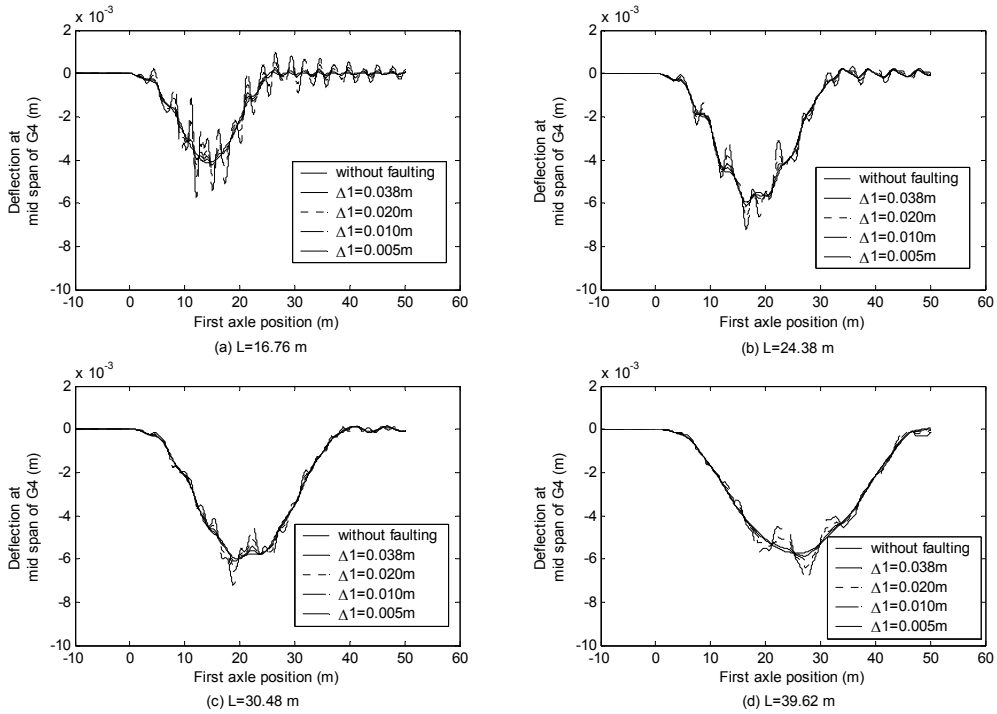

Fig. 6-16 Dynamic deflection of bridges under different faulting condition (G4, load case3)

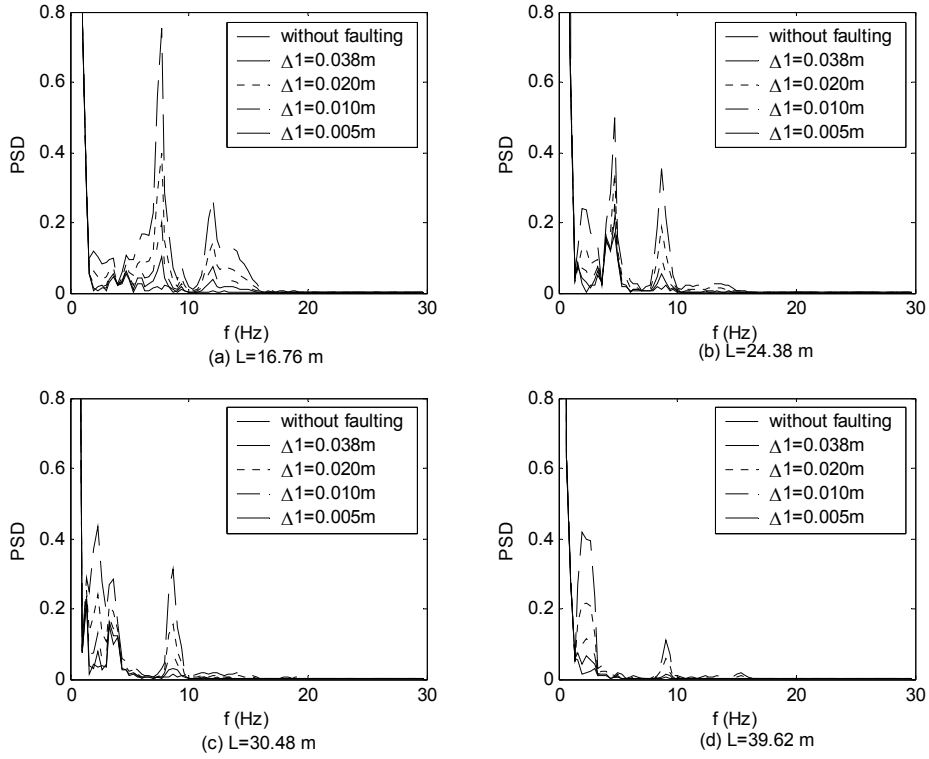

Fig. 6-17 Spectral analysis of dynamic deflection under different faulting condition (G4, load case3)

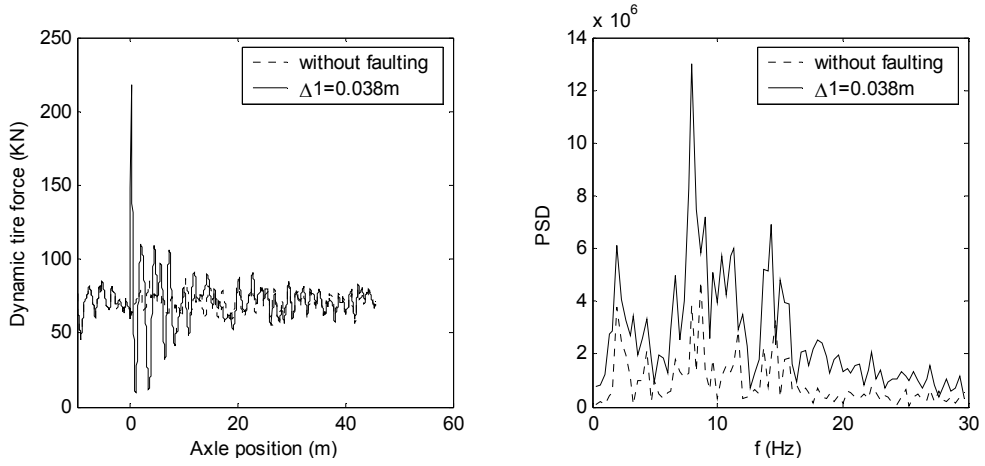

(a) time domain (b) frequency domain

Fig. 6-18 Dynamic tire force of the second axle

Fig. 6-18 shows the time history and spectral analysis of dynamic tire force (interaction force between the vehicle and the bridge). As the vehicle passes over the expansion joint, the faulting triggers an impact tire force. The larger the faulting value, the higher the impact force. Under the faulting condition of 0.038 m, the impact force in the second axle (218.1 KN) can be as much as three times of the static tire force (71.8KN). The impact force is dissipated gradually by the vehicle damping system, but the tire force applied on the bridge is still large and causes larger bridge dynamic response, which explains why the larger faulting causes larger bridge response.

On the other hand, the abrupt faulting also excites the higher modes of the vehicle, most probably the wheel-hop mode, which increases the frequency of the dynamic load (Fig. 6-18 (b)), while the smaller faulting or more gradual change in road surface mainly excites the modes of vehicle body motion. Compared with the dynamic tire force under the condition without faulting, the characteristics of the vehicle tire force under the faulting condition are clear, i.e., the contribution from the modes of body motion is still considerable, but the wheel-hop mode with higher frequency is dominant. The dynamic tire force with higher frequency in turn excites the higher modes of bridge, which explains why the larger faulting increases the contribution of higher modes to dynamic response of bridges with a span length less than 30.48 m. For the bridge with a span length of 39.62 m, since the vehicle body motion frequency (2.69 Hz) is in coincidence with the frequency of the bridge's first mode (2.64 Hz), the contributions of higher modes caused by larger faulting value are much smaller than the other bridges.

6.5.2 Impact Factor (IM)

To predict the dynamic responses of bridges resulting from a moving vehicle is a significant problem in bridge design, most design codes assign an approximate quantity for the dynamic response for a normal design procedure, i.e., by amplifying the static response with an impact factor (IM). The impact factor is defined as

$$IM(\%) = (\frac{R_d}{R_s} - 1) \times 100\% \quad (6\text{-}8)$$

in which R_d and R_s are the maximum dynamic and static responses of the bridge, respectively.

To investigate the bridge impact behavior caused by the faulting (bump) problem, the three load cases shown in Fig. 6-6 are considered. To analyze the effect of approach span conditions, four different faulting conditions are considered, respectively.

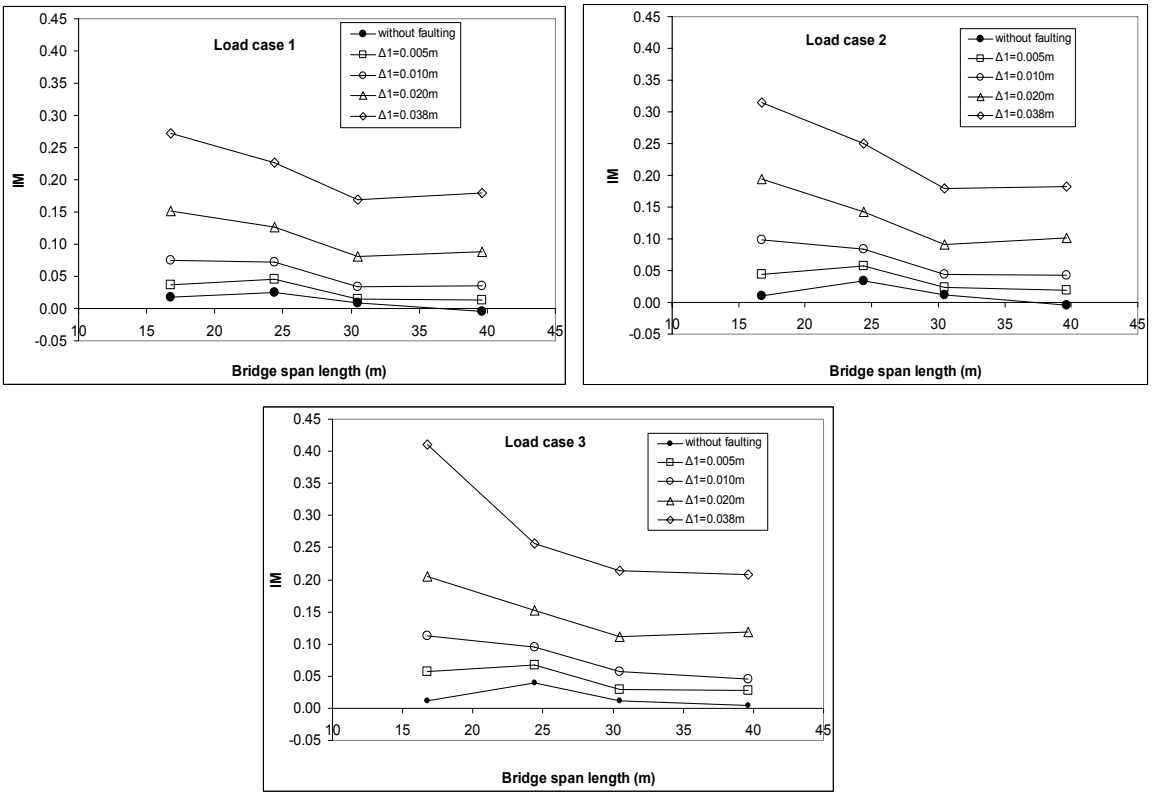

Fig. 6-19 IM versus span length

6.5.2.1 IMs of Bridges with Different Span Lengths

Fig. 6-19 shows the effects of different faulting conditions on IMs of all four bridges. Only IMs of girders that carry the largest load for each load case are presented. It is obvious that the same large faulting condition has a much larger influence on shorter bridges than it does on longer bridges. For example, for the faulting of 0.038 m, the impact factors for bridges (subjected to load case 3) with span lengths of 16.76 m, 24.38 m, 30.48 m, and 39.62 m are 0.41, 0.26, 0.21, and 0.21, respectively. As is mentioned earlier, after the truck passed over the faulting at the bridge entrance, the bump causes a large tire force (the sharp peak in Fig. 6-18). For longer span bridges, after the truck received the bump disturbance, it has more time to dissipate the initial disturbance and to become more stable before it comes to the mid-span of the bridge. Thus, the dynamic tire load applied on a longer bridge is smaller than on a shorter bridge under the same faulting condition.

6.5.2.2 IMs of Different Girders

Fig. 6-20 presents the impact factors of each girder for all four bridges with different faulting conditions. It is found that the distribution of impact factor along lateral direction is quite different, especially for shorter bridges. Generally, the increase in faulting increases the impact factors; and the increase in impact factors for the exterior girders caused by the increase in faulting is much larger than those for interior girders. For the bridge with a span length of 16.76 m subjected to load case 1, the impact factor of exterior girder (G1) is increased by 3.37 while the IM of the fifth girder (G5) by 0.13, when the faulting increases from 0 to 0.020 m. However, for longer span bridges, the difference of increase in impact factors between exterior and interior girders decreases. For bridge with a span length of 24.38 m, the impact factors of the exterior girder (G1) and interior girder (G5) are increased by 0.37 and 0.12, respectively. This can also be explained by the spectral analysis mentioned earlier, i.e., the large faulting causes the higher modes of the bridge, which includes bridge torsion modes that causes the vibration of the exterior girders. For example, for bridge with a span length of 16.76 m under the faulting condition of 0.020 m, the dominant mode of exterior girder (G1) is the first torsion mode while the dominant mode of interior girder (G5) is the first bending mode, as is shown in Fig. 6-21. For longer span bridges, although the dominant mode in both exterior and interior girders remains to be first bending mode, the contribution of torsion modes to exterior girder is larger than that to interior girder.

The IMs calculated according to AASHTO codes (both standard and LRFD) for all four bridges are also shown in Fig. 6-20. Since the current design codes use the impact factor for the girder that takes the largest load, only the impact factors of the girder with the maximum load is compared with the AASHTO specifications, i.e. G5 for load case 1, G3 for load case 2, and G4 for load case 3. It is evident that the impact factor caused by faulting can be larger than that is specified by AASHTO codes. Under the faulting condition of 0.038 m, the impact factors exceed the value specified in AASHTO standard code (designated as AASHTO STD) , except for the bridge with a span length of 30.48 m subjected to a single lane load. When the faulting condition is no larger than 0.020 m, IMs in most cases are within the values specified in the AASHTO standard codes. Fig. 6-20 also shows that for most cases, the impact factors of bridges with span lengths of 24.38 m to 39.62 m are less than the values in AASHTO LRFD specifications (designated as AASHTO LRFD). For the bridge with a span length of 16.76 m, the impact factors may still exceed that in AASHTO LRFD specifications if the faulting condition is as large as 0.038 m.

6.5.2.3 IMs along Longitudinal Direction

Fig. 6-22 compares impact factors of the quarter span and mid-span points for all four bridges subjected to load case 3. The impact factors at the quarter span point are quite different from that at the mid-span point. For all four bridges, the impact factors at the quarter span are larger than those at mid-span. This is caused by the larger faulting which excites the higher vibration modes including the second bending mode in bridge responses. As shown in Fig. 6-23, the second bending mode has more influence on the response at the quarter span than at the mid-span. The larger IM at quarter span needs to be noticed in design and rating prestressed girder at the section with harped strands.

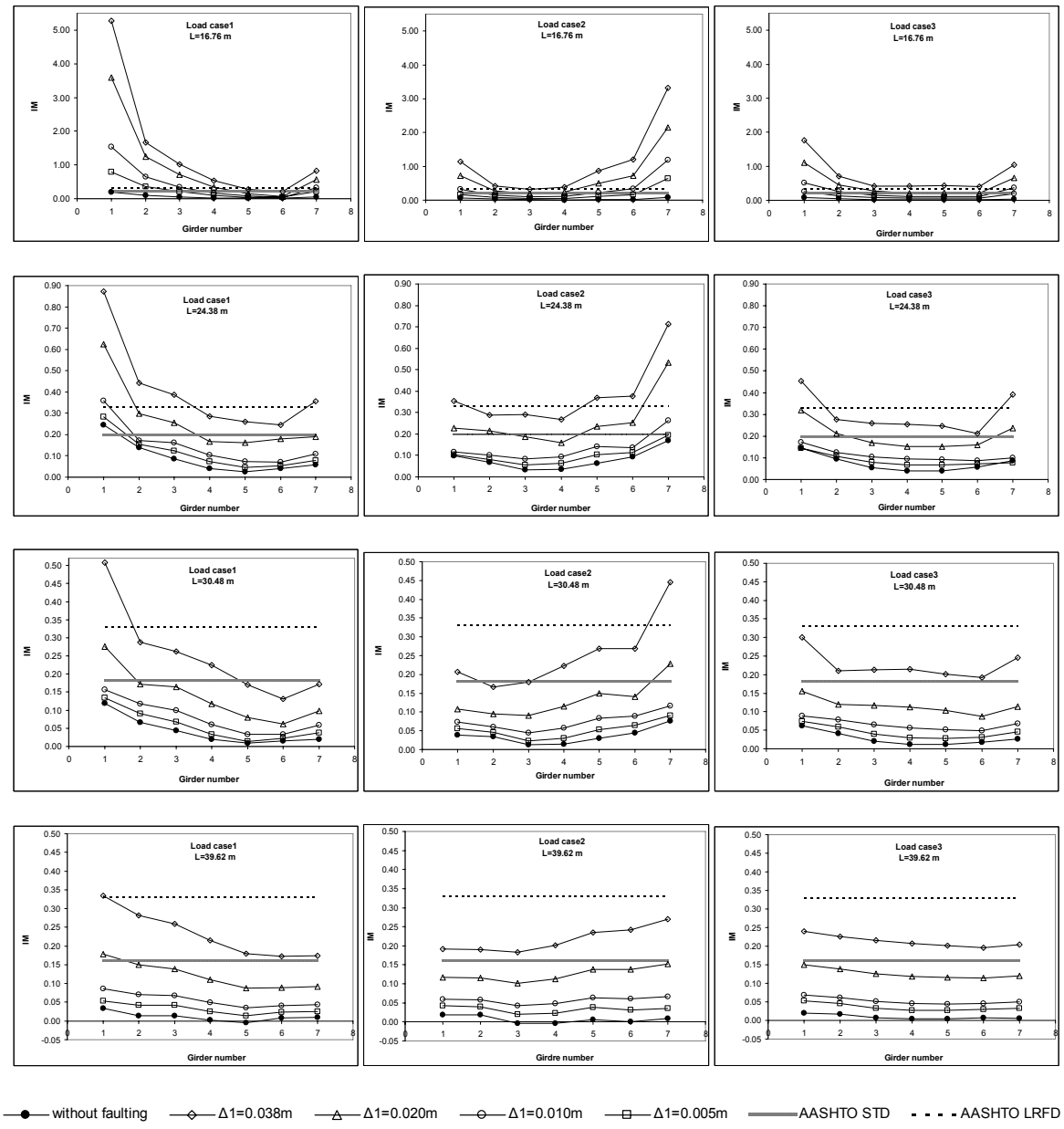

Fig. 6-20 IM of bridges under different faulting conditions

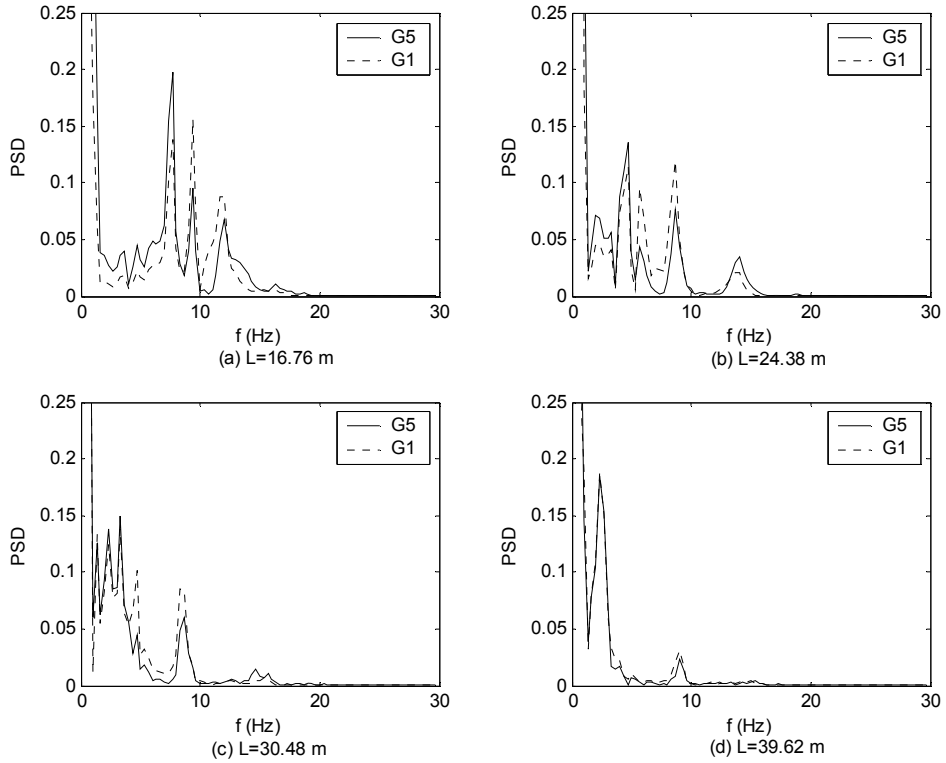

Fig. 6-21 Spectral analysis of dynamic deflection of exterior girder (G1) and interior girder (G5) under the faulting condition of 0.02 m (load case1)

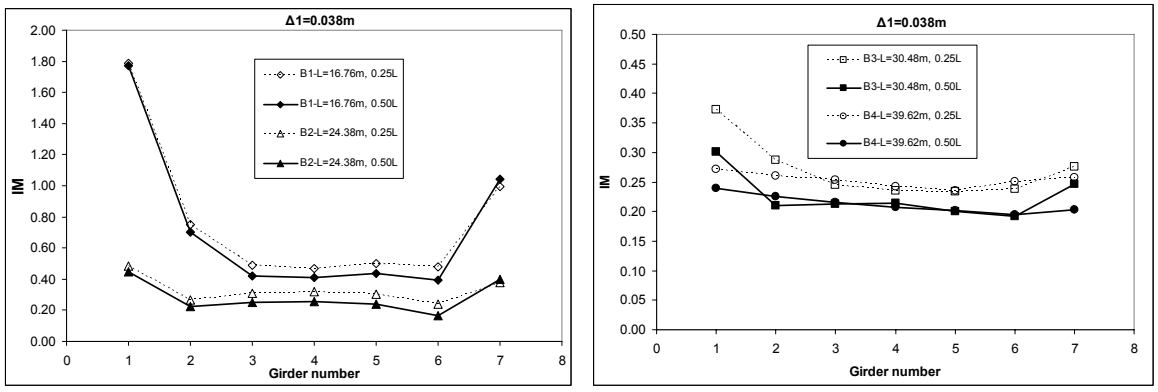

Fig. 6-22 IM at different sections (load case3, faulting=0.038 m)

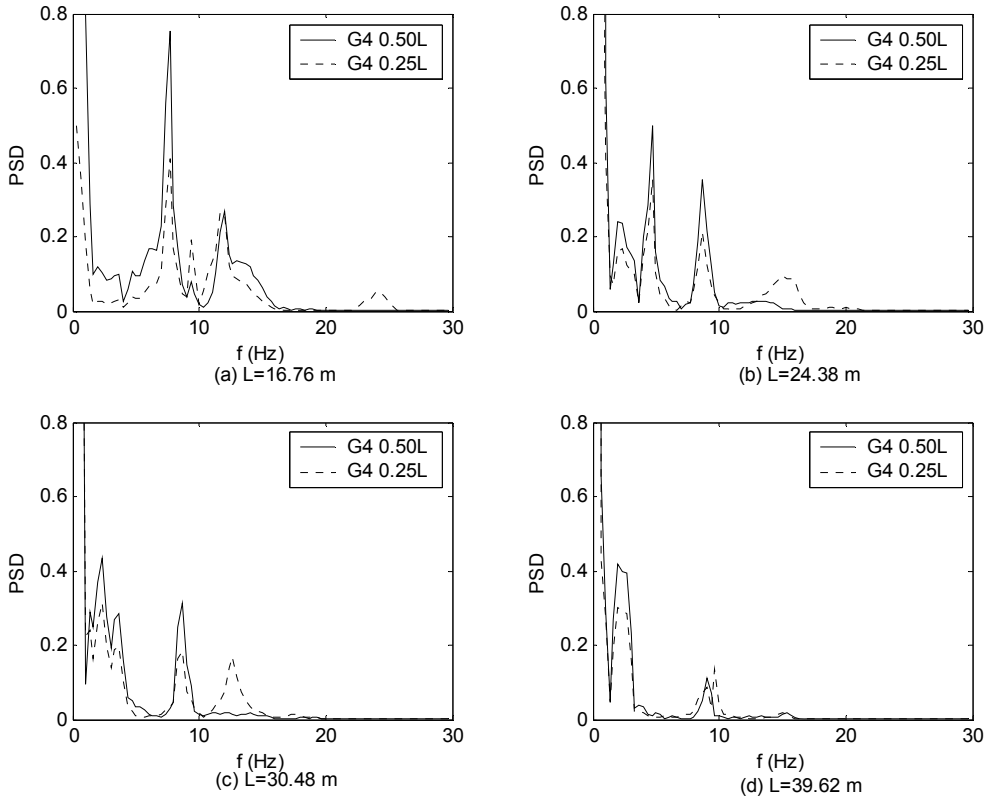

Fig. 6-23 Spectral analysis of dynamic deflection at different sections (load case3, faulting=0.038 m)

6.5.3 Load Distribution Factor (LDF)

The LDF is important for a rational design and rating of bridges. According to Ghosen et al. (1986), LDF of each girder is assumed to be equal to the ratio of its strain to the sum of the strains of all girders. The weighted strains were used by Stallings and Yoo (1993) to consider the different section modulus of the girders. Thus the LDF for the *i*th girder can be expressed as follows:

$$LDF_i = \frac{M_i}{\sum_{j=1}^{n} M_j} = \frac{ES_i\varepsilon_i}{\sum_{j=1}^{n} ES_j\varepsilon_j} = \frac{\frac{S_i}{S_T}\varepsilon_i}{\sum_{j=1}^{n}\frac{S_j}{S_T}\varepsilon_j} = \frac{w_i\varepsilon_i}{\sum_{j=1}^{n} w_j\varepsilon_j} \tag{6-9}$$

where M_i = bending moment of *i*th girder; E = modulus of material; S_i = section modulus; S_T = typical section modulus; ε_i = strain at the bottom of *i*th girder; w_i = ratio of the section modulus of the *i*th girder to that of the typical girder; and n = total number of the girders. For the bridges considered in this study, all girders have the same cross section, i.e. w_i are equal to 1 for all girders. The LDFs of girders for all four bridges, under different faulting conditions, calculated by Eq. (6-9) are presented in Fig. 6-24.

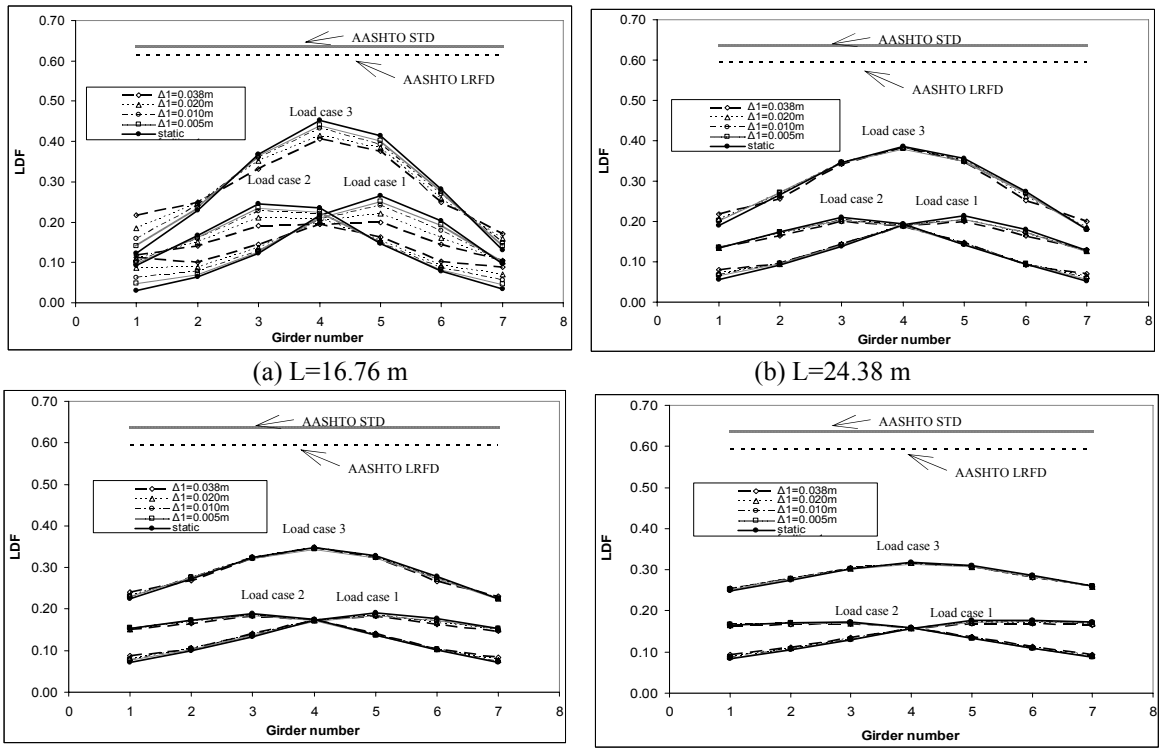

(a) L=16.76 m (b) L=24.38 m

(c) L=30.48 m (b) L=39.62 m

Fig. 6-24 LDF (moment) under different faulting conditions

It is found that the load distribution along the lateral direction under a large faulting condition is different from that under a static truck load, especially for short-span bridges. For the bridge with a span length of 16.76 m, the LDF of exterior girders increases when the faulting increases, whereas the LDF of interior girder decreases, which results in more uniform LDFs among girders. The more uniform LDF under a larger faulting condition indicates that the exterior girders more efficiently participate in dynamic load carrying. However, for longer bridges this change caused by large faulting is comparatively slight. A longer span bridge has more uniform values of LDF for each girder even when the faulting condition is large, i.e., the effect of faulting on LDF for a longer bridge is smaller than that for shorter bridge.

In Fig. 6-24, the values of LDFs, for two-lane loading, according to the AASHTO specifications are also presented and compared with the LDFs from the numerical analysis. The factors specified in the AASHTO codes are much larger than the values from the FEM analysis. For the 16.76 m bridge, the AASHTO LRFD and standard codes specify 29.8% and 35.3% larger LDFs than the maximum factors from FEM analysis, respectively, which indicate that using LDFs specified in AASHTO codes are conservative.

6.6 Conclusions

A fully computerized vehicle-bridge coupled model has been developed. The methodology is validated by field tests on a typical slab-on-girder bridge. The results from the tests indicate that this vehicle-bridge coupled model is reliable for predicting the dynamic response of bridges induced by heavy vehicles with consideration of road surface irregularities.

The dynamic responses of four different slab-on-girder bridges under HS20 trucks are obtained in time domain by using the bridge-vehicle coupled model. Parameters such as the bridge span length, road surface conditions, and the faulting values are investigated. Based on the results, the conclusions can be drawn as follows:

(1) Initial conditions of vehicles entering bridges excited by a large faulting at the approach slab end have a significant influence on bridge dynamic response. The local unevenness of expansion joints at the approach slab ends tremendously increases the dynamic response of shorter bridges. Moreover, the bridge dynamic response under a large faulting condition is much higher than that under the rough road surface with a good condition.

(2) The same faulting value has a much larger influence on shorter bridges than it does on longer bridges. Longer span bridges have more time for the initial disturbance to be dissipated and for the vehicle to become more stable before it comes to the mid-span of the bridge.

(3) The vehicle bumping caused by large faulting condition excites higher modes in the vehicle, which in turn triggers higher modes in the bridge dynamic response. Among these higher modes, the torsion modes contribute more to dynamic response for exterior girders, which results in larger increase in IMs for exterior girders than that for interior girders.

(4)The higher modes not only affect the IMs along transverse direction but also affect the IMs along the longitudinal direction. The higher bending modes of bridges excited by the vehicle bumping, may cause larger IMs at the quarter span than that at the mid-span, which needs to be noticed in design and evaluation of prestress girders at sections with harped strands.

(5) Provided that the faulting condition is not larger than 0.020 m, the impact factors of all four bridges are generally smaller than those computed by the AASHTO specifications (both standard and LRFD codes). However, AASHTO specifications may underestimate the impact factors for these bridges with larger faulting conditions at uneven joints at the bridge ends. This situation should be emphasized in practice, especially in rating existing bridges.

(6) The bridges with vehicles moving across them under larger faulting conditions have more uniform LDFs than under static loads. The variations of LDFs for all four bridges are similar. The LDFs are consistently lower than those according to AASHTO specifications.

6.7 References

American Association of State Highway and Transportation Officials (AASHTO). (2004). *LRFD bridge design specifications,* Washington, DC.

American Association of State Highway and Transportation Officials (AASHTO). (2002). *Standard specifications for highway bridges,* Washington, DC.

Bruni, S., Bocciolone, M., and Beretta, S. (2003). "Simulation of bridge-heavy road vehicle interaction and assessment of structure durability." *International Journal of Vehicle Design*, 20(1), 70-85.

Cai, C.S. and Shahawy, M. (2004). "Predicted and Measured Performance of Prestressed Concrete Bridges". Journal of Bridge Engineering, ASCE, 9(1), 4-13.

Cai, C. S., Shi, X. M., Voyiadjis, G. Z. and Zhang, Z. J. (2005). "Structural performance of bridge approach slab under given embankment settlement." *Journal of Bridge Engineering,* 10(4), 482-489.

Calcada, R., Cunha, A. and Delgado, R. (2005). "Analysis of traffic-induced vibrations in a cable-stayed bridge. Part II: numerical modeling and stochastic simulation." *Journal of Bridge Engineering.* 10(4), 386-397.

Cebon, D. (1999). *Handbook of vehicle-road interaction*, 2nd Ed., Swets & Zeitlinger B.V., Lisse, the Netherlands.

Chatterjee, P.K., Datta, T. K., and Surana, C. S. (1994). "Vibration of continuous bridges under moving vehicles." *Journal of Sound and Vibration*, 169(5), 619-632.

Green, M. F., Cebon, D. and Cole, D. J. (1997). "Effects of heavy vehicle suspension design on the dynamics of highway bridges." *Journal of Structural Engineering*, 121(2), 272-282.

Green, M.F. and Cebon, D. (1994). "Dynamic response of highway bridges to heavy vehicle loads: theory and experimental validation." *Journal of Sound and Vibration.* 170(1), 51-78.

Huang, D.Z., Wang, T.L., and Shahaway, M. (1993). "Impact studies of multi-girder concrete bridges," *Journal of Structural Engineering*, 119(8), 2387-2402.

Hwang, E. S. and Nowak, A. S. (1991). "Sumulation of dynamic load for bridges." *Journal of Structural Engineering*, 117(5), 1413-1434.

International Organization for Standardization (ISO). (1995). "Mechanical vibration –Road surface profiles-Reporting of measured data." *ISO 8068: 1995 (E),* ISO, Geneva.

Kim, S. and Nowak, A.S. (1997). "Load distribution and impact factors for I-girder bridges." *Journal of Bridge Engineering.* 2(3), 97-104.

Kostem, C.N. (1977), "Effects of Diaphragms on Lateral Load Distribution in Beam-Slab Bridges." *Transportation Research Record no.645*, Transportation Research Board, Washington D.C., 6-9.

Li, C.Y. (1996). "Bridge vibration and impact under moving vehicles." *Proceedings of the 1996 3rd Joint Conference on Engineering Systems Design and Analysis, ESDA.* Jul 1-4 1996*,* Montpellier, v 81, n 9, p 17-23.

Sammartino, G., Amirouche, F., Chen, Z. L., and Wang, M. L. (1999). "Effects of heavy vehicle speeds on the structure and vibration of bridges." *American Society of Mechanical Engineers, Design Engineering Division (Publication) DE*, v 101, 139-147.

Shi, X. M., and Cai, C. S. (2006). "Vehicle induced dynamic behavior of short span slab bridges considering effect of approach span." *Journal of Bridge Structur,* (submitted)

White, D., Sritharan, S., Suleiman,M., Mekkawy, M., and Chetlur, S. (2005). "Identification of the best practices for design, construction, and repair of bridge approaches." Rep. No. *CTRE Project 02-118*, Iowa Department of Transportation, Ames, IA.

Wang, T. L. and Liu, C.H. (2000). "Influence of Heavy Trucks on Highway Bridges," Rep. No. *FL/DOT/RMC/ 6672-379*, Florida Department of Transportation, Tallahassee, FL.

Wang, T. L. and Huang, D. Z. (1992). "Computer modeling analysis in bridge evaluation." Rep. No. *FL/DOT/RMC/0542-3394*, Florida Department of Transportation, Tallahassee, FL.

CHAPTER 7 SUPRESSION OF VEHICLE INDUCED BRIDGE VIBRATION USING TUNED MASS DAMPER (TMD)

7.1 Introduction

The importance of bridge vibrations induced by moving vehicles, which act as oscillators on a bridge as well as time variant forces, has long been recognized by engineers. Vibration that occurs in bridges can amplify the propagation of existing cracks resulting in further damage to the bridge. It has become one of the causes of reduction in long-term serviceability of the bridge, although major bridge failures are not usually caused directly by moving vehicles, and it is also a critical factor to bridge's structure fatigue and rapid deterioration (Sammartino et al. 1999). Extensive researches (e.g., Green and Cebon 1994; Wang and Liu 2000), including both experimental and theoretical works, have been conducted to determine the dynamic behavior of bridges under moving vehicles. The results of field tests and analytical researches have shown significant dynamic response exceeding that anticipated on certain small and medium span bridges (Huang et al. 1993; Karoumi 2000).

One method of reducing the vibration of structures is to add an energy dissipative system to the primary structure to control the dynamic response. The tuned mass damper (TMD), which is a secondary vibration system connected to the primary structure at suitable points, is a classical device to dissipate a substantial amount of vibration energy of the main structure. A typical TMD generally consists of a mass, a spring, and a dashpot. Since Den Hartog firstly investigated the optimum values of TMD parameters using a two-degree of freedom model in 1950s, the TMDs have been extensively studied and applied to suppress vibrations of buildings and bridges. It is well known that the TMD is effective in suppressing the single-mode resonant vibration when its frequency is tuned to the modal frequency of the structure (Igusa and Xu 1991; Das and Dey 1992). Much of research efforts were focused on developing the design procedure and optimizing the TMD parameters. Although excessive studies (e.g. Chen and Cai 2004; Chen and Kareem 2003; Jo et al. 2001;) have been conducted on TMDs for suppressing vibration of structures under wind and seismic loads, little research has been done on applying TMDs to control vehicle-induced bridge vibration (Li et al. 2005).

The objective of this research is to study the possible effectiveness of TMDs for suppressing vibrations of bridges under vehicle loads. In order to achieve this objective, a general formulation of the vehicle-induced bridge vibration controlled with a TMD system is first developed, which takes into account the road surface conditions. Then, a comprehensive investigation is made to investigate the efficiency of the TMD for suppressing vibrations of different bridges under two vehicle load patterns, i.e. two trucks moving side by side and several trucks passing over the bridge in a traffic flow. Such a study is helpful in evaluating the control performance before real control devices are designed in practice. These analytical results will also be useful in carrying out further studies of control strategies in order to suppress the vehicle-induced bridge vibration.

7.2 Vehicle-Bridge System with TMD

As shown in Fig. 7-1, the system consists of a bridge with a TMD installed at a desired position of the bridge and a series of vehicles. Each vehicle is idealized as a combination of a number of rigid bodies connected by a series of springs and dampers. For demonstration purposes, a 3-axle articulated truck consisting of up to 11 independent degrees of freedoms is shown in Fig. 7-1. The equations of motion for the vehicle are derived based on the following matrix form:

$$[M_v]\{\ddot{d}_v\}+[C_v]\{\dot{d}_v\}+[K_v]\{d_v\}=\{F_v{}^G\}+\{F_c\} \tag{7-1}$$

where the vehicle mass matrix $[M_v]$, damping matrix $[C_v]$, and stiffness matrix $[K_v]$ are obtained by considering the equilibrium of the forces and moments of the vehicle system; $\{d_v\}$ is the displacement vector of vehicle; $\{F_v{}^G\}$ is the self-weight of the vehicle; and $\{F_c\}$ is the vector of wheel-bridge contact forces acting on the vehicle.

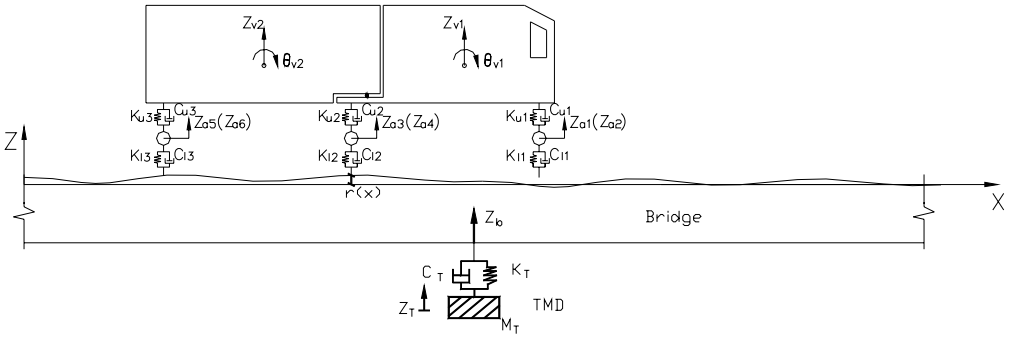

(a) side view

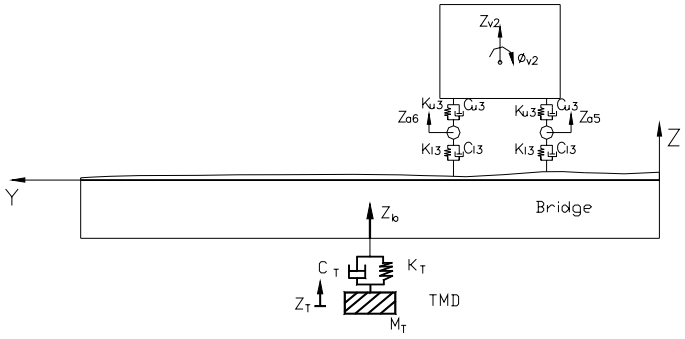

(b) section view

Fig. 7-1 Illustration of vehicle-bridge system with TMD

The bridge is modeled using the conventional finite element method, and the equations of motion for the bridge can be expressed as

$$[M_b]\{\ddot{d}_b\}+[C_b]\{\dot{d}_b\}+[K_b]\{d_b\}=\{F_b\}+\{F_T\} \tag{7-2}$$

where $[M_b]$ is the bridge mass matrix, $[C_b]$ is the damping matrix, and $[K_b]$ is the stiffness matrix; $\{F_b\}$is the wheel-bridge contact force on the bridge; and $\{F_T\}$is the interacting force between the TMD and the bridge.

The equations of motion for the vehicle and bridge are coupled through the interaction forces, i.e. $\{F_b\}$ and $\{F_c\}$. $\{F_b\}$and $\{F_c\}$are action and reaction forces existing at the contact points of the two systems and are expressed as a function of the deformation of the vehicle's lower springs $\{\Delta_l\}$ (Zhang et. al 2006):

$$\{F_b\} = -\{F_c\} = [K_l](Z_a - Z_b - r(x)) + [C_l](\dot{Z}_a - \dot{Z}_b - \dot{r}(x)) \quad (7\text{-}3)$$

in which $r(x)$ is the road surface profile of the bridge deck (Fig. 7-1) and it can be simulated using reversed Fourier transformation. $\dot{r}(x) = \frac{dr(x)}{dx}\frac{dx}{dt} = \frac{dr(x)}{dx}V(t)$ and $V(t)$ is the vehicle velocity; Z_a is vehicle axle suspension displacement in vertical direction, and Z_b is the displacement of bridge at wheel-road contact points.

The TMD is installed at a desired position of the bridge where its response becomes a maximum. The equations of motion which represent the interaction between the TMD and the bridge are

$$[M_T]\ddot{d}_T + [C_T](\dot{Z}_T - \dot{Z}_b) + [K_T](Z_T - Z_b) = 0 \quad (7\text{-}4)$$

where $[M_T]$ is the mass of TMD, $[C_T]$ is the damping of TMD, $[K_T]$ is the spring coefficient, and Z_T is the displacement of TMD. At time t, the interacting force, $\{F_T\}$, between bridge and TMD is

$$\{F_T\} = [K_T](Z_T - Z_b) + [C_T](\dot{Z}_T - \dot{Z}_b) \quad (7\text{-}5)$$

By substituting Eqs. (7-3) and (7-5) into Eqs. (7-1) and (7-2), the final equations of motion of bridge, TMD, and vehicle system can be rewritten in matrix form as in the following equation.

$$\begin{bmatrix} M_b & & \\ & M_T & \\ & & M_v \end{bmatrix}\begin{Bmatrix} \ddot{d}_b \\ \ddot{d}_T \\ \ddot{d}_v \end{Bmatrix} + \begin{bmatrix} C_b + C_{bb} + C_T & C_{bT} & C_{bv} \\ C_{Tb} & C_T & 0 \\ C_{vb} & 0 & C_v \end{bmatrix}\begin{Bmatrix} \dot{d}_b \\ \dot{d}_T \\ \dot{d}_v \end{Bmatrix} + \begin{bmatrix} K_b + K_{bb} + K_T & K_{bT} & K_{bv} \\ K_{Tb} & K_T & 0 \\ K_{vb} & 0 & K_v \end{bmatrix}\begin{Bmatrix} d_b \\ d_T \\ d_v \end{Bmatrix}$$
$$= \begin{Bmatrix} F_b^{\,r} \\ 0 \\ F_v^{\,r} + F_v^{\,G} \end{Bmatrix} \quad (7-6)$$

The additional terms C_{bb}, C_{bv}, C_{vb}, K_{bb}, K_{bv}, K_{vb}, $F_b^{\,r}$, and $F_v^{\,r}$ in Eq. (7-6) are due to the expansion of the contact force vector expressed by Eq. (7-3) and Eq. (7-5). As a vehicle passes over a bridge not only the position but also the magnitude of the contact force are changing with respect to time. This is caused by the fact that the position the vehicle, the response of bridge and vehicle, and the road roughness r(x) at the wheel and bridge deck contact points no longer

remain the same. The change of contact force with time indicates that the additional terms in Eq. (7-6) are time-dependent and will change as the vehicle moves across the bridge.

To simplify the modeling procedure, the bridge mode superposition technique is used based on the obtained bridge mode shapes and the corresponding natural circular frequencies. Since the ratio of the TMD mass to the bridge mass is assumed to be very small, the attachment of TMD does not cause a meaningful change to the static equilibrium of the bridge, and the mode shapes of the bridge remain the same as those of the original bridge without the TMD. The mode superposition makes it possible to separate the bridge modal analysis from the vehicle-bridge coupled model. Consequently, the number of equations in Eq. (7-6) and the complexity of the entire procedure are greatly reduced.

A computer program is developed based on the above methodology. The mass matrix, stiffness matrix, and damping matrix of vehicle and bridge are automatically assembled using the fully computerized approach. The equations of motion are solved in time domain by using the Runge-Kutta method. By solving the equations, the dynamic response of the vehicle, bridge, and TMD can be obtained in time history.

7.3 Numerical Examples

Two numerical examples of different truck load cases, i.e. two trucks moving side by side and several trucks moving one following another, are investigated by using the developed method. Different bridges are also considered to study the effectiveness of TMD. An AASHTO HS20-44 truck, whose configuration is shown in Fig. 7-1, is used in the following numerical analyses. The static wheel loads for the first, second, and third axle are 17.8 KN (4 kips), 71.2 KN (16 kips), and 71.2 KN (16 kips), respectively, which makes the total weight of the truck as 320 KN (72 kips). The truck was assumed to pass a step up of 0.0381 m, which is used to simulate the differential faulting between the bridge deck and approach slab (Cebon, 1999), and then move on a smooth surface of bridge deck at a constant speed of 20 m/s (45mph).

7.3.1 Case One: Two Trucks Moving Side by Side

To investigate the effectiveness of TMD on different bridges, four slab bridges and four slab-on-girder bridges with different span lengths are analyzed. The four concrete slab bridges are simply supported with the width of 12 m and the span lengths ranging from 6 m, 8 m, 10 m, to 12 m, which is the normal range of span lengths for slab bridges. The four slab-on-girder bridges, with span lengths of 16.76 m (55 ft), 24.38 m (80 ft), 30.48 m (100 ft), and 39.62 m (130 ft), are of Type II, Type III, Type IV and Type VI prestressed concrete girders, respectively. The slab-on-girder bridges consist of seven girders that are simply supported with girder spacing of 2.13 m (7 ft). The bridges have a roadway width of 14.32 m (47 ft) and a bridge deck thickness of 0.20 m (8 in). For all eight bridges, twenty modes of each bridge are taken into account in the analysis of dynamic response after a sensitivity study. The primary data of the bridges and the first modes of each bridge are listed in Table 7-1. The damping ratios of all bridges are assumed to be 0.02.

Table 7-1 Modal frequencies of bridges

Mode	Slab bridge span length				Girder bridge span length			
	B1	B2	B3	B4	B5	B6	B7	B8
	6m	8m	10m	12m	16.76m	24.38m	30.48m	39.62m
First bending mode (Hz)	12.92	9.64	7.68	6.38	7.56	4.45	3.44	2.64
Second bending mode (Hz)	51.75	38.57	30.72	25.52	24.47	15.98	12.54	9.69
First torsional mode (Hz)	15.37	12.71	11.27	10.39	9.34	5.77	4.50	3.50
Second torsional mode (Hz)	23.04	22.26	22.61	23.53	11.86	8.68	8.52	9.08

Since the bridges considered in the present study have two traffic lanes, two vehicles, one in each lane, is considered at any given moment. In this case, two trucks are assumed to move side by side when passing over bridges (Fig. 7-2), which agrees also with the critical live load specifications of AASHTO codes (AASHTO 2002, 2004).

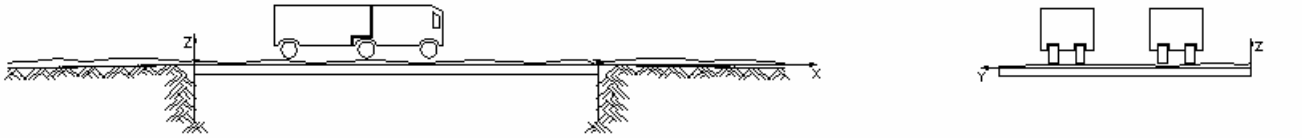

Fig. 7-2 Two trucks moving side by side

According to the preliminary analyses, the bridge's first mode is dominant in the dynamic response for all eight bridges. To reduce the bridge dynamic response, it is desirable to tune the TMD to the fundamental frequency (the first frequency) of the bridge. The TMD is positioned at the center of the bridge (Fig. 7-1) where the first mode response is at the maximum. The mass ratio of 1% is selected in this study, though ratios between 1% and 5% have generally been used in other studies (Soong and Dargush 1997; Lin et al. 2005; Jo et al. 2001). The damping ratio of TMD is set as 6%, which is the optimal damping ratio for single TMD proposed by Den Hartog (1956).

Figs. 7-3 and 7-4 display the time history of the deflection of all the bridges with and without TMD. It is observed that the maximum dynamic deflection when the vehicle is on the bridge (forced vibration period) is slightly reduced by TMD. For instance, the maximum dynamic deflections of the 8 m slab bridge and the 39.62 m girder bridge without TMD are 5.42 mm and 7.03 mm, respectively. After the installation of the TMD, the deflections of these two bridges are reduced to 5.16 mm and 6.99 mm, respectively. This indicates that the reducing effect of the forced vibration is only 4.86% for the 8 m slab bridge, and 0.60% for the 39.62 m girder bridge. It is evident that the TMD does not significantly suppress the forced vibration in these bridges. However, it is obvious from Figs. 7-3 and 7-4 that the vibration level of all bridges is greatly reduced during the free vibration period, which means the TMD is effective in reducing the free vibration although it is difficult to control the forced vibration. Figs. 7-5 to 7-6 present the spectral analysis of the dynamic displacement of all bridges.

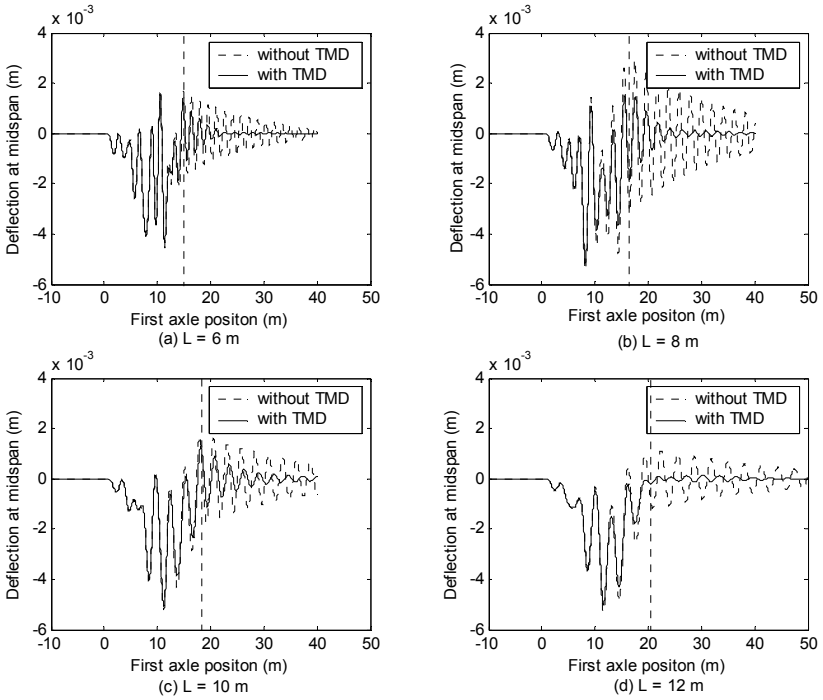

Fig. 7-3 Time history of deflection at mid-span of slab bridges with and without TMD

The forced vibration for the passage of two side by side trucks is very short for the bridges considered in this study. In this short period of passage of vehicle, the bridge only vibrates for very few cycles (Figs. 7-3 to 7-4). Although the TMD increases the overall damping of the bridge, it needs time to respond to the vibration before it can effectively absorb vibration energy from the main structure and then suppress the vibration. Figs. 7-7 and 7-8 present the time history of the TMDs' stroke for the slab bridges and girder bridges, respectively. The results clearly show that since the vehicle passage time on the bridge is too short the TMDs only experience very few cycles of vibration during the forced vibration period of the bridge. Therefore, it is not surprising that the response of TMD is not active and that the forced vibration of bridge is hardly suppressed.

Table 7-2 summarizes the reduction of displacement for different bridges, which displays that the suppression effect for the shorter bridges (B1, B2, B3, B4, and B5) is generally better than that for relatively longer bridges (B6, B7, and B8). This is probably due to the fact that the vibration of the shorter bridges is more active (i.e., with higher frequencies) than the longer bridges. Since the fundamental frequency of B1 to B5 is relatively high, during the forced vibration period, there are more excited vibration cycles in the TMDs for the shorter bridges than for the longer bridges (Figs. 7-7 and 7-8). On the other hand, compared with B6, B7, and B8, the multi-axle truck loads applied on the relatively short bridge (B1, B2, B3, B4, and B5) can be considered as repeated loads (similar to the train load on short bridges) although the number of axles of the truck is small, because the bridge span is short compared to the 4.26 m spacing of the HS20 truck axles. Whereas, for longer bridge, since the bridge span is relatively long compared to the axle spacing there is only one half-cycle of loading as the truck crosses the span (Li and Su 1999). Thus, the loading frequency for shorter bridge is higher than that of the longer bridge, which causes more actively vibration in the shorter bridges.

Table 7-2 Maximum response of bridges with and without TMD (Case one)

Span length	Deflection (mm)		Acceleration (m/s^2)	
	without TMD	With TMD	without TMD	with TMD
L=6m	4.550	4.376 (-3.83%)*	17.43	15.83 (-9.18%)*
L=8m	5.423	5.159 (-4.86%)	11.61	10.12 (-12.86%)
L=10m	5.196	5.031 (-3.24%)	5.75	4.99 (-13.23%)
L=12m	5.274	4.990 (-5.37%)	3.71	3.00 (-18.90%)
L=16.76m	5.743	5.470 (-4.75%)	10.24	9.13 (-10.83%)
L=24.38m	7.200	7.091 (-1.51%)	2.79	2.64 (-5.12%)
L=30.48m	6.902	6.872 (-0.44%)	1.25	1.21 (-5.12%)
L=39.62m	7.034	6.992 (-0.60%)	0.92	0.89 (-5.12%)

Note: * Reduction

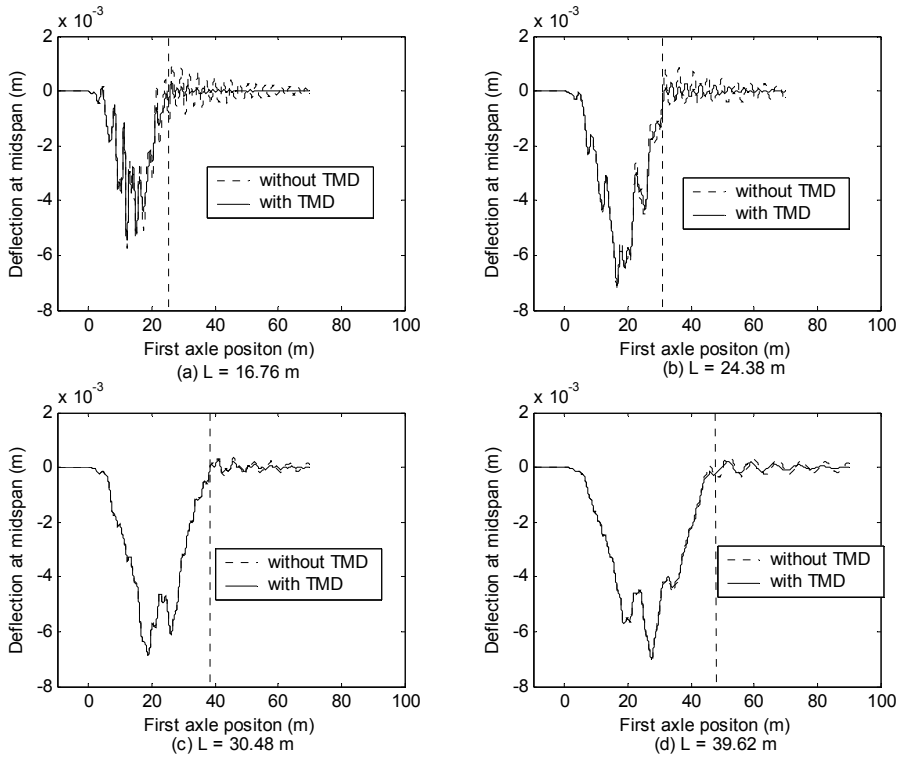

Fig. 7-4 Time history of deflection at mid-span of girder bridges with and without TMD

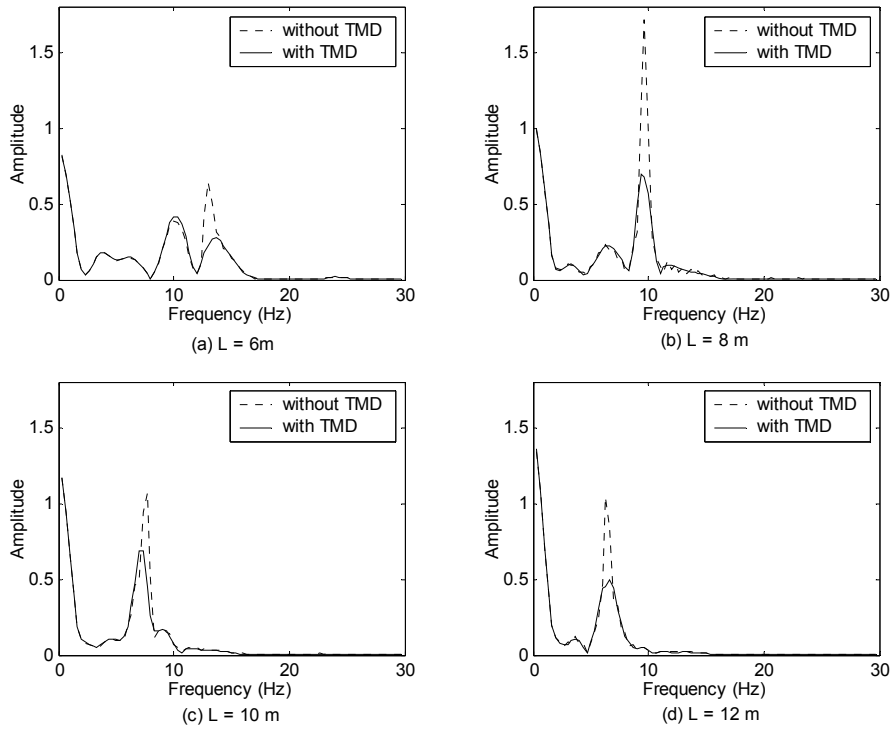

Fig. 7-5 Spectral analysis of deflection at mid-span of slab bridges with and without TMD

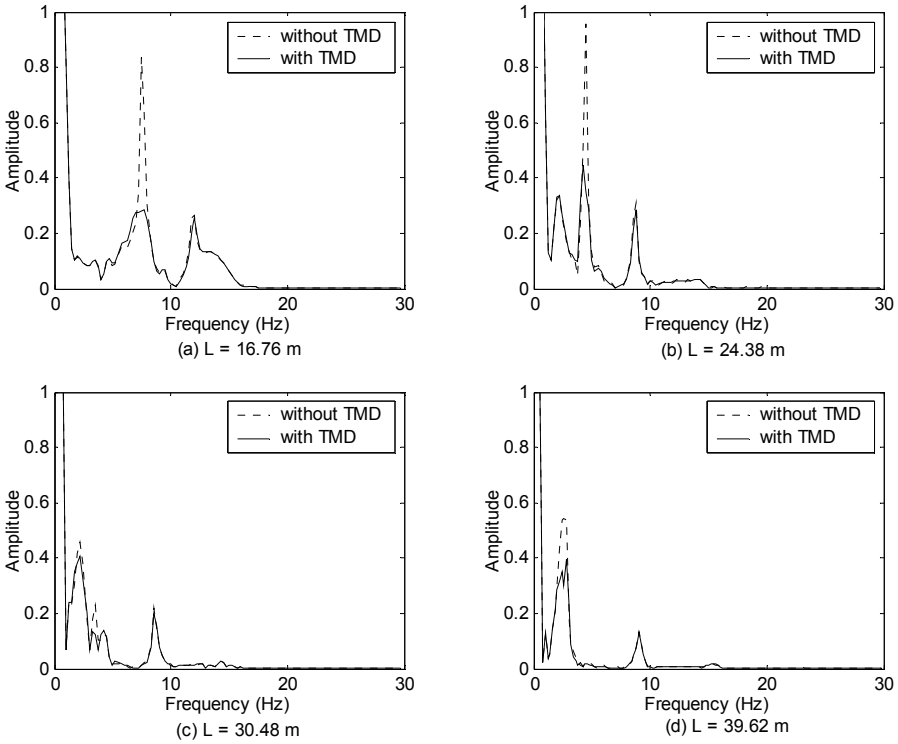

Fig. 7-6 Spectral analysis of deflection at mid-span of girder bridges with and without TMD

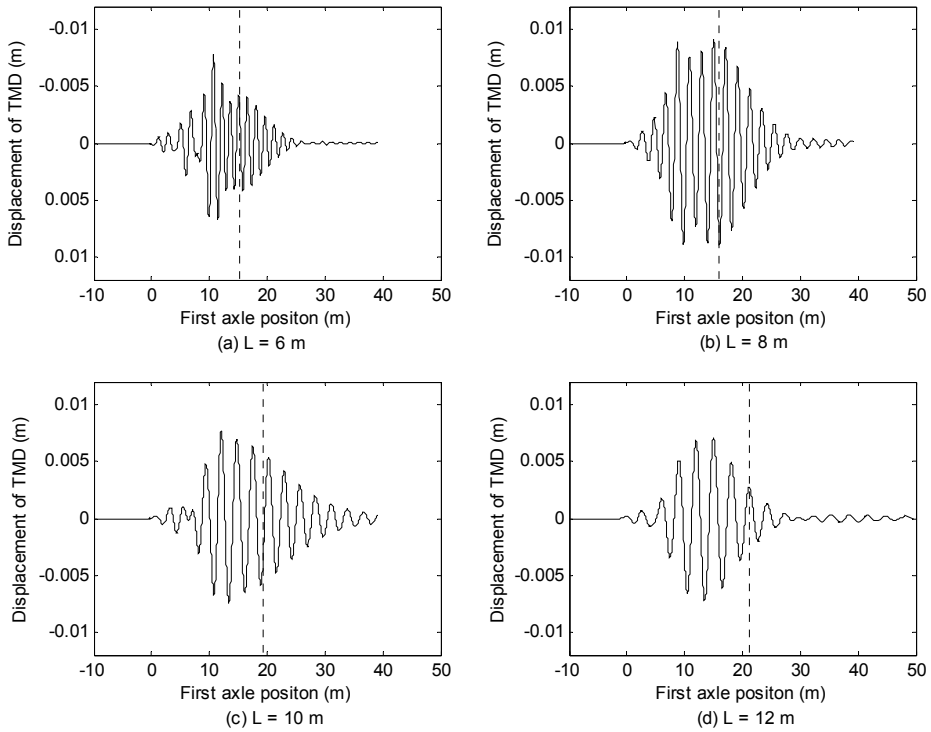

Fig. 7-7 Time history of TMD stroke for slab bridges

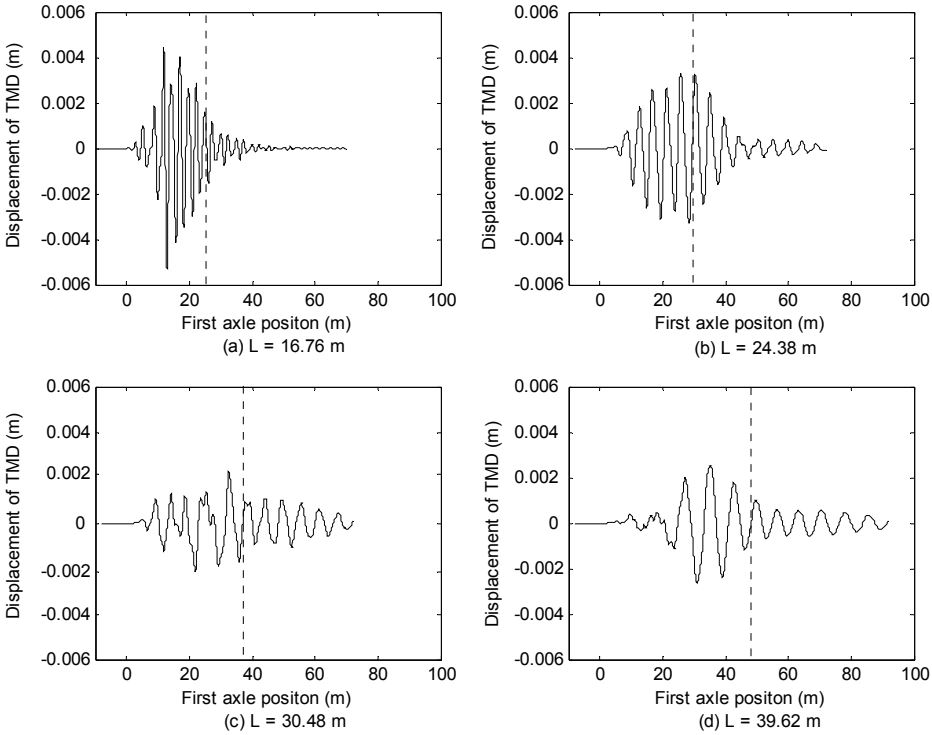

Fig. 7-8 Time history of TMD stroke for girder bridges

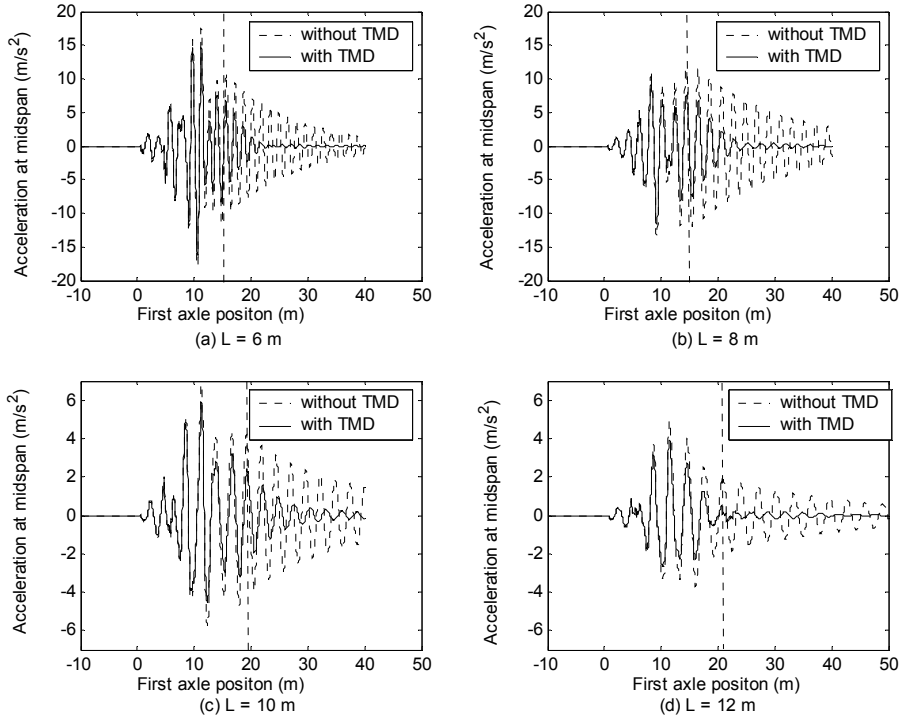

Fig. 7-9 Time history of acceleration at mid-span of slab bridges with and without TMD

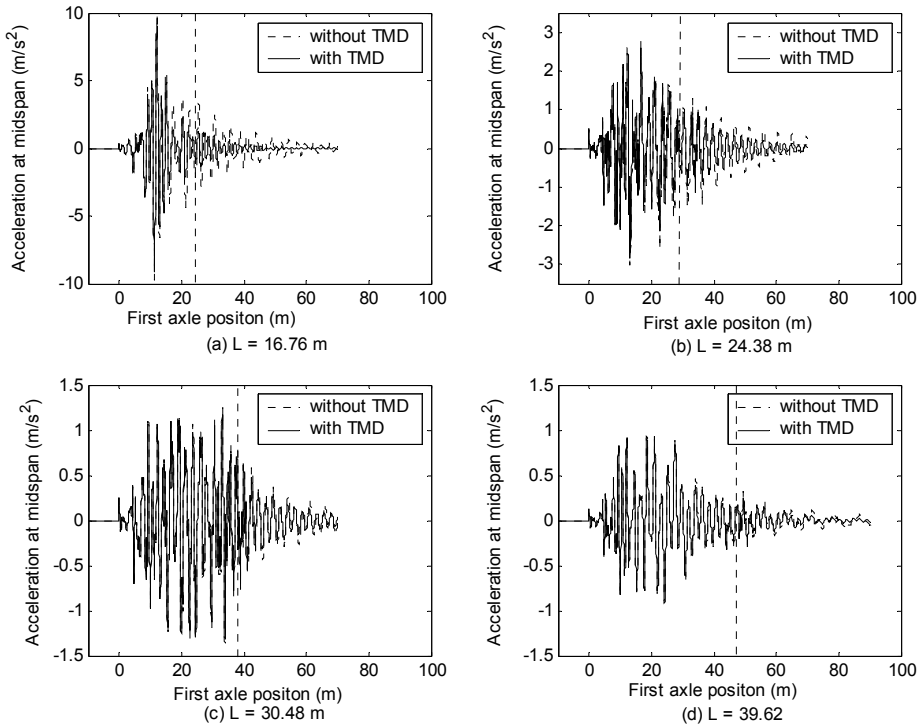

Fig. 7-10 Time history of acceleration at midspan of girder bridges with and without TMD

The bridge dynamic responses of acceleration for all the bridges are also presented in Table 7-2 and Figs. 7-9 to 7-10. It is revealed that the suppression effect of TMD on acceleration is better than on deflection. For example, the accelerations of the 8 m bridge and 39.62 m bridge are reduced by 12.86% and 5.12%, respectively, while the deflections of these two bridges are only reduced by 4.86% and 0.60%, respectively. Moreover, it is observed that the TMD tuned to the first bending mode shows more significant improvement in reduction of acceleration for shorter bridges (B1 to B5) compared to longer bridges (B6 to B8). The spectral analysis of acceleration (Figs. 7-11 to 7-12) indicates that for shorter bridges the first mode is dominant in response of acceleration while for longer brides the contribution of higher modes is relatively larger and the first mode (to which the TMD is tuned) may not be as dominant as in the cases of shorter bridges. In fact, the second torsional mode dominates in the response of acceleration for B6, B7, and B8. Therefore, the TMD tuned to the first mode cannot be very effective for suppression of acceleration for these bridges. This result also implies that the TMD effectiveness for vehicle-induced bridge vibration is highly frequency-dependent.

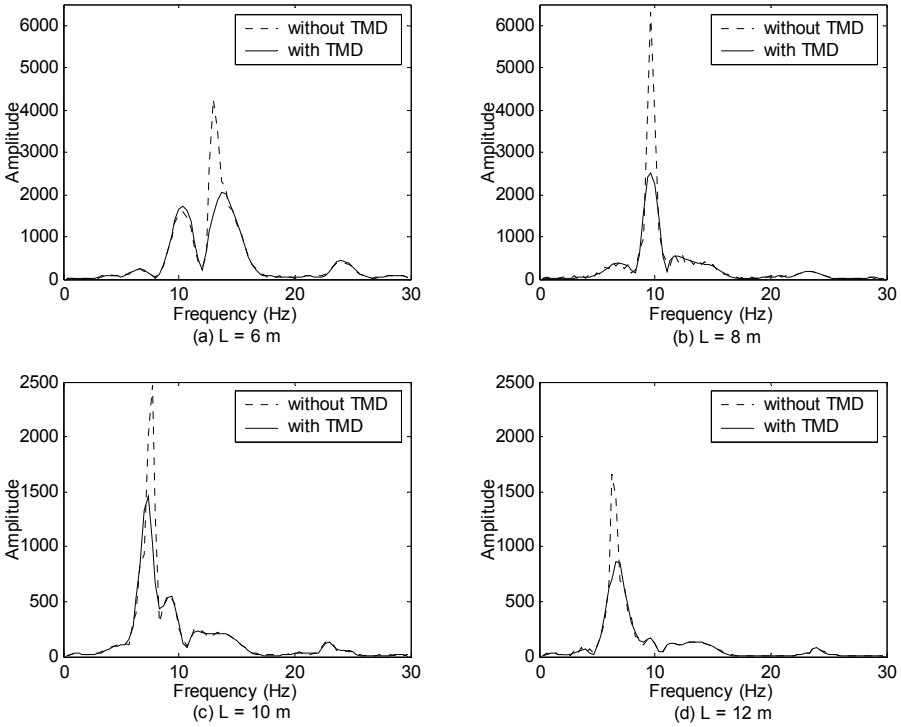

Fig. 7-11 Spectral analysis of acceleration at midspan of slab bridges with and without TMD

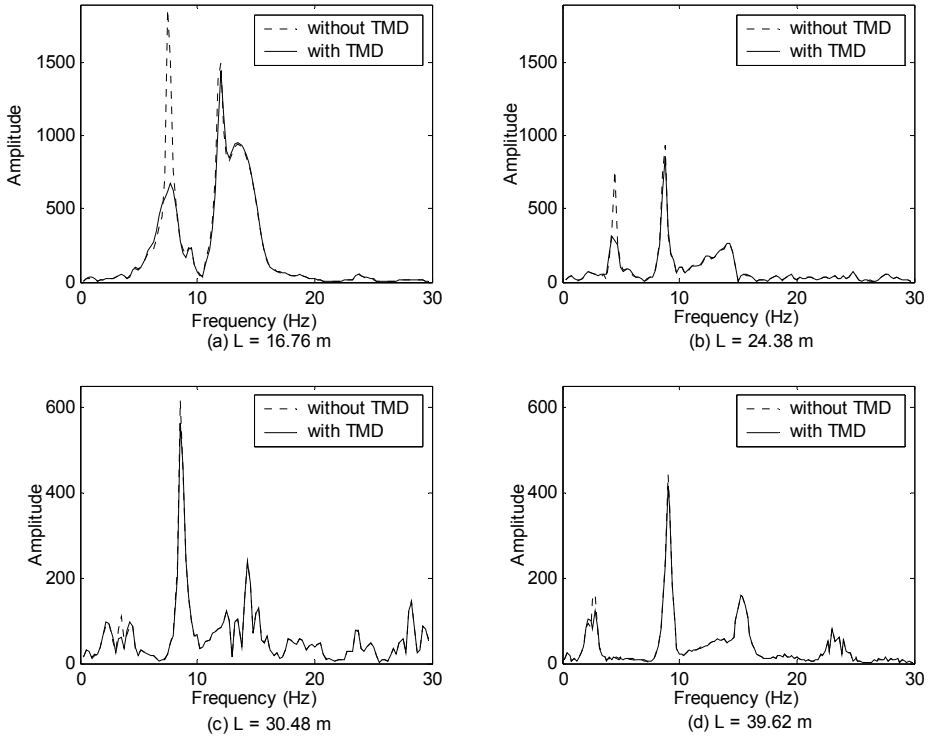

Fig. 7-12 Spectral analysis of acceleration at midspan of girder bridges with and without TMD

7.3.2 Case Two: Trucks Moving in a Traffic Flow

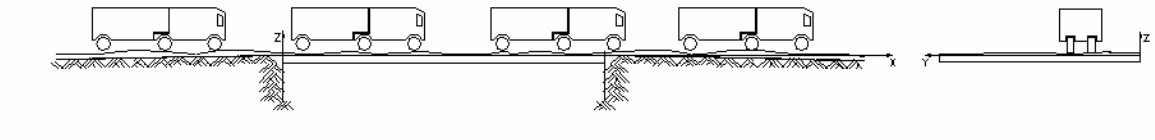

Fig. 7-13 Traffic flow

In the case of a traffic flow, the bridge undergoes a forced vibration for longer time when the trucks are on the bridge. The effectiveness of TMD under this circumstance is also investigated. To properly simulate the traffic on the bridge, the actual vehicle type and distribution of traffic flow is required. However, vehicles passing over the bridge may have quite different numbers and random distributions at any different moment. Due to the complexity of each vehicle model (multi degrees of freedom), it is technically difficult to simulate a real traffic flow using current computer techniques, which is especially true when the traffic is very busy. The common practice in analyzing the vehicle-induced bridge vibration is to choose only one vehicle or a series of identical vehicles in one line (Guo and Xu 2001). Therefore, in this section, only one line of up to six vehicles is assumed to be evenly distributed along the side lane of the bridge with an interval of 6.5 m (Fig. 7-13). The interval setting of vehicles is decided based on some preliminary analyses and the consideration of the random nature of the traffic flow, in which the distance of vehicles is assumed as a random variable characterized by a beta

distribution (Calcada et. al 2005). The effect of the number of vehicles has also been studied in the following numerical analysis.

Table 7-3 lists the effectiveness of TMD for bridge vibrations caused by the different number of trucks in a traffic flow. For the 8 m slab bridge, the maximum deflection and acceleration are reduced by 6.46% and 20.52% by The MD when there is only one truck passing over the bridge, while these reductions are increased to 11.12% and 21.83%, respectively, when there are two trucks passing over the bridge. In the case of this slab bridge, the number of trucks will not affect the effectiveness of TMD when there are more than two trucks in the traffic flow. For the 39.62 m girder bridge, however, as the number of trucks increases from 1, 2, 3, to 4, the reduction of displacement is increased from 0.52%, 1.15%, 2.07%, to 3.37%, and the reduction of acceleration is increased from 0.66%, 1.52%, 7.08%, to 11.16%. For this girder bridge, the number of trucks will not affect the effectiveness of TMD when there are more than four trucks in the traffic flow. From these results, it can be easily observed that the same TMD has better effect to suppress the bridge vibration for the case of several trucks in a traffic flow than for the case of two trucks moving side by side. Again, the dynamic response of the TMD shown in Figs. 7-14 and 7-15 probably explains this phenomenon. As the number of trucks in the traffic flow increase, the maximum amplitude of the TMD vibrations increases. It indicates that more trucks in a traffic flow extends the period of forced bridge vibration, which provides the TMD more time to respond to bridge vibration and to effectively suppress the vibration.

Table 7-3 Maximum response of bridges with and without TMD (Case two)

Bridge	# of trucks in row	Deflection (mm)		Acceleration (m/s^2)	
		without TMD	with TMD	without TMD	with TMD
L=8m	1	3.428	3.207 (6.46%)*	10.54	8.38 (20.52%)*
	2	3.750	3.333 (11.12%)	11.97	9.36 (21.83%)
	3	3.750	3.333 (11.12%)	11.97	9.36 (21.83%)
	4	3.750	3.333 (11.12%)	11.97	9.36 (21.83%)
	5	3.750	3.333 (11.12%)	11.97	9.36 (21.83%)
	6	3.750	3.333 (11.12%)	11.97	9.36 (21.83%)
L=39.62m	1	3.909	3.889 (0.52%)	0.350	0.348 (0.66%)
	2	5.786	5.719 (1.15%)	0.495	0.488 (1.52%)
	3	6.193	6.065 (2.07%)	0.534	0.496 (7.08%)
	4	6.305	6.093 (3.37%)	0.571	0.508 (11.16%)
	5	6.305	6.093 (3.37%)	0.571	0.508 (11.16%)
	6	6.305	6.093 (3.37%)	0.571	0.508 (11.16%)

Note: * Reduction

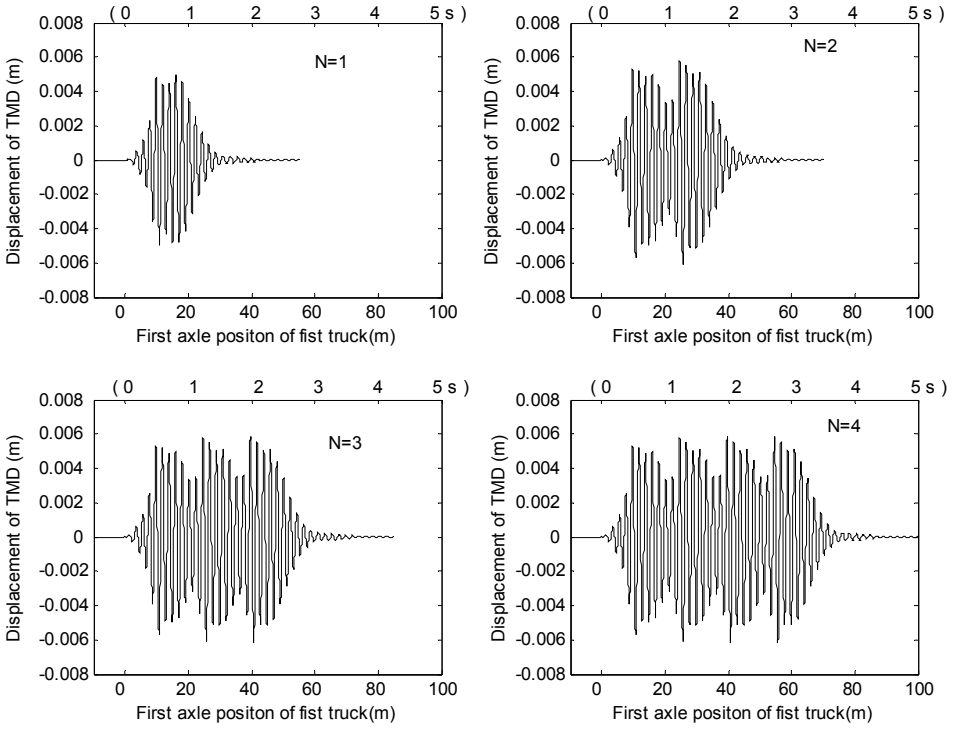

Fig. 7-14 Time history of TMD stroke for the 8 m bridge with different trucks moving across

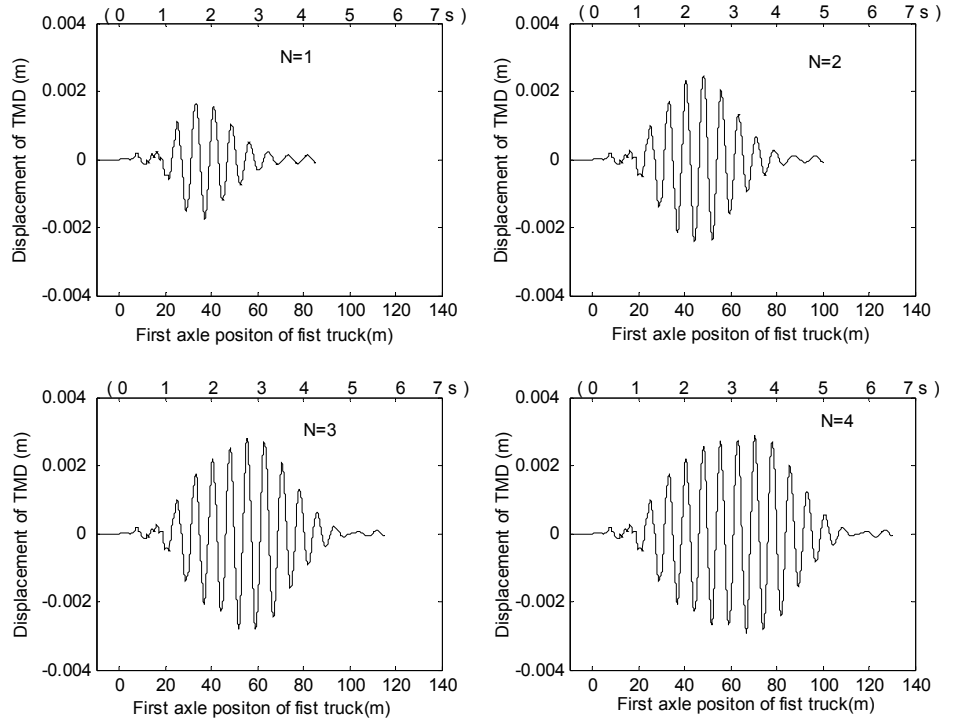

Fig. 7-15 Time history of TMD stroke for the 39. 62 m bridge with different trucks moving across

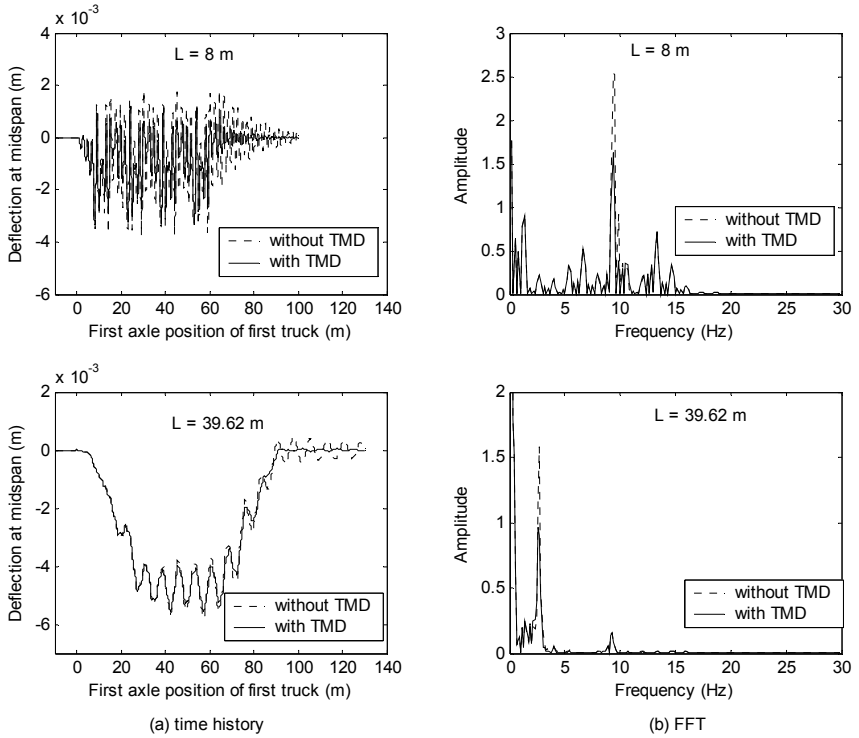

Fig. 7-16 Dynamic response of deflection for bridges with four trucks moving across

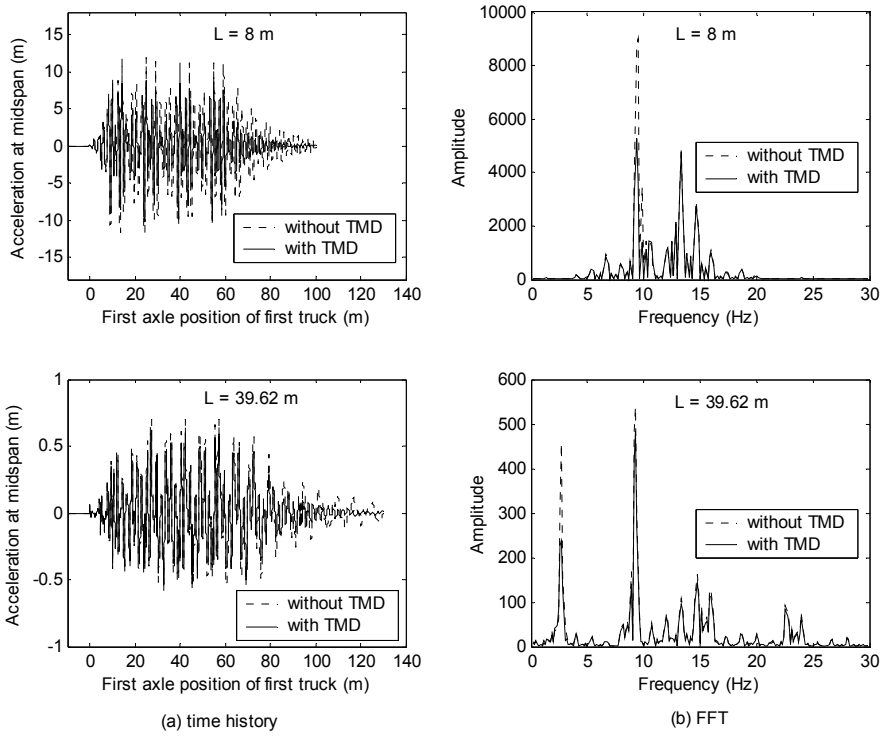

Fig. 7-17 Dynamic response of acceleration for bridges with four trucks moving across

Fig. 7-16 presents the time history and the fast Fourier transform of the deflection at bridge mid-span. Similarly, the acceleration at bridge mid-span in time domain and frequency domain is shown in Fig. 7-17. It can be seen that the reduction of forced vibration is still smaller than that of free vibration.

7.4 Conclusions

The vehicle-induced bridge vibration may affect the durability of the structure and the safety and comfort of passengers. It also can lead to deterioration and reduction in service life of the bridge. Although the major bridge failures are not normally caused by vehicle-induced vibration, it causes more subtle problems and contributes to fatigue, surface wear, and cracking of concrete deck and beams, which leads to corrosion. In this study, the TMD is investigated for the purpose to suppress the vehicle-induced vibration of bridges by a finite element approach. Based on the numerical analyses of short and mediate bridges, the following conclusions can be drawn:

A conventional TMD control approach usually focuses on suppressing the resonant vibration by supplying additional damping to the concerned modes. However, in the case of two trucks passing the bridge side by side, it was found that the addition of damping provided by the TMD does not result in an appreciable reduction of the maximum dynamic displacement during the forced vibration period (i.e. when the vehicle is on the bridge) due to the reason that the forced vibration period is too short and that the TMD does not have enough time to respond. Although this approach could be inefficient for forced vibration, it is evident from the analysis results that the TMD is effective in reducing the vibration level in free vibrations. On the other hand, for all the bridges investigated in this study, the reduction of acceleration is larger than that of the displacement.

It is emphasized that the performance of TMD may be influenced by the dynamic characteristics of bridge vibrations induced by moving vehicles. The TMD has more effect on short bridges with large fundamental frequencies than on longer bridges. This is due to the fact that the vibration of short bridge is more “active” than longer bridge because of the relatively higher natural frequency and multi-axle load frequency of short bridges, which excites more cycles of TMD vibrations.

More generally, it can be concluded that for the same TMD, for the case of several trucks moving in a row, the TMD for reducing the forced bridge vibration is more effective than the case with only two trucks moving side by side.

The evaluation of the control performance is helpful before real control devices are designed in practice. For example, in a given condition the most effective way to reduce bridge response may or not be to install a TMD. The analytical result will be useful in carrying out further studies of control strategies in order to make decisions to suppress the vehicle-induced bridge vibration.

7.5 References

Calcada, R., Cunha, A. and Delgado, R. (2005). "Analysis of traffic-induced vibrations in a cable-stayed bridge. Part II: numerical modeling and stochastic simulation." *Journal of Bridge Engineering.* 10(4), 386-397.

Cebon, D. (1999). *Handbook of vehicle-road interaction*, 2nd Ed., Swets & Zeitlinger B.V., Lisse, the Netherlands.

Chen, S. R. and Cai, C. S**.** (2004) "Coupled Vibration Control with Tuned Mass Damper for Long-Span Bridges ", *Journal of Sound and Vibration,* Elsevier, 278(1-2), 449-459.

Chen, X. Z. and Kareem, A. (2003). "Efficacy of tuned mass dampers for bridge flutter control." *Journal of Structural Engineering*, 129(10), 1290-1300

Das, A. K. and Dey, S. S. (1992). "Effects of tuned mass dampers on random response of bridges." *Journal of Computers and Structures*, 43(4), 745-750

Den Hartog, J. P. (1956). Mechanical Vibration, 4th edition, McGraw-Hill

Green, M.F. and Cebon, D. (1994). "Dynamic response of highway bridges to heavy vehicle loads: theory and experimental validation." *Journal of Sound and Vibration.* 170 (1), 51-78.

Guo, W. H. and Xu, Y. L. (2001). "Full computerized approach to study cable-stayed bridge-vehicle interaction." *Journal of Sound and Vibration,* 248(4), 745-761.

Huang, D.Z., Wang, T.L., and Shahaway, M. (1993). "Impact studies of multi-girder concrete bridges." *Journal of Structural Engineering*, ASCE, 119 (8), 2387-2402.

Igusa, T. and Xu, K. (1991). "Vibration reduction characteristics of distributed tuned mass dampers." *Proc. 4th International Conf. on Recent Advances in Structural Dynamics,* 596-605.

Jo, B. W., Tae, G. H., and Lee, D. W. (2001). "Structural vibration of tuned mass damper-installed three-span steel box bridge." *International Journal of Pressure Vessels and Piping*, 78(10), 667-675.

Karoumi, R. (2000). "Modeling of cable-stayed bridges for analysis of traffic induced vibrations." *Proceedings of the International Modal Analysis Conference – IMAC,* v 1, p 842-848.

Li, J. Z., Su, M. B., and Fan, L. C. (2005). "Vibration control of railway bridges under high-speed trains using multiple tuned mass dampers." *Journal of Bridge Engineering*, 10(3), 312-320.

Lin, C. C., Wang, J. F., and Chen, B. L. (2005). "Train-induced vibration control of high-speed railway bridges equipped with multiple tuned mass dampers." *Journal of Bridge Engineering*, 10(4), 398-414.

Sammartino, G., Amirouche, F., Chen, Z. L., and Wang, M. L. (1999). "Effects of heavy vehicle speeds on the structure and vibration of bridges." *American Society of Mechanical Engineers, Design Engineering Division (Publication) DE*, v 101, 1999, 139-147.

Soong, T. T. and Dargush, G. F. (1997). *Passive Energy Dissipation Systems in Structural Engineering*, JohnWiley & Sons, Chichester, England.

Wang, T. L. and Liu, C.H. (2000). *Influence of Heavy Trucks on Highway Bridges.* Rep. No. FL/DOT/RMC/ 6672-379, Florida Department of Transportation, Tallahassee, FL.

Zhang, Y., Cai, C. S., Shi, X. M. and Wang, C. (2005). "Vehicle Induced Dynamic Performance of a FRP Versus Concrete Slab Bridge." *Journal of Bridge Engineering*, ASCE, 11 (4), 410-419.

CHAPTER 8 CONCLUSIONS AND RECOMMENDATIONS

8.1 Performance of Approach Slab under Given Embankment Settlement

In most cases, the approach slab is partially in contact and partially separated from the embankment soil because of soil settlement. Thus, its deformation depends on embankment settlement as well as on external force. To investigate the effect of embankment settlements on the performance of the approach slab, a 3-D finite element analysis is conducted. The contact element is used to model the separation and contact mechanics between the approach slab and the soil.

The predicted deflections and internal moments of the slab and stresses of the embankment soil increase with the increase of the embankment settlement. For the particular example used in Chapter 2, when the settlement increases to 152 mm (6.0 in.), the approach slab becomes a simply-supported beam. This result indicates that LaDOTD's current slab design is good for cases without embankment settlement, but the ultimate strength is not adequate if settlement larger than 15 mm is considered. This implies that either more reinforcement, thicker slab section, and/or settlement control are needed to satisfy the AASHTO structural design requirement. Similar issues may exist in other states and modifications of concrete slab design may be warranted.

Correlations of the faulting and deflection of the approach slab with approach embankment settlement and the approach slab parameters (length and flexural rigidity) are also developed. This correlation will be used to evaluate the effectiveness of approach slabs and develop guidelines for their structural design. It provides a simpler design procedure so that engineers do not need to use complicated finite element analysis in a routine design. Instead, the developed coefficients can be multiplied with the simple beam response to consider the interaction of the embankment soil and slab under a given embankment settlement. The more rational design considering a given settlement will eventually lead to a more reliable practice in using approach slabs.

In addition, to alleviate the "bump" problem at bridge ends, a ribbed concrete approach slab (similar to slab-on-beam bridge decks) is developed in place of the pile/column-supported approach span and/or flat slab system. The ribbed approach slab can reduce the slab thickness compared with the flat approach slabs. The present study has investigated the effect of the embankment settlement on the structural performance of the ribbed approach slab. The deflections and internal moments of the beam, and reaction forces of the beam at the sleeper slab end have been predicted to increase with the increase of the embankment settlement. Since the beams with different spacing are also investigated, with the given settlement and deflection limit, proper beam spacing can be determined. The preliminary results indicate that the beam spaced at 32 ft is good for cases with an embankment settlement less than 3 in. The strength of beams with spacing of 16 and 12 ft is adequate when the settlement is larger.

The information from the present study, along with other information, such as time-dependent embankment settlement, and comfort criteria of bump from other related studies, will help decide when settlement controls are necessary and how to choose an appropriate configuration to have an economical design for the approach slabs.

8.2 Effect of Approach Slab Deformation on Vehicle-Bridge Interaction

Vehicle-induced impact load on highway bridges is one of the primary problems that the structural engineers should be concerned. To consider dynamic effects introduced by moving vehicles on bridges, engineers generally rely on dynamic amplification factors specified in bridge design codes. This is the traditional method used today for design purpose and can yield a conservative and expensive design for some bridges but might underestimate the dynamic effects for others. Improved analytical techniques that consider all the important parameters influencing the dynamic response are required in order to check the true capacity of existing bridges to heavier traffic and for proper design of new bridges.

The uneven joint of the bridge deck and approach is the initial excitation of vehicle vibration that affects the dynamic responses of both the bridge and vehicles. To take into account the influence of the unevenness, the vehicle induced dynamic bridge responses are calculated by modeling the bridge and vehicle in one coupled system. A fully computerized vehicle-bridge coupled model has been developed. This model is validated by field dynamic test on a typical slab-on-girder bridge. The numerical outcomes of the bridge dynamic response are compared to the experimental results, which show a satisfactory agreement. This indicates that the proposed model is reliable for predicting the vehicle-induced dynamic response of bridges with consideration of road surface irregularities.

The approach span condition that consists of faulting at the ends and deformation along the span is considered in the analysis. While the effect of the along-span deformation on the dynamic response of bridges is trivial, the faulting condition of the approach span is found to cause significantly dynamic responses in short span bridges.

For slab bridges with small span lengths, critical truck speeds that result in peaks of dynamic response are found to follow the rule governing the resonant vibration of bridges due to train loading. The local unevenness of expansion joints at the approach slab ends tremendously increases the dynamic response of short slab bridges. Moreover, the bridge dynamic response under the condition of a large approach span deformation, especially the faulting, is much higher than that under the rough road surface with an ISO classified good condition. The same faulting value has a much larger influence on short bridges than it does on longer bridges since the longer span bridges have more time for the initial disturbance to be dissipated and allow the vehicle to become stable before it comes to the mid-span of the bridge. Provided that short bridges have a good road surface condition and smooth joints (small faulting) at the bridge ends, the impact factors are generally smaller than those computed by the AASHTO specifications (both standard and LRFD codes). However, AASHTO specifications may underestimate the impact factors for short bridges with uneven joints at the bridge ends. This situation should be emphasized in practice, especially in rating existing short span bridges.

For slab-on-girder bridges, the faulting condition of the approach span is found to cause significant dynamic responses and to have considerable effect on the distribution of impact factors along transverse and longitudinal directions. The vehicle bumping caused by large faulting condition excites higher modes in the vehicle, which in turn triggers higher modes in the bridge dynamic response. Among these higher modes, the torsion modes contribute more to the

dynamic response of exterior girders, which results in larger increase in IMs (impact factors) for exterior girders than that of interior girders. The higher modes not only affect the IMs along transverse direction but also affect the IMs along the longitudinal direction. The higher bending modes of bridges excited by the vehicle bumping, may cause larger IMs at the quarter span than that at the mid-span, and this needs to be noticed in design and evaluation of prestressed concrete girders at sections with harped strands where the section strength could be more critical than at the mid span. AASHTO specifications may also underestimate the impact factors for these slab-on-girder bridges with larger faulting conditions at the bridge ends. The bridges with vehicles moving across them under larger faulting conditions have more uniform LDFs (load distribution factors) than under static loads, and they are consistently lower than those in AASHTO specifications.

8.3 Suppression of Vehicle-Induced Bridge Vibration

TMD is investigated with the purpose to suppress the vehicle-induced vibration of bridges by a finite element approach. A model for the vehicle-induced bridge vibration controlled with the TMD system takes into account the road surface conditions. The damping provided by TMDs does not result in an appreciable reduction of the maximum dynamic displacement during the period of forced vibration (i.e. when the vehicle is on the bridge). However, it is evident from the analysis results that TMD is effective in reducing the free vibration. On the other hand, for all the bridges investigated in this study, the reduction of acceleration is more significant than that of the displacement. Generally speaking, it can be concluded that for the same TMD installed in the same bridge, it is more effective for cases that trucks pass the bridge in row than for cases having only one truck. Such a study is helpful in evaluating the control performance before real control devices are designed in practice. The TMD has more effect on short bridges than on longer bridges. This is due to the fact that the vibration of short bridge is more active than longer bridge for its relatively higher natural frequencies and multi-axle load frequencies.

In summary, for a given condition the most effective way to reduce bridge response may or may not be to install a TMD. The analytical result will be useful in carrying out further studies of control strategies for suppressing the vehicle-induced bridge vibration.

8.4 Recommendations for Further Research

From current analysis and results, recommendations of future related researches are as follows:

- Regardless of the efforts made to improve the structural rigidity and long-term performance of the approach slab, the magnitude of the bump will be a function of the total settlement. A more rigid approach slab will reduce the change of the slope angle (θ_1 in Fig 1-1), but may also increase the local soil pressure beneath the contact area (sleeper slab), thereby may increase the faulting deflection (Δ_1 in Fig. 1). Therefore, a balanced/optimal approach slab design is desirable and should be addressed. This requires collaboration between structural and geotechnical engineers to implement the developed procedure.

- The research on static structural performance of approach slab is based on a given differential settlement. Therefore, developing a more accurate settlement prediction procedure based on field data is necessary. Field instrumentation will help improve the prediction accuracy in terms of settlements and soil stress. Without a known settlement, the developed procedure in this study cannot be fully implemented, though the approach slab can be conservatively designed as a simple beam.

- Since the "bump" is a subjective description, a further study may focus on establishing an acceptance guideline for "bump", i.e., the criteria for an acceptable slope change and faulting of approach spans. Without this information, the approach design can only be based on a strength requirement as the present study does, though deformation has been predicted. A dynamic analysis simulating the truck system and driver response will help develop such a guideline.

- According to the results in Chapter 7, the TMD-based system may or may not be the most appropriate countermeasure for suppressing vehicle-induced vibration in bridges. It is worthwhile to investigate other vibration reduction approaches or even to improve vehicular technologies to solve this problem more adequately.

APPENDIX A: EFFECT OF EMBANKMENT SETTLEMENT ON BRIDGE APPROACH SLAB DESIGN – A FEW CONCERNED ISSUES

A.1 Introduction

The excessive differential settlement between a bridge and the adjacent pavement causes "bumps" or uneven joints at the bridge ends. When vehicles, especially heavy trucks, enter and leave the bridge, the bumps cause large impact loads to the bridge and the pavement. To provide a smooth transition between the bridge deck and the roadway pavement, a reinforced concrete approach slab that connects the bridge deck and the adjacent roadway is commonly used. When the approach slab is initially built on the embankment soil, it has full contact with the embankment fill. However, the long-term embankment soil settlement (due to the embankment soil consolidation and erosion) will form a gap between the slab and the soil and will cause the approach slab to lose its contacts and supports from the soil (Fig. 1-1). When the soil settlement occurs, the slabs will bend in a concave manner that causes a sudden change in slope grades of the approach slab (Fig. 1-1). The loads and weight of the slab will also be redistributed to the ends of the slab and faulting may occur, which in turn will cause a secondary deformation in the approach slab. Field observations indicated that a large deformation (either faulting or a sudden change in slope grades) of approach slabs still causes this "bump", even though the approach slab is used to alleviate the bump problem.

Several comprehensive studies on the performance of bridge approach slabs have been sponsored over the years by various state DOTs. The majority of the previous researches can be categorized as (1) syntheses of practice (Ha et al. 2003; Mahmood 1990; Stewart 1985), (2) identification of the sources of differential settlement (Chini et al. 1992; Kramer and Sajer 1991; Zaman et al. 1991), and (3) soil improvement (Briaud et al. 1997). Although the bump-related problems have been commonly recognized and the causes are clearly identified, no unified engineering solutions have emerged, primarily because of the number and complexity of the factors involved.

In order to solve the bump problem, it is necessary to treat it as a stand-alone design issue. Since its deformation and damage due to embankment soil settlement still causes the bump problem, the approach slab must be provided with enough stiffness and strength for such a settlement. Field observations revealed some broken approach slabs in Louisiana due to excessive soil settlement. Engineering calculations of the conventional or standard approach slab are typically not conducted since the information for the interaction of the approach slab and the embankment settlement is unknown for a routine office design. There are no guidelines in the AASHTO code specifications (AASHTO 2002, AASHTO 2004) regarding the structural design of approach slabs considering the effects of embankment settlements. Similarly, the LADOTD design manual (LADOTD 2002) specifies only the minimum reinforcement requirement, but it does not specify how to conduct the structural design of the approach slabs.

The Louisiana Department of Transportation and Development has launched a major effort to alleviate this problem by changing the design of approach slabs where differential settlement is expected (LQI 2002). The objective is to find a feasible solution that allows approach slabs that are strong enough to lose a portion of their contact supports without detrimental deflection,

perhaps by increasing the flexural rigidity (EI) of the approach slabs. To help design engineers develop such a solution, correlations between the approach slab's deflection and the approach embankment settlement are required.

A.2 Objective and Research Approach

In the point view of approach slab design, there are two extreme cases. One extreme case assumes that the slab has a full contact with the embankment soil and that the performance of the slab is the same as that of the concrete floors on the ground. This assumption is not realistic in many cases due to the embankment settlement discussed above, and it may result in an unconservative design. In the other extreme case, an approach slab can be designed as a simple beam spanning the bridge end and the pavement end, assuming that no soil supports the beam between the two ends. This assumption, while conservative, will definitely result in an uneconomical design. In the majority of these cases, the approach slab is both partially separating from and partially contacting the soil. The supports provided to the concrete slab by the embankment soil will reduce the internal force in the slab. The extent of this support and reduction depends on the slab and soil interaction for a given embankment soil settlement. As the embankment soil settlement results in the separation of the slab from the soil, the slab must be designed to provide enough strength and stiffness for such a settlement.

In the study of bridge approach slab performance under different embankment settlement, which is one of the components of the LQI program, Cai et al. (2005) developed design aids which considered the effect of embankment settlement on the internal forces and deformation of approach slabs. In this method a correlation among the slab parameters, deflection of the slab, internal moment of the slab, and the differential settlement was developed by analyzing the results using the finite element analysis. The results were normalized with respect to the traditional simply-supported beams (with pin and roller supports). For a given embankment differential settlement, the predicted maximum internal moments and deflections due to the total load and dead load only were normalized and were expressed by an exponential function as follows:

$$\frac{M_T}{M_{T0}} = \left(0.955 - 0.78e^{-1.8\times10^7(\frac{\delta h^2}{L^4})} \right) = K_{TM} \qquad \text{(A-1)}$$

$$\frac{M_D}{M_{D0}} = \left(0.95 - 0.8e^{-2.3\times10^7(\frac{\delta h^2}{L^4})} \right) = K_{DM} \qquad \text{A-2)}$$

$$\frac{d_T}{d_{T0}} = \left((3.05 - 2.58e^{-1.6\times10^7(\frac{\delta h^2}{L^4})}) \times (\frac{h}{L})^{0.3} \right) = K_{Td} \qquad \text{(A-3)}$$

$$\frac{d_D}{d_{D0}} = \left((3.01 - 2.63e^{-2.0\times10^7(\frac{\delta h^2}{L^4})}) \times (\frac{h}{L})^{0.3} \right) = K_{Dd} \qquad \text{(A-4)}$$

where M_T and M_D are the maximum moment of the approach slab due to the total load and the dead load respectively; δ = the differential settlement (ft), shown in Fig. 1-1; h = the thickness

of approach slab (ft); L = the length of the approach slab (ft); K_{DM} and K_{TM} are the moment coefficients that are self-evidenced in the equations; M_{T0} and M_{D0} are the maximum moment of simply-supported beam due to the total load and the dead load respectively; d_T and d_D are the maximum deflection of approach slab due to the total load and the dead load respectively; K_{Dd} and K_{Td} are the deflection coefficients that are self-evidenced in the equations; d_{T0} and d_{D0} are the maximum deflection of simply-supported beam due to the total load and the dead load respectively. The maximum internal moment and deflection in the approach slab due to the live load is then calculated as follows:

$$M_L = M_T - M_D = K_{TM} M_{T0} - K_{DM} M_{D0} \quad \text{(A-5)}$$

$$d_L = d_T - d_D = K_{Td} d_{T0} - K_{Dd} d_{D0} \quad \text{(A-6)}$$

Eqs. (A-1) to (A-6) take into account the effect of different soil settlement by considering the approach slab as partially supported by and partially separated from the soil. They also provide engineers with a convenient method which can be used to obtain the slab response by multiplying the slab response of the simply-supported beam with a computed coefficient. The information (deformation and internal force) can be used for the structural evaluation and design of approach slabs without conducting a complicated finite element analysis. For example, the predicted internal moments can be used to design the slab reinforcement for a given settlement (δ). Engineers can also control the excessive settlement by either improving embankment fills or foundations or by selecting a stiffer approach slab based on the predicted deformation. However, there may be some limits in their applications because these equations are based on HS20-44 truck loads and right angle slabs. Whether they are applicable to the AASHTO LRFD HL93 truck load and to skewed approach slab needs to be confirmed.

In this paper, the applicability of the previous design aids to approach slabs under HL93 truck load and to skewed approach slabs was investigated. The effect of embankment settlement was also considered. Moreover, the capacity of the approach slab to some special truck loads is rated in order to evaluate the approach slab designed by using the design aids. These results will eventually be used to systematically evaluate the effectiveness of approach slabs and develop guidelines for their structural design. This information will also help decide when settlement controls are necessary in order to have an economical design of approach slabs.

In the present study, a linear settlement of embankment is assumed, as shown in Fig. 1-1. The embankment settlement, a known parameter in the present finite element analysis, will be determined in another on-going research project supported by the LADOTD LQI program. Since one end of the slab sits on the relatively stiffer abutment while the other end on the relatively weaker soil or sleeper slab, a differential movement occurs between the two ends of the slab, which results in a gap between the slab and the embankment soil (Fig. 1-1).

In this study, a typical approach slab, shown in Fig. A-1, was used. The dimensions of the approach slab and the properties of soil used as embankment fill in Louisiana are listed in Table A-1 and Table A-2, respectively. A 3D finite element model was established, as shown in Fig. A-1(b), where eight-node hexahedron elements, Solid 45 (*ANSYS*, Canonsburg, PA,), were used to form the finite element mesh. A contact and target pair surface element available in the *ANSYS* element library was used to simulate the interaction between the soil and the slab. This surface

element is compressive only and can thus model the contacting and separating process between the slab and the soil. In addition to the dead load of the slab, two lanes of HL93 truck loads were applied on the slab. The present research will provide essential information needed for the structural design of the approach slab considering embankment settlement.

A.3 Applicability of Design Aids

A.3.1 Analysis of Approach Alab Aubjected to HL93 Highway Load

As discussed earlier, Eqs. (A-1) to (A-6) were derived (Cai et al. 2005) to simplify the calculation of internal forces and deformations based on the HS20-44 truckload. In this study, the investigation of the applicability of the equations to the HL 93 highway load was conducted by using the finite element method. The geometries and the material conditions of the FE model are shown in Fig. A-1. The HL93 highway load, consisting of the lane load and the HS20-44 truckload, is applied on the approach slab.

A parametric study was conducted by changing the slab thickness, span length, and soil settlement to investigate whether the previous equations are applicable to the HL93 highway load. The slab parameters, i.e., length (L) and thickness (h), were investigated for the following cases: (1) h was varied from 1 to 1.5 ft for the fixed L = 40 ft; and (2) h was varied from 1.5 to 2.25 ft for the fixed L = 60 ft. For each case the settlement was varied from 0.5 to 2, to 6 inches.

The results of the FE analyses for approach slabs subjected to HL 93 truck loads under different settlements are shown in Fig. A-2. Meanwhile, the results obtained by using equations (1) to (6) are also plotted to compare them with the FE analyses. The M_0 and d_0 used in the equations were calculated by applying HL 93 loads to a simply-supported slab. For the approach slab with a span length of 40 ft and thickness of 1.5 ft, the internal moment of the slab calculated by using the equations is almost the same as those from the FE analyses.

Table A-1 Dimension of approach slab, sleeper slab, abutment, embankment and natural Soil

Approach slab		Sleeper slab		Abutment		Embankment Soil						Natural Soil				
L1 (ft)	S4	L2 (ft)	H3 (ft)	L3 (ft)	L4 (ft)	W1 (ft)	H1 (ft)	H2 (ft)	S1	S2	L5 (ft)	W2 (ft)	H4 (ft)	H5 (ft)	S3	L6 (ft)
40, 60	2%	4	2	2	4	45	4	5	6	4	40	15	5	50	2	10

Table A-2 Parameters of soil

	Elastic modulus E (psi)	Poisson's ratio μ	Cohesion c (psi)	Friction angle φ(°)	Density γ (pcf)
Embankment Soil	37700	0.3	11.6	30	127.4
Natural Soil	4360	0.3	7.25	30	95.6

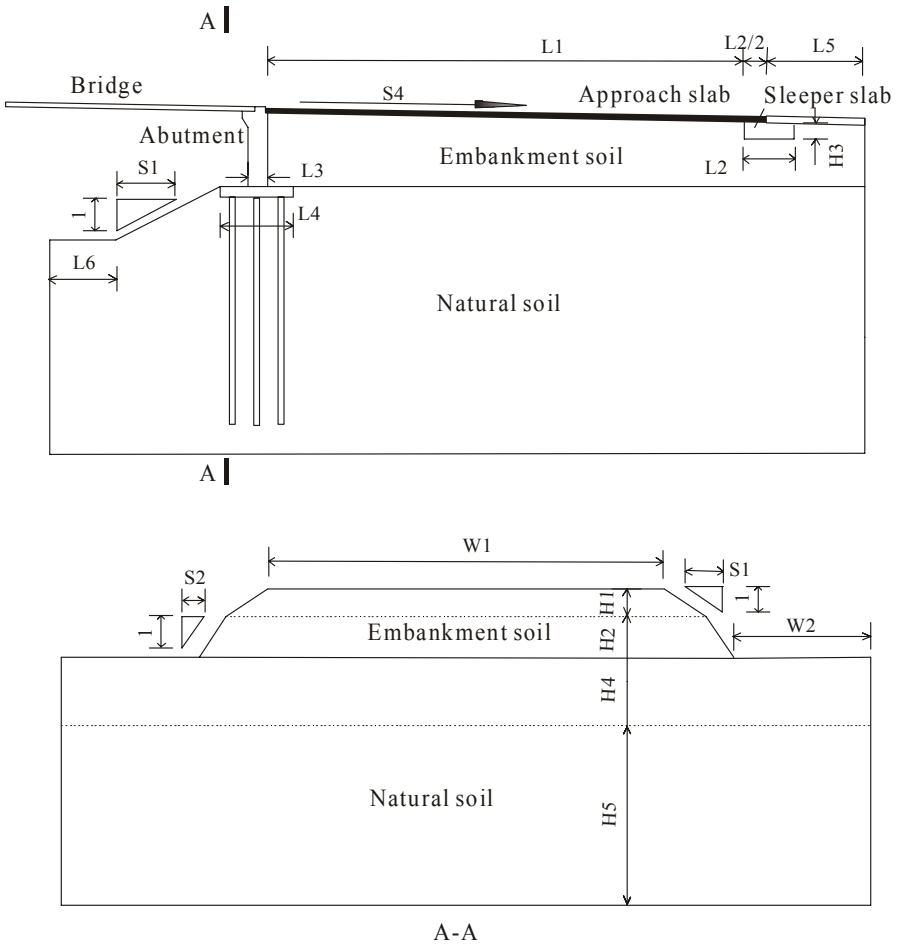

(a) Sketch of bridge abutment

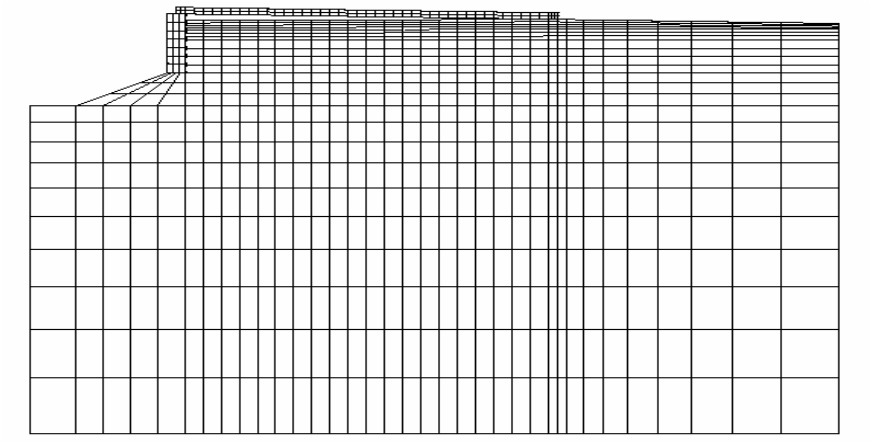

(b) Typical finite element mesh with 8 node cubic element

Fig. A-1 Approach slab and abutment model

This figure shows that for different approach slabs with different dimensions under different embankment settlements the moment and deformation obtained from the equations are close to those from FE analyses. Based on the investigation of different cases, we can conclude that the equations are applicable to approach slabs subjected to the HL93 highway load.

While the derived equations are applicable for both HS20-44 and HL93 highway loads, the internal forces and the load factors in the design method are different. The results of the reinforcement design for the approach slab subjected to HS20-44 and HL93 highway loads are listed in Table A-3. It is observed that when the settlement is zero, the required reinforcement at the bottom of the slab (L=40', h=12") is 0.65 $in.^2$/ft. (ρ=0.0063), and it increases to 1.57 $in.^2$/ft. (ρ=0.0145) when the settlement increases to 0.6 in. This indicates that the current design (LADOTD 2002), 0.88 $in.^2$/ft. (ρ=0.00815), is good only for the case of zero settlement and is not adequate for a settlement larger than 0.6 in. When the embankment settlement increases, more reinforcement is required and the required reinforcement ratio, ρ, will exceed the allowed maximum reinforcement ratio, ρ_{max}, namely 75% of the balanced reinforcement ratio (AASHTO 2002). In this case, either the slab thickness should be increased or the soil should be improved to control the settlement within the allowable limit.

A.3.2 Performance of Skewed Approach Slab

It is not unusual for bridges to end with large skews to pavements. In order to confirm the applicability of the previously derived equations to the skewed approach slab, skewed approach slabs with a skew angle of 45^o for a few different span lengths under different differential embankment settlements were analyzed using the FE method. The geometry, material properties, and load conditions of the FE model (Fig. A-3) are the same as those used in the normal (right) approach slab analysis, except for the skew angle. Approach slabs with different span lengths, 40 ft and 60 ft, and different thicknesses, 1 ft and 1.5 ft for 40 ft long slabs, and 1.5 ft and 2.25 ft for 60 ft long slabs, were investigated. Two AASHTO HS20-44 design truckloads were applied on the slab under different embankment settlements. Application of the uniform lane loads is not necessary for this applicability study since it has been proven that the HS20-44 is equivalent to the HL93 in terms of the approach slab performance.

Fig. A-4 shows the stress distribution in a skewed slab under different embankment settlements. When the settlement is small, the slab is partially supported by the soil near the sleeper slab end and separates from the embankment soil near the abutment end. The performance of the slab under this condition is more like that of a triangular slab, as shown in Fig. A-4 (a). Although the maximum moment of the total section is in the rectangular part, the maximum stress is located in the triangular part. Therefore, using the moment per unit width to describe the internal force of the slab is more reasonable for design purposes. In the following study of skewed approach slabs, the moment per unit width is thus used instead of the total moment of the section.

Table A-3 Reinforcement ratio of slab under different settlement (HL93 and HS20-44)
(f'c = 4000 psi and fy = 60,000 psi)

Differential settlement (in)	40-ft Slab			60-ft Slab		
	ρ for thickness of 12 in	ρ for thickness of 18 in	ρ for thickness of 24 in	ρ for thickness of 21 in	ρ for thickness of 27 in	ρ for thickness of 36 in
0	0.0063 (0.0061)(*)	0.0025 (0.0024)	0.0014 (0.0014)	0.0035 (0.0034)	0.0022 (0.0022)	0.0014 (0.0014)
0.6	0.0145 (0.0137)	0.0081 (0.0077)	0.0058 (0.0056)	0.0060 (0.0056)	0.0046 (0.0043)	0.0036 (0.0034)
1.2	0.0213 (0.0207)	0.0114 (0.0110)	0.0074 (0.0072)	0.0083 (0.0077)	0.0065 (0.0061)	0.0052 (0.0049)
2.4	NA(**)	0.0143 (0.0138)	0.0080 (0.0079)	0.0121 (0.0112)	0.0093 (0.0087)	0.0068 (0.0066)
3.6	NA	0.0151 (0.0147)	0.0081 (0.0079)	0.0151 (0.0140)	0.0110 (0.0104)	0.0074 (0.0072)
4.8	NA	0.0153 (0.0149)	0.0081 (0.0079)	0.0174 (0.0162)	0.0120 (0.0115)	0.0077 (0.0075)
6	NA	0.0154 (0.0149)	0.0081 (0.0079)	0.0191 (0.0178)	0.0126 (0.0121)	0.0077 (0.0075)
7.2	NA	0.0154 (0.0150)	0.0081 (0.0079)	NA (0.0191)	0.0130 (0.0124)	0.0078 (0.0076)

Note: (*) The numbers in brackets are the results of approach slab due to HS20-44 truck load.

(**) The required reinforcement ratio ρ exceeds the allowed maximum reinforcement of flexure, i.e., $\rho > \rho_{max} = 0.75\rho_b$, meaning that section dimension needs to be increased.

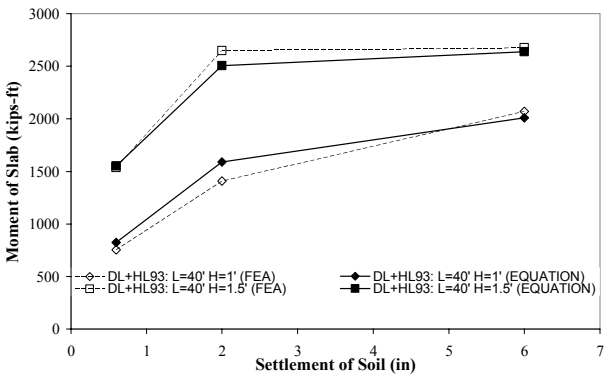

(a) Moment of slab with span of 40 ft

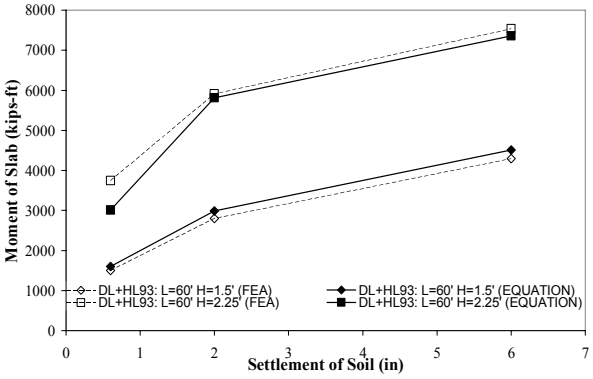

(b) Moment of slab with span of 60 ft

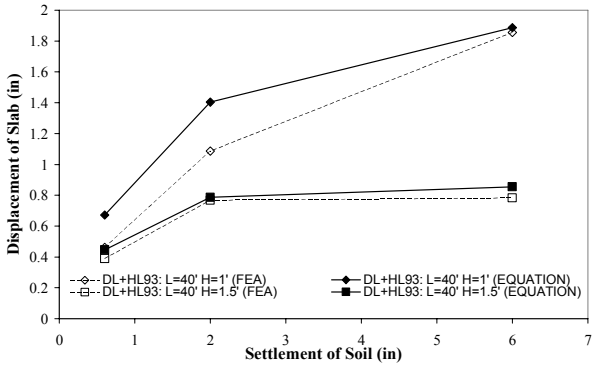

(c) Displacement of slab with span of 40 ft

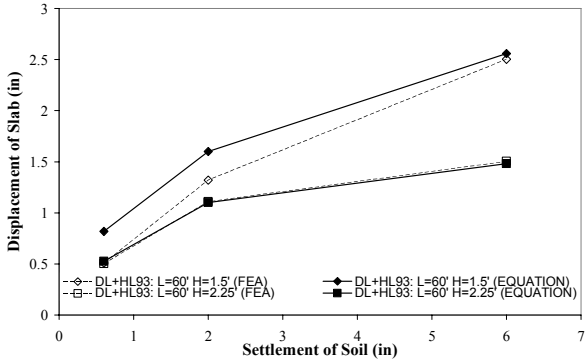

(d) Displacement of slab with span of 60 ft

Fig. A-2 Moment and displacement of approach slab versus soil settlement

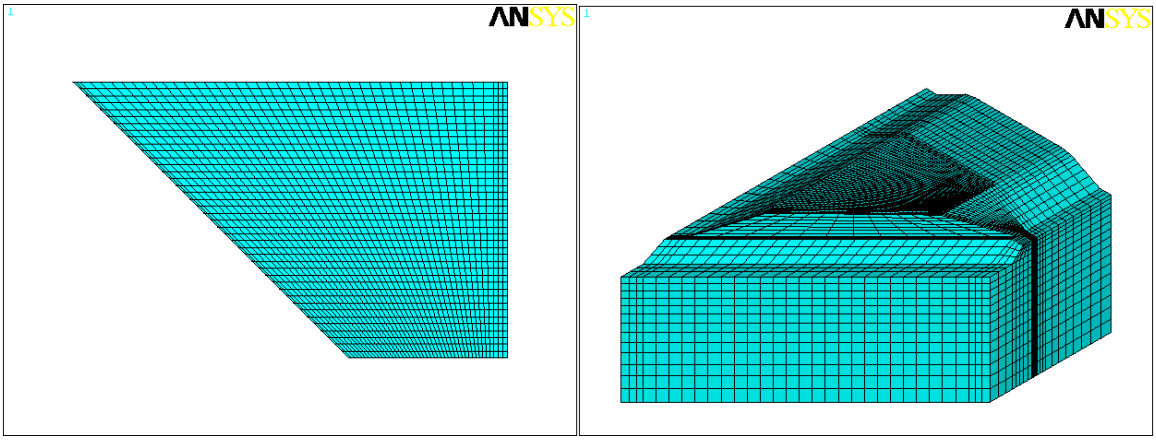

Fig. A-3 FE model of skewed approach slab

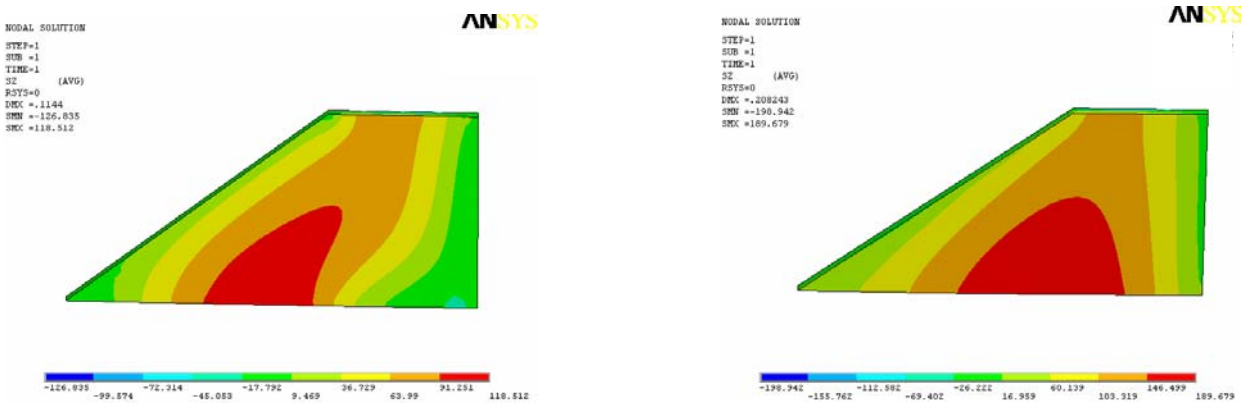

(a) Settlement = 0.5 inches (b) Settlement = 6 inches

Fig. A-4 Stress distribution of skewed approach slab

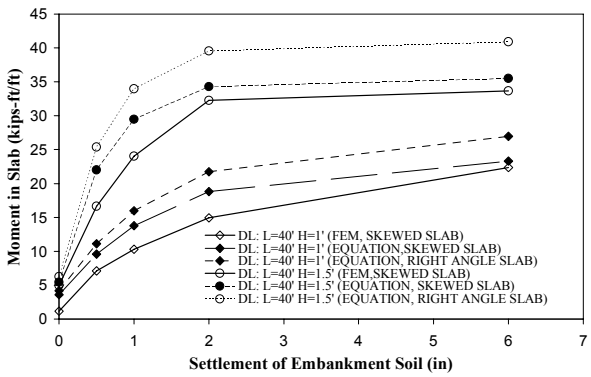

(a) Skewed approach slab with span of 40 ft due to self weight

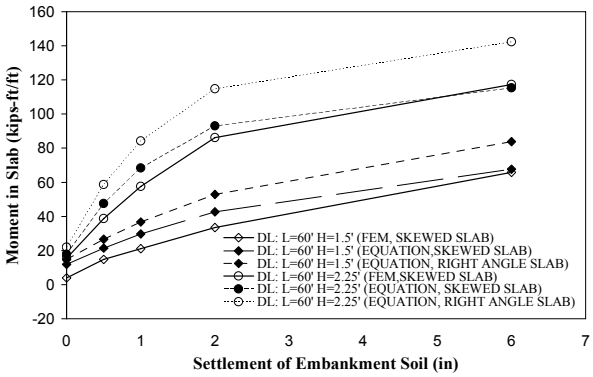

(b) Skewed approach slab with span of 60 ft due to self weight

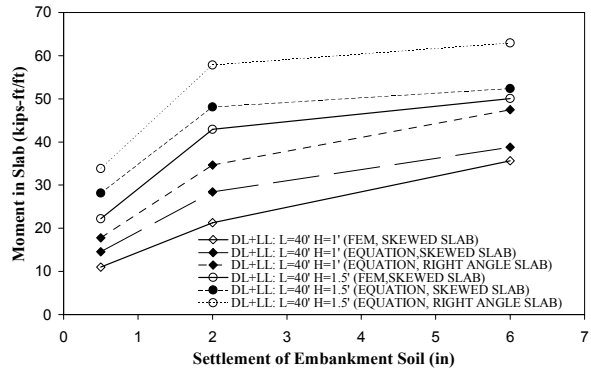

(c) Skewed approach slab with span of 40 ft due to Total Load

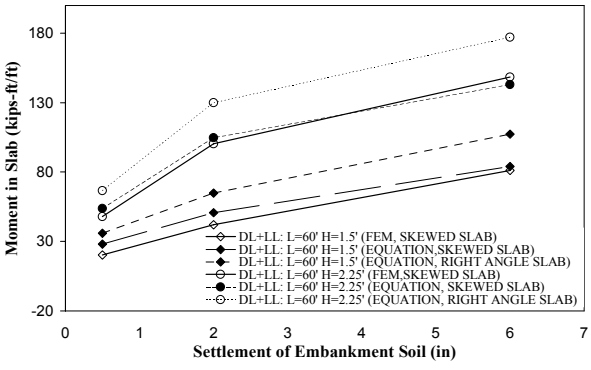

(d) Skewed approach slab with span of 60 ft due to Total Load

Fig. A-5 Moment of skewed approach slab versus embankment settlement

Fig. A-5 shows the moment per unit width of a skewed approach slab with a span length of 40 ft and 60 ft under different settlements of embankment soil due to the dead load and total load, respectively. The span length L for the skewed slab used here represents the length of the slab along the mid-width line. It is recalled that in the previous derived Eqs. (A-1) to (A-6), the internal force and displacement of the approach slab considering the settlement effects are calculated by using a coefficient to multiply the corresponding value of a simply-supported beam. Therefore, in these figures, in addition to the moment predicted directly from the FE analysis that is labeled "FEM, SKEWED SLAB", two more calculations based on the derived equations were conducted. In the first one, the moment per unit width was obtained by using previously derived equations, but the M_0 (moment of a simply-supported beam) was based on a simply-supported skewed slab using a finite element modeling since a direct calculation of M_0 for skewed slabs is not available. This calculation is labeled "EQUATION, SKEWED SLAB". In the second calculation, the unit width moment was calculated by using the derived equations, but the M_0 is based on an equivalent simply-supported normal (right) slab where its span length is taken to be the same as the length along the mid-width line of the skewed slab. This calculation is labeled "EQUATION, RIGHT ANGEL SLAB". The displacement of the skewed approach slab due to the dead load and total load are shown in Fig. A-6. Similarly, the displacement was calculated by using the equations with d_0 based on a simply-supported skewed slab and a simply-supported normal slab.

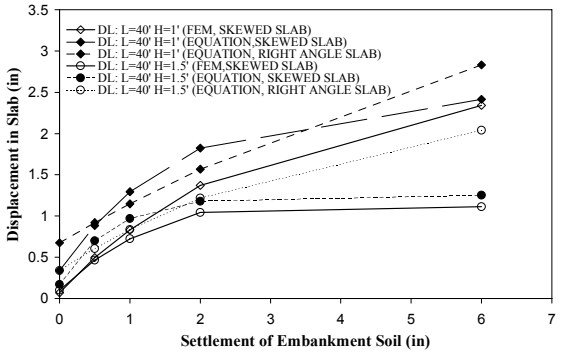

(a) Skewed approach slab with span of 40 ft due to self weight

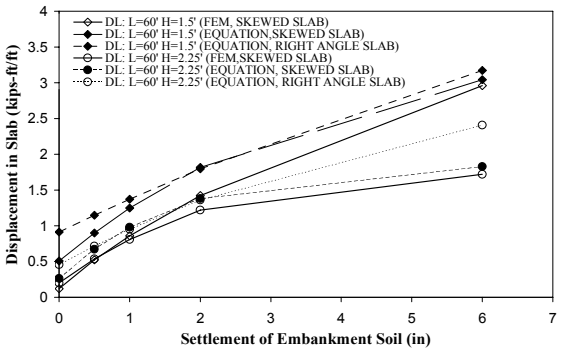

(b) Skewed approach slab with span of 60 ft due to self weight

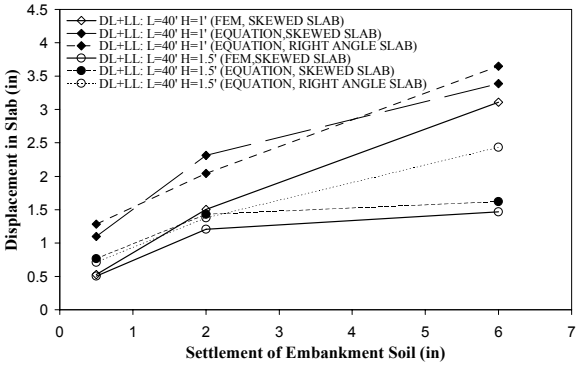

(c) Skewed approach slab with span of 40 ft due to Total Load

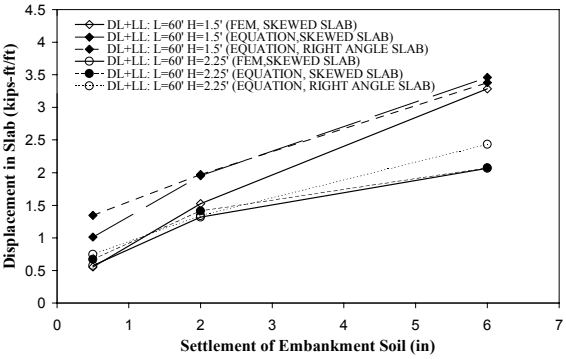

(d) Skewed approach slab with span of 60 ft due to Total Load

Fig. A-6 Displacement of skewed approach slab versus embankment settlement

From Fig. A-5, it is obvious that the moment of skewed approach slabs based on FEM is close to that obtained from equations based on the simply-supported skewed slab, which indicates that the equations derived for the normal approach slab can be used to calculate the internal forces of the skewed approach slab. However, the simply-supported skewed slab is complicated and a hand calculation for the internal force analysis is not available because of its irregular shape. Thus a FE analysis is usually necessary. The moment obtained from the equations based on the equivalent simply-supported normal slab is larger than that of the skewed slab from the FE analysis, as shown in Fig. A-5. Therefore, it is conservative and more convenient to use the moment calculated from the equations based on an equivalent normal slab in the skewed approach slab design.

The displacements of skewed slabs obtained from the FE analysis and equations based on a *simply-supported skewed slab* are close to each other, as shown in Fig. A-6, which means if the displacement of a simply-supported skewed slab is known, the equations derived for a normal approach slab can also be used to analyze the displacement of a skewed approach slab. However, the displacement obtained from equations based on an equivalent *simply-supported normal slab* is much smaller than that from the FE analysis of the skewed slab, which is caused by the large displacement of the long side of the skewed approach slab. Therefore, to use the developed equations, a longer nominal span length than that used for moment is needed.

The comparison of results from the FE analysis and the results calculated by using the previous derived equations indicates that the internal force and deflection of skewed approach slabs can be obtained by using the equations derived for normal approach slabs, where M_0 and d_0 in the equations are internal forces and deformation of the simply-supported skewed approach slab respectively. Since the calculation of a simply-supported skewed approach slab is more complicated than a simply-supported normal slab, the FE method is also needed to analyze the simply-supported skewed slab, which makes the equation inconvenient for design purposes. Therefore, the internal forces of skewed approach slabs are compared to those of simply-supported normal slabs with the same nominal span. Results show that the internal forces of a skewed slab are less than that obtained from equations using a simply-supported normal slab, which indicates that using the equations with M_0 of an equivalent normal slab to calculate a skewed approach slab internal force is conservative.

A.4 Capacity Rating of Special Trucks

The objective of the approach slab rating is to determine (1) the safe load-carrying capacity of the slab designed by using the design aids, and (2) whether a specific overweight vehicle may cause damage to the slab. In this study, approach slabs were rated by using trucks that may be more critical to the approach slab design. Three special trucks provided by LADOTD were used, as shown in Fig. A-7.

For approach slabs, the same FE model (Fig. A-1) is used to analyze the internal force of the approach slabs subjected to different rating truck loads. The internal moments of different approach slabs under embankment settlement of 6.0 in. are listed in Table A-4.

Load rating was performed in accordance with the procedures given in the AASHTO Manual for Condition Evaluation of Bridges (AASHTO, 1994). The following strength condition equation was used to determine the load rating of the structure:

$$R.F. = \frac{\phi M_n - \sum \gamma_D M_D}{\gamma_L M_L (1 + I)} \tag{A-7}$$

where *R.F.* is the rating factor, Φ is the strength reduction factor, γ_D, and γ_L are the dead load and live load factors, respectively, M_n is the nominal moment capacity, M_D and M_L are the moment due to the dead load and the live load, respectively. The coefficients γ_D, and γ_L may have different values depending on the type of loading rating (inventory or operating).

Load rating of the approach slabs, with reinforcement designed for HS20-44 and HL93 highway loads (Table A-3), was also conducted based on the standard AASHTO specifications and AASHTO LRFR (AASHTO 2003). The AASHTO LRFR specifications adopt three levels of rating methodology. They are: design load rating, legal load rating, and permit load rating. While the provided trucks should fit in either the legal or permit truck, all three levels of rating were conducted. The rating factors for different cases shown in Table A-5 are larger than one, which indicates that the available live load capacity of approach slabs is larger than that produced by the loads being investigated.

Table A-4 Internal force of approach slab subjected to rating truck

Truck Type	Moment of slab with L=40' h=18" (kips-ft)	Moment of slab with L=40' h=24" (kips-ft)	Moment of slab with L=60' h=21" (kips-ft)	Moment of slab with L=60' h=27" (kips-ft)
	DL+LL (DL: M=1697.9)	DL+LL (DL: M=2293.1)	DL+LL (DL: M=4429.1)	DL+LL (DL: M=5724.5)
Rating truck 1	2508.4	3098.6	5636.9	7519.4
Rating truck 2	3236.6	3831.9	6222.3	8611.6
Rating truck 3	2645.9	3236.3	5764.1	7746.5

A.5 Conclusions

The approach slabs are supposed to prevent "bump", but the large deformation of approach slabs designed according to conventional methods still causes this "bump". The current approach slab design is still more an art than a science. There are no AASHTO guidelines for designing approach slabs with embankment settlements (due to embankment soil long-term consolidation and erosion). An appropriate approach slab design will directly affect the safety and economy of the transportation infrastructure. It will be a trend to assign the responsibility of this design issue to an engineer. A rational design is necessary not only for the serviceability requirement of the transition approach slab, but also for the life-expectancy of the whole highway system, including bridges and pavements.

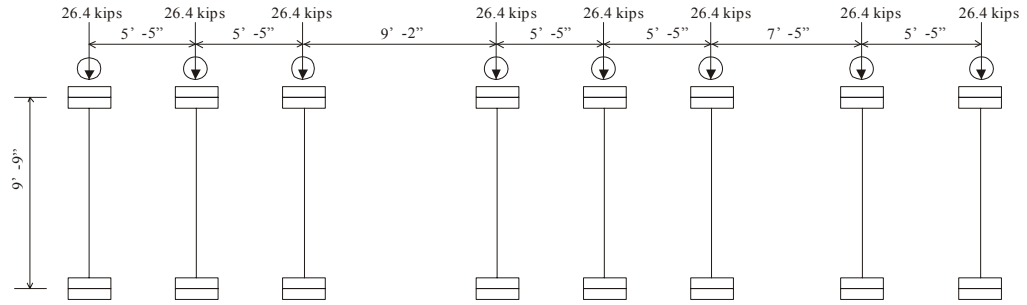

(a) Rating vehicle 1

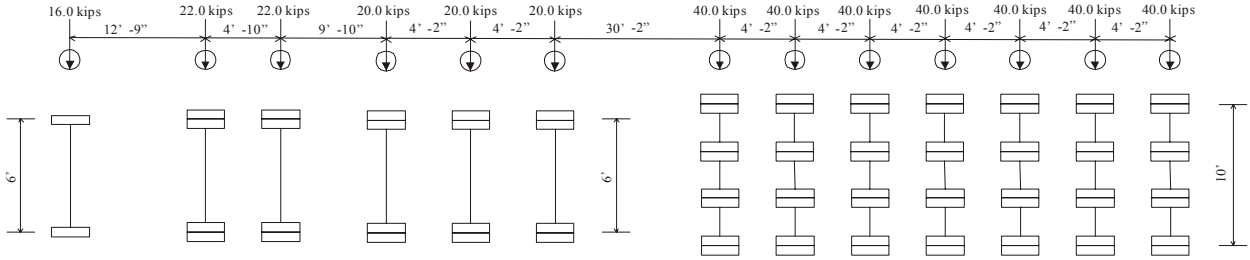

(b) Rating vehicle 2

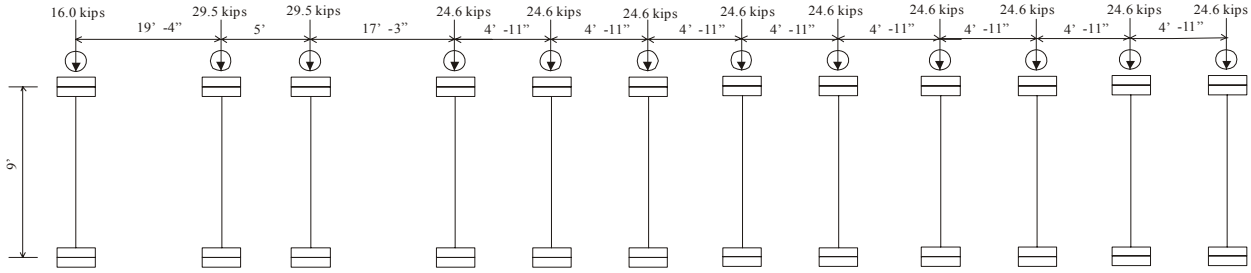

(c) Rating vehicle 3

Fig. A-7 Rating vehicle (plan view) with axle loads marked

Table A-5 Rating result of approach slab

	AASHTO Standard Rating (*)								AASHTO LRFR Design Load Rating (**)								AASHTO LRFR Legal Load Rating (***)				AASHTO LRFR Permit Load Rating(****)			
	L=40' h=18"		L=40' h=24"		L=60' h=21"		L=60' h=27"		L=40' h=18"		L=40' h=24"		L=60' h=21"		L=60' h=27"		L=40' h=18"	L=40' h=24"	L=60' h=21"	L=60' h=27"	L=40' h=18"	L=40' h=24"	L=60' h=21"	L=60' h=27"
	(1)	(2)	(1)	(2)	(1)	(2)	(1)	(2)	(1)	(2)	(1)	(2)	(1)	(2)	(1)	(2)	(2)	(2)	(2)	(2)	(2)	(2)	(2)	(2)
v1	2.18	3.63	2.19	3.66	2.10	3.50	1.59	2.65	2.68	3.48	2.72	3.52	2.62	3.40	1.99	2.58	2.61	2.64	2.55	1.94	3.61	3.66	3.53	2.68
v2	1.15	1.91	1.15	1.91	1.41	2.36	0.99	1.65	1.41	1.83	1.42	1.84	1.77	2.29	1.24	1.61	1.37	1.38	1.72	1.20	1.90	1.91	2.38	1.67
v3	1.86	3.11	1.87	3.12	1.90	3.17	1.41	2.35	2.29	2.97	2.32	3.01	2.37	3.08	1.77	2.29	2.23	2.26	2.31	1.72	3.09	3.12	3.19	2.38

Note: (*) Standard rating: (1) Inventory rating: $\gamma_D = 1.3$; $\gamma_L = 1.3 \times 1.67 = 2.17$; (2) Operating rating: $\gamma_D = 1.3$; $\gamma_L = 1.3$;

(**)LRFD design load: (1) Inventory rating: $\gamma_D = 1.25$; $\gamma_L = 1.75$; (2) Operating rating: $\gamma_D = 1.25$; $\gamma_L = 1.35$;

(***)LRFD legal load: (2) Operating rating: $\gamma_D = 1.25$; $\gamma_L = 1.8$;

(****)LRFD-Permit Load: (2) Operating rating: $\gamma_D = 1.25$; $\gamma_L = 1.3$;

In the present study a 3-D finite element analysis has been conducted to consider the effect of embankment settlement on the approach slab performance. The parametric study has led to the confirmation of a set of equations for the prediction of internal forces and deformation of the slab for a given settlement.

Based on a parametric study, we can conclude that the equations are applicable to approach slabs subjected to the HL93 highway load and also applicable for skewed slabs. The internal force and deflection of the skewed approach slabs can be obtained by using the equations, where M_0 and d_0 are the internal forces and deformation of the simply-supported skewed approach slab respectively. However, the calculation of a simply-supported skewed approach slab is complicated. Results show that using the equations with M_0 , the moment of an equivalent normal slab, to calculate the skewed approach slab internal force is conservative. Furthermore, the results of capacity rating of the approach slab indicate that the designed slab has sufficient capacity for the three special vehicles.

By using the design aids confirmed in this study, engineers, without using finite element analysis in their routine design, can conveniently design the approach slabs. This performance-based design will eventually lead to a more reliable practice in using approach slabs. These results can also be used to systematically evaluate the effectiveness of the approach slabs and develop guidelines for their structural design. This information will help decide when settlement controls are necessary in order to have an economical design of the approach slabs.

A.6 References

AASHTO. *Standard Specifications for Highway Bridges*. American Association of State Highway and Transportation Officials, Washington, D.C., 2002

AASHTO. *LRFD Bridge Design Specifications*. American Association of State Highway and Transportation Officials, Washington, DC., 2004

AASHTO. *Manual for Condition Evaluation of Bridges*. American Association of State Highway and Transportation Officials, Washington, D.C., 1994

AASHTO. *Guide Manual for Condition Evaluation and Load and Resistance Factor Rating (LRFR) of Highway Bridges*. American Association of State Highway and Transportation Officials, Washington, D.C., 2003

Briaud, J. L., James, R. W., and Hoffman, S. B. *Settlement of Bridge Approaches (the Bump at the End of the Bridge)*. NCHRP Synthesis 234, Transportation Research Board, National Research Council, Washington, D.C., 1997

Cai, C. S., Shi, X. M., Voyiadjis, G. Z. and Zhang, Z. J. Structural Performance of Bridge Approach Slab under Given Embankment Settlement. *Journal of Bridge Engineering, ASCE*, Vol. 10, No. 4, 2005, pp 482-489

Chini, S. A., Wolde-Tinsae, A. M., and Aggour, M. S. *Drainage and Backfill Provisions for Approaches to Bridges*. University of Maryland, College Park, 1992

Kramer, S.L., & Sajer, P. *Bridge Approach Slab Effectiveness*. Washington State Transportation Center, Seattle., 1991

LADOTD. *Bridge Design Metric Manual.* Louisiana Department of Transportation and Development, Baton Rouge, LA., 2002

LQI. *Louisiana Quality Initiative: Preservation of Bridge Approach Ride Ability*. Louisiana Department of transportation and Development, Baton Rouge, LA., 2002

Mahmood, I. U. *Evaluation of Causes of Bridge Approach Settlement and Development of Settlement Prediction Models*. Ph.D. Thesis, University of Oklahoma, Norman., 1990

Ha, H., Seo, J. B., Briaud, J. L. *Investigation of Settlement at Bridge Approach Slab Expansion Joint: Survey and Site investigations*. Report No. 4147-2 to the Texas Department of Transportation, published by the Texas Transportation Institute, Texas A&M University System., 2003

Stewart, C. F. *Highway Structure Approaches*. California Department of Transportation, Sacramento., 1985

Zaman, M., Gopalasingam, A. and Laguros, J. G. Consolidation settlement of bridge approach foundation. *Journal of Geotechnical Engineering*, Vol. 117, No.2, 1991, pp 219-239.

APPENDIX B: PERMISSIONS

AMERICAN SOCIETY OF CIVIL ENGINEERS LICENSE
TERMS AND CONDITIONS

Oct 25, 2006

This is a License Agreement between xiaomin shi ("You") and American Society of Civil Engineers ("American Society of Civil Engineers"). The license consists of your order details, the terms and conditions provided by American Society of Civil Engineers, and the payment terms and conditions.

License Number	1575730268289
License date	Oct 25, 2006
Licensed content title	Structural Performance of Bridge Approach Slabs under Given Embankment Settlement
Licensed content author	C. S. Cai; X. M. Shi; G. Z. Voyiadjis; Z. J. Zhang
Licensed content publication	Journal of Bridge Engineering
Licensed content publisher	American Society of Civil Engineers
Type of Use	Doctoral Thesis
Portion used	Excerpt
Institution	Louisiana State University
Title of your work	Structural performance of approach slab and its effect on vehicle indeced bridge dynamic response
Publisher of your work	UMI Company
Publication date of your work	12/30/2006
Website	http://etd.lsu.edu/issues/index.htm
Usage	electronic

2nd November 2006
To: Xiaomin Shi
Louisiana State University

Dear Ms. Shi:

The Transportation Research Board grants permission to use in your doctoral dissertation your paper "Design of Ribbed Concrete Approach Slab Based on Interaction with the Embankment," coauthored with C. S. Cai, G. Voyiadjis, and Z. Zhang, as identified in your e-mail of October 31, 2006. Please note the following conditions:

1. Please credit as follows:
   From Transportation Research Record: Journal of the Transportation Research Board, No. 1936, Transportation Research Board of the National Academies, Washington, D.C., 2005, pp. 181-191. Reprinted with permission.
2. None of this material may be presented to imply endorsement by TRB of a product, method, practice, or policy.

Every success with your dissertation. Please keep the Record in mind for future submissions.
Sincerely,
Javy Awan
Director of Publications
Transportation Research Board
Email: PBARBER@nas.edu

-----Original Message-----
From: Xiaomin Shi [mailto:xshi1@lsu.edu]
Sent: Tuesday, October 31, 2006 11:01 AM
To: Barber, Phyllis
Subject: Permission request
Dear Phyllis Barber:

This is Xiaomin Shi from Louisiana State University writing you this letter. I am completing a doctoral dissertation at entitled "Structural Performance of Approach Slab and Its Effect on Vehicle Induced Bridge Dynamic Response". I would like your permission to reprint in my dissertation the following article published in "Journal of the Transportation Research Board": Shi, X. M., Cai, C. S., Voyiadjis, G. Z., and Zhang, Z. J. (2005) "Design of Ribbed Concrete Approach Slab Based on Its Interaction with Embankment" Transportation Research Record, J. of the Transportation Research Board, National Research Council, 1936, 181-191.

I am the author of the above paper and it will be reproduced as chapter 3 in my dissertation. The requested permission extends to any future revisions and editions of my dissertation including non-exclusive world rights in all languages, and to the prospective publication of my dissertation by UMI Company. These rights will in no way restrict republication of the material in any other form by you or by others authorized by you. Your permission of this request will also confirm that you own (or your company owns) the copyright to the above-described material. If these arrangements meet with your approval, please response this email.
Thank you very much.
Sincerely,
Xiaomin Shi

VITA

Ms. Xiaomin Shi was born in 1976 in Jiangsu Province, P.R.China. She received her Master of Science degree from the Department of Civil Engineering at Tsinghua University, P.R.China, in 2002, her Bachelor of Science degree from the Department of Civil Engineering at Tongji University in 1999. Ms. Shi has worked as a Graduate Research Assistant at Louisiana State University since January 2003.

Ms. Shi has been involved in research in several areas, such as Interaction between Approach Slab and Embankment Soil, Vehicle-Bridge Coupled System, Bridge Vibration Control, and Bridge Test. She has 15 publications, which are listed as follows:

- Cai, C. S., **Shi, X. M.**, Araujo, M., and Chen, S. R. (2006) "Influence of approach span condition on vehicle-induced dynamic response of slab-on-girder-bridges: field and numerical simulations." J. of the Transportation Research Board, (submitted).
- **Shi, X. M.**, Cai, C. S., Voyiadjis, G. Z., and Zhang, Z. J. (2005) "Effect of embankment settlement on bridge approach slab design: a few concerned issues" J. of the Transportation Research Board, (submitted).
- **Shi, X. M.**, Cai, C. S., Chen, S. R. (2006) "Vehicle induced dynamic behavior of short span slab bridges considering effect of approach span condition." Journal of Bridge Engineering, ASCE, (accepted).
- Cai, C. S., Nie, J. G., and **Shi, X. M.**(2006) "Interface Slip Effect on Bonded Plate Repairs of Concrete Beams." Engineering Structures, (accepted and in press)
- Zhang, Y., Cai, C. S., **Shi, X. M.** and Wang, C. (2006) "Vehicle Induced Dynamic Performance of a FRP Versus Concrete Slab Bridge" J. of Bridge Engineering, ASCE, 11(4), 410-419.
- Cai, C.S., Wu, W.J. and **Shi, X. M.** (2006) "Cable Vibration reduction with a Hung-on TMD System: I. Theoretical Study." J. of Vibration and Control, 12(7), 801-814.
- **Shi, X. M.**, Cai, C. S., Voyiadjis, G. Z., and Zhang, Z. J. (2005) "Design of Ribbed Concrete Approach Slab Based on Its Interaction with Embankment" Transportation Research Record, J. of the Transportation Research Board, National Research Council, 1936, 181-191.
- Cai, C. S., **Shi, X. M.**, Voyiadjis, G. Z. and Zhang, Z. J. (2005) "Structural Performance of Bridge Approach Slab under Given Embankment Settlement." Journal of Bridge Engineering, ASCE, 10(4), 482-489.
- Wang, Y.Q., **Shi, X. M.**, and Chen, H. (2003) "Design and Analysis of Steel Portal Frame in Hydropower Plant Building", Journal of Water Power, v29, n3, 63-66.
- **Shi, X. M.**, Wang, Y. Q. and Zhang, Y. (2003) "Application of Large-Span Portal Frame with Prestressed Cable-Strut", Journal of Industrial Construction, v33, n2, 68-71.
- Wang, Y. Q., Wu, Y. M., Wang, X. Z., **Shi, X. M.** (2002) "3-D stresses in a flat slab with a crack in tension and the effect on brittle fracture." Journal of Tsinghua University (Science and Technology), v42, n6, 832-834+842.
- Zhang, Y., Cai, C. S., **Shi, X. M.** (2006) "Vehicle Load-Induced Dynamic Performance of FRP Slab Bridges" 2006 Structures Congress, ASCE, May 18-21, St. Louis, Missouri, USA
- **Shi, X. M.**, Cai, C. S., and Wu, W.J. (2005) "Effect of Approach Slab on Bridge-Vehicle

Coupled Vibration: Numerical Analysis." The joint /ASME/ASCE/SES Engineering Mechanics and Materials Conference, June 2005, Baton Rouge, Louisiana. (also presented)

- **Shi, X. M.**, Cai, C. S., Voyiadjis, G. Z. and Zhang Z. J. (2004) "3-D Finite Element Analysis of Interaction of Concrete Approach Slab and Soil Embankment", Geo-Trans 2004, the Geo-Institute of the American Society of Civil Engineers, Los Angeles, CA, July 27-31, 2004, ASCE Geotechnical Special Publication No. 126, 393-402. (also presented)
- Cai, C. S., Voyiadjis, G. Z., and **Shi, X. M.** (2005) "Determination of Interaction between Bridge Concrete Approach Slab and Embankment Settlement." Final Report, LTRC Project No. [03-4GT, State Project No. [736-99-1149], submitted to Louisiana Transportation Research Center.

The degree of Doctor of Philosophy will be awarded to Ms. Shi at the December 2006 commencement.